

**OPTICAL PROPERTIES OF LANTHANIDE IONS DOPED IN
BORATE, PHOSPHATE AND OXYFLUORIDE GLASSES**

A THESIS
SUBMITTED FOR THE DEGREE OF
DOCTOR OF PHILOSOPHY

BY
P. NACHIMUTHU

SCHOOL OF CHEMISTRY
UNIVERSITY OF HYDERABAD

HYDERABAD 500 046

INDIA

MAY 1996

Dedicated to
my father S. Ponnusamy
and to
my mother P. Kandayammal

CONTENTS

Statement	(i)
Certificate	(ii)
Acknowledgments	(iii)
List of Publications	(v)
Preface	(vii)
Chapter 1 Introduction	1
1.1 Introduction-the vitreous state	1
1.2 A Brief Review of Optical Properties of Lanthanide Ions in Crystalline and Glassy Hosts	3
Chapter 2 Experimental Techniques and Methodology	39
2.1 Experimental Techniques	39
2.2 Spectral Analysis	44
Chapter 3 Absorption and Emission Spectral Studies of Lanthanide Ions in Borate Glasses	55
3.1 Influence of Cations on the Optical Properties of Nd^{3+} , Eu^{3+} and Er^{3+} Doped Borate Glasses	55
3.2 Optical Absorption and Emission Spectral Studies of Pr^{3+} , Nd^{3+} , Sm^{3+} , Eu^{3+} , Tb^{3+} , Dy^{3+} , Ho^{3+} , Er^{3+} and Tm^{3+} Ions in $\text{CaO-Al}_2\text{O}_3\text{-B}_2\text{O}_3$ Glass System	72
Chapter 4 Absorption and Emission Spectral Studies of Lanthanide Ions in Phosphate Glasses	120
Chapter 5 Absorption and Emission Spectral Studies of Lanthanide Ions in Lead Oxyfluoride Glasses	149
5.1 Absorption and Emission Spectral Studies of Pr^{3+} and Tm^{3+} Ions in PbO-PbF_2 Glasses	153
5.2 Optical Properties of Nd^{3+} , Ho^{3+} and Er^{3+} Ions in PbO-PbF_2 Glasses	158
5.3 Absorption and Emission Spectral Studies of Sm^{3+} and Dy^{3+} Ions in Oxyfluoride Glasses	164
5.4 Absorption and Emission Spectral Studies of Eu^{3+} Doped in PbO-PbF_2 Glass System	171
5.5 Tb^{3+} Fluorescence as a Probe for Cluster Formation in Lead Oxyfluoride Glasses	176
Summary	231
Appendix 1 Thermal and Optical Properties of PbO-KF Glasses	235

STATEMENT

I hereby declare that the matter embodied in this thesis is the result of investigations carried out by me in the School of Chemistry, University of Hyderabad, Hyderabad, under the supervision of Professor **R Jagannathan**.

In keeping with the general practice of reporting scientific observations, due acknowledgments have been made wherever the work described is based on the findings of other **investigators**



P. Nachimuthu

Hyderabad

May 1996

CERTIFICATE

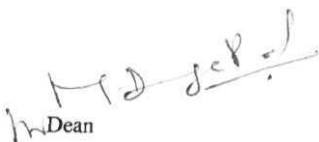
Certified that the work contained in this thesis entitled "**Optical Properties of Lanthanide Ions Doped in Borate, Phosphate and Oxyfluoride Glasses**" has been carried out by Mr. P Nachimuthu, under my supervision and same has not been submitted elsewhere for a degree.



R. Jagannathan
(Thesis supervisor)

Hyderabad

May 1996


Dean

School of Chemistry

University of Hyderabad

ACKNOWLEDGMENTS

I express my deep sense of gratitude with profound respect to Professor R. Jagannathan for his constant guidance, encouragement and cooperation throughout the course of this **work**

Thanks are due to

Professor K.D. Sen, the former Dean and Professor P.S. Zacharias, present **Dean**, School of Chemistry for their constant encouragement and providing necessary facilities to complete this work.

Dr D. Narayana Rao, School of Physics for lifetime measurements and discussions.

Dr. K.V. Reddy, Principal Scientific Officer, Central Instruments Laboratory for his help in some of the spectral measurements.

Dr. M. Vithal, Department of Chemistry, Saifabad College, Osmania University for encouragement and fruitful discussions throughout the course of the work.

Dr P. Balaya for introducing to preparative techniques, Dr. G. **Subramaniam** for computer programming and Dr. P. Murali for help in spectral analysis.

Dr M.V. **Rajasekharan**, **Dr** T.P. **Radhakrishnan**, Dr. Anunay **Samanta** and M. Durga Prasad, School of Chemistry, Dr. Ranjit Singh and Dr. C.S. Sunandana, School of Physics for discussions and suggestions, all the faculty members in the School of Chemistry for the help and encouragement.

Mr S Sivaprakasam and **Mr. V. Nirmal Kumar** for **refractive** index and life time measurements, **Ms M. Prasanna**, **Mr. C. Sivaram**, **Ms D. Ramalakshmi**, **Ms. M.S. Ameerunnisha Begum**, **Ms. H. Anitha**, **Ms. Sindhu Menon**, **Ms K Bhagyalakshmi** and **Ms. T. Banu** for their help in the course of experimental works.

Mr. C.S. Murthy, **Mrs. Nirmalananda**, **Mr. S. Manjunath**, **Mr. V. Bhaskar Rao**, **Vijaya Bhaskar**, **Mrs. Asia Perwaz** and **Mrs. B Vijayalakshmi** for their help in collecting various spectral **data**

Dr. K.C. Kumaraswamy for his generous gesture in providing the laser **printout** facility.

My **friends** **Dr. V. Saravanan**, **Dr. A.D Sagayaraj**, **Dr. K. Fanneerselvam**, **Dr. N. Karthikeyan**, **Mr. P.N. Rajesh**, **Mr. L Venkatraman**, **Mr. P Bharathi**, **Mr. S. Amanulla**, **Dr. K. Narkunan**, **Mr. U Radhakrishnan**, **Dr. S. Pandiyaraju**, **Mr. C.R. Ramanathan**, **Mr. C. Ramesh Kumar**, **Mr. K. Muthukumaran**, **Mr. S. Arounagui**, **Mr. V. Sathish**, **Mr. S. Senthil**, **Mr. K.R. Lakshmikanthan** and **Mr. D. Loganathan** for their lively company and timely help whenever required.

The University Grants **Commission**, Special Assistance Programme and the Council of Scientific and **Industrial Research**, New Delhi for the financial **support**

Finally, I wish to express my gratitude to my parents, brother and sister for their love, inspiration and constant encouragement throughout the course of academic career.

P. Nachimuthu.

List of Publications

- 1 Optical absorption spectral studies of Pr^{3+} , Nd^{3+} , Er^{3+} and Tm^{3+} ions in the $\text{CaO-Al}_2\text{O}_3\text{-B}_2\text{O}_3$ glass system P Nachimuthu and R Jagannathan, *Phys. Chem. Glasses* 36(1995)204.
- 2 Absorption and emission spectral studies of Pr^{3+} and Tm^{3+} ions in PbO-PbF_2 glasses. P. Nachimuthu and R. Jagannathan, *Phys. Chem. Glasses* 36 (1995) 77.
3. Absorption and emission spectral studies of Eu^{3+} doped PbO-PbF_2 glass system. P. Nachimuthu and R Jagannathan, *Proc. Indian Acad. Sci. (Chem. Sci.)* 107 (1995) 59.
- 4 Tb^{3+} fluorescence as a probe of cluster formation in lead oxyfluoride glasses P. Nachimuthu and R Jagannathan, *J. Non-Cryst. Solids* **183** (1995) 208
- 5 Thermal and optical properties of PbO-KF glasses P. Nachimuthu and R Jagannathan, *J. Appl. Phys* 78 (1995) 7323

Presented at Conferences

- 1 *Solid state physics symposium* at Bhaba Atomic Research Centre, Bombay, in December 1993. The posters were presented (a) Oscillator strengths and radiative properties of Pr^{3+} in PbO-PbF_2 glass. P. Nachimuthu and R Jagannathan. (b) Absorption and emission spectral studies of Eu^{3+} doped phosphate glasses, P. Nachimuthu, M. Prasanna and R Jagannathan.
2. *National laser symposium* at IRDE, Dehradun, in February 1995. The poster was presented. (a) Lead based oxyfluoride glass as host for rare earth lasers, P. Nachimuthu and R Jagannathan.
3. *Modern trends in inorganic chemistry* at University of Hyderabad, Hyderabad in August 1995 The poster was presented (a) Thermal and optical properties of PbO-KF glasses, P. Nachimuthu and R Jagannathan,
4. XXIII National symposium of the optical society of India on *Optics and Opto-electronics* at IRDE, Dehradun, in March 1996 The poster was presented. (a) An hitherto unreported energy transfer in rare earth systems, Pr^{3+} to Tb^{3+} ions in PbO-PbF_2 glass P. Nachimuthu, C Sivaram and R Jagannathan

PREFACE

The interest in the study of glasses in the early stages pertained to the role of glass forming and modifying inorganic ions on the structure and properties of glasses. Most of the studies were made on glass systems such as borates, silicates and **phosphates**. Transition metal ions as dopants in glasses attracted attention for introducing color and optical properties desirable for use as filters. Subsequent developments include new glass formers such as tellurites, gallates and germanates. Due to the advent of applications that glasses find in the field of optics and electronics, recent interest extends to fast ion conductors, lasers and non-linear optical materials. The search for transparent glasses over a wide spectral range resulted in the recent developments in fluoride glasses. Ever since the advent of Nd:YAG laser, rare earth ions as dopants in glasses have attracted considerable attention.

The present thesis deals with rare earth ions as dopants in borate, phosphate and oxyfluoride glasses. The oxyfluoride glasses as host materials for rare earth ions are subject to more detailed investigations than the borate and phosphate glasses. It is felt that these glasses deserve more attention as they are easy to prepare, relatively stable and should in principle exhibit properties intermediate between heavy metal oxide glasses and fluoride **glasses**. Further the scope in these systems to vary the relative amounts of fluoride and oxide ions present by varying the composition leading to consequent changes in the properties of interest can provide an additional feature of interest in such **systems**. We give below a brief account of the material presented in the thesis chapterwise.

Chapter 1 presents the salient features of the spectroscopic properties of the lanthanide ions from Pr^{3+} to Tm^{3+} . In this context the **Judd-Ofelt** model extensively used in the analysis of lanthanide absorption spectra is briefly dealt **with**. The so called hypersensitive transitions, in the emission and absorption spectra, the selection rules that

govern these transitions and the structural factors that influence their relative intensities and profiles are **presented**. One of the most interesting features of rare earth spectroscopy pertains to energy transfer in codoped systems. The pairs of lanthanide ions that show this phenomenon are tabulated and the mechanisms suggested for energy transfer presented. Under the individual members of the rare earth family the following features relevant to the present investigations are presented. (1) The significance of the **Judd-Ofelt** parameters, Ω_2 , Ω_4 and Ω_6 as obtained in widely varying host materials. (2) The results pertaining to hypersensitive transitions in the absorption and emission spectra as found in recent literature. (3) Features of interest in the emission spectral studies of these ions doped in crystalline and glassy systems. The presentation includes, wherever appropriate, highlighting recent studies on laser transitions, upconversion studies, energy transfer studies and suggested applications of the end results.

Chapter 2 entitled 'Experimental techniques and spectral analysis' provides details about various techniques used in the present study. This includes density measurements, refractive index measurements, absorption and emission spectral techniques and excited state lifetime measurements. The methods employed for the analysis of transition energies in the absorption spectra of Pr^{3+} , Nd^{3+} , Er^{3+} and Tm^{3+} for Racah parameters, spin-orbit coupling and configuration interaction terms are presented. The method used for obtaining oscillator strengths for the different transitions observed in the region 300 to 2200 nm is given. The least square fit procedure employed for obtaining the Judd-Ofelt parameters from the oscillator strengths is **described**. The various relationships useful in obtaining emission transition probabilities (A , A_T), branching ratios (β_R), stimulated emission cross sections (σ_p) and excited state lifetimes (τ_R) from the Judd-Ofelt parameters are presented.

Chapter 3 dealing with borate glasses as hosts consists of two parts. The first part of this chapter deals with optical spectral studies of Nd^{3+} , Eu^{3+} and Er^{3+} ions in the $\text{Li}_2\text{O-B}_2\text{O}_3$, $\text{CaO-B}_2\text{O}_3$ and $\text{BaO-B}_2\text{O}_3$ glass systems. The influence of the large variations in

the ionic radii of the cations present as major constituents in these borates on energy parameters, **Judd-Ofelt** parameters and radiative parameters are **presented**. The ionic size of the constituent cations and coordination preferences intrinsic to the Nd^{3+} and Er^{3+} ions as evidenced by structural characteristics exhibited by related crystalline borates are invoked to account for the variations in the Judd-Ofelt **parameters**. The emission and excitation spectra of Eu^{3+} ion doped in these glasses are **presented**. Information on the covalent character of the dopant ion is obtained from the red to orange emission intensity ratios of Eu^{3+} and is found to follow the behavior similar to Nd^{3+} as deduced from the Judd-Ofelt parameters. It is shown that the phonon side band studies of Eu^{3+} can be used as a novel tool for insight into the guest-host relationship. The phonon side bands associated with ${}^7\text{F}_0 \rightarrow {}^5\text{D}_2$ transition of Eu^{3+} can be resolved into two major components due to BO_3 and BO_4 groups. An increase in the BO_4 component relative to BO_3 accompanied by a **corresponding** increase in the electron phonon coupling strength in the order $\text{Li}^+ < \text{Ca}^{2+} < \text{Ba}^{2+}$ provides evidence for increasing dimensionality in the glass network resulting in stronger interaction between the glass matrix and the dopant Eu^{3+} ion. The second part presents the results of investigations on calcium aluminoborate glasses doped with Ln^{3+} ions. These glasses are chosen because of their unique features such as high stability, machinability and solubility of lanthanide ions. The results of analyses of transition energies for Pr^{3+} , Nd^{3+} , Er^{3+} and Tm^{3+} ions in these glass matrices in terms of Racah parameters, spin-orbit coupling and configuration interaction terms by full matrix **diagonalisation** procedure are **presented**. Supporting evidence for suggested coordinations are obtained from absorption and emission transitions which are influenced by the coordination but not by other mechanisms. The absorption spectral intensities of the above ions and those of Sm^{3+} , Dy^{3+} and Ho^{3+} ions doped in these glass matrices are analyzed for the Judd-Ofelt parameters and radiative **parameters**. The variation in the Judd-Ofelt parameters across the lanthanide series are compared with observations in the crystalline systems and are accounted for on the basis of site asymmetries, possible differences in covalency, coordination number, vibrational levels characteristic of the lanthanide ions and the dielectric of the **medium**. The radiative parameters obtained from

Judd-Ofelt parameters *viz.*, transition probabilities, branching ratios and excited state **lifetimes** are compared with values reported for phosphate, fluoride and other related bonte glasses. The emission spectra of **Sm³⁺**, **Eu³⁺**, **Tb³⁺** and **Dy³⁺** in these glasses are **presented** The other rare earth ions, *viz.*, **Pr³⁺**, **Ho³⁺**, **Er³⁺** and **Tm³⁺** gave rise to no significant emissions. It is shown that unlike in the case of phosphate and silicate glasses, the presence of **Al³⁺** does not significantly influence the emission spectra of **Eu³⁺** ion.

Chapter 4 deals with phosphate glasses with and without **Al³⁺** ions as host materials chosen for the following two reasons. Compared to borates, phosphate glasses have very high optical homogeneity and a matrix characterized by lower phonon energies favoring radiative decay. Secondly, presence of **Al³⁺** is known to influence significantly emission characteristics and it would therefore be of interest to study phosphates with and without **Al³⁺** In this chapter we present results of investigations of **Ln³⁺** doped in **CaO-P₂O₅** and **CaO-Al₂O₃-P₂O₅** glasses. The variation in the Judd-Ofelt parameters as we go higher up in the series from **Pr³⁺** to **Tm³⁺** for the two glasses are presented. The radiative parameters obtained from the Judd-Ofelt parameters *viz.*, transition probabilities, branching ratios and stimulated emission cross sections are compared for the two glassts. The emission spectra which could be recorded for **Pr³⁺**, **Eu³⁺**, **Dy³⁺** and **Tm³⁺** are analyzed for branching ratios and compared with values obtained from Judd-Ofelt **parameters** For **Eu³⁺** the results of phonon side band spectra are also presented.

Chapter 5 presents an extensive study of absorption and emission spectra of **Ln³⁺** ions in the heavy metal oxyfluoride glass system **PbO-PbF₂**. The rare earth ions used as dopants include **Pr³⁺**, **Nd³⁺**, **Sm³⁺**, **Eu³⁺**, **Tb³⁺**, **Dy³⁺**, **Ho³⁺**, **Er³⁺** and **Tm³⁺**. The Judd-Ofelt parameters obtained for different rare earth ions in these glasses are compared with values obtained for the corresponding rare earth ions in borate, phosphate and fluoride glasses. In addition a comparison is made for the variation in the Judd-Ofelt parameters as we go along the lanthanide series in the oxyfluoride glasses and other glass hosts such as phosphates and borates as host materials to establish whether the trend is general or

differs from system to system. The influence of host matrices on the hypersensitive transitions in the absorption spectra of Nd^{3+} , Ho^{3+} and Er^{3+} ions are presented. The plots of the sum of **Judd-Ofelt** parameters against the oscillator strengths vividly bring out the sensitivity of hypersensitive transitions to glass hosts in contrast to the nonhypersensitive transitions. The observed differences in the hypersensitive transitions are rationalized in terms of the influence of the bonding characteristics of the dopant ions with the different glass matrices as hosts. The transitions of Pr^{3+} and Nd^{3+} in the absorption spectra and Eu^{3+} in the emission spectra which are characteristic of coordination number provide evidence for 8-9 coordination around the rare earth ions in the oxyfluoride glasses. Taking this coordination and other factors such as the observation of the high energy fluorescence transitions into account a structure has been proposed for Ln^{3+} site with eight fluoride and oxide ligands from six PbO_nF_m octahedra linked by Pb-O-Pb linkages from OPb_4 tetrahedra. The emission spectra of Pr^{3+} and Tm^{3+} ions are discussed. The observation of temperature dependence in the case of the former is explained in terms of Boltzmann population. The emission spectra of Pr^{3+} also provide evidence for strong J-J mixing. The radiative parameters viz., transition probabilities, branching ratios, and lifetimes obtained from Judd-Ofelt parameters for Pr^{3+} and Tm^{3+} ions are presented. The β_R values deduced from Judd-Ofelt parameters are compared with values derived from their emission spectral intensities. The fluorescence efficiency of these ions in this glass system has been compared with those observed for other glass hosts such as phosphate, tellurite and germanate glasses.

For Sm^{3+} and Dy^{3+} in the oxyfluoride glasses the radiative properties viz., transition probabilities, branching ratios, stimulated emission cross sections and excited state lifetimes deduced from the Judd-Ofelt parameters are compared with values obtained for the same ions in borate, phosphate and fluoride glasses. For these ions in addition to emission spectral measurements, studies of excited state lifetimes are also **reported**. For these systems the branching ratios derived from Judd-Ofelt parameters show good agreement with values deduced from emission spectral intensities. The

magnitude of the stimulated emission cross sections for different transitions for these ions evaluated for the first time are found to be an order of magnitude less than those reported for other rare earth ions. The quantum efficiencies for ${}^4G_{5/2}$ of Sm^{3+} and for ${}^4F_{9/2}$ of Dy^{3+} have been obtained from calculated and measured lifetimes. The decay curves for Dy^{3+} could be fit to single exponential. At higher Dy^{3+} concentration the shortening of the decay times are observed due to concentration quenching. Sm^{3+} decay at higher dopant concentration could be accounted for taking into account energy transfer due to cross relaxation involving levels ${}^4G_{5/2}$, ${}^6H_{9/2} \rightarrow {}^6F_{9/2}$, ${}^6F_{7/2}$, ${}^6F_{9/2}$, ${}^6F_{9/2}$, ${}^6F_{7/2}$, ${}^6F_{9/2}$ and ${}^6F_{5/2}$ $F_{11/2}$.

The emission spectra of Eu^{3+} in 30PbO-70PbF₂ and 70PbO-30PbF₂ are presented. The radiative transition probabilities, branching ratios and stimulated emission cross sections obtained for the laser transition ${}^5D_0 \rightarrow {}^7F_2$ of Eu^{3+} are compared with values obtained for phosphate glasses. The branching ratios obtained from Judd-Ofelt parameters compare well with values obtained from emission spectral intensities. The emission spectra in the high energy region which are usually not prominent in most of the glasses are found to be prominent in the present glass system. These transitions prominently appearing in the 440-570 nm region, provide evidence for less nonradiative decay due to low phonon energies characteristic of the host *viz.*, PbO-PbF₂. The phonon energy maximum for this glass is 930 cm⁻¹ and is comparable to tellurite, germanate and fluoride glasses. The electron phonon coupling strengths are deduced from the phonon side band spectra of Eu^{3+} in 30PbO-70PbF₂ and 70PbO-30PbF₂ glasses. The relative emission intensities of the low energy transitions to high energy transitions and the ratios of the intense transitions ${}^5D_0 \rightarrow {}^7F_2$ / ${}^5D_0 \rightarrow {}^7F_1$ significantly vary for the two compositions providing evidence for clustering of Eu^{3+} ions with increase in its concentration and increasing PbO content.

For Tb^{3+} ions doped in oxyfluoride glasses the ratios of the low energy emissions to high energy emissions are found to be quite sensitive to the concentration of the

dopant **ions** The change in this ratio with increasing Tb^{3+} concentration is investigated in detail. The observed behavior of this ratio with respect to dopant concentration is found to run parallel to the observations of Tb^{3+} fluorescence in crystalline systems which provide evidence for absence of cluster formation at low concentrations and clustering at much higher concentration of Tb^{3+} . It is therefore submitted that Tb^{3+} fluorescence studies can be used as a probe to throw light on clustering behavior in glass systems as **well** The observation of non occurrence of clusters at low Tb^{3+} concentrations is also in accordance with the structure proposed above for lanthanide ions in this glass matrix as it can accommodate even near neighbor rare earth ions far **apart**

An attempt is made to extend the above studies to other oxyfluoride glass systems such as **PbO-KF**. Emission spectral studies of rare earth ions in this glass matrices could not be made due to interference by very significant lead fluorescence. As a result the investigations were modified. The influence of composition on lead fluorescence, optical absorption edge, refractive index and thermal stability are investigated for **PbO-KF** glass systems and these results are presented in appendix **1**.

Introduction

1.1 Introduction - the vitreous state

The large amount of work on glasses pertains to silicates, borates and phosphates¹⁻³ The pioneering work of Zachariasen gave us a good understanding of the structure of these **glasses**.⁴ Their structures mostly consisting of rigid tetrahedra as in silicates or phosphates and in addition planar triangular coordination as in the case of the borates have been well **established**.^{1,5} Till the seventies most of the work done on glasses pertain to these systems. In the relatively recent times new glass formers other than those mentioned above have been **identified** For instance the work of Stanworth on glasses constituting glass formers such as tellurium oxide and heavy metal oxides such as lead oxide as conditional glass formers invoked renewed interest in glasses with better optical **properties**.⁶ Such oxide glass systems were subsequently extended to germanate and tantalate glasses^{3,7} Recently Shelby *et al* have reported a number of heavy metal oxide glass systems containing rare earth oxide as one of the major constituent. These glasses have high paramagnetic susceptibilities and Verdet constants and they exhibit high chemical durability, variable thermal expansion coefficient with rare earth content and high transformation temperatures which make them excellent candidates for Faraday rotator applications, either as bulk optics or as optical fibers.^{8,11} Besides the oxide glasses new nonoxide glass forming systems have also been **identified** These include the chalcogenide and the halide **glasses**.^{3,12} While the above glasses attracted attention because of their optical properties, an entirely new family of glassy materials, the so called metallic glasses with fascinating magnetic properties kindled renewed **efforts** in our understanding of materials with random distribution of the constituent atoms in solids.¹³

Chapter 1

An important aspect that rightly deserved attention in the area of glasses pertains to new methods in their preparations. Pol Duwez pioneered the method of roller quenching and preparation of metallic **glasses**¹⁴. This method found a useful extension in the preparation of new glasses which could not be prepared by simple melt quenching. While traditional methods of preparation of glasses involved quenching the melts from relatively high temperatures, attempts to prepare glasses by soft chemistry using the sol-gel technique has enabled preparation of glasses with high optical **homogeneity**.¹⁵⁻²⁴ The sol-gel route for preparation of glasses is attracting great deal of attention as reflected by the large amount of literature appearing on the subject.

The initial interest of introducing metal ions into glasses is to impart color. Introduction of metal ions as dopants subsequently shifted towards use of glasses as convenient matrices for bringing about added features of interest in their optical properties and their uses as filters and more recently as parent matrices for **lasers**. Transition metal ions have been considered as suitable dopants for introducing color or magnetism through the impurity ions and the nature of the sites occupied by these ions has been extensively investigated in the seventies.^{2,3,25} The interest in the dopant ions has subsequently shifted from the first transition metal ions to the lanthanides as many of them give rise to lasing **transitions**.^{3,26,27} Use of glasses as host materials has several **advantages**. The composition of the hosts can be changed to improve the desired optical properties. The host materials can be prepared with relative ease either by melt quenching or by the more recent sol-gel **technique**.¹⁵⁻²⁴ The host material can be prepared in large scale and in many cases with scope for machining into convenient shapes or in fiber forms. These advantages have led to exhaustive studies by way of identifying suitable transitions of the dopant ions with lasing properties and doping these in glass matrices with optical properties that will enable realizing potential devices using these materials in the bulk form or as optical fibers.^{28,29} These studies have been successful in making glass lasers commercially **viable**.^{3,27} The development of lasers has further catalyzed interest in the field of nonlinear optics and in materials giving rise to second

harmonic **generation** This in turn has created interest in making glass systems for non linear optical properties as **well**.²⁹⁻³²

1.2 A brief review of optical properties of lanthanides in crystalline and glassy hosts

The lanthanides are characterized by progressive filling of the 4f shell in their electronic configuration. The series begins with the element cerium (**Z=58**) and ends with the element **lutetium** (Z=71). The neutral lanthanides possess the common feature of a xenon configuration with two or three outer electrons ($6s^2$ or $5d6s^2$). As we proceed from La to Lu,, the nuclear charge and the number of 4f electrons increase by one at each step. The shielding of one 4f electron by another is very imperfect owing to the shapes of the orbitals, so that with each addition the effective nuclear charge experienced by each 4f electron increases, thus causing a reduction in size of the entire **4f^N** shell. The accumulation of these successive contractions is the total lanthanide contraction. This results in a change in the atomic radii of the lanthanides from 1.061 to 0.848 Å.^{33,34}

The lanthanides may be ionized by successive removal of electrons. The first stage of ionization, with the sole exception of Lu, results from the removal of a 6s electron. In the second stage of ionization, further removal of 6s electron occurs, and at the third stage, all the 6s- and 5d-electrons or more frequently a 4f-electron are removed resulting in the electronic configuration consisting of the closed shell xenon configuration and **4f^N** electrons. N=1 for cerium and increases regularly to N=14 for lutetium. The 3+ oxidation state dominates the entire lanthanide **series** Other oxidation states are also known for several of the lanthanides, although these valence states are relatively much less **stable**.^{33,34} Many of these lanthanide ions have their first excited states at quite low energies and the corresponding absorption bands which occur in the far infrared region have been reported only **recently** **Gd³⁺** is an exception in this regard with the electronic configuration corresponding to the half filled shell, **4f⁷** and its first excited state at **32,100 cm⁻¹**.^{3,26,27} The optical spectra of the first row transition metal ions have only a remote

Chapter 1

similarity with free ion **transitions**. On the other hand, in the lanthanides the narrow absorption bands are close to the free ions. The spectral transition energies for the same ion do not differ from system to system as much as they do in the case of first row transition metal **ions**. The differences although small are significant in that they are dependent on a number of spectral parameters as discussed below. The spectral assignments below 40,000 cm^{-1} were almost completed by Carnall *et al.*^{35,36} The energy level scheme for all the lanthanide ions are shown in figure 1.1. The 4f-4f spectral transition energies can be analyzed on the basis of the Hamiltonian containing Racah parameters, configuration interaction terms and spin-orbit coupling as discussed in detail by Carnall.³⁷ The analysis of 4f-4f spectral intensities are based on the original works of Racah and the phenomenological model independently put forward by Judd and Ofelt.^{38,39} The salient features of the theory and the methods of analysis are given in some detail in the next **chapter**. The Judd-Ofelt model is being extensively used for the analysis of spectral intensities in terms of the so called Judd-Ofelt parameters (Ω_λ , $\lambda=2,4,6$). This model is quite successful in providing an insight into information such as covalency, coordination of central lanthanide ions and radiative properties. The model is however based on certain assumptions and hence has some limitations. In the following account under individual rare earths we highlight the success or limitations in the applicability of this model to different lanthanide **ions**.

Some of the 4f-4f transitions of the trivalent lanthanide ions are very sensitive to the **ligating** atoms and coordination, compared to other **transitions**. Jorgensen and Judd referred to such transitions as hypersensitive **transitions**.^{26,27,40-43} These authors have noted that **all** known hypersensitive transitions obeyed selection rules $|AJ|$, $|AL| < 2$ and $AS = 0$. As these selection rules happen to be the same as those for electric quadrupole transitions they are also referred to as pseudo quadrupolar transitions. In the Judd-Ofelt model it is found that the hypersensitive or pseudo quadrupolar transitions significantly influence the value of Ω_2 . As a result, transitions which affect Ω_2 due to change in environment are in general referred to as hypersensitive **transitions**. The hypersensitive transitions for all the lanthanide ions are given in table 1.1.⁴⁰⁻⁴³

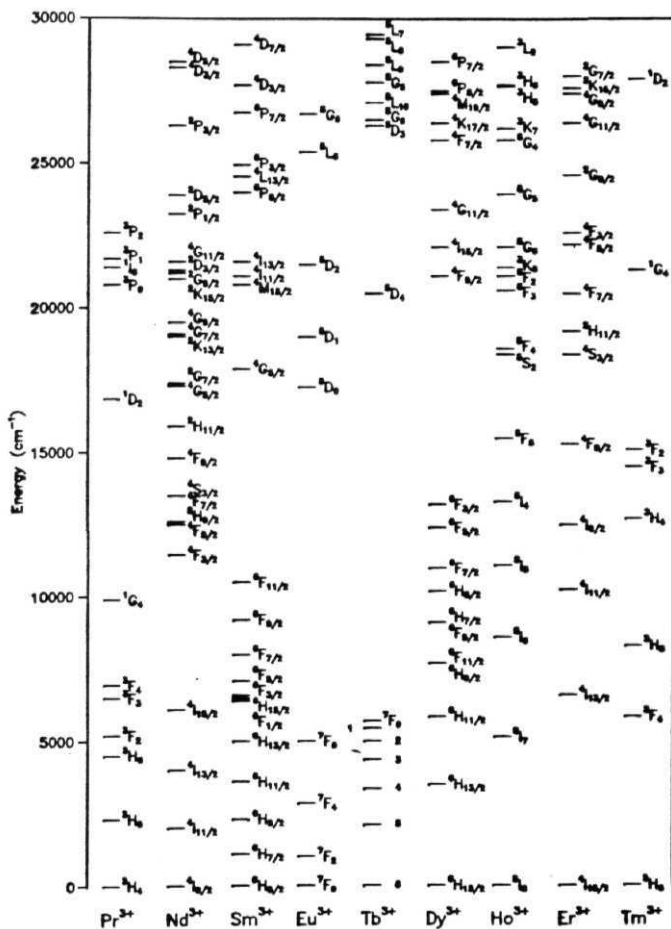


Figure 1.1 Energy levels of the **trivalent** lanthanide ions

Chapter 1

Table 1. Hypersensitive transitions for the lanthanide ions.⁴⁰ⁿ⁴³

Lanthanide ion	Transition	Approximate wavenumber (cm ⁻¹)
Pr ³⁺	$^3H_4 \rightarrow ^3F_2$	5200
	$^3H_4 \rightarrow ^3P_2$	22500
Nd ³⁺	$I_{9/2} \rightarrow G_{5/2}$	17300
Pm ³⁺	$^5I_4 \rightarrow ^5G_3 \ ^5G_2$	18000
Sm ³⁺	$H_{5/2} \rightarrow F_{1/2} \ F_{3/2}$	6400
	$G_{5/2} \rightarrow F_{9/2}$	8700
	$G_{5/2} \rightarrow H_{9/2}$	15600
Eu ³⁺	$^7F_0 \rightarrow ^5D_2$	21500
	$^5D_0 \rightarrow ^7F_2$	16300
	$^5D_1 \rightarrow ^7F_1$	18700
Gd ³⁺	$^8S_{7/2} \rightarrow ^6P_{3/2} \ ^6P_{7/2}$	32500
Tb ³⁺	$^5D_4 \rightarrow ^7F_6$	20400
	$^5D_4 \rightarrow ^7F_2$	15400
Dy ³⁺	$H_{15/2} \rightarrow F_{11/2}$	7700
	$F_{9/2} \rightarrow H_{13/2}$	17250
	$F_{9/2} \rightarrow H_{5/2}$	10600
Ho ³⁺	$^5I_8 \rightarrow ^5G_6$	22100
		27700
Er ³⁺	$I_{15/2} \rightarrow H_{11/2}$	19200
	$I_{15/2} \rightarrow G_{11/2}$	26400
Tm ³⁺	$^3H_6 \rightarrow ^3F_4$	5900
	$^3H_6 \rightarrow ^3H_4$	12700
	$^3H_6 \rightarrow ^1G_4$	21300

A number of transitions in the lanthanide ions has also been identified as potential laser **transitions**.^{3,26} Many of the emission transitions of the rare earth ions including the laser transitions are favorably influenced by the addition of other rare earth ions as **sensitizers**. The spectroscopic properties of rare earths as dopants in crystalline and glassy systems are being currently reinvestigated in detail for optical phenomena which are recently discovered and are of current **interest**. These include studies such as upconversion, fiber **lasers**,⁴⁷⁻⁴⁹ fiber amplifiers,^{50,52} photo darkening effects,⁵³ hole burning⁵⁴ and second harmonic generation by doped single mode optical fibers.^{29,30,45,55} On account of present interest on these aspects and by way of giving a sense of completeness to this review, these features of interest in various rare earths have also been **highlighted**. In addition we include brief mention of systems or properties with potential for **applications**.

1.2.1 Cerium(III) and (IV)

Cerium exists both as trivalent as well as tetravalent ion of which Ce^{3+} is the more stable **state**. Ce^{3+} has the $4f^1$ electronic configuration with $^2F_{5/2}$ ground state. The energy difference between the ground state $^2F_{5/2}$ and the only excited state $^2F_{7/2}$ is about $2,257 \text{ cm}^{-1}$ and the corresponding transition appears in the infrared region. Ce^{3+} also exhibits an absorption band due to $4f \rightarrow 5d$ transition in the near ultraviolet **region**.^{26,56} Recently Malashkevich *et al* have reported the optical centers of cerium ions in silica glasses obtained by the sol-gel **process**. They have concluded from their experimental observations that there are two optical centers present in the system, viz., Ce^{3+} and Ce^{4+} occurring as near neighbors. Their relative concentrations depended upon the total concentration of cerium and the conditions in which the sol-gel silica glasses were derived, viz., in air or in vacuum. The resonance transfer of excitation occurs to **the** $\text{Ce}^{3+} - \text{O}^{2-}$ complexes when Ce^{4+} is photoreduced to the triply charged **state**.⁵⁷

Cerium doped materials show enhanced optical stability even when exposed to high radiation conditions and also find use as light filters absorbing ultraviolet **radiation**.⁵⁸

Ce^{3+} ion is widely used for energy transfer studies as an activator doped in crystalline and glassy hosts with the ions Tb^{3+} and Dy^{3+} .^{46,59-61} Green emitting Ce^{3+} codoped with Tb^{3+} in $\text{GdMgB}_3\text{O}_{10}$ is used as lamp phosphor.⁶² Cerium doped glasses find use as photo and cathodic luminophors, magnetoactive and photosensitive elements and as ionizing radiation detectors.⁵⁸ Ce^{4+} is relatively unstable and its compounds are used as an oxidizing reagent in organic synthesis. Ce^{3+} with one electron in the 4f orbital acts as a good electron spin resonance probe which gives good signals at low temperature with g tensor values indicative of unusually large anisotropy as shown for instance in Ce^{3+} doped p"-alumina with $g_x=2.58$, $g_y=2.15$ and $g_z=0.85$.⁶³ It will be of interest to extend such studies to glassy matrices to gain insight on crystal field distribution.

1.2.2 Praseodymium(III)

Pr^{3+} has the $4f^2$ electronic configuration with $^3\text{H}_4$ ground state. The transition $^3\text{H}_4 \rightarrow ^3\text{P}_0$ of Pr^{3+} in the absorption spectra is characteristic of coordination of the Pr^{3+} ion in the crystalline and glassy host matrices. For example, the effective coordination numbers of Pr^{3+} ion in $\text{Na}_2\text{Pr}(\text{OOCCH}_2\text{-OCH}_2\text{COO})_3 \cdot 2\text{NaClO}_4 \cdot 6\text{H}_2\text{O}$ and in aqueous solution are 9.8 and 11.2 respectively. Differences in the coordination leads to a variation in the energy of the above transition from 20,580 to 20,750 cm^{-1} .⁵⁶ For Pr^{3+} ions the concentration dependence of vibronic transitions has been investigated in detail by Strek *et al*.⁶⁴⁻⁶⁶ in the absorption spectra of Pr^{3+} doped single crystals of $\text{LiLaP}_4\text{O}_{12}$, LaF_3 and $\text{Cs}_2\text{NaLaCl}_6$ and by Blasse and coworkers in the excitation and emission spectra of Pr^{3+} doped powder samples of La_2O_3 , $\text{La}_2\text{O}_2\text{S}$, $\text{Y}_2\text{O}_2\text{S}$, LaOCl , $\text{Na}_3\text{La}(\text{MoO}_4)_4$, $\text{Na}_3\text{La}(\text{WO}_4)_4$ and LaNbO_4 .⁶⁷⁻⁷¹ Strek *et al* have reported that increasing Pr^{3+} concentration leads to enhancement of the $^3\text{H}_4 \rightarrow ^3\text{P}_{1,2}$, $^1\text{D}_2$ electronic absorption as well as the vibronic absorption lines, but results in systematic decrease in the intensity of $^3\text{H}_4 \rightarrow ^3\text{P}_0$ transition. These authors suggest that the vibronic transitions being essentially cooperative, the concentration dependence arises due to exchange of virtual phonons between coupled Pr^{3+} ion pairs.⁶⁴⁻⁶⁶ Blasse *et al* reported that increase in the concentration of Pr^{3+} increases the intensities of the vibronic lines in the excitation spectra of Pr^{3+} ion relative

to the $H_4 \rightarrow {}^3P_0$ zero phonon line whereas the vibronic lines in the emission spectra are not observably affected. These authors attributed their observation to superexchange interaction between Pr^{3+} ions.⁶⁷⁻⁷¹ In their subsequent work these authors have reported that the enhancement of the intensities of vibronic transitions in the excitation spectra with increasing dopant concentration is due to saturation of the absorption transitions. They concluded that both their own earlier observations and those reported by Streck *et al* arise due to similar saturation effects. Further, they have shown that the saturation effects are more pronounced for transitions with higher oscillator strengths even when samples with low concentrations of Pr^{3+} and narrow optical paths typically of the order of millimeters are used. This is attributed to spurious line broadening and masked relative intensities in the **absorption/excitation** spectra.⁷² The transition ${}^3H_4 \rightarrow {}^3F_4$ in the absorption spectra of Pr^{3+} is hypersensitive by quadrupole selection rules. Two other transitions, ${}^3H_4 \rightarrow {}^1D_2$ and ${}^3H_4 \rightarrow {}^3P_2$ are hypersensitive by experimental **observations** in that they are strongly influenced by ligand environments. The 5d level of Pr^{3+} is low lying and contributes considerably to the oscillator strengths of 4f-4f transitions. This is principally responsible for the hypersensitive nature of the latter transition. Inclusion of the intensity of this transition in particular invariably leads to large errors in the Judd-Ofelt parameters. The application of the Judd-Ofelt theory, in general, works less well for Pr^{3+} than for other lanthanides as the number of observed transitions is limited to seven out of which three are **hypersensitive**.⁴⁰⁻⁴³ The emission spectra of Pr^{3+} in crystalline hosts such as YAG and LaF_3 and glasses such as fluorozirconate are well **studied**.⁷³⁻⁷⁸ The transitions ${}^3P_0 \rightarrow {}^3H_5$ and ${}^3P_0 \rightarrow {}^3F_3$ are unique examples with significant intensities in Pr^{3+} emission spectra due to J **mixing**.⁷⁹ J mixing contributes to the intensities of these transitions through Judd-Ofelt parameters with odd X values. Interestingly terms corresponding to even λ values do not contribute for these two transitions as the even reduced matrix elements vanish in these cases with $U^2, U^4, U^6=0$.⁷⁶ This also invalidates the frequently applied three parameter Judd-Ofelt model for Pr^{3+} ion. The radiative parameters *viz.*, transition probability, branching ratios and excited

Chapter 1

state lifetimes are reported for Pr^{3+} ion in many crystalline and glassy hosts. Though the Judd-Ofelt theory is not fully valid for Pr^{3+} for reasons mentioned above, the radiative parameters calculated from Judd-Ofelt parameters obtained excluding the hypersensitive $^3\text{H}_4 \rightarrow ^3\text{P}_2$ transition from the calculation, show fairly good agreement with observed values from emission spectra and life time measurements. '

Studies of multiphonon decay in Pr^{3+} have brought to light many interesting features de Mello Donega *et al* have recently measured the non radiative decay rates of $^3\text{P}_0 \rightarrow ^1\text{D}_2$ and the transition probabilities for the vibronic transitions associated with the $^3\text{H}_4 \rightarrow ^3\text{P}_0$ excitation transition in several host lattices ranging from those where the non radiative decay is negligible ($\text{LiYF}_4:\text{Pr}^{3+}$) to hosts where it dominates ($\text{Lu}_2\text{O}_3:\text{Pr}^{3+}$) depending on covalency of the central ion and the electron phonon coupling strength. When the force constant in the low lying 4f5d states is stronger than in the $4f^2$ states, the fast $^3\text{P}_0 \rightarrow ^1\text{D}_2$ non radiative relaxation via inter system crossing through 4f5d state becomes dominant even at 4.2 K. These mechanisms, unless suppressed, can reduce the potential of Pr^{3+} for practical applications as scintillator materials⁸⁰

Emission studies show that in Pr^{3+} systems energy transfer can occur by cross relaxation between Pr^{3+} ions. Life time measurements of $^3\text{P}_0$ and $^1\text{D}_2$ levels over a wide temperature range provide experimental evidence for cross relaxations. Nonradiative decay by cross relaxation from $^3\text{P}_0$ is possible through three path ways, viz., $(^3\text{P}_0, ^3\text{H}_4) \Rightarrow (^1\text{D}_2, ^3\text{H}_6)$, $(^1\text{G}_4, ^3\text{H}_4)$ and $(^3\text{H}_6, ^1\text{D}_2)$. In the case of $^1\text{D}_2$ level the cross relaxation paths can be $(^1\text{D}_2, ^3\text{H}_4) \Rightarrow (^1\text{G}_4, ^3\text{F}_4)$ and $(^3\text{H}_6, ^1\text{G}_4)$.^{77,81}

Laser action has been observed in PrCl_3 and also in $\text{PrP}_5\text{O}_{14}$.⁸² Quantum yields exceeding unity in the conversion of ultraviolet excitation into visible emission in $\text{Pr}_x\text{Y}_{1-x}\text{F}_3$, prove that the Pr^{3+} doped crystals are attractive for light converters.⁸² $^3\text{P}_0 \rightarrow ^3\text{H}_4$ upconversion emission transition has been observed for Pr^{3+} in LaF_3 and YAG by

excitation of the 1D_2 level.^{83,84} In energy transfer studies reported so far, Pr^{3+} acts as acceptor with the ions Nd^{3+} , Tb^{3+} , Tm^{3+} and Mn^{2+} .⁸⁵⁻⁸⁸

Wei *et al* and Simons *et al* have simultaneously reported the suitability of Pr^{3+} doped in Ge-Ga-S and GeS_x glasses respectively for fiber amplifiers at 1.3 μm due to the transition $G_4 \rightarrow H_5$. The radiative properties associated with the above transition have been determined by absorption and fluorescence measurements coupled with Judd-Ofelt analysis. They have shown that Pr^{3+} doped in these glasses have a longer fluorescence life time and a larger stimulated emission cross section than ZBLAN glass, factors which are favorable for an efficient fiber amplifier.^{50-52,89,90}

The narrow absorption bands of solutions containing Pr^{3+} continue to be used to monitor separation of colored lanthanides having adjacent atomic numbers, and historically were major tools used by Auer von Welsbach for separating praseodymium and neodymium in 1885.²⁷ The corresponding bands in glasses continue to serve as wavelength standards in spectrophotometers.

1.2.3 Neodymium(III)

Nd^{3+} has the $4f^3$ electronic configuration with $^4I_{9/2}$ ground state. The absorption and emission spectra of Nd^{3+} in several crystalline and glassy host lattices have been extensively investigated because of its potential in laser applications.^{26,27,56} The transition $^4I_{9/2} \rightarrow ^2P_{1/2}$ of Nd^{3+} in the absorption spectra is characteristic of coordination of the rare earth ion in the crystalline and glassy host matrices. The effective coordination number of Nd^{3+} ion varies from 6 to 9. Differences in the coordination leads to a variation in the energy of the above transition from 23,217 to 23,385 cm^{-1} .⁵⁶ The fairly intense transition $^4I_{9/2} \rightarrow ^4G_{5/2}$ occurring in the visible region is hypersensitive.⁴⁰⁻⁴² The hypersensitivity of this transition is well brought out as shown by the influence of cations in borate glasses and addition of trivalent aluminium in silicate glasses.²¹ This transition absorbs selectively the two yellow sodium lines, circumventing interference by potassium and rubidium

Chapter 1

spectral lines in gas flames.²⁷ Thus glasses containing Nd^{3+} are being used to give protection to glassblowers while seeing the red glow of glass objects under work.

The Judd-Ofelt theory works very well for this ion. The radiative parameters can therefore be conveniently evaluated from Judd-Ofelt parameters for Nd^{3+} ion in several hosts before embarking on detailed emission studies and their suitability for laser systems intelligently guessed. The useful parameters that could be obtained from absorption, emission and excited state lifetime measurements on small samples include radiative transition probability, branching ratios, excited state lifetimes, quantum yield, nonradiative relaxation rate, energy transfer probabilities and laser cross sections.²⁷

The maximum focus in the emission studies of Nd^{3+} pertains to the influence of the host matrix on the lasing transition ${}^4\text{F}_{3/2} \rightarrow {}^4\text{I}_{11/2}$. In many cases most of the doped Nd^{3+} ions are unavailable for laser action because of partial microscopic clustering. In the case of glass hosts inhomogeneous distribution of the neodymium ions can further lead to low fluorescence intensity of the lasing transition. Several approaches have been made to minimize such effects. For instance small amount of trivalent aluminum or phosphorus peroxide as codopant makes microscopic clustering of Nd^{3+} ions disappear and render the coordination around the Nd^{3+} ions favorable for laser application in silicate glasses.⁹¹

The ability to prepare silicate glasses by sol-gel route enables incorporation of Nd^{3+} ions in a glass host with high homogeneity and results in marked improvement in the lasing properties with high quantum yield and wide tunability.²¹ The method also provides superior physical properties of sol-gel derived silica. These include low non-linear refractive index coefficient, low strain birefringence, coefficient of thermal expansion close to zero, low temperature dependence of expansion coefficient and low impurity levels. The method also provides further scope for improvement by incorporation of cations such as trivalent aluminium to avoid concentration quenching in addition to

homogeneous dispersion of the active ions. However care is required for the removal of residual OH^- detrimental to fluorescence.

Many different Nd^{3+} doped glasses and crystals have been identified as active media for solid state lasers. The most commonly used systems employ Nd^{3+} in $\text{Y}_3\text{Al}_5\text{O}_{12}$ (YAG), LiYF_4 (YLF) and phosphate glasses. Trivalent lanthanide ions doped yttrium aluminum garnet $\text{Y}_3\text{Al}_5\text{O}_{12}$ (YAG) have been extensively studied during the last decade, because $\text{Nd}^{3+}:\text{YAG}$ is the most **successful** solid state laser material. $\text{Nd}^{3+}:\text{YAG}$ lasers have found extensive applications as range finders and have also become laboratory standard equipment for research in photo chemistry and related fields. $\text{Nd}^{3+}:\text{YLF}$ some times used in place of YAG, when it is appropriate to trade off the inferior **thermo** mechanical properties of YLF for its lower thermal lensing, longer emission life time and broader emission line width. Research on Nd^{3+} lasers increased rapidly because of the requirement of large Nd^{3+} glass lasers for **fusion** research. All glass lasers developed to date have used a rare earth as the active ion and optical pumping for excitation. Of these, flash lamp pumped Nd^{3+} glass lasers are the most widely investigated and the most frequently **used**. Examples of other Nd^{3+} hosts that are some times used include $\text{LaMgAl}_{11}\text{O}_9$ (LMA), YAlO_3 (YALO), $\text{LiNdP}_4\text{O}_{12}$ (LNP), $\text{Gd}_3\text{Sc}_2\text{Ga}_3\text{O}_{12}$ (GSGG), $\text{La}_2\text{Be}_2\text{O}_5$ (BEL) and many **others**. Each of these materials is useful for specific but limited applications because of its unique **attribute**.²⁷

Recently Wang *et al* have reported the fabrication, spectroscopy and laser performance of Nd^{3+} doped lead silicate glass fibers.²⁸ Glass fiber lasers developed to date have mostly been based on two glass compositions, silicate glasses and ZBLAN fluoride glass containing zirconium, barium, lanthanum, aluminum and sodium. Early experiments on glasses as bulk laser host for rare earth ions showed that the lead glass was not suitable for lasing ions on account of its poor thermal optic and non linear refractive index **coefficient**. These factors cause either a low optical damage threshold or a detrimental effect of self focusing which impose severe constraints on the output power

Chapter 1

of a laser. However in fiber lasers, the poor thermal optical behavior is irrelevant because the fiber structure allows excellent heat dissipation and thus avoids self-focusing. Thus lead glass can be employed as a suitable fiber laser host for rare earth ions, with the possible benefit of having narrower absorption and fluorescence spectral line widths than the alkali silicate glass host. These attributes provide a larger emission cross section, hence a higher gain and a lower threshold for fiber laser action in lead silicate fibers compared to the conventional silica based active fibers.

Goh *et al* have recently demonstrated the technologically important lasing action in the blue (488 nm) and red (635, 717 nm) region of the visible spectrum in a new $\text{Nd}^{3+}:\text{Pr}^{3+}$ codoped ZBLANP glass fiber with 796 nm pump. They have explained the lasing action in the above system on the basis of an upconversion and resonant energy transfer mechanism.⁸⁵

1.2.4 Promethium(III)

Pm^{3+} has the electronic configuration of $4f^4$ with $^4\text{I}_4$ ground state.⁵⁶ Promethium is the only lanthanide that lacks stable isotopes. For chemical investigation the isotope ^{147}Pm with a half life of about two years is usually employed. Though promethium is highly radioactive, some absorption spectral studies have been carried out on Pm^{3+} in aqueous solutions and in molten nitrates.^{56,92} The Judd-Ofelt model accounts well for the absorption spectra. The transitions $^4\text{I}_4 \rightarrow ^5\text{G}_2$, $^4\text{I}_4 \rightarrow ^5\text{G}_3$ in the absorption spectra are hypersensitive.⁴⁰⁻⁴²

1.2.5 Samarium (III) and (II)

Samarium has variable valency viz., Sm^{3+} and Sm^{2+} . Sm^{3+} is quite stable compared to Sm^{2+} . Sm^{3+} has the $4f^5$ electronic configuration with $^6\text{H}_{5/2}$ ground state.⁵⁶ Reisfeld has shown that the oscillator strengths of Sm^{3+} ions may be arranged in two groups, one referring to transitions upto $10,700 \text{ cm}^{-1}$ and the second to transitions in the range $17,600\text{-}32,800 \text{ cm}^{-1}$ and they calculated the Judd-Ofelt parameters separately for

these two **regions**.⁴⁰ The parameters obtained for the high energy region are higher by a factor of 30 in the τ_2 . This was attributed to the splitting **off** configuration being smaller than the f-d energy **gap**.⁴⁰ In such a case it is incorrect to use the oscillator strengths of transitions which are about $10,000 \text{ cm}^{-1}$ for calculations of Ω_λ parameters by means of the Judd-Ofelt theory. The transitions $^6\text{H}_{5/2} \rightarrow ^4\text{F}_{1/2}$, $^4\text{F}_{3/2}$ of Sm^{3+} occurring in the absorption spectrum in the near infrared region are hypersensitive.⁴⁰⁺⁴² In the emission spectra of Sm^{3+} , the transitions, $^4\text{G}_{5/2} \rightarrow ^6\text{F}_{9/2}$ and $^4\text{G}_{5/2} \rightarrow ^6\text{H}_{9/2}$ occurring in the near infrared and visible region respectively are also **hypersensitive**.⁴⁰⁻⁴³ The quantum efficiency for $^4\text{G}_{5/2}$ level of Sm^{3+} has been determined in hydrated salts and is found to be low due to the smaller energy gap between $^4\text{G}_{5/2}$ and the next lower level, $^6\text{F}_{11/2}$ ($\Delta E = 7,400 \text{ cm}^{-1}$).⁹³

For Sm^{3+} , the energy levels are **such** that cross relaxation takes place easily resulting in fluorescence **quenching**. Recently Rodriquez *et al* have reported that cross relaxations occur for Sm^{3+} doped in fluoride glasses even at low concentrations via dipole-dipole mechanism.⁹⁴ Sm^{3+} ions can act both as sensitizer as well as **activator**.⁹⁵⁻⁹⁸ When Sm^{3+} is used as sensitizer, energy transfer takes place via dipole-dipole or dipole-quadrupole mechanism depending upon the host **matrices**.⁹⁵

Sm^{2+} is also relatively stable in crystalline and glass hosts. Sm^{2+} easily stabilizes in crystalline hosts such as CaSO_4 .⁹⁹ Recently Hirao *et al* and Izumitani and Payne have investigated Sm^{2+} ions doped in oxide and fluoride glass matrices **respectively**.^{54,100} Hirao *et al* have shown that Sm^{2+} doped glasses show many features of interest such as persistent hole **burning**.⁵⁴ These authors have shown that by using a suitable laser beam corresponding to $^7\text{F}_0 \rightarrow ^5\text{D}_0$ transition it is possible to excite ions to saturation. This requires that the excited ions resonate with the narrow laser beam whose energy varies within the homogeneous line width of the transition under study. Thus, with narrow band excitation very narrow and photochemically stable holes can be burnt into the absorption bands of the rare earth in the glass. Persistent hole burning experiments with glass hosts

Chapter 1

have the potential for developing devices with optical memory superior to other devices which use polymers doped with dyes. An optical memory based on persistent hole burning uses frequency multiplexing to facilitate writing and reading with light of various frequencies at one spot so that the recording density can be increased 2 to 10 times that of conventional optical memories. Persistent hole burning optical memories are studied primarily for the polymer materials that are doped with organic dye but such materials fail to produce holes at room temperature and the working temperatures are limited to cryogenic temperatures lower than 80 K. Also, use of an organic dye raises the problem of fatigue during many read/write cycles. For these reasons persistent hole burning studies in glass systems doped with rare earth ions are pursued with vigour. Recently room temperature persistent hole burning has been observed in Sm^{2+} doped halide single crystals and oxide glasses.⁵⁴

1.2.6 Europium(III) and (II)

Europium has variable valency state, Eu^{3+} and Eu^{2+} . Eu^{3+} is quite stable even at high temperatures in crystalline and glassy host matrices. The spectroscopy of europium is widely investigated as it finds large number of applications. Eu^{3+} has the $4f^6$ electronic configuration with 7F_0 ground state.⁵⁶ One of the early but most extensive studies on absorption spectra of Eu^{3+} in glasses is due to Gallegar which includes study of the influence of glass modifying cations and glass forming anions on the absorption spectra.¹⁰¹ The transitions $^7F_0 \rightarrow ^5D_2$ in the absorption spectra and $^5D_0 \rightarrow ^7F_2$ in the emission spectra of Eu^{3+} are hypersensitive.⁴⁰⁻⁴³ The transition $^5D_0 \rightarrow ^7F_0$ in the emission spectra is characteristic of coordination of the Eu^{3+} ion.¹⁰² The transitions $^5D_0 \rightarrow ^7F_2$ and $^5D_0 \rightarrow ^7F_1$ occur in the visible in the red and orange region respectively and their integrated emission intensity ratio (R/O ratio) is strongly influenced by site asymmetry and covalency of the bonds with the ligand anions.¹⁰³ Oomen and van Dongen have shown that the Eu^{3+} emission intensity of the transitions $^5D_0 \rightarrow ^7F_2$ and $^5D_0 \rightarrow ^7F_4$ depend on the Judd-Ofelt parameters Ω_2 and Ω_4 respectively. The intensity of the emission 5D_0

$\rightarrow F_2$ and the value of the Ω_2 parameter depend on the short range effects such as covalency and structural changes in the vicinity of the Eu^{3+} ion. On the other hand the intensity of the emission transition ${}^5D_0 \rightarrow {}^7F_6$ and the value of Ω_6 parameter depend mainly on long range effects related to the bulk properties of the glasses.¹⁰⁴ Recent studies of Hirao *et al* in phosphate and borophosphate glasses doped with Eu^{3+} suggest that the **inhomogeneous** broadening of the emission lines can be systematized in terms of factors such as the presence of non bridged oxygens in the coordination sphere of the Eu^{3+} ion and the extent of polymerization in the glass **structure**.¹⁰⁶ The laser induced fluorescence line narrowing technique involving ${}^5D_0 \rightarrow {}^7F_0$ emission has been used to investigate the local structure and structural inhomogeneities of **glasses**.¹⁰²

Todoroki *et al* were the first to report a low intensity peak in the high energy side of the ${}^7F_0 \rightarrow {}^5D_2$ transition in the excitation spectra of Eu^{3+} ion and **identified** it as the phonon side **band**.¹⁰⁷ It arises due to excitation by incident light a transition corresponding to the sum of the energies of the ${}^7F_0 \rightarrow {}^5D_2$ transition and the excess energy of the vibrational mode characteristic of the **matrix**. The energy gap between the phonon side band and the pure electronic transition ${}^7F_0 \rightarrow {}^5D_2$ corresponds to the energy of one phonon, $\hbar\omega$ owing to the lattice vibration around the Eu^{3+} ion. The integrated intensity ratio of the phonon side band to the pure electronic transition ${}^7F_0 \rightarrow {}^5D_2$ corresponds to the electron phonon coupling strength, g . Todoroki *et al* have shown that the integrated emission intensity of the transitions from 5D_J ($J=3,2,1$) levels of Eu^{3+} decreases with increasing phonon energy, $\hbar\omega$.¹⁰⁸ Tanabe *et al* have observed that addition of $AlPO_4$ into fluoride glass host results in a systematic decrease in the integrated emission intensity of the transitions from 5D_J ($J=3,2,1$) levels of Eu^{3+} due to increase in the electron phonon coupling **strength**. Enhancement in the phonon energy and/or electron phonon coupling strength lead to higher **multiphonon** relaxation from 5D_J ($J=3,2,1$) levels to lower levels of Eu^{3+} .¹⁰⁹ Tanaka and Kushida have observed at 2 K three phonon side bands associated with ${}^7F_0 \rightarrow {}^5D_0$, ${}^7F_0 \rightarrow {}^5D_1$ and ${}^7F_0 \rightarrow {}^5D_2$ transitions of Eu^{3+} doped in calcium phosphate

Chapter 1

glass.¹¹⁰ The intensity of the phonon side band of ${}^7F_0 \rightarrow {}^5D_2$ transition is higher than the integrated intensities of the other two phonon side bands associated with ${}^7F_0 \rightarrow {}^5D_1$ and ${}^7F_0 \rightarrow {}^5D_0$ transitions. This is attributed to the J-mixing effect as originally suggested by **Stavola**.^{111,112} Support for assignments of phonon side bands is invariably derived from **infrared** and Raman spectra of the parent matrix. The phonon side bands involve the same infrared active intramolecular vibrational modes characteristic of the ligand groups in the parent matrix.

The Eu^{3*} ions also show spectral features characterized by energy transfer. As in the case of Sm^{3+} discussed earlier Eu^{3*} can act both as donor as well as acceptor. The energy transfer scheme is particularly useful in certain cases in discriminating the specific radiative transitions. For example, excited state absorption induced upconversion at 452 and 480 nm in Tm^{3+} doped ZBLAN fiber was observed for a single pump laser source at 650 nm. Codoping with Eu^{3+} increases the 452 nm emission while the 480 nm emission is reduced.⁴⁴ In glass hosts when Eu^{3+} is codoped with UO_2^{2+} , Bi^{3+} , Pb^{2+} , Mn^{2+} , Sm^{3+} or Tb^{3+} energy transfer occurs with Eu^{3+} ion acting as acceptor.^{46,95,113,114} On the other hand Eu^{3+} is known to act as donor when codoped with Nd^{3+} or Ho^{3+} ions in coordination complexes.¹¹⁵ Eu^{3+} activated phosphors as the red emitting component is used in color television tubes and blue emitting $\text{BaMgAl}_{10}\text{O}_{17}$ Eu^{2*} in present day luminescent lamps.⁶² Eu^{3*} is widely used as a luminescent probe in biological systems.¹¹⁶ Levy *et al* followed by McDonegh *et al* have shown that the optical spectroscopy of Eu^{3*} ion can be used as a probe to monitor the glass formation by sol-gel technique.¹¹⁷⁻¹¹⁹ They measured the decay time of 5D_0 level of Eu^{3*} ion at different stages of the sol-gel process and attributed the changes in the lifetimes to structural changes around the Eu^{3*} ion.¹¹⁹

Eu^{2*} is stabilized by using strong reducing atmosphere and/or reducing agents in the reaction mixture in the course of doping.¹²⁰ Optical transitions of Eu^{2*} ions have been investigated in many systems.^{62,93,120,121} The spectra of Eu^{2*} ions are generally due to parity allowed electric dipole transitions involving $4f^7$ and $4f^65d$ states which overlap

with the weak but sharp lines due to parity forbidden **intraconfigurational $4f^7 \rightarrow 4f^7$ transitions**. Because of their efficient luminescence **Eu²⁺** containing systems have been extensively studied for possible use as lamp phosphors and tunable solid state lasers.^{62,121} For **Eu²⁺** in some compositions, sharp emission lines due to the **$^6P_{7/2} \rightarrow ^8S_{7/2}$** transitions are observed next to **$4f^65d \rightarrow 4f^7$** broad emission. This can be the case when the lowest **$4f^65d$** level is at higher energy than the **$^6P_{7/2}$ level**. It is well established that the presence of sharp emission line in addition to broad emission band may appear resolved or overlap depending on the coordination number, covalency and crystal field strength at the **Eu²⁺ site**. The dependence of the position of **$4f^65d$** state on covalency is well brought out in the studies of **BaFCl:Eu²⁺** and **BaFBr:Eu²⁺**. In the more covalent **BaFBr:Eu²⁺**, the center of gravity of the **$4f^65d$** state is at lower energy and only a broad band emission is observed. In the less covalent **BaFCl:Eu²⁺** a sharp emission line also appears due to **$^6P_{7/2} \rightarrow ^8S_{7/2}$** of **Eu²⁺**.¹²¹ Studies on **Eu²⁺** doped in alkali borate, phosphate and aluminate glasses show that the position of the **$4f^65d \rightarrow 4f^7$** transition of **Eu²⁺** shifts to lower energy monotonically with increase in the theoretical optical basicity of the glass, irrespective of the glass systems.¹²⁰

1.2.7 Gadolinium(III)

Gd³⁺ ion has a half filled 4f shell with **$4f^7$ configuration**. The ground term, **$^8S_{7/2}$** is located quite deeply far below the excited states.⁵⁶ Consequently the absorption spectrum of **Gd³⁺** lies entirely in the ultraviolet region.^{26,27,56} Analysis of the intensities in the absorption spectrum of the **Gd³⁺** aquo ion was the subject of one of the early studies on this ion.⁵⁶ Though the absorption transitions of **Gd³⁺** ion lie principally in the ultraviolet region, accurate spectroscopic measurements became possible only with ultraviolet tunable lasers and/or x-ray excitation.^{26,27,93} The optical spectral studies reported so far are confined to crystalline systems.^{122,123} The emission transitions **$^6P_J \rightarrow ^8S$** occur over an energy gap (AE) of about **32,000 cm⁻¹**.^{122,123} Nonradiative transitions cannot compete with this radiative one because it occurs over such a large AE. Thus even water

molecules ($\nu=3,500\text{ cm}^{-1}$) do not quench the Gd^{3*} emission. The emission can only be quenched by transfer of energy to other luminescent centers.⁹³

In some host lattices such as GdF_3 emission has also been observed from the higher excited levels, $^6\text{I}_7$, $^6\text{D}_7$ and even $^6\text{G}_7$.^{93,122,123} In the case of borates and hydrates, all these emissions are quenched in favor of the $^6\text{P}_7$ emission.^{93,122,123} This is a clear demonstration that higher frequency vibrations promote the radiationless transitions to the $^6\text{P}_7$ levels. Cooperative vibronic emission transitions are reported for Gd^{3+} in $\text{NaLa}(\text{SO}_4)_2 \cdot \text{H}_2\text{O}$. They involve the electronic $^6\text{P}_{7/2} \rightarrow ^8\text{S}_{7/2}$ transition of the Gd^{3+} ion and the asymmetric valence vibrational levels of the SO_4^{2-} anion and the H_2O molecule both of which are coordinated to the Gd^{3*} ion.^{93,122,123}

Gd^{3*} ions are used in lamp phosphors and x-ray phosphors. In cases of lamp phosphor such as $(\text{Gd,Ce,Tb})\text{MgB}_5\text{O}_{11}$, Gd^{3+} ion plays an intermediary role. The excitation occurs in the Ce^{3*} ion which transfers its energy to the Gd^{3+} sub lattice. Energy migration over the Gd^{3+} ions transports the excitation energy to the Tb^{3*} activator. The $\text{Gd}^{3+}-\text{Tb}^{3+}$ energy transfer rate is $10^6-10^7\text{ sec}^{-1}$ which is much higher than the Gd^{3*} radiative rate ($10^2-10^3\text{ sec}^{-1}$).⁶²

Gd^{3+} ion is used as electron spin resonance probe to determine the local site symmetry of the lanthanide ion doped glass systems and in crystalline hosts such as zeolites.^{124,125} In glass systems such as soda-silica glass the lanthanide ion shows the presence of several sites with distribution in the crystal fields as evidenced by broad spectral profiles around g values 2.0, 4.0 and 6.0.¹²⁴

1.2.8 Terbium(III)

Tb^{3+} has the electronic configuration, $4f^8$ with $^7\text{F}_6$ ground state.⁵⁶ Carnall *et al* assigned the transitions for the terbium aquo ion absorption spectrum upto $40,000\text{ cm}^{-1}$.³⁵ The $4f-4f$ transitions with energy values higher than $36,000\text{ cm}^{-1}$ are

superimposed by more intense and broad bands centered at $\sim 38,000$ and $46,000 \text{ cm}^{-1}$ resulting from 4f-5d transitions.⁵⁶ The intensities and positions of these two 4f-5d transitions are strongly influenced by the symmetry at the metal ion site and the nature of bonding with the coordinating ligands and thus enable characterization of the host.¹²⁶ The overlap between the above mentioned transitions however renders a correct analysis of the intensities of the Tb^{3+} absorption spectra difficult.

The Tb^{3+} ion gives fairly intense fluorescence in the ultraviolet and visible region. Emission lines of Tb^{3+} ion under ultraviolet excitation occur in two regions, one centered around 550 nm (green) and the other in the high energy region centered around 440 nm (blue). For some host matrices, only the low energy emission lines are observed whereas for certain other host matrices intense emission lines occur both in the low energy as well as in the high energy regions. The above two groups of emission lines originate from two different levels and their relative integrated emission intensities give insight about cluster formation of the guest ion.¹²⁷ The emission transition occurring around 545 nm corresponding to the transition $^5\text{D}_4 \rightarrow ^7\text{F}_6$ is hypersensitive.⁴⁰⁻⁴³

Recently Atkins and Carter have reported that the Tb^{3+} doped phosphosilicate and germanosilicate optical fibers show the permanent photo darkening effect when they are exposed to 488 nm Ar^+ laser light corresponding to $^7\text{F}_6 \rightarrow ^5\text{D}_4$ transition of Tb^{3+} .⁵³ The photo darkening effect is a three photon process and involves the sequential two photon absorption for reaching the $4f^75d$ level of Tb^{3+} ion and a third photon for carrying out the photo ionization step, leading to the removal of the 5d electron to form Tb^{4+} . The sensitivity of the three photon process to 488 nm light raises the possibility of realizing side writing refractive index gratings in silica based optical fibers with the above wavelength.

The Tb^{3+} ions act as an efficient sensitizer in solution, crystalline and glassy host matrices when codoped with Ce^{3+} , Pr^{3+} , Sm^{3+} , Eu^{3+} or Er^{3+} ions.^{59,60,86,96,113,128,129} It also

Chapter 1

provides a convenient platform for the study of ion-ion interactions in different matrices. All studies of energy transfer between Tb^{3+} and other Ln^{3+} ions so far studied suggest that the interactions between the ions is dipole-dipole in nature.

Tb^{3+} doped crystalline borate, $\text{GdMgB}_5\text{O}_{11}$ is used as green emitting lamp phosphor and other hosts such as GaTaO_4 , Gd_2SiO_5 and $\text{Gd}_3\text{Ga}_5\text{O}_{12}$ doped with Tb^{3+} ions are used as x-ray storage phosphors.^{62,93} Tb^{3+} is widely used as a fluorescent probe in the study of biological systems. For instance in biological substrates such as yeast tRNA the magnesium ions are effectively replaced by Tb^{3+} ions as evidenced by the emission intensity of the hypersensitive transition ${}^5\text{D}_4 \rightarrow {}^7\text{F}_6$ of Tb^{3+} ion.^{116,40-43} The high sensitivity of this intense hypersensitive transition of Tb^{3+} ions to its interactions with biological substrates seem to be a promising tool in the study of the binding stoichiometries and of the resulting conformational changes.

1.2.9 Dysprosium(III)

Dy^{3+} has the electronic configuration, $4f^9$ with ${}^6\text{H}_{15/2}$ ground state.⁵⁶ It gives rise to a large number of absorption and emission lines in the ultraviolet to near infrared region ranging from 300 nm to 3000 nm. The ${}^6\text{H}_{15/2} \rightarrow {}^6\text{F}_{11/2}$ transition occurring at 1285 nm in the absorption spectrum is hypersensitive.^{40,43} Absorption spectral studies have been reported for a number carboxylato and amino acid complexes.^{56,130,131} Both absorption and emission spectral studies have been reported for Dy^{3+} doped crystalline hosts such as $\text{KY}_x\text{Dy}_{1-x}(\text{MoO}_4)_2$ and glass systems.¹³²⁻¹³⁴ The Judd-Ofelt model works well for this ion as in the cases of Nd^{3+} and Sm^{3+} ions on account of the large number of transitions easily observed in their absorption spectra. Recently Cases *et al* have reported the optical properties of Dy^{3+} in fluoride glasses.¹³³ Based on the Judd-Ofelt parameters, these authors conclude that the bonding between Dy^{3+} ion and the ligand anions is more ionic in the fluorozincate glasses than in fluorozirconate glasses

Dy^{3+} ions show reasonably intense fluorescence at 575 nm (yellow) and at 485 nm (blue) corresponding to the transitions ${}^4\text{F}_{9/2} \rightarrow {}^6\text{H}_{13/2}$ and ${}^4\text{F}_{9/2} \rightarrow {}^6\text{H}_{15/2}$ respectively. The integrated emission intensity ratio of these two transitions (Y/B ratio) is a sensitive function of covalency and ligand asymmetry around the rare earth ion in the host.¹⁰³ The yellow line is hypersensitive.⁴⁰⁻⁴³ The influence of symmetry and electronegativity of the ligand atoms on the intensity of the yellow line is thus greater than on the blue line. The site symmetry due to coordination and the nature of the metal ligand bonding significantly influence the Y/B ratio and shows a trend similar to that on R/O ratio of Eu^{3+} discussed earlier.¹⁰⁴ Thus by suitably varying the site symmetry and the ligands in a systematic manner the yellow to blue intensity ratio (Y/B) may be suitably altered in order that Dy^{3+} emits white light.¹⁰³ Thus luminescent materials doped with Dy^{3+} in suitable matrices are potential two primary color phosphors. Further the Y/B ratio can also be influenced by the presence of a suitable sensitizer such as UO_2^{2+} which brings about the overlap of absorption transition of the donor UO_2^{2+} and emission transition of Dy^{3+} ion appearing as white light. Such materials find applications in thermo luminescent dosimetry.¹³⁵

While the other rare earth ions can be potential for laser applications in the visible and/or near infrared region, recent works show that Dy^{3+} ions doped materials could be invaluable for laser in the 3 urn wavelength region.¹³² This becomes possible using the ${}^6\text{H}_{13/2} \rightarrow {}^6\text{H}_{15/2}$ transition. In order to realize the most suitable host for the Dy^{3+} ion the search for the spectroscopic behavior of the ion in various hosts needs further studies.

Recently Wei *et al* have investigated the spectral characteristics of Dy^{3+} doped chalcogenide glasses and their suitability for 1.3 urn fiber optical amplifier applications.¹³⁶ These glasses exhibit high refractive indices and very low phonon energy maxima. These characteristics enable observation of the emission transitions ${}^6\text{H}_{9/2}$, ${}^6\text{F}_{11/2} \rightarrow {}^6\text{H}_{15/2}$, ${}^6\text{H}_{11/2} \rightarrow {}^6\text{H}_{15/2}$ and ${}^6\text{H}_{13/2} \rightarrow {}^6\text{H}_{15/2}$ at 1.3, 1.8, 2.9 urn respectively. The emission intensities of Dy^{3+} ion are generally much less compared to the intensities of the emission

Chapter 1

lines of many other lanthanides and consequently the observation in chalcogenide glasses assume **significance**. In general the above characteristics of the parent **matrices** lead to a large stimulated emission cross section of potential lasing transitions and low nonradiative decay.

1.2.10 Holmium(III)

Ho^{3*} has the electronic configuration, $4f^{10}$ with $^5\text{I}_8$ ground state.^{26,56} It gives a large number of well resolved absorption and emission transitions in the ultraviolet, visible and near infrared region. Thus for absorption spectral calibration it is even recommended as a standard. The initial studies reported on the optical properties of trivalent holmium pertain to Ho^{3*} ions doped in crystalline hosts such as LaF_3 , YAlO_3 and $\text{KNO}_3 + \text{LiNO}_3$ melt and borate, phosphate and tellurite glasses^{26,27,40} The Judd-Olfelt model works well for this ion as in the cases of Nd^{3+} , Sm^{3+} and Dy^{3+} ions. The two transitions of Ho^{3*} in the absorption spectra viz., $^5\text{I}_8 \rightarrow ^5\text{G}_6$ and $^5\text{I}_8 \rightarrow ^5\text{H}_6$ are **hypersensitive**.⁴⁰⁻⁴³ The former is governed by the quadrupole selection rules ($\Delta S = 0$, ΔL , $\Delta J < 2$) Weak visible fluorescence of Ho^{3*} has been observed in phosphate glasses from $^5\text{S}_2$, $^5\text{F}_4$ and $^5\text{F}_3$ levels to the terminal $^5\text{I}_8$ level.⁴⁰ The intensities of the above fluorescence transitions are higher by two orders of magnitude in the tellurite glass because of the favorable low phonon energy maximum characteristic of the tellurite glass.⁴⁰ Many of the emission transitions of Ho^{3*} are lasing transitions in crystals but only one laser transition has been identified in glass hosts, viz., $^5\text{I}_7 \rightarrow ^5\text{I}_8$.³ Stimulation of $^5\text{I}_7 \rightarrow ^5\text{I}_8$ transition of Ho^{3*} at about 2.0 μm has received considerable attention in the past because efficient optical pumping is possible by codoping with ions such as Er^{3*} , Tm^{3*} and Yb^{3+} .¹³⁷ Stimulated emission in Ho^{3*} was first reported in singly doped $\text{Ho}^{3+}:\text{CaWO}_4$ at 77 K.⁴⁰ Observation of energy transfer between Er^{3+} - Ho^{3+} led to the first report of efficient continuous wave operation at 77 K in Ho^{3*} doped yttrium aluminum **garnet**.⁴⁰ Ho^{3*} lasing action assisted by energy transfer has been reported in glass and yttrium iron **garnet**.⁴⁰ Low threshold, room temperature Ho^{3*} continuous wave operation in multiple

sensitized hosts has been reported in $\text{Ca}_2\text{Er}_3\text{F}_{19}$ and yttrium aluminum garnet and such hosts containing several rare earths in varied proportions are commonly referred to as "alphabet materials".⁴⁰

Optical transitions of Ho^{3+} in fluorozirconate glasses have been well characterized and lasing has been observed for the transition $^5\text{I}_7 \rightarrow ^5\text{I}_8$ in this glass.³ Continuous wave operation of Ho^{3+} doped fluorozirconate fiber laser emitting at 2.9 μm corresponding to the transition $^5\text{I}_6 \rightarrow ^5\text{I}_7$ is based on the depletion of the lower laser level, $^5\text{I}_7$ by excited state absorption of the appropriately selected pump wavelengths. This additional absorption process limits the efficiency of this laser transition. This can however be overcome by codoping Ho^{3+} with suitable another rare earth element such as Pr^{3+} or Eu^{3+} .

The conversion of long wave into short wave radiation by multiphonon mechanisms is known as upconversion. In the upconversion process energies of absorbed photons are added into the energy level scheme of a rare earth ion by excited state absorption or by energy transfer. This results in a more efficient process of populating the higher excited state than can be accomplished by one photon absorption. Subsequent emission from the higher excited state yields photons with higher energy than the energy of the absorbed photons.^{108,109} Upconversion was extensively studied in particular in the late sixties and early seventies. Afterwards the interest in upconversion diminished because of the lack of practical applications and suitable excitation means in the infrared region. However, the recent demand for compact, efficient and reliable laser devices that operate in the blue to green spectral region for use in optical data storage, color displays, laser printing, barcode reading, etc. and the availability of powerful laser diodes have led to a renewed interest in upconversion. This phenomenon is of great value as it permits building up a new laser system. In the case of Ho^{3+} excitation by ca. 645 nm leads to absorption by the ground state as well as the excited states, $^1\text{I}_6$ and $^5\text{I}_7$, all the three processes leading to significant enhancement of the population and upconverted

fluorescence from 5F_4 , 5S_2 levels to ground state at 545 nm. The above described upconversion fluorescence at room temperature in a Ho^{3+} doped glass system was first reported in a tellurite glass matrix.¹³⁹ Upconversion in Ho^{3+} can be sensitized by codoping with Yb^{3+} ions.¹³⁷

1.2.11 Erbium(III)

Er^{3+} ion has the electronic configuration, $4f^{11}$ with $^4I_{15/2}$ ground state.⁵⁶ It gives rise to a large number of absorption and emission transitions in the ultraviolet, visible and near infrared region. Reisfeld *et al* were the first to report detailed absorption and emission spectral studies of Er^{3+} ion in borate, phosphate, germanate and tellurite glasses.^{26,27,40} The transitions $^4I_{15/2} \rightarrow ^2H_{11/2}$ and $^4I_{15/2} \rightarrow ^4G_{11/2}$ of Er^{3+} in the absorption spectra are hypersensitive and their intensities are greatly influenced by the host matrices.⁴⁰⁻⁴³ The dopant concentration dependence of lifetime of $^4S_{3/2}$ level for Er^{3+} in these glasses has also been reported.⁴⁰ The lifetime decreases with increasing concentration of the active ion due to cross relaxation involving the levels $^4G_{11/2}$, $^4I_{15/2} \rightarrow ^4F_{7/2}$, $^4I_{13/2}$ and $^2H_{11/2}$, $^4S_{3/2}$, $^4I_{15/2} \rightarrow ^4I_{9/2}$, $^4I_{13/2}$. The fluorescent quantum efficiency in tellurite glass is much higher than in germanate glass.⁴⁰ No fluorescence could be observed for Er^{3+} doped borate glasses even at low temperatures.⁴⁰ However very weak fluorescence was obtained in phosphate glasses.⁴⁰ The emission transitions, $^2H_{11/2} \rightarrow ^4I_{15/2}$ and $^4S_{3/2} \rightarrow ^4I_{15/2}$ of Er^{3+} in tellurite glass exhibit thermalization effects.⁴⁰

Many laser transitions have been identified for Er^{3+} ion in crystalline hosts over a wide region.^{3,26} Laser action at 1.663 μm involving the transition from $^4S_{3/2} \rightarrow ^4I_{9/2}$ level has been observed for Er^{3+} doped $YAlO_3$ single crystals.^{26,27,40} Laser action occurs for the transition $^4I_{13/2} \rightarrow ^4I_{15/2}$ of Er^{3+} ion in silicate, phosphate and fluorozirconate glasses at about 1.6 μm .³ Erbium is an attractive candidate for pulsed solid state lasers at 1.54 μm , and this falls well within the "eye-safe" region.^{26,40} However, since erbium has only weak pumping bands, it is necessary to assist the pumping by resonant transfer donors such as

Yb³⁺,^{26,40,46} Four level lasing involving $^4S_{3/2} \rightarrow ^4I_{13/2}$ transition has been reported for **Er³⁺** at ambient temperatures in several hosts including **YAlO₃**.^{26,40} This transition is of interest because of the existence of sensitive photo detection at around 850 nm where the second harmonic of the above transition **occurs**. Continuous wave operation of **Er³⁺** doped fluorozirconate glass fiber laser emitting at 2.7 **μm** corresponding to the transition, $I_{11/2} \rightarrow I_{13/2}$ is based on the depletion of the lower level by excited state absorption of the appropriate pump **wavelength**. The additional absorption process limits the efficiency of this laser transition and as in the case of Ho³⁺ can be avoided by codoping with **Pr³⁺**.

It is now well established that fibers made of doped germanosilicate glasses can efficiently generate second harmonic signals from **infrared** and visible laser radiation, owing to a photo induced χ^2 grating written in the fiber core by means of a preparation process involving exposure for long duration. The phenomenon is however not fully understood. The preparation can be reduced to a few minutes by the injection of a second harmonic light seed in addition to the fundamental pump radiation. It was initially believed that defects associated with **GeO₂** in the fiber core were the major factor in the efficiency of the second harmonic generation process in germanosilicate fibers. However, it was subsequently shown that not only the **GeO₂** defects but the rare earth and tantalum as dopants also strongly affect the infrared second harmonic generation efficiency in silica based optical fibers. Recently, the generation of a two photon resonant photo induced second harmonic signal at 660 nm in **Er³⁺** doped **GeO₂-Al₂O₃-SiO₂** single mode optical fibers pumped by a **Nd³⁺**:YAG laser at 1.319 **μm** has been **reported**. Defect states in the band gap are thus optically excited through a resonant two photon absorption process connecting the energy levels $^4I_{15/2}$ and $^4F_{9/2}$ of the erbium ions in the fiber **core**. As a result a periodic χ^2 grating is formed, and efficient second harmonic generation takes **place**. For **Er³⁺** free **GeO₂** doped silica test fibers no such second harmonic signal has been detected, even after hours of seeded preparation process^{29,45,55}

Chapter 1

Recently, much attention has been given to the development of 1.5 μm optical amplifiers for long distance communication **systems**.^{140,141} Glass fiber amplifiers with low Er^{3+} ion concentrations have been demonstrated to be quite efficient for the above **application**.¹⁴² Parallel to the development of a fiber amplifier having a length of several meters, there is a strong interest in developing planar waveguide amplifiers with small dimensions of around a few **centimeters**.¹⁴¹ These have potential applications in optical telecommunication and signal processing systems as integrated **devices**.¹⁴¹ For such amplifiers a high Er^{3+} concentration and a high pump power density are needed to obtain sufficient optical amplification gains because the optical interaction path is shorter. At high Er^{3+} concentration, however, the luminescence will be quenched by energy transfer processes due to ion-ion interactions and besides, another cooperative upconversion process occurs due to simultaneous application of high pump power. These two luminescence quenching processes strongly influence the amplifier **efficiency**.¹⁴⁰⁻¹⁴³

Er^{3+} doped phosphate glasses have proved to be optical glasses with good homogeneity and the laser transition $^4\text{I}_{13/2} \rightarrow ^4\text{I}_{15/2}$ around 1.5 μm is being used for laser action with the bulk glasses as the host **matrix**.¹⁴¹ The conventionally prepared phosphate glasses contain residual hydroxyl groups which are serious quenchers for the lasing **transition**. It has been demonstrated that the heat treatment performed on the as melted phosphate glass samples enhances the luminescence efficiency at 1.5 μm . The photo luminescence lifetime of Er^{3+} ions for the $^4\text{I}_{13/2} \rightarrow ^4\text{I}_{15/2}$ transition increases substantially, typically from 3 msec upto 7 msec for a sample doped with 2.0 mol % Er_2O_3 due to the heat treatment. The increase of the lifetime was ascribed to a decrease in concentration of hydroxyl groups incorporated in the glass. The photo luminescence peak intensity also increases on careful drying by a factor of 3 to 7 depending upon the glass **composition**.¹⁴¹

Recently Tanabe *et al* have reported that the upconversion properties of Er^{3+} ions in fluorophosphate glasses with the use of the infrared radiation from a (Ga, Al)As laser diode ($\lambda = 802 \text{ nm}$) as an excitation **source**.¹⁴⁴ They have observed green upconversion

fluorescence due to the $^4S_{3/2} \rightarrow ^4I_{15/2}$ transition of Er^{3+} in fluoride glasses. The upconversion fluorescence intensity decreased drastically with increasing AlPO_4 content. This is attributed to the enhanced nonradiative decay of $^4S_{3/2}$ level to the lower levels of Er^{3+} ion due to the presence of P-O stretching vibrations.¹⁴⁴

1.2.12 Thulium(III)

The electronic configuration of Tm^{3+} is $4f^{12}$ and is characterized by the same states as the $4f$ configuration of Pr^{3+} .^{26,56} However, according to Hund's rule the levels of ground multiplet are reversed and the lowest lying level is 3H_6 . Both in solutions and crystals the transitions from the ground level to all excited levels except for the highest 1S_0 have been observed in the absorption spectra of Tm^{3+} .^{26,56} A thorough theoretical analysis of the absorption spectrum for Tm^{3+} in crystal matrices of LaF_3 with allowance for electric and magnetic interactions of the higher orders has been carried out by Carnall *et al.*¹⁴⁵ The $^3H_6 \rightarrow ^3F_4$ transition is hypersensitive.⁴⁰⁻⁴³

The optical properties of Tm^{3+} ion in borate, phosphate, germanate and tellurite glasses have been reported.⁴⁰ The oscillator strengths of Tm^{3+} in tellurite, borate and phosphate are higher than in germanate glasses.⁴⁰ Since most of the transitions are of electric dipole nature, these results imply that the non symmetric component of the electric field acting on the rare earth in the tellurite, borate and phosphate glasses is stronger than in germanate glasses.⁴⁰⁻⁴³ Fluorescence has been observed from 1D_2 and 1G_4 levels of Tm^{3+} in all the above glasses.⁴⁰ Temperature dependence studies of visible fluorescence of Tm^{3+} ion in all the above glasses have also been investigated.⁴⁰

The lasing action has been found for the transitions $^3F_4 \rightarrow ^3H_5$ and $^1D_2 \rightarrow ^3H_4$ at 2.35 and 0.45 μm respectively in crystals and $^3H_4 \rightarrow ^3H_6$ at 1.95 μm in glasses for Tm^{3+} ion.^{3,26} Sanz *et al* have reported the optical properties of Tm^{3+} ion in fluorozirconate glasses.¹⁴⁶ Carter *et al* have reported laser studies of Tm^{3+} doped in fluorozirconate fibers.¹⁴⁷ Pumping of thulium doped fluorozirconate fiber lasers at wavelengths available from semiconductor diodes around 790 nm has enabled continuous laser operation at

Chapter 1

806 nm, 1.47 μm , 1.97 μm and 2.3 μm corresponding to the transitions $^3\text{F}_4 \rightarrow ^3\text{H}_6$, $^3\text{F}_4 \rightarrow ^3\text{H}_4$, $^3\text{H}_4 \rightarrow ^3\text{H}_6$ and $^3\text{F}_4 \rightarrow ^3\text{H}_5$ respectively. Many of these transitions may occur simultaneously. Output powers of 200 mW and a slope efficiency of 15 % have been obtained for a pump power of 2 W at 0.78 μm . In addition, continuous tunability of this laser from 2.20 to 2.46 μm is obtained.

Upconversion of red light into blue light in Tm^{3+} doped halide and oxide glasses has been investigated by many workers. Recently Oomen has done a detailed study of upconversion in Tm^{3+} doped fluorozirconate glasses.¹⁴⁸ Upconversion in Tm^{3+} involves excitation by red light with a wavelength of about 650 nm leading to emission of blue light of two wavelengths at 450 and 475 nm, corresponding to the $^1\text{D}_2 \rightarrow ^3\text{H}_4$ and the $^1\text{G}_4 \rightarrow ^3\text{H}_6$ transitions respectively. The emission intensities of both bands vary quadratically with the excitation power. The upconversion mechanisms for these bands are elucidated from the results of the emission and excitation spectra and decay time measurements of Tm^{3+} doped with varying concentrations in fluoride glasses. The upconversion efficiency can be improved by codoping with other rare earth ions such as Pr^{3+} and Eu^{3+} which act as sensitizers^{44,138}

1.2.13 Ytterbium(III)

The energy level scheme for Yb^{3+} with electronic configuration $4f^{13}$ is similar to that for Ce^{3+} ion having electronic configuration $4f^1$. The ground state of Yb^{3+} is $^2\text{F}_{7/2}$. This level is separated from the $^2\text{F}_{5/2}$ excited state by as much as $10,300 \text{ cm}^{-1}$ and the corresponding transition can be observed both in absorption and emission spectra.^{26,56} In the solution media the absorption spectra of Yb^{3+} has been examined in deuterated perchloric acid and ethylacetate and in molten $\text{LiNO}_3\text{-KNO}_3$.^{56,92} The only absorption transition observed for this ion in these media corresponds to the weak magnetic dipole transition, $^2\text{F}_{7/2} \rightarrow ^2\text{F}_{5/2}$ with oscillator strength of the order $(2-8) \times 10^{-7}$.⁵⁶ Yb^{3+} ion has been used as sensitizer to improve the laser efficiency and/or upconversion efficiency of Er^{3+} , Ho^{3+} and Tm^{3+} ions by energy transfer.^{137,149,150}

References

- 1] A Wong and C A Angel, *Glass: Structure by Spectroscopy* (Marcel Dekker, New York, 1976)
2. I. Fanderlik, *Optical Properties of Glass 5* (Elsevier, New York, 1983)
- 3 G Fuxi, *Optical and Spectroscopic Properties of Glass* (Springer-Verlag, New York, 1992)
4. W.H Zachariasen, *J. Am. Chem. Soc.* **54** (1932) 3841.
5. J. Krogh-Moe, *J. Non-Cryst. Solids* **1** (1969) 269.
6. J.E. Stanworth, *Nature* **169** (1952) 581.
- 7 P.L Higby and I.D Aggarwal, *J. Non-Cryst. Solids* **163** (1993) 303.
- 8 J.T Kohli and J.E Shelby, *Phys. Chem. Glasses* **32** (1991) 67
- 9 M.S Spess and J.E. Shelby, *Phys. Chem. Glasses* **33** (1992) 87.
- 10 J.E Shelby, S.M. Minton, C.E Lord and M.R Tuzzolo, *Phys. Chem. Glasser* **33** (1992)93.
- 11 J A Ruller and J.E. Shelby, *Phys. Chem. Glasses* **33** (1992) 177.
12. R.M. Almeida, *Handbook on the Physics and Chemistry of Rare Earths*, (Eds.) K.A. Gschneidner and L. Eyring, **15** (North-Holland, New York, 1991) 287.
- 13 A.K. Bhatnagar and R. Jagannathan, *Metallic Glasses* (Ed.) T. Anantharaman (Trans Tech Publications, Switzerland, 1984) 89
14. W. Klement, R.H. Willens and P. Duwez, *Nature* **187** (1960) 869.
- 15 B.E Yoldas, *J. Mater. Sci.* **10** (1975) 1856.
16. F. Pancrazi, J. Phalippou, F. Sorrentino and J. Zarzycki, *J. Non-Cryst. Solids* **63** (1984)81.
- 17 C.J. Brinker and GW. Scherer, *Sol-Gel Science* (Academic Press, California, 1990).
18. V.S. Nagarajan and K.J. Rao, *Philosophical Magazine A* **65** (1992) 771.
19. D.S. Wang and C.G. Pantano, *J. Non-Cryst. Solids* **142** (1992) 225.
- 20 S. Roy and D Ganguli, *J. Non-Cryst. Solids* **151** (1992) 203.
21. I.M Thomas, S.A Payne and G.D. Wilke, *J. Non-Cryst. Solids* **151** (1992) 183

Chapter 1

22. L. Montagne and G. Palavit, *J. Non-Cryst. Solids* 155 (1993) **115**.
23. J. **Gopalakrishnan**, *Chem. Mater.* 7 (1995) 1265.
24. T.K. Kundu and D. Chakravorty, *Appl. Phys. Lett.* 67 (1995) 2732.
25. A. Paul, *Phy. Chem. Glasses* 17 (1976) 7.
- 26** R. Reisfeld and C.K. Jorgensen, *Lasers and Excited States of Rare Earths* (**Springer-Verlag**, New York, 1977).
27. R. Reisfeld and C.K. Jorgensen, *Hand Book on the Physics and Chemistry of Rare Earths*, (Eds.) K.A. Gschneidner and L. Eyring, 9 (North-Holland, New York, 1987) chap. 58.
28. J. Wang, L. Reekie, W.S. Brocklesby, Y.T. Chow and D N. Payne, *J. Non-Cryst. Solids* 180 (1995) 207.
- 29 J.M. Hickmann, E A. **Gouveia**, A.S. Gouveia-Neto, D.C Dini, and S Celaschi, *Opt. Lett* 20(1995)1692.
- 30** EM. **Vogel**, M.J. Weber and DM. **Krol**, *Phy. Chem. Glasses* 32 (1991) **231**.
31. K. **Shioya**, T. **Komatsu**, H.G. Kim, R. Sato and K. **Matusita**, *J. Non-Cryst. Solids* 189(1995) 16.
- 32** H. Nasu, K. Kurachi, A. Mito, H. **Okamoto**, J. Matsuoka and **K Kamiya**, *J. Non-Cryst. Solids* 181 (1995) 83.
- 33** F.A. Cotton and G. Wilkinson, *Advanced Inorganic Chemistry* (A **Wiley**-interscience Publication, New York, 1988) **960**
34. B.G. **Wybourne**, *Spectroscopic Properties of Rare Earths* (Interscience Publishers, New York, 1965).
- 35** W.T. **Carnall**, *Arogonne National Laboratory Report (1978)* ANL-78-XX-95
36. W.T. Carnall, PR. Fields and K. Rajnak, *J. Chem. Phys.* 49 (1968) **4424**
37. W.T. Carnall, PR. Fields and **K** Rajnak, *J. Chem. Phys.* 49 (1968) 4412.
- 38** B.R. Judd, *Phys. Rev.* 127 (1962) 750.
- 39** G S. **Ofelt**, *J. Chem. Phys.* 37 (**1962**) **511**
- 40** R. Reisfeld, *Structure and Bonding* 22 (**Springer-Verlag**, New York, 1975) 123 and **refs** therein.

- 41 D.E Henrie, R L. Fellows and G.R Choppin, *Coord. Chem. Rev.* 18 (1976) 199
- 42 R.D Peacock, *Structure and Bonding* 22 (Springer-Verlag, New York, 1975) 83
- 43 W.D Horrocks, Jr and M Albin, *Prog. Inorg. Chem.* 31 (An Interscience Publication, New York, 1984) 1.
- 44 G Tohmon, H Sato, J Ohya and T Fujita, *J. Appl. Phys.* 73 (1993) 1528.
- 45 E.M Dianov, L.S Kornienko, V.I Stupina and P.V Chernov, *Opt. Lett* 20 (1995) 1253.
- 46 R Reisfeld, *Structure and Bonding* 30 (Springer-Verlag, New York, 1976) 65 and refs therein
- 47 M.P Le Flohic, J Y Allain, G.M. Stephan, G Maze, *Opt. Lett.* 19 (1994) 1982.
- 48 J E Roman, M Hempstead, C Ye and S. Nouth, *App. Phys. Lett.* 67 (1995) 470
- 49 Y. Zhao, *Opt. Lett.* 20 (1995) 566.
- 50 K Wei, D.P Machewirth, J. Wenzel, E Snitzer and G.H Sigel, Jr *Opt. Lett.* 19 (1994)904.
- 51 D R Simons, A J. Faber and D de Waal, *Opt. Lett.* 20 (1995) 468
- 52 Y. Ohishi, M Yamada, A Mori, T. Kanamori, M. Shimizu and S Sudo, *Opt. Lett.* 20(1995)382.
- 53 G R Atkins and A.L.G. Carter, *Opt. Lett.* 19 (1994) 874
- 54 (a) K Hirao, S. Todoroki, D.H Cho and N.Soga, *Opt. Lett.* 18 (1993) 1586, (b) A. Kurita, T. Kushida, T Izumitani and M. Matsukawa, *Opt. Lett.* 19 (1994) 314
- 55 J.M Hickmann, E.A Gouveia, A.S. Gouveia-Neto, D.C Dini, and S Celaschi, *Opt. Lett.* 19(1994) 1726.
- 56 K.B Yatsimirskii and N.K. Davidenko, *Coord. Chem. Rev.* 11 (1979) 223 and refs therein
- 57 G.E. Malashkevich, E.N Poddenezhny, I.M Melnichenko and A.A Boiko, *J. Non-Cryst. Solids* 188 (1995) 107.
- 58 G Blasse, *J. Lumin.* 60 & 61 (1994) 930.
- 59 R. Reisfeld and J Hormadaly, *J. Solid State Chem.* 13 (1975) 283.

60. Q. Changhong and G. **Fuxi**, *J. Lumin.* 31 & 32 (1984) **339**
61. S. Taniguchi, N. **Takeuchi**, Y. Fukuda and H. Ohtaki, *J. Meter. Sci. Lett.* 12 (1993) 268.
62. G. Blasse, *J. Alloys Compds.* 192 (1993) 17.
63. J.D. Barrie, L.A. **Momoda**, B. **Dunn**, D. Gourier, **G** Aka and **D** Vivien, *J. Solid State Chem.* 86(1990)94.
64. M. Galczynnski and **W** Strek, *J. Phys. Chem. Solids* 52 (1991) **681**
65. M. Galczynnski, **M** Blazej and **W** Strek, *Mat. Chem. Phys.* 31 (1992) 175.
66. W. Strek, **J** Sztucki, presentd at **9th Int Conf on Luminescence and Optical Spectroscopy of Condenced Matter**, (Storrs, Connecticut, USA, August 1993)
67. C. de **Mello Donega** and **G** Blasse, *Chem. Phys. Lett.* 183 (1991) 367.
68. C. de Mello **Donega**, **A** Ellens, **A** Meijerink and **G** Blasse, *J. Phys. Chem. Solids* 54 (1993) 293.
69. **C** de Mello Donega, H. **Lambaerts**, **A**. Meijerink and **G** Blasse, *J. Phys. Chem. Solids* 54 (1993) **873**
70. C. de Mello Donega, M.J.D. Crombag, **A**. Meijerink and **G** Blasse, *J. Lumin.* 60 & 61 (1994) 74.
71. **A**. Meijerink, **C** de Mello **Donega**, **A** Ellens, **J** **Sysma** and **G** Blasse, *J. Lumin.* 58 (1994) 26
72. C. de Mello Donega, **A**. Meijerink and **G** Blasse, *J. Lumin.* 62 (1994) **189**
73. **M** Malinowski, **R** Wolski and W. Wolinski, *Solid State Commun.* 74 (1990) 17
74. **S.T.**Lai, **S** Huang and W M. Yen, *Phys. Rev. B* 26 (1982) **2349**
75. J L. Adam and W. A. Sibley, *J. Non-Cryst. Solids* 76 (1985) 267.
76. M. **Eyal**, E. Greenberg and R. Reisfeld, *Chem. Phys. Lett.* **117**(1985) 108.
77. A.B. Arauzo, R. Cases and R. Alcala, *Phys. Chem. Glasses* 35 (1994) 202.
78. **M.A.** Bunel, R. Cases, MA. **Chamarro** and R. Alcala, *Phys. Chem. Glasses* 33 (1992) 16.

- 79 **W Streck**, **C Szafranski**, **P Deren**, **K Jablonski** and **B Jezowska-Trzebiaatowska**, *Rare Earth Spectroscopy* (Eds.) **B Jezowska-Trzebiaatowska**, **J Legendziewicz** and **W. Streck** (World **Scientific**, Philadelphia, 1985) 340.
- 80 **C de Mello Donega**, **A Meijerink** and **G Blasse**, *J. Phys. Chem. Solids* **56** (1995) 673.
- 81 **R.C. Naik**, **N.P. Karanjikar** and **MAN. Razvi**, *J. Lumin.* **54** (1992) 139.
- 82 **Z Mazurak**, **E Lukowiak**, **B Jezowska-Trzebiaatowska**, **D Schultze** and **Ch Waligora**, *J. Phys. Chem. Solids* **45** (1984) 487.
- 83 **D J Zalucha**, **J C Wright** and **F.K Fong**, *J. Chem. Phys.* **59** (1973) **997**
- 84 **O.L. Malta**, **E Antic-Fidancev**, **M Lemaitre-Blaise**, **J Dexpert-Ghys** and **B Piriou**, *Chem. Phys. Lett.* **129** (1986) 557.
- 85 **S.C Goh**, **R Pattie**, **C. Byrne** and **D. Coulson**, *Appl. Phys. Lett.* **67** (1995) **768**
- 86 **H.C. Kandpal**, **A K Agarwal** and **H B Tripathi**, *Ind. J. Pure & Appl. Phys.* **17** (1979) 583.
- 87 **B.C. Joshi** and **M C Joshi**, *J. Non-Cryst. Solids* **142** (1992) 171.
- 88 **B.C. Joshi**, **M C Joshi** and **B.D. Joshi**, *J. Phys. Chem. Solids* **52** (1991) 939.
- 89 **D.R Simons**, **A.J. Faber** and **H de Waal**, *J. Non-Cryst. Solids* **185** (1995) **283**
- 90 **K Wei**, **DP. Machewirth**, **J. Wenzel**, **E Snitzer** and **G.H Sigel Jr.**, *J. Non-Cryst. Solids* **182** (1995) 257.
- 91 **K Arai**, **H. Namikawa**, **K. Kumata** and **T. Honda**, *J. Appl. Phys.* **59** (1986) 3430.
- 92 **W T Carnall**, **J.P Hessler** and **F Wagner Jr.**, *J. Phys. Chem.* **82** (1978) **2152**
- 93 **G Blasse**, *Advances in Inorganic Chemistry* **35** (Academic Press, New York, 1990)319.
- 94 **V D Rodriguez**, **I.R Martin**, **R Alcala** and **R. Cases**, *J. Lumin.* **54** (1992) **231**.
- 95 **R Reisfeld** and **L Boehm**, *J. Solid State Chem.* **4** (1972) 417.
- 96 **H.C. Kandpal** and **K C Joshi**, *J. Phys. Chem. Solids* **49** (1988) 555.
97. **A.K. Agarwal**, **N.C. Lohani**, **T.C. Pant** and **K.C Pant**, *J. Solid State Chem.* **54** (1984)219.

98. W. Xu, X. Zhang and X. **Xu**, *J. Lumin.* **31 & 32** (1984) 808.
99. R. J. **danby**, K. **Holliday** and N.B. Manson. *J. Lumin.* **42** (1988) 83.
100. T. Izumitani and S.A. Payne, *J. Lumin.* **54** (1993) 337.
101. P.K. Gallagher, C.K. Kurkjian and P.M. Bridenbaugh, *Phys. Chem. Glasses* **6** (1965)95.
102. G. Boulon, M. Bouderbala and J. Seriot, *J. Less-Common Mets.* **112** (1985) **41**
103. Q. Su, Z. Pei, L. Chi, H. Zhang, Z. Zhang and F. Zou, *J. Alloys Compds.* **192** (1993)25.
- 104 **E.W.J.L.** Oomen and A.M A. va **Dongen**, *J. Non-Cryst. Solids* **111** (1989) **205**
105. **H.C** Kandpal and K.C. Joshi, *J. Non-Cryst. Solids* **101** (1988) 243.
106. K. Hirao, S. Todoroki and N. Soga, *J. Non-Cryst. Solids* **175** (1994) 263.
107. S. Todoroki, K. Hirao and N. Soga, *J. Appl. Phys.* **72** (1992) 5853.
108. S. Todoroki, **K** Hirao and N. Soga, *J. Non-Cryst. Solids* **143** (1992) 46.
- 109 **S** Tanabe, **K.** Hirao and N. **Soga**, *J. Non-Cryst. Solids* **142** (1992) 148.
- 110 M. Tanaka and **T** **Kushida**, *J. Alloys Compds* **193** (1993) 183.
- 111 **M** Stavola and D.L. Dexter, *Phys. Rev. B* **20** (1979) **1867**.
- 112 M. **Stavola**, L. Isganitis and M. Sceats, *J. Chem. Phys.* **74** (1981) 4228.
- 113 B.C. **Joshi**, *J. Non-Cryst. Solids* **180** (1995) 217.
- 114 J. Garcia **M** and W.A. Sibley, *J. Lumin.* **42** (1988) 109.
- 115 **H.C.** Kandpal and H.B. Tripathi, *Ind. J. Pure & Appl. Phys.* **17** (1979) **587**
116. G. Linger, R. Mohan, S. Knittel and G. Duportail, *Spectrochimica Acta* **46A** (1990) 797.
117. D. Levy, R. Reisfeld and D. Anvir, *Chem. Phys. Lett.* **109** (1984) 593.
118. C. McDonagh, G. Ennis and P. **Morrison**, B. O'Kelly, Z.R. Tang and J.F. **McGlip**, *J. Non-Cryst. Solids* **147 & 148** (1992) 97.
119. K. Devlin, B. O'Kelly, Z.R. Tang, C. McDonagh and **J.F** **McGlip**, *J. Non-Cryst. Solids* **135** (1991) **8**

- 120 **K Tanaka**, **T Ohyagi**, **K Hirao** and **N. Soga**, *Bull. Chem. Soc. Jpn.* 66 (1993) 1121.
121. **A Ellens**, **A. Meijerink** and **G Blasse**, *J. Lumin.* 59 (1994) 293.
122. **G Blasse**, *Inorganica Chimica Acta* 132 (1987) 273.
- 123 **G Blasse** and **L H Brixner**, *Inorganica Chimica Acta* 161 (1989) 13
- 124 **C.M Broadbeck** and **L E. Iton**, *J. Chem. Phys.* 83 (1985) 4285
- 125 **L E Iton**, **C.M Broadbeck**, **S.L Suib** and **G D Stucky**, *J. Chem. Phys.* 79 (1983) 1185.
- 126 **R Reisfeld**, **L Bohem**, **M Ish-Shalom** and **R Ficher**, *Phys. Chem. Glasses* 15 (1974) 76.
127. **A.M A. van Dongen**, *J. Non-Cryst. Solids* 139 (1992) 271.
- 128 **J.C Joshi**, **B C. Loshi**, **N.C. Pandey**, **R Belwal** and **J Joshi**, *J. Solid State Chem.* 72 (1977) 439.
- 129 **B.C Joshi** and **U.C. Pandey**, *J. Phys. Chem. Solids* 50 (1989) 599
- 130 **J Legendziewicz**, **T Glowiak**, **G Oczko** and **C N. Dao**, *J. Less-Common Mets.* 125(1986)45.
- 131 **T Glowiak**, **J Legendziewicz**, **C.N Dao** and **E Huskowska**, *J. Less-Common Mets.* 168(1991)237.
- 132 **J Hanuza**, **L. Macalik**, **P Deren**, **W. Ryba-Romanowski**, **W. Strek**, and **B. Jezowska-Trzebiaatowska**, *Rare Earth Spectroscopy* (Eds) **B Jezowska-Trzebiaatowska**, **J. Legendziewicz** and **W. Strek** (World Scientific, Philadelphia, 1985)209.
133. **R. Cases**, **M.A Chamarro**, **R Alcala** and **V.D. Rodriguez**, *J. Lumin.* 48 & 49 (1991)509.
- 134 **V.M Orera**, **P.J. Alonso**, **R. Cases** and **R Alcala**, *Phys. Chem. Glasses* 29 (1988) 59.
135. **T Yamamura**, **Y.Y. Park** and **H Tomiyasu**, *J. Alloys Compds.* 193 (1993) 186.
- 136 **K. Wei**, **D.P. Machewirth**, **J. Wenzel**, **E. Snitzer** and **G.H Sigel Jr.**, *Opt. Lett.* 19 (1994)904.

Chapter 1

- 137. X. Zou and H. Toratani, *J. Non-Cryst. Solids* **181** (1995) 87.
- 138. L. Wetenkemp, G F. West and H. Tobben, *J. Non-Cryst. Solids* **140** (1992) 25.
- 139. **K.** Hirao, S. Kishimoto, **K Tanaka**, S. Tanabe and N. Soga, *J. Non-Cryst. Solids* 139(1992)151.
- 140. W.J. Miniscalco, *J. Lightwave Technol* 9 (1991) 234.
- 141. Y. Yan, A **J** Faber and H. de Waal, *J. Non-Cryst. Solids* **181** (1995) 283.
- 142. N. Kagi, **A** Oyobe and K. **Nakamura**, *IEEE Photon. Technol. Lett.* 2 (1990) 559.
- 143 D.L. Dexter and **J H Schulman**, *J. Chem. Phys.* 22 (1954) 1063.
- 144. S. Tanabe, **S** Yoshii, K. Hirao and N. Soga, *Phys.Rev. B* 45 (1992) 4620.
- 145. **W.T** Carnall, **P.R.** Fields, J. Morrison and R. Sarup, *J. Chem. Phys.* 52 (1970) 4054.
- 146 **J** Sanz, **R** Cases and R. **Alcala**, *J. Non-Cryst. Solids* 93 (1987) 377
- 147 J.N. Carter, R G. Smart, **A.C** Tropper and **D.C Hanna**, *J. Non-Cryst. Solids* **140** (1992) 10.
- 148. **E.W.J.L. Oomen**, *J. Lumin.* 50 (1992) 317.
- 149. **W** Xu, D G. Ozen, A. **Kermaoui**, F. **Pelle** and **B** Blanzat, *J. Appl. Phys.* 75 (1994) 4180
- 150 D G. Ozen, J P. Denis, **W** Xu, F. Pelle and B. Blanzat, *J. Non-Cryst. Solids* 176 (1994) 147.

Chapter 2

Experimental Techniques and Methodology

In this chapter we provide brief accounts of experimental techniques and methodology used for spectral analyses. The preparations of glass samples are presented in the respective chapters.

2.1 Experimental Techniques

2.1.1 X-Ray Diffraction

The x-ray diffraction spectra of all the glass samples prepared in the course of the study were recorded at room temperature on a Seifert x-ray powder **diffractometer** with nickel filtered Cu K_{α} radiation. Powder specimens are best prepared for XRD study by placing the finely ground powder in a recess in plastic or teflon plate, compacting it under just sufficient pressure to cause cohesion without use of a binder and smoothing **off** the surface. Sometimes vacuum grease was also used as a binder.

2.1.2 Density Measurements

The density of irregular shaped solids can be determined by the Archimede's principle. The density of the glass samples under study were obtained using a 25 cm³ specific gravity bottle, Dhona single pan balance for weight measurements and xylene as the inert immersion liquid. The density is obtained from the relation

$$\rho = \frac{W_a \rho_l}{(W_a - W_l)} \quad (2.1)$$

where p is the density of the sample, W_a is the weight of the sample in air, W_l is the weight of the sample fully immersed in liquid and p_l is the density of the liquid used. The error in the density measurements is within $\pm 0.04 \text{ g cm}^{-3}$.

2.1.3 Refractive Index Measurements

The **refractive** indices of the glass samples are carried out using two different methods depending upon the range. For refractive indices lying in the range 1.33 to 1.60 Abbe's **refractometer** is used. The apparatus is standardised with the standard glass sample with **refractive** index of 1.528 supplied with the instrument. For glass samples with **refractive** index greater than 1.6 the Brewster angle method is employed.

(i) Refractive Index Measurement by Abbe's Refractometer¹

The Abbe's refractometer consists of a glass prism, K, with **refractive** index $n_0 = 1.6$. On the upper surface of the prism, the edges of which have been slightly bevelled, is placed a small specimen plate, G, of the glass the **refractive** index (n) of which is to be measured (figure 2.1).

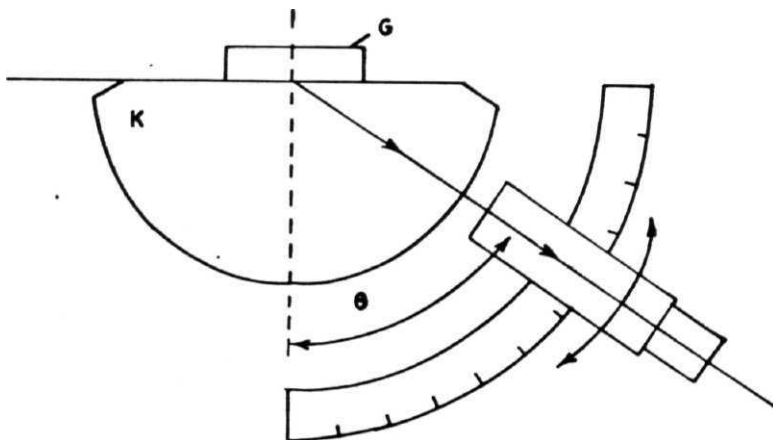


Figure 2.1 Measurement of refractive index using Abbe's refractometer.

The surface of the glass specimen adjoining prism K is polished, and the contact between the two adjoining surfaces were kept free from air columns with the help of 1-bromo naphthalene with relatively high refractive index of **1.658** to avoid interference to the measurement of refractive index for the specimen under study. The glass specimen is illuminated from one side by sodium arc lamp radiation. The ray of light falls on the boundary between the two indices of refraction, η and η_o , from different directions within the limits of the largest possible angle of incidence (right angle). The light is reflected into prism K at the critical angle. The telescope is set to a position where the cross wires lie on the dark edge of the field of view. This reading is noted (9). Knowing the absolute refractive index of the prism (η_o) the refractive index (r) of the glass specimen is obtained from the relationship,

$$\eta = \eta_o \sin \theta \quad (2.2)$$

The scale attached to the telescope is calibrated to give the refractive index of the glass sample **directly**

(ii) Refractive Index Measurement by Brewster Angle Method²

Ordinary light is completely polarized in the plane of incidence when it gets itself reflected from the transparent medium at a particular angle known as the angle of **polarization**. The angle is also referred to as Brewster angle after the discoverer of the phenomenon. The tangent of the angle of polarization is numerically equal to the refractive index of the medium, *i.e.*, the refractive indices are given by $\tan \theta$ where θ is the Brewster angle. Under these conditions, the reflected and the refracted light rays are perpendicular to each other.

The schematic diagram of the set up used is shown in figure 2.2. The polished transparent glass sample with dimension 2x1x0.2 cm is vertically mounted on a

Chapter 2

spectrometer base A He-Ne laser (Model No. 127) is used as the light source. The **reflected** light is allowed to fall on a sensitive photodiode and the output voltage **measured** with a Keithley multimeter (Model No. 175). The sample was rotated to **approximately** determine the point at which the reflected light intensity goes through the minimum. The intensity was then measured in steps of 10° on either side of the point at **which** minimum intensity is obtained. A plot of angle vs. voltage enables determination of the **Brewster** angle accurately at which minimum intensity is **obtained**. the refractive **index** could be measured to an accuracy of ± 0.001 .

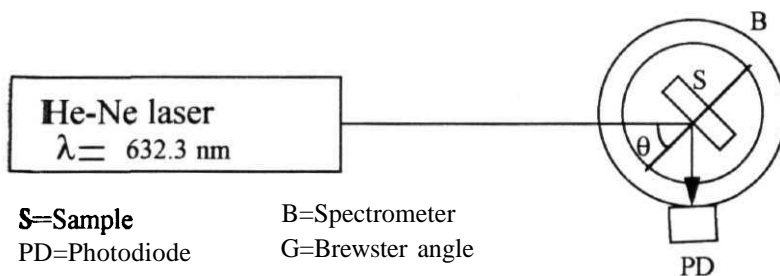


Figure 2.2 The schematic diagram of the measurement of refractive index by Brewster angle method

2.1.4 Infrared Spectral Measurements

A JASCO FT IR-5300 spectrometer has been used for the present study. This spectrometer enables measurement in the transmission mode in the region 4600 to 400 cm^{-1} with good resolution ($\pm 2 \text{ cm}^{-1}$). The infrared spectra were recorded at room temperature by KBr pellet method using powder samples.

2.1.5 Absorption Spectral Measurements

The absorption spectra of samples were recorded at room temperature with JASCO Model-7800 spectrophotometer in the ultraviolet and visible region 300-900 nm and Cary 17D spectrophotometer in the near infrared region 800-2200 nm with undoped glass as **reference**. The glass samples used had the dimensions approximately 2.0x1.0x0.2 cm. The second derivative spectra also were recorded wherever required.

2.1.6 Emission Spectral Measurements

The emission and excitation spectra of our glass samples were recorded with JASCO FP-777 and Hitachi-3010 **spectrofluorometers**. Emission spectral studies require choosing the most appropriate excitation energy or frequency. This requires in turn measurement of the excitation spectra as well. To start with approximate excitation frequencies are chosen depending upon the lanthanide ions from existing literature of emission spectral data for recording the emission spectra. From the emission spectra the most intense emission transition is chosen for the fixed emission frequency required for recording the excitation spectra. The appropriate intense transition in the excitation spectra are chosen for exciting the sample for the emission spectra taking into consideration the spectral region of interest. The emission spectra thus recorded are corrected for the background. Appropriate optical filters were used to avoid the noise due to the instrument and the background.

2.1.7 Excited State Lifetime Measurements

For measurements of excited state lifetimes, the polished glass samples were excited with first(As1) or second(As2) antistokes line from a home built **H₂** Raman shifter operating at 3500 KPa. The second harmonic (532 nm) of Nd(III):YAG laser (Continuum Inc. U.S.A Model No. 660B-10, 6 nsec, 10 Hz) is used as the pump source for the Raman **shifter** As1 and As2 for the **H₂** gas are 368.9 nm and 435.7 nm **respectively**. The spectra recorded with Jobin Yvon Hrs2 monochromator and the same spectra recorded with JASCO FP-777 **spectrofluorometer** were found to have identical

Chapter 2

features. The data and hard copies for fluorescent decay curves were obtained with a DCS01GPH camera and Tektronix 2465B oscilloscope controlled by a personal computer.

2.2 Spectral Analysis

2.2.1 Analysis of Transition Energies

The absorption spectra of trivalent lanthanide ions in glasses may be represented by the Hamiltonian³

$$H = H_e + H_{so} + H' \quad (2.3)$$

where H_e corresponds to interaction between pairs of electrons and H_{so} to spin-orbit coupling. In **addition**, the terms representing configuration interaction, H' are found to be important for realizing good fit with experimental energies and are given by³

$$\beta G(G_2) + \gamma G(R_7) + \text{three - particle terms} \quad (2.4)$$

where a , β and γ are linear combinations of radial integrals $L = 0, 1, 2, \dots$ for the states S, P, D, and are treated as adjustable **parameters** $G(G_2)$ and $G(R_7)$ are eigenvalues of **Casimir's** operator for the groups G_2 and R_7 respectively and have been tabulated by **Wybourne**.⁴ The effects of the three-particle terms are smaller than those of a , β and γ and **the** accuracy of the present data does not warrant their consideration here.

The absorption spectra of Ln^{3+} ions doped in glass were recorded both in the normal as well as second derivative forms. The latter give better resolution for overlapping transitions and thus enable determination of transition energies with better accuracy in such cases (figure 2.3). For Pr^{3+} , Nd^{3+} , Er^{3+} and Tm^{3+} , the transition energies are analysed by a least square fit procedure using the above Hamiltonian. Thus the

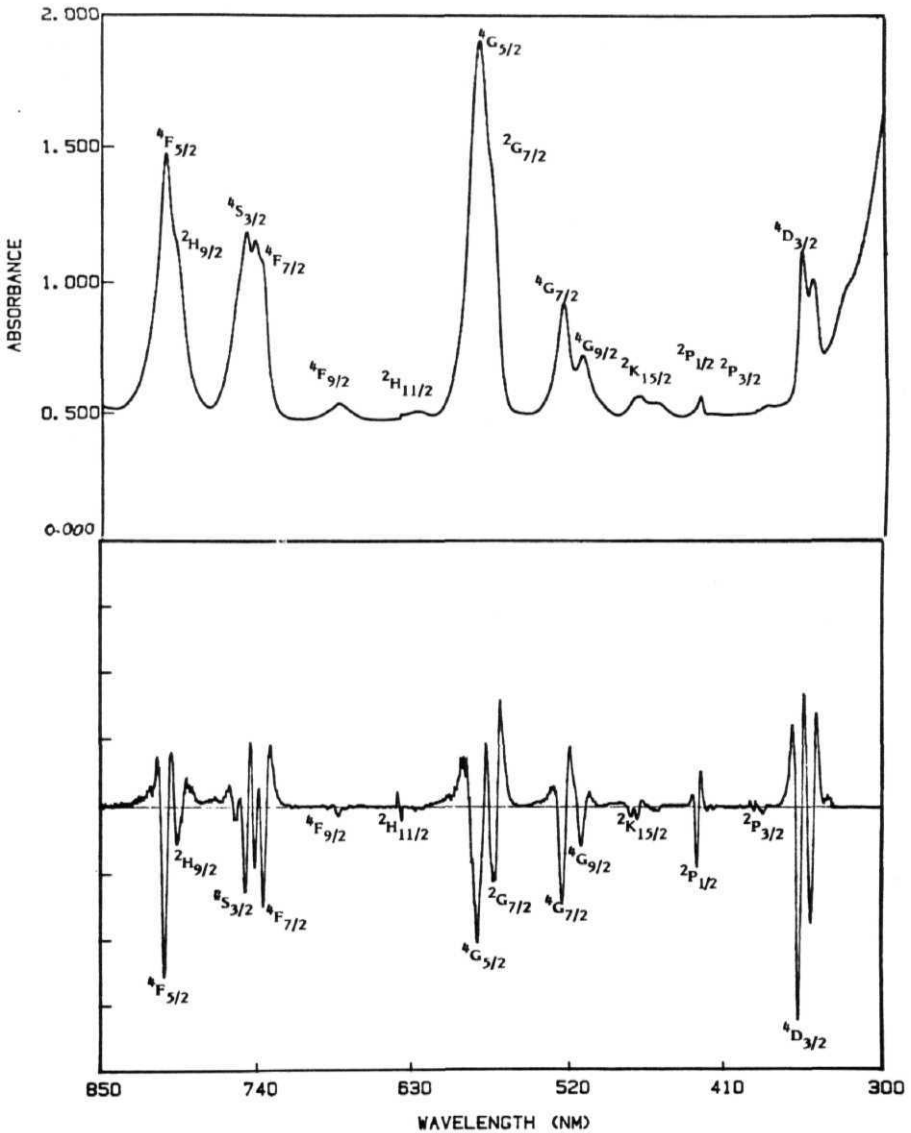


Figure 2.3 Absorption spectrum of Nd^{3+} ion in $CaO-Al_2O_3-B_2O_3$ glass system (a) Normal and (b) Second derivative.

Chapter 2

relevant matrix elements can be expressed in terms of the **Racah** parameters (E^k , $k=1,2,3$), spin-orbit coupling constant (4) and configuration interaction terms (a , p , γ) in the intermediate coupling scheme. The required matrix elements in terms of E^k , a , P , γ and ξ are taken from literature.^{4,7} Whereas most of the earlier workers have used the Taylor series method³, we have used the full matrix diagonalisation procedure.⁸ As only seven transitions each were observed for Pr^{3+} and Tm^{3+} , and the fit involves as many parameters the fitting procedure is modified by deriving suitable relationships between the matrix elements and experimentally observed transition energies and imposing these relationships as conditions to be satisfied during the fit. These are derived from the matrix elements corresponding to the terms $^3\text{H}_4$, $^3\text{P}_1$, $^3\text{P}_0$, and $^3\text{F}_3$ for Pr^{3+} and $^3\text{H}_6$, $^3\text{F}_3$ and $^3\text{H}_5$ for Tm^{3+} and observed transition energies and are given below

$$\begin{aligned} & \text{Pr}^{3+}: (^3\text{P}_1 \leftarrow ^3\text{H}_4) - (^3\text{P}_0 \leftarrow ^3\text{H}_4) \\ & \frac{(1 - kR_1)Y + (12 - 10kR_1)\alpha + \left(1 + \frac{kR_1}{2}\right)\beta + \gamma + \sqrt{(1 - kR_1)Y + (12 + 10kR_1)\alpha + \left(1 + \frac{kR_1}{2}\right)\beta + \gamma - \xi + 48\xi^2}}{2} \end{aligned} \quad (2.5a)$$

where $k = 3/11$ and Y is given by

$$Y = (^3\text{P}_1 \leftarrow ^3\text{H}_4) - (^3\text{F}_3 \leftarrow ^3\text{H}_4) = 33E^3 - 10\alpha + 0.5\beta \quad (2.5b)$$

where the transition energy differences corresponding to $(^3\text{P}_1 \leftarrow ^3\text{H}_4) - (^3\text{P}_0 \leftarrow ^3\text{H}_4)$ and $(^3\text{P}_1 \leftarrow ^3\text{H}_4) - (^3\text{F}_3 \leftarrow ^3\text{H}_4)$ are obtained from the absorption maxima of the relevant transitions.

$$\begin{aligned} & \text{Tm}^{3+}: X^2 + 2X \left(2E^3R - \left(\frac{2}{9}\right)P + 68\alpha + \left(\frac{37}{18}\right)\beta + 2.5\xi + 2.4\gamma \right) + \\ & 42E^3R + \left(-JP + 56a + \left(\frac{14}{9}\right)\beta + 1.4\gamma \right)j(-P + 12a + 0.5P + 2.5\xi + \gamma) - 6\xi^2 = 0 \end{aligned} \quad (26a)$$

$$\text{where } X = 2(^3F_3 \leftarrow ^3H_6) + \xi - 24\alpha - \beta - \gamma \quad (2.6b)$$

$$P = (^3F_3 \leftarrow ^3H_6) - (^3H_5 \leftarrow ^3H_6) = 9E^3 - 18\alpha - 0.5p \quad (2.6c)$$

$$R = R_1 + 35R_2 \quad (2.6d)$$

R_1 and R_2 are given by the ratios of the Racah parameters, E^1/E^3 and E^2/E^3 respectively. The transition energies were found to be sensitive **functions of ξ and p** . To start with the free ion values of R_1 , R_2 , a , γ and ξ as input parameters and evaluated p from eqns. (2.5) and (2.6) for Pr^{3+} and Tm^{3+} respectively before proceeding with diagonalisation. The input parameters were varied systematically to obtain a good fit between observed and calculated transition energies. E^3 is then evaluated from eqns. (2.5b) and (2.6c) for Pr^{3+} and Tm^{3+} respectively. Using its value E^1 and E^2 are obtained from R_1 and R_2 . The spectra of Nd^{3+} and Er^{3+} gave rise to as many as 11 and 12 transitions respectively. The transition energies were least square fit by diagonalising the 41×41 matrix with terms corresponding to all the J values. The corresponding eigenvectors are used for intensity calculations. For other rare earth ions the number of matrix elements corresponding to the Hamiltonian is too large and no attempts were made to analyze the transition energies in those cases.

2.2.2 Intensities of the Transitions

The absorption intensities are determined experimentally by the area method and the oscillator strength (P_{exp}) calculated from the reduced expression⁹

$$P_{\text{exp}} = \frac{2303mc^2}{N\pi e^2} \int \epsilon(\tilde{\nu}) d\tilde{\nu} \quad (2.7)$$

where m and e are the electron mass and charge respectively, c is the velocity of light and $E(V)$, the molar absorptivity is given by⁹

Chapter 2

$$\epsilon(\bar{\nu}) = \left(\frac{l}{cl} \right) \log \left(\frac{I_0}{I} \right) \quad (2.7a)$$

where c (moles/litre) is the concentration of Ln^{3+} , l is the optical path length (cm) and $\log(I_0 / I)$ is the absorptivity.

In evaluating the integral *viz.*, $\int \epsilon(\bar{\nu}) d\bar{\nu}$ normally one of the following three methods **adopted** (i) Half width method, (ii) Area method and (iii) Weight method. The first method *viz.*, half width method is applicable where the starting and ending points of the profile of the band do not deviate very much from the base line. Either second or third method is employed in all other cases.

In the present work the second method was adopted to evaluate the necessary values of the integrals. In this method, the number of squares within the band profile are counted and multiplied by a suitable factor related to molar extinction coefficient and energy in cm^{-1} to obtain the integrated area. In the weight method, the band part of the paper is cut, its weight taken and from its known density and thickness the area within the profile is calculated.

The theory dealing with calculation of intensities of spectral transitions has been looked into in considerable **detail**.⁴ Neglecting higher multipole mechanism such as electric quadrupole **etc.**, the oscillator strength is given by⁴

$$P = P_{ed} + P_{md} \quad (2.8)$$

where P_{md} represents contribution to intensity by magnetic dipole mechanism and P_{ed} by electrical dipole mechanism. The latter is given by **Judd-Ofelt** theory a brief outline of which is presented below.

According to Judd-Ofelt theory the intensities for electric dipole transitions connecting states A and B is given by⁴

$$\left(A \left| P_{\rho}^{(1)} \right| B \right) = - \sum_k \frac{\left(\psi J J_z \left| V \right| k \right) \left(k \left| P_{\rho}^{(1)} \right| \psi' J' J'_z \right)}{E(\psi J J_z) - E(k)} - \sum_k \frac{\left(\psi J J_z \left| P_{\rho}^{(1)} \right| k \right) \left(k \left| V \right| \psi' J' J'_z \right)}{E(\psi' J' J'_z) - E(k)} \quad (29)$$

where $P_{\rho}^{(1)}$ represents the component of the electric dipole operator, $(\psi J J_z)$ and $(\psi' J' J'_z)$ are the two states of configuration n^N which get mixed by crystal field with states, k . The summations are to be made over all the perturbing states. As it stands this summation is intractable. Judd and Ofelt approximated the above expression by replacing the energy denominator by a single average denominator, E_{ave} when it reduces to⁴

$$\left(A \left| P_{\rho}^{(1)} \right| B \right) = \sum_{\lambda, q} Y(\lambda, q, \rho) \left(l^N \alpha S L J_z \left| U_{\rho+q}^{(\lambda)} \right| l^N \alpha' S' L' J'_z \right) \quad (2.10)$$

where $Y(\lambda, q, \rho)$ is a complex expression relating the crystal field parameters and inter configurational radial integrals and the U^{λ} parameters are the reduced matrix elements. The summation in eqn. (2.10) is limited to even values *i.e.*, 2, 4, 6 for f electrons. The selection rules follow on the application of triangular conditions to the $3j$ and $6j$ symbols that occur in $Y(\lambda, q, \rho)$ in eqn. (2.10). These are as follows.⁴

$$\Delta l = \pm 1; \Delta S = 0; \Delta L = < 2l; \Delta J = < 2l.$$

The oscillator strengths (P_e) of a transition at a wavenumber σ in a medium of refractive index, n , is given by⁴

Chapter 2

$$P_e = \frac{8\pi^2 mc}{3\hbar e^2} \sigma \left(A \left| P_p^{(1)} \right| B \right)^2 \frac{(\eta^2 + 2)^2}{9} \quad (2.11)$$

$$= \sigma \sum_{\lambda, q} \xi(\lambda, q, \rho) \left(l^N \alpha SLJ_z \left| U_{\rho+q}^{(\lambda)} \right| l^N \alpha' SL' J' J'_z \right)^2 \quad (2.12)$$

where

$$\xi(\lambda, q, \rho) = \frac{8\pi^2 mc}{3\hbar e^2} \frac{(\eta^2 + 2)^2}{9} Y^2(\lambda, q, \rho) \quad (2.13)$$

Assuming that all the components associated with a transition are equally populated, the oscillator strength may be written as⁴

$$P = \sigma \sum_{\lambda} T_{\lambda} \left(l^N \alpha SLJ \left| U^{\lambda} \right| l^N \alpha' SL' J' \right)^2 \quad (2.14)$$

$$\text{where } T_{\lambda} = \sum_{q, \rho} \xi(\lambda, q, \rho)$$

The Judd-Ofelt parameters often represented by Ω_{λ} are related to T_{λ} as follows.¹⁰

$$\Omega_{\lambda} (\text{cm}^2) = \frac{3\hbar}{8\pi^2 mc} \frac{9\eta(2J+1)T_{\lambda}}{(\eta^2 + 2)^2} \quad (2.15)$$

where \hbar is the refractive index of the medium, $(2J+1)$ is the degeneracy of the ground level of the particular ion of interest. Application of Judd-Ofelt theory to the intensities of transitions between various Stark levels is dependent upon the availability of reliable crystal field eigenstates. When ions reside at low symmetry the states cannot be calculated and the intensity parameters have to be obtained from experimental data. Thus using the reduced matrix elements given in literature and the experimental oscillator strengths the intensity parameters, T_{λ} and hence Ω_{λ} have been calculated by least square analysis. The reduced matrix elements of the unit tensor operators U^{λ} evaluated in the

intermediate coupling scheme are almost insensitive to the ion environment and hence values obtained for one host may be used for other hosts as discussed by Reisfeld, Riseberg and Weber.^{5,11,12} We have used the U^λ values given by Carnall *et al.*¹³

In the intermediate coupling scheme, the states of f^N electronic configuration are taken as linear combinations¹⁰

$$|f^N \psi J\rangle = \sum_{\alpha, S, L} C(\alpha, S, L) |f^N \alpha SLJ\rangle \quad (2.16)$$

where $c(\alpha, S, L)$ are the numerical coefficients resulting from the diagonalisation of electrostatic, spin-orbit and configuration interaction matrices. The details of the matrix elements and the procedure for obtaining the linear combinations have been presented in section 2.2.1.

The electric and magnetic dipole strengths are calculated from the formulae¹⁰

$$S_{ed} = e^2 \sum_{2,4,6} \Omega_\lambda \langle \psi J \| U^\lambda \| \psi' J' \rangle^2 \quad (2.17)$$

$$S_{md} = \frac{e^2 h^2}{16\pi^2 m^2 c^2} \langle \psi J \| L + 2S \| \psi' J' \rangle^2 \quad (2.18)$$

where h is the Planck's constant. The matrix values of $\langle \psi J \| L + 2S \| \psi' J' \rangle$ are evaluated using the formulae given by Wybourne.

$$(1) J = J$$

$$(\alpha SLJ \| L + 2S \| \alpha SLJ) = g[J(J+1)(2J+1)]^{1/2} \quad (2.19a)$$

Chapter 2

where $g = 1 + \frac{J(J+1) + S(S+1) - L(L+1)}{2J(J+1)}$

(2) $J = J' - 1$

$$(\alpha SLJ \| L + 2S \| \alpha SLJ - 1) = \left[\frac{(S + L + J + 1)(S + L + 1 - J)(J + S - L)(J + L - S)}{4J} \right]^{1/2} \quad (2.19b)$$

(3) $J = J' + 1$

$$(\alpha SLJ \| L + 2S \| \alpha SLJ + 1) = \left[\frac{(S + L + J + 2)(S + L + 1 - L)(L + J + 1 - S)(S + L - J)}{4(J + 1)} \right]^{1/2} \quad (2.19c)$$

The matrix elements calculated from eqn. (2.19) were transformed into the intermediate coupling scheme before computation of the magnetic dipole contribution represented by eqn. (2.18).

The total oscillator strength (P_{cal}) of a band with energy σ (cm^{-1}) is⁹

$$P_{cal} = \frac{8\pi^2 mc\sigma}{3he^2 (2J + 1)} \left[\frac{(\eta^2 + 2)^2}{9\eta} S_{ed} + \eta S_{md} \right] \quad (220)$$

2.2.3 Evaluation of transition probabilities, lifetimes, branching ratios and stimulated emission cross sections

The radiative transition probability $A(\psi J, \psi' J')$ between the states ψJ and $\psi' J'$ is given by⁹

$$A(\psi J, \psi' J') = \frac{64\pi^4 \bar{\nu}^3}{3h(2J + 1)} \left[\frac{\eta(\eta^2 + 2)^2}{9} S_{ed} + \eta^3 S_{md} \right] \quad (2.21)$$

where ν is the energy difference in wave numbers (cm^{-1}) between the two levels concerned. The total radiative transition probability $A_T(\psi J)$ is obtained from⁹

$$A_T(\psi J) = \sum_{\psi' J'} A(\psi J, \psi' J') \quad (2.22)$$

where the sum runs over all $\psi' J'$ lower in energy than ψJ . The radiative life time τ_R of a transition is calculated using the relationship⁹

$$\tau_R = \frac{1}{A_T(\psi J)} \quad (2.23)$$

The branching ratios (PR) are obtained from the relationship⁹

$$\beta_R(\psi J, \psi' J') = \frac{A(\psi J, \psi' J')}{A_T(\psi J)} \quad (2.24)$$

The experimental branching ratios were obtained from the areas under the emission bands. The stimulated emission cross section $\sigma_p(\lambda_p)$ of a given emission transition is calculated using the relationship¹⁴

$$\sigma_p(\lambda_p) = \frac{\lambda_p^4}{8\pi c \eta^2 \Delta \lambda_p} A(\psi J, \psi' J') \quad (2.25)$$

where λ_p is the average emission wavelength and $\Delta \lambda_p$ is the effective emission band width, η , the refractive index and $A(\psi J, \psi' J')$ the radiative transition probability.

Chapter 2

References

1. I. **Fanderlik**, *Optical Properties of Glass* 5 (Elsevier, New York, 1983) 103.
2. N. Subrahmanyam and B. **Lal**, *A Text Book of Optics* (S. Chand & Company Ltd., New Delhi, 1976)424.
3. W.T. Carnall, **P.R** Fields and K. Rajnak, *J. Chem. Phys.* 49 (1963) 4424.
4. B.G. Wybourne, *Spectroscopic Properties of Rare Earths* (Interscience Publishers, New York, 1965).
5. S.V.J. **Lakshman** and **C.K.** Jayasankar, *J. Phys.C: Solid State Phys.* **17** (1984) 2967.
6. B.R. Judd and R. Loudon, *Proc. Roy. Soc. (London)* **A251** (1959) 127.
7. C.W. Nielson and G.F. **Koster**, *Spectroscopic Coefficients for P^n , d^n and f Configurations* (M.I.T Press, Cambridge, Mass, 1964).
8. **P.R.** Srikanth Sharma, R. Jagannathan and M. Vithal, *J. Chem. Soc. Dalton Trans.* (1992)723.
9. W.T. Carnall, J.P. Hessler and F. Wagner Jr., *J. Phys. Chem.* 82 (1978) 2152.
10. R. Reisfeld, *Structure and Bonding* **22** (Springer-Verlag, New York, 1975) 123
11. R. Reisfeld, L. **Boehm**, N. Lieblich, B. Barnett, *Proc. Tenth Rare Earth Conference* 2 (1973) 1142.
12. **L.A.** Riseberg and M.J. Weber, *Relaxation Phenomena in Rare Earth Luminescence in Prog. Optics XIV* (Ed.) E. Wolf (North Holland, Amsterdam, 1975).
13. W.T. **Carnall**, *Argonne National Laboratory Report* (1978) ANL-78-XX-95.
14. M. **Eyal**, E. Greenberg, R. Reisfeld and N. Spector, *Chem. Phys. Letts.* **117** (1985) 108.

Chapter 3

Absorption and Emission Spectral Studies of Lanthanide Ions in Borate Glasses

In this chapter we report the results of our study on borate glasses pertaining to two aspects. Accordingly the material is submitted in two parts. The first part deals with the influence of cations on the optical properties of borate glasses doped with Nd^{3+} , Eu^{3+} and Er^{3+} . The borate glasses taken differ in the cations present as one of the constituents as glass modifiers. The second part deals with optical absorption spectral studies of Pr^{3+} , Nd^{3+} , Sm^{3+} , Dy^{3+} , Ho^{3+} , Er^{3+} and Tm^{3+} and emission spectral studies of Sm^{3+} , Eu^{3+} , Tb^{3+} and Dy^{3+} in the cabal glass viz., $\text{CaO-Al}_2\text{O}_3\text{-B}_2\text{O}_3$. The reasons for the choices of the dopant ions and host matrices are presented in the respective parts

3.1 Influence of Cations on the Optical Properties of Nd^{3+} , Eu^{3+} and Er^{3+} Doped Borate Glasses

Glasses are found to be good host matrices for rare earth lasers.¹⁻⁴ The optical properties of rare earths doped glasses are chiefly influenced by the glass forming anions and glass forming/modifying cations and to a lesser extent by the methods of preparation and heat treatments.^{4,11} Systematic studies on the influence of cations on the optical properties of glasses are limited although they do show many Subtle influences.⁶⁻⁹ In this part we present the results of our study on the influence of cations Li^+ , Ca^+ and Ba^+ on the optical properties of $\text{Li}_2\text{O-B}_2\text{O}_3$, $\text{CaO-B}_2\text{O}_3$ and $\text{BaO-B}_2\text{O}_3$ glasses doped with Nd^{3+} , Eu^{3+} and Er^{3+} ions. These glasses are chosen as they are relatively simple binary systems with large variations in the ionic sizes of the cations and detailed crystal structure studies on related borates are available.¹²⁻¹⁶ The influence of the matrices with different cations on the absorption spectra of $\text{Nd}^{3+}(4f^3)$ and $\text{Er}^{3+}(4f^{11})$ have been investigated. The

spectroscopic energy parameters and the Judd-Ofelt **parameters**, obtained from absorption spectra and radiative parameters *viz.*, the transition probabilities and branching ratios of emission lines of interest evaluated from the Judd-Ofelt parameters are **compared** For Eu^{3+} ions, where the excitation and emission spectra are more **informative**,¹⁷⁻²⁰ we present the influence of the parent matrices on the relative intensities of the emission transitions and the phonon side bands observed in the excitation **spectra**. The results of our study on the influence of the cations on the Urbach energies and optical band gaps on the neat glasses are also **presented**.^{21,22}

3.1.1 Preparation of Alkali and Alkaline Earth Borate Glasses

The glass samples with compositions in mol % $30\text{Li}_2\text{O}-69\text{B}_2\text{O}_3-1\text{Ln}_2\text{O}_3$, $30\text{CaO}-69\text{B}_2\text{O}_3-1\text{Ln}_2\text{O}_3$ and $30\text{BaO}-69\text{B}_2\text{O}_3-1\text{Ln}_2\text{O}_3$ (Ln = Nd, Eu, or Er) were **prepared** Lithium carbonate (BDH), calcium carbonate (BDH), barium carbonate (BDH), boric acid (Analar) and respective rare earth oxides (Aldrich **Chem. Co**) were used as starting materials. The calculated amounts of starting materials for 10 g of glass in single batch were ground to give a homogeneous mixture. The finely ground mixture was then placed in a silica crucible and heated in an electric furnace. A slow heating rate was initially maintained until the temperature **reached** 300 °C and the dehydration of H_3BO_3 was complete. Then the temperature was increased to 730 °C, 830 °C and 900 °C for glasses for which the cation component corresponded to lithium carbonate calcium carbonate and barium carbonate respectively. The mixture was kept at this temperature until the decomposition was complete. Though the decomposition temperature of barium carbonate is above 1740 °C, when it is in the glass mixture it is found to decompose at 900 °C **itself**. Complete decomposition of barium carbonate could be ensured by keeping the mixture for sufficiently long time at 900 °C. Then the temperature was rapidly increased to 950 °C in the case of all the glasses. The crucible containing the melt was constantly agitated to ensure homogeneous mixing. Sufficient time was allowed for the melt to become visibly homogeneous and bubble **free**. Then the melt was poured into a slot in a stainless steel plate and quenched rapidly by pressing with another stainless steel

plate Typical weight loss on melting under experimental conditions indicated that the actual compositions should be within 1 % of the values quoted for the components. The samples were annealed at a temperature 20 °C below T_g and subsequently polished with commercial media and water free lubricant. The samples could be obtained with good transparency and uniform thickness of 0.2 cm and 2.0 cm diameter. The amorphous nature of the glass samples were confirmed by recording their powder x-ray diffraction spectra.

The method of obtaining the optical band gaps and Urbach energies for neat glasses is presented in detail in appendix 1.

3.1.2 Results and Discussion

Table 3.1 reproduces refractive index (η), the optical band gap (E_{opt}), Urbach energy (AE), the emission intensity ratio (R/O) of Eu^{3+} , phonon energy ($\hbar\omega$) and the electron phonon coupling strengths (g) for $Li_2O-B_2O_3$, $CaO-B_2O_3$ and $BaO-B_2O_3$ glass systems. The energy parameters derived from absorption spectra for Nd^{3+} and Er^{3+} doped glasses are given in table 3.2. The corresponding transition energies are reproduced in tables 3.3 and 3.4 respectively. The Judd-Ofelt parameters Ω_λ ($\lambda=2,4,6$) for Nd^{3+} and Er^{3+} derived from their experimental oscillator strengths are given in table 3.5. As the number of transitions observed for the absorption spectra of Eu^{3+} are limited due to strong self absorption below 400 nm and as a result the Judd-Ofelt parameters could not be obtained reliably, no attempts were made to extend these calculations for this ion. The observed and calculated oscillator strengths for Nd^{3+} and Er^{3+} ions in the above glass matrices are reproduced in tables 3.6 and 3.7 respectively. The typical values for the electric dipole strengths, magnetic dipole strengths, transition probabilities, total transition probabilities, radiative lifetimes and branching ratios for excited states of Nd^{3+} and Er^{3+} are given for the case of these ions doped in $CaO-Al_2O_3-B_2O_3$ in the next part of this chapter. We therefore confine to giving the transition probabilities (A) and the

corresponding branching ratios (PR) calculated from Judd-Ofelt parameters for Nd^{3+} and Er^{3+} in borate glasses only for transitions identified for their potential as lasers.¹⁻⁴ These values are reproduced in table 3.8. The excitation spectra of Eu^{3+} doped glasses were measured by monitoring the emission at 613 nm corresponding to the transition ${}^5\text{D}_0 \rightarrow {}^7\text{F}_2$. The low intensity peak in the higher energy side of ${}^7\text{F}_0 \rightarrow {}^5\text{D}_2$ transition is the phonon side band associated with this transition.^{19,20} The phonon side bands obtained for Eu^{3+} in different glass matrices are reproduced in figure 3.1. The energy gap between the phonon side band and the pure electronic transition ${}^7\text{F}_0 \rightarrow {}^5\text{D}_2$ corresponds to the phonon energy, $\hbar\omega$.¹⁹⁻²⁰ The integrated intensity ratio of the phonon side band to the pure electronic transition ${}^7\text{F}_0 \rightarrow {}^5\text{D}_2$ gives the electron phonon coupling strength, g .^{19,20} The values of $\hbar\omega$ and g for different hosts are included in table 3.1. The emission spectra of Eu^{3+} in borate glasses were measured by exciting at 395 nm corresponding to the ${}^7\text{F}_0 \rightarrow {}^5\text{L}_6$ transition and are reproduced in figure 3.2. The two dominant emissions for Eu^{3+} occur due to ${}^5\text{D}_0 \rightarrow {}^7\text{F}_2$ at 613 nm in the red region and ${}^5\text{D}_0 \rightarrow {}^7\text{F}_1$ at 590 nm due to orange emission. The relative integrated intensity ratio, R/O, of these two transitions are included in table 3.1 as mentioned earlier.

Table 3.2 shows that the full matrix diagonalisation procedure adopted leads to good agreement between calculated and observed transition energies as shown by the small rms deviations. In the case of Nd^{3+} doped borate glasses, the values of electrostatic parameters (E^k , $k=1,2,3$) and the configuration interaction parameters (α, β, γ) show a decreasing trend in the order $\text{Li}_2\text{O}-\text{B}_2\text{O}_3 > \text{CaO}-\text{B}_2\text{O}_3 > \text{BaO}-\text{B}_2\text{O}_3$. Such a systematic trend is found to arise due to the increasing red shifts in the corresponding absorption spectral maxima of Nd^{3+} transitions as we go along the above order (table 3.3). The variations in the spectroscopic parameters for Er^{3+} in different glass matrices are far less than those observed for Nd^{3+} due to more shielding effect in Er^{3+} .²³ The ${}^4\text{I}_{9/2} \rightarrow {}^2\text{P}_{1/2}$ transition of Nd^{3+} lies in the range 23,228-23,255 cm^{-1} characteristic of 8-9 coordination.^{24,25}

Among the Judd-Ofelt parameters Ω_2 is the most sensitive to structure and shows an increase with increasing covalency in the bonding between the lanthanide ion and the ligand atoms and/or site asymmetry of the lanthanide ion.¹⁷⁻¹⁸ For Nd^{3+} Ω_2 shows an increase with increasing ionic size of the constituent cations, a result akin to that observed for this ion in silicate glasses.^{1,6} The Ω_2 values reflect the nature of the sites occupied by the Nd^{3+} and Er^{3+} ions in the glass matrices. Recent studies suggest that in glasses the rare earth ions occupy sites closely similar to those in related crystalline systems.⁵ No doubt in a glass matrix dopant ions will have distribution of sites and associated crystal fields. The differences should therefore be attributed to the dominant site symmetry and covalency effects. Nd^{3+} gives rise to Ω_2 values in $\text{BaO-B}_2\text{O}_3$ and $\text{CaO-B}_2\text{O}_3$ which are comparable but significantly larger than the value in $\text{Li}_2\text{O-B}_2\text{O}_3$ glass suggesting a more ionic site in the last case. The lanthanide ions are known to have different coordination and site symmetries in crystalline borates. Some of these structures relevant to the present discussion are illustrated in figure 3.3. In borates the early members of the lanthanides from La^{3+} to Gd^{3+} strongly favor 9 coordination with aragonite structure with an average La-O bond length of ~ 2.6 Å as in LaBO_3 .^{13,14} In $\text{Li}_2\text{O-B}_2\text{O}_3$ a more ionic site may result due to higher coordination such as 10 as for instance observed for $\text{La}_2\text{O}_3\text{-}3\text{B}_2\text{O}_3$ with an average La-O bond length of ~ 2.68 Å leading to smaller Ω_2 value.^{13,15} A comparison of Ω_2 values between Nd^{3+} and Er^{3+} in the same glass matrix in general shows significantly larger values for Er^{3+} . The end members of the rare earth series from Er^{3+} to Lu^{3+} strongly prefer 6 coordination characterized by less ionic environment although instances of isomorphous series with higher coordination are also known.^{13,26} Occupation of sites with 6 closely situated neighbors as in calcite isotype LuBO_3 ¹³ can result in the larger Ω_2 value. The relatively smaller value of Ω_2 observed for Er^{3+} in $\text{BaO-B}_2\text{O}_3$ glass within the three erbium doped borate glasses suggests occupation of relatively more ionic sites with larger coordination such as in $\text{LnMg}(\text{B}_5\text{O}_{10})$ with 9 coordination, such a site occupancy being facilitated by the

Chapter 3

presence of the large Ba^{2+} ions.¹⁶ The analogy is put forward on the basis that transition metal ions and lanthanide ions are likely to occupy sites in glasses similar to those found in related crystalline systems as suggested by Wang *et al* on the basis of crystal chemistry approach.⁵

The Judd-Ofelt parameters Ω_2 , Ω_4 and Ω_6 together decide the radiative properties. The branching ratios, β_R are given by A/A_T , where A is the transition probability for the transition in question and A_T is the total transition probability from the relevant excited state. A higher A or β_R thus signifies a higher stimulated emission cross section for the transition in question in the host matrix under study. For the widely used lasing transition, $^4F_{3/2} \rightarrow ^4I_{11/2}$ for Nd^{3+} , lithium borate glass shows the largest β_R value. A similar result has been deduced for this transition of Nd^{3+} in borate and silicate glasses containing alkali ions.¹⁹ For the most important lasing transition $^4I_{11/2} \rightarrow ^4I_{13/2}$ of Er^{3+} occurring at 2.7 μm , the β_R has the highest value for the $\text{BaO-B}_2\text{O}_3$ glass.

It may be reasonably assumed that the boron coordination in these glasses will have planar and tetrahedral boron in a ratio closely related to those observed in crystalline systems such as $\text{Li}_2\text{O-2B}_2\text{O}_3$, $\text{CaO-2B}_2\text{O}_3$ and $\text{BaO-2B}_2\text{O}_3$.¹² The infrared studies for these systems show presence of both types of coordination.¹² The characteristic infrared frequencies corresponding to BO_3 and BO_4 groups center around 1375 and 1065 cm^{-1} respectively.^{12,19} The phonon side bands associated with $^7F_0 \rightarrow ^5D_2$ transition of Eu^{3+} doped in these glass systems could be resolved into two major components centered around the above energies which could be assigned to BO_3 and BO_4 groups (figure 3.1).^{19,20} The ratios of the integrated areas under the two components, *i.e.*, $(\text{BO}_4)/(\text{BO}_3)$ are found to be 2.6, 4.3 and 6.2 for $\text{Li}_2\text{O-B}_2\text{O}_3$, $\text{CaO-B}_2\text{O}_3$ and $\text{BaO-B}_2\text{O}_3$ glass matrices respectively. These ratios signify that the electron phonon coupling gets associated with more of tetrahedral boron when smaller cations are replaced by larger ones. If this is the case one would also expect the tetrahedral boron to

lead towards a more three dimensional network resulting in a higher electron phonon coupling strength for the glass lattice with larger cations. The observation of increasing g values in the order $\text{Li}_2\text{O-B}_2\text{O}_3 < \text{CaO-B}_2\text{O}_3 < \text{BaO-B}_2\text{O}_3$ is in conformity with such a conclusion.

The emission spectra of Eu^{3+} consist of transitions only from the $^5\text{D}_0$ level. The absence of emission transitions from higher excited states viz., $^5\text{D}_1$ ($J=1,2,3$) is due to the high phonon energy characteristic with a maximum of $1340\text{-}1480\text{ cm}^{-1}$ of the host leading to nonradiative decay of these transitions.⁶ The value of R/O ratio is a sensitive function of covalency and site asymmetry of the Eu^{3+} ion.^{17,18} This value is larger when the ion is in a more covalent environment and/or present in higher asymmetry.^{17,18} The R/O value increases in the order, $\text{Li}_2\text{O-B}_2\text{O}_3 < \text{CaO-B}_2\text{O}_3 < \text{BaO-B}_2\text{O}_3$. This trend shows that the bonding between Eu^{3+} and the ligand atoms is more covalent, larger the ionic size of the cation present. In these respects Eu^{3+} behaves similar to Nd^{3+} in these glass matrices.

As these studies pertain to the influence of cations, we also measured the optical band gaps and Urbach energies for these glasses. The Urbach energies (AE) obtained for these glasses lie in the narrow range reported in literature for glasses.^{27,28} The optical band gap energies (E_{opt}) obtained for borate glasses are found to be in the order $\text{Li}_2\text{O-B}_2\text{O}_3 > \text{CaO-B}_2\text{O}_3 > \text{BaO-B}_2\text{O}_3$ (table 3.1). The optical band gap in amorphous systems is closely related to the energy gap between valence band and conduction band. In glasses although the latter is influenced by the anions, the cations play an indirect role. The s and p orbitals of boron and p orbitals of oxygen interact with each other to form bonding and antibonding states which contribute to valence and conduction band respectively.² Replacement of more covalent Li^+ by less covalent Ca^{2+} or highly ionic Ba^{2+} results in an increase in the presence of strong -B-O-B- linkages in the above order.² This in principle should result in reduction of the band gap between the valence

Chapter 3

band and conduction band and in turn the optical band gap, as the cations introduced are made increasingly ionic.

3.1.3 Conclusions

The transitions in the absorption spectra of Nd^{3+} ions show a red shift with increasing ionic radius of the cation present as major constituent of the borate glass. The energy parameters show a corresponding decrease. For Er^{3+} the changes observed for these parameters are relatively small. The constituent alkali or alkaline earth ions considerably influence the Judd-Ofelt and radiative parameters. The ionic size of the constituent cations and coordination preferences intrinsic to the Nd^{3+} and Er^{3+} ions as evidenced by structural characteristics shown by related crystalline borates account for the variations in the Judd-Ofelt parameters. The Judd-Ofelt parameter Ω_2 for Nd^{3+} in different borate glasses and the red to orange emission intensities of the Eu^{3+} show increasing covalent character for the dopant with increasing ionic size of the cation present as glass constituent. The phonon side bands of the ${}^7\text{F}_0 \rightarrow {}^5\text{D}_2$ transition of Eu^{3+} show components due to BO_3 and BO_4 groups. An increase in the BO_4 component accompanied by a corresponding increase in the electron phonon coupling strength in the order $\text{Li}^+ < \text{Ca}^{2+} < \text{Ba}^{2+}$ provide evidence for increasing dimensionality in the network resulting in stronger interaction between the glass matrix and the dopant Eu^{3+} ion. The optical band gaps for the undoped glasses show decreasing trend with increasing cationic radius.

Table 3.1 Refractive index (η), the optical band gap (E_{opt}), Urbach energy (AE), the emission intensity ratio (R/O^\dagger) of Eu^{3+} , phonon energy (ha) and the electron phonon coupling strengths (g) for (a) $Li_2O-B_2O_3$, (b) $CaO-B_2O_3$ and (c) $BaO-B_2O_3$ glass systems

Glass matrix	$r \setminus$	$E_{opt}(eV)$	AE (eV)		ha (cm $^{-1}$)	g (10^{-3})
	± 0.001	± 0.03	± 0.001	R/O^\dagger	± 10	± 1
Li₂O-B₂O₃	1.560	3.31	0.212	3.5	1060, 1387	6.9
CaO-B₂O₃	1.593	3.26	0.226	36	1083 , 1375	11.8
BaO-B₂O₃	1.597	3.12	0.360	3.7	1065, 1374	18.3

[†] See text

Table 3.2 The spectroscopic parameters Nd^{3+} and Er^{3+} ions doped in (a) $30Li_2O-69B_2O_3-1Ln_2O_3$, (b) $30CaO-69B_2O_3-1Ln_2O_3$ and (c) $30BaO-69B_2O_3-1Ln_2O_3$ glass systems.

Parameters (cm $^{-1}$)	Nd^{3+}			Er^{3+}		
	a	b	c	a	b	c
F^2	76518	76408	76030	98007	98084	97660
F⁴	51818	51581	51150	69637	69837	69723
F⁶	37903	37823	37393	52024	52245	51625
H ¹	5011.69	4999.90	4963.70	6601.20	6615.28	6579.19
E^2	25.93	25.94	25.84	32.58	32.58	32.34
E^3	505.79	504.87	503.05	639.51	639.54	638.74
a	24.24	24.11	24.02	15.76	16.07	15.98
P	-634.70	-629.90	-628.90	-683.34	-707.14	-682.03
Y	1493.09	1537.79	1695.99	1523.90	1472.99	1516.70
	880.57	884.67	886.58	2436.46	2437.55	2443.88
E^1/E^3	991	9.90	9.87	10.32	10.34	10.30
E^2/E^3	0.0512	0.0513	0.0513	0.0509	0.0509	0.0506
rms	± 31	± 35	± 36	± 41	± 43	± 45

Table 3.3 Observed and calculated energy levels in cm^{-1} of Nd^{3+} ion in (a) $30\text{Li}_2\text{O}-69\text{B}_2\text{O}_3-1\text{Nd}_2\text{O}_3$, (b) $30\text{CaO}-69\text{B}_2\text{O}_3-1\text{Nd}_2\text{O}_3$ and (c) $30\text{BaO}-69\text{B}_2\text{O}_3-1\text{Nd}_2\text{O}_3$ glass systems.

System	a		b		c	
Terms	E_{obs}	E_{cal}	E_{obs}	E_{cal}	E_{obs}	E_{cal}
from $I_{9/2}$	(cm^{-1})	(cm^{-1})	(cm^{-1})	(cm^{-1})	(cm^{-1})	(cm^{-1})
${}^4F_{3/2}$	11441	11455	11435	11441	11409	11407
${}^4F_{5/2}$	12468	12487	12461	12478	12430	12447
${}^2H_{9/2}$	12620	12676	12610	12670	12602	12666
${}^3S_{3/2}$	13386	13350	13377	13344	13351	13316
${}^4F_{7/2}$	13513	13470	13522	13466	13477	13438
${}^3F_{9/2}$	14716	14764	14716	14769	14684	14752
${}^3H_{11/2}$	16000	15989	16000	16002	16012	16010
${}^4G_{5/2}$	17152	17177	17108	17154	17050	17097
${}^2G_{7/2}$	17241	17256	17238	17245	17235	17220
${}^4G_{7/2}$	19047	19057	19047	19050	19011	19018
${}^4G_{9/2}$	19569	19499	19569	19495	19531	19459
${}^2G_{9/2}$	21075	21023	21074	21094	21074	21086
${}^3K_{15/2}$	21786	21780	21777	21783	21762	21772
${}^2P_{1/2}$	23255	23247	23255	23246	23228	23220
	28653	28639	28612	28606	28490	28517
rms	± 31		± 35		± 36	

Table 3.4 Observed and calculated energy levels in cm^{-1} of Er^{3+} ions in (a) $30\text{Li}_2\text{O}-69\text{B}_2\text{O}_3-1\text{Er}_2\text{O}_3$, (b) $30\text{CaO}-69\text{B}_2\text{O}_3-1\text{Er}_2\text{O}_3$ and (c) $30\text{BaO}-69\text{B}_2\text{O}_3-1\text{Er}_2\text{O}_3$ glass systems

System	a		b		c	
Terms	E_{obs}	E_{cal}	E_{obs}	E_{cal}	E_{obs}	E_{cal}
from $I_{15/2}$	(cm^{-1})	(cm^{-1})	(cm^{-1})	(cm^{-1})	(cm^{-1})	(cm^{-1})
$II_{3/2}$	6634	6668	6636	6671	6678	6691
$I_{11/2}$	10256	10285	10251	10287	10251	10301
	12370	12360	12360	12363	12355	12360
	15361	15283	15360	15290	15360	15286
	18450	18527	18450	18539	18416	18494
$III_{1/2}$	19193	19168	19193	19165	19193	19148
$^4F_{7/2}$	20492	20511	20492	20522	20492	20510
$^4F_{5/2}$	22222	22179	22222	22188	22173	22162
$^4F_{3/2}$	22573	22529	22598	22540	22598	22520
$G_{9/2}$	24570	24572	24570	24577	24570	24584
$^4G_{11/2}$	26455	26455	26455	26455	26455	26456
$^4G_{9/2}$	27397	27437	27397	27436	27397	27436
rms	± 41		± 43		± 45	

Table 3.5 The Judd-Ofelt parameters for Nd^{3+} and Er^{3+} ions doped in (a) $30\text{Li}_2\text{O}-69\text{B}_2\text{O}_3-1\text{Ln}_2\text{O}_3$, (b) $30\text{CaO}-69\text{B}_2\text{O}_3-1\text{Ln}_2\text{O}_3$ and (c) $30\text{BaO}-69\text{B}_2\text{O}_3-1\text{Ln}_2\text{O}_3$ glass systems.

Lanthanide ion	Glass matrix	$\Omega_2 (10^{-20} \text{ cm}^2)$	$\Omega_4 (10^{-20} \text{ cm}^2)$	$\Omega_6 (10^{-20} \text{ cm}^2)$
Nd^{3+}	a	2.271	1.516	2.440
	b	3.436	3.452	3.155
	c	3.952	2762	3.312
Er^{3+}	a	4.576	0 807	1.463
	b	4673	1.372	1.336
	c	3.651	0.694	0.798

Table 3.6 Observed and calculated Oscillator strengths of Nd^{3+} ions in (a) $30\text{Li}_2\text{O}-69\text{B}_2\text{O}_3-1\text{Nd}_2\text{O}_3$, (b) $30\text{CaO}-69\text{B}_2\text{O}_3-1\text{Nd}_2\text{O}_3$ and (c) $30\text{BaO}-69\text{B}_2\text{O}_3-1\text{Nd}_2\text{O}_3$ glass systems.

System	a		b		c	
Transition	P(10^{-8})		P (10^{-8})		P (10^{-8})	
from $^4\text{I}_{9/2}$	obs	cal	obs	cal	obs	cal
$^4\text{F}_{3/2}$	82	83	69	171	71	145
$^4\text{F}_{5/2} \text{ } ^2\text{H}_{9/2}$	302	311	446	484	457	468
$^4\text{S}_{3/2} \text{ } ^4\text{F}_{7/2}$	323	344	475	471	468	487
$^4\text{F}_{9/2}$	25	26	45	38	37	38
$^2\text{H}_{11/2}$	7	7	13	10	12	10
$^4\text{G}_{5/2} \text{ } ^2\text{G}_{7/2}$	847	855	1488	1496	1532	1542
$^4\text{G}_{7/2} \text{ } ^4\text{G}_{9/2}$	347	232	525	416	520	416
$^2\text{K}_{15/2} \text{ } ^2\text{G}_{9/2} \text{ } ^2\text{D}_{3/2} \text{ } ^4\text{G}_{11/2}$	68	51	120	90	89	82
$^2\text{P}_{1/2}$	16	19	28	46	27	37
$^4\text{D}_{3/2}$	374	398	-	-	708	722
rms	± 38		± 52		± 59	

Table 3.7 Observed and calculated Oscillator strengths of Er^{3+} ions in (a) $30\text{Li}_2\text{O}-69\text{B}_2\text{O}_3-1\text{Er}_2\text{O}_3$, (b) $30\text{CaO}-69\text{B}_2\text{O}_3-1\text{Er}_2\text{O}_3$ and (c) $30\text{BaO}-69\text{B}_2\text{O}_3-1\text{Ln}_2\text{O}_3$ glass systems.

System	a		b		c	
Transition	P (10^{-8})		P(10^{-8})		P(10^{-8})	
from $^4\text{I}_{15/2}$	obs	cal	obs	cal	obs	cal
$^4\text{I}_{13/2}$	211	143	191	140	103	84
$^4\text{I}_{11/2}$	49	68	67	65	33	41
$^4\text{I}_{9/2}$	20	18	19	30	13	15
$^4\text{F}_{9/2}$	177	161	184	202	130	111
$^4\text{S}_{3/2}$	65	56	64	53	48	31
$^2\text{H}_{11/2}$	733	680	676	752	574	556
$^4\text{F}_{7/2}$	170	201	163	207	116	120
$^4\text{F}_{5/2}$	56	68	52	64	34	38
$^4\text{F}_{3/2}$	29	39	23	37	17	22
$^2\text{G}_{9/2}$	63	80	64	78	36	46
$^4\text{G}_{11/2}$	1176	1205	1374	1332	976	985
$^4\text{G}_{9/2} \rightarrow ^2\text{G}_{7/2}$	193	204	281	239	119	139
rms	± 29		± 35		± 13	

Table 3.8 The calculated radiative properties (A , β_R) for selected transitions of Nd^{3+} and Er^{3+} in (a) $30\text{Li}_2\text{O}-69\text{B}_2\text{O}_3-1\text{Ln}_2\text{O}_3$, (b) $30\text{CaO}-69\text{B}_2\text{O}_3-1\text{Ln}_2\text{O}_3$ and (c) $30\text{BaO}-69\text{B}_2\text{O}_3-1\text{Ln}_2\text{O}_3$ glass systems.

Lanthanide	Transitions	a		b		c	
ion		$A \text{ sec}^{-1}$	β_R	$A \text{ sec}^{-1}$	β_R	$A \text{ sec}^{-1}$	β_R
Nd^{3+}	$^4\text{F}_{3/2} \rightarrow ^4\text{I}_{9/2}$	443	0.358	946	0.439	799	0.401
	$\rightarrow ^4\text{I}_{11/2}$	651	0.526	1015	0.471	991	0.497
	$\rightarrow ^4\text{I}_{13/2}$	136	0.110	186	0.086	193	0.097
Er^{3+}	$^4\text{S}_{3/2} \rightarrow ^4\text{I}_{15/2}$	1291	0.676	1264	0.673	755	0.676
	$\rightarrow ^4\text{I}_{13/2}$	516	0.270	505	0.269	299	0.268
	$\rightarrow ^4\text{I}_{11/2}$	40	0.021	40	0.022	23	0.021
	$\rightarrow ^4\text{I}_{9/2}$	61	0.032	67	0.036	38	0.035
	$^4\text{I}_{11/2} \rightarrow ^4\text{I}_{15/2}$	155	0.779	154	0.762	98	0.703
	$\rightarrow ^4\text{I}_{13/2}$	44	0.221	48	0.238	42	0.297
	$^4\text{I}_{13/2} \rightarrow ^4\text{I}_{15/2}$	256	1.000	277	1.000	233	1.000

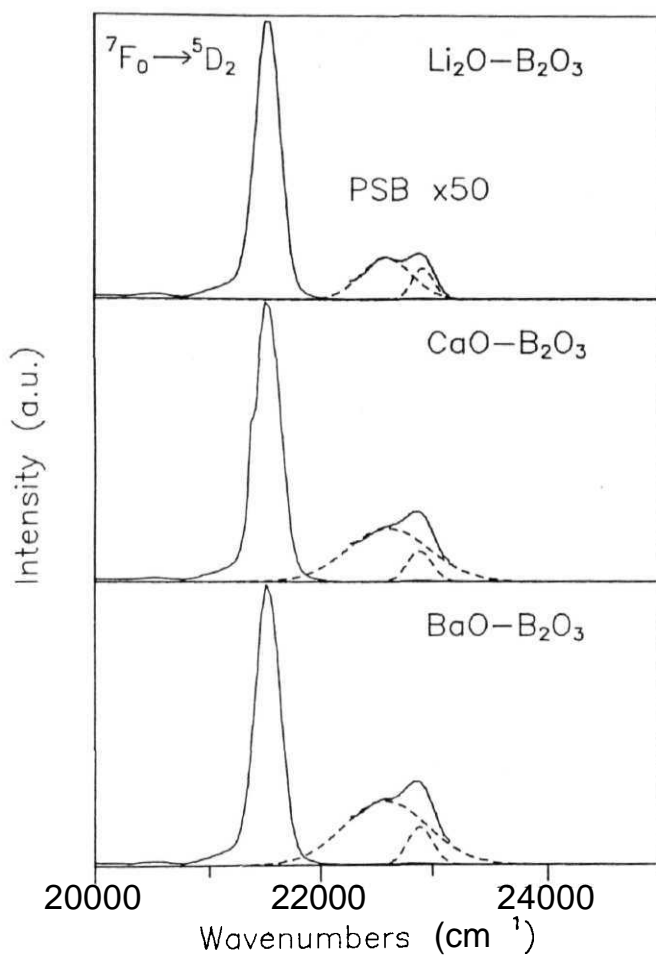


Figure 3.1 Phonon side band spectra of Eu^{3+} doped $\text{Li}_2\text{O}-\text{B}_2\text{O}_3$, $\text{CaO}-\text{B}_2\text{O}_3$ and $\text{BaO}-\text{B}_2\text{O}_3$ glasses. The dashed curves represent the resolved gaussians of the spectra. The solid curves are the experimental spectra $\lambda_{\text{em}}=613 \text{ nm}$.

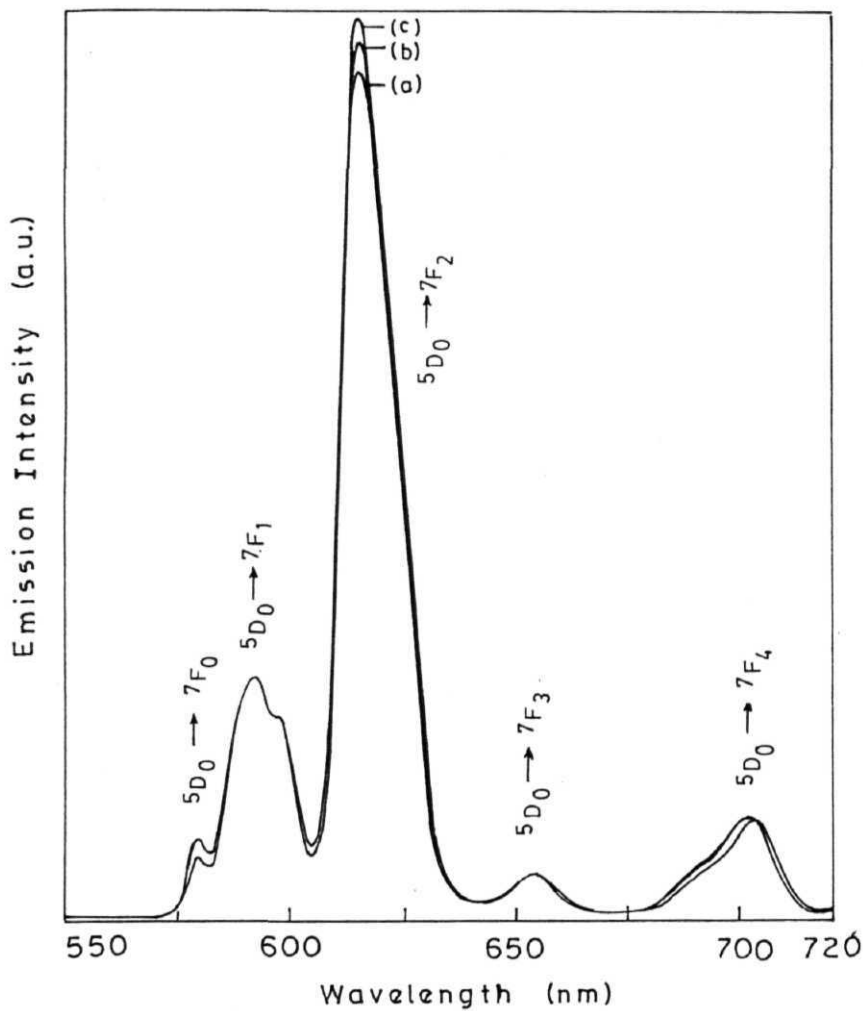


Figure 3.2 Room temperature emission spectra of Eu^{3+} doped (a) $\text{Li}_2\text{O-B}_2\text{O}_3$, (b) $\text{CaO-B}_2\text{O}_3$ and (c) $\text{BaO-B}_2\text{O}_3$ glasses. $\lambda_{\text{ex}}=395$ nm. All spectra are normalized to unit ${}^5\text{D}_0 \rightarrow {}^7\text{F}_1$ peak intensity.

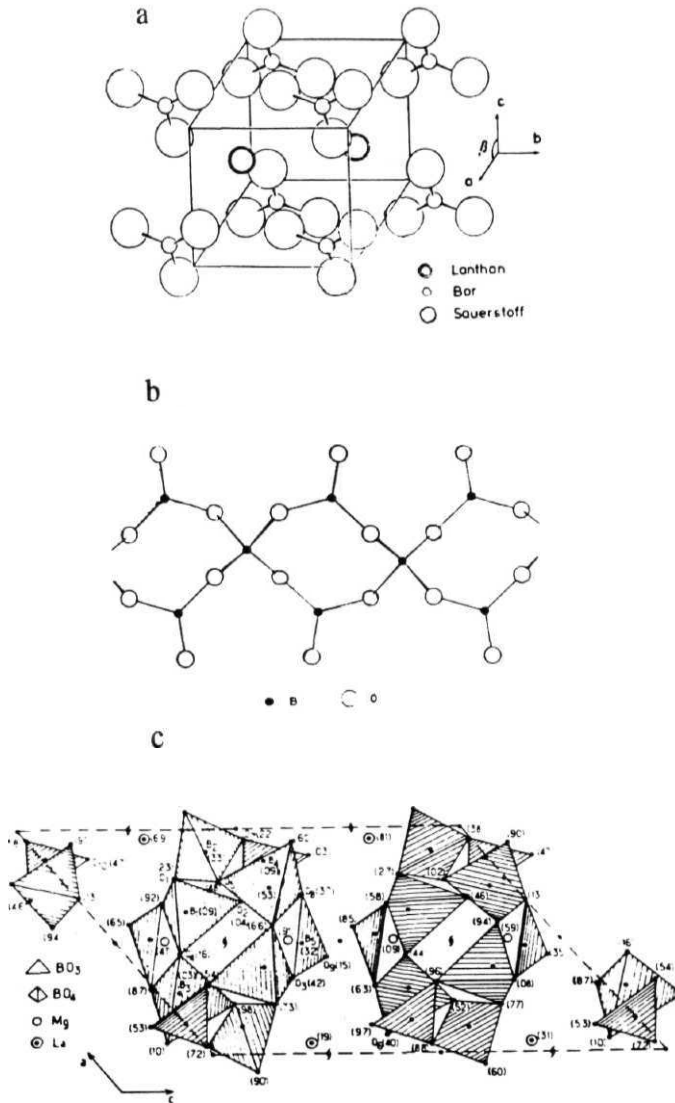


Figure 3.3 (a) The structure of LaBO_3 (b) $[\text{B}_3\text{O}_6]_\alpha$ network in $\text{La}_2\text{O}_3-3\text{B}_2\text{O}_3$ and (c) Projection of the structure, $\text{LaMg}(\text{B}_5\text{O}_{10})$ on the (010) plane.

3.2 Optical Absorption and Emission Spectral Studies of Pr^{3+} , Nd^{3+} , Sm^{3+} , Eu^{3+} , Tb^{3+} , Dy^{3+} , Ho^{3+} , Er^{3+} and Tm^{3+} Ions in $\text{CaO-Al}_2\text{O}_3\text{-B}_2\text{O}_3$ Glass System

The $\text{CaO-Al}_2\text{O}_3\text{-B}_2\text{O}_3$ (calabo) glass system has several features of interest. the early interest in this glass pertains to its unusually low d.c. conductivity properties.²⁹⁻³¹ Bishop and Bray have carried out detailed nuclear magnetic resonance studies to determine the influence of concentration of CaO on the coordinations of aluminium and boron atoms.³² They established that this ternary glass may in principle be treated as a binary glass with CaO as the modifier oxide and B_2O_3 and Al_2O_3 serving jointly as the network formers. Our own interest in this glass as host matrix for the lanthanide ions stems from the following features. Relatively large concentration of transition metal ions in the oxide forms can be dissolved in this glass.⁵ The glass can be prepared with relative ease even in bulk quantities from a melt at fairly low temperatures. The ternary glasses in this family exhibit high thermal stability and transparency in the visible region. The glass can be conveniently machined to desired shapes. If required the glasses in this family can be prepared with high optical homogeneity by sol-gel route.

The optical spectra of lanthanides in glasses are of interest for two reasons. The absorption spectral studies of lanthanide ions are of interest for the following reasons. The effects of chemical bonding and weak covalency of the lanthanide ions are of basic interest and can be well studied conveniently through their absorption spectra.¹ Further, the absorption spectral studies can be extended to obtaining radiative parameters of the emission transitions. Secondly many of the Ln^{3+} ions exhibit potential laser transitions.^{1,2} The radiative properties derived from the absorption spectra together with emission spectral studies can throw light on identifying suitable host matrices for development of new laser systems. We present here the results of detailed absorption spectral studies of almost the entire series of the rare earths ions, Pr^{3+} , Nd^{3+} , Sm^{3+} , Dy^{3+} , Ho^{3+} , Er^{3+} and Tm^{3+} doped in the calabo glass with composition 32 CaO -16 Al_2O_3 -49 B_2O_3 -

1 6Ln₂O₃ These rare earth ions are chosen as they give rise to a large number of absorption transitions in the spectral region viz., 300 to 2200 nm.²⁴ The Judd-Ofelt parameters in all these cases can be reliably evaluated. While in crystalline systems the Judd-Ofelt parameters have been systematically evaluated over the entire rare earth series, to our knowledge work of this nature extended over the entire series in glass systems is limited.^{33,34} We also report here the emission spectral studies of **Sm³⁺**, **Eu³⁺**, **Tb³⁺** and **Dy³⁺** doped in this borate glass. Yet another reason for undertaking studies of this kind in this glass matrix is that investigations of optical properties of lanthanide ions in this glass matrix lends itself for a comparative study in borate glass matrices with and without **Al³⁺**. The results of such a study in the related glass without **Al³⁺**, viz., **CaO-B₂O₃** has been presented in the earlier section. Such a comparative study is of interest as the presence of trivalent aluminium is known to influence not only the solubility of the rare earth ions in glass systems but also the optical properties of the dopant ions significantly.^{5,11} For the same reason such a comparative study has been extended to **Ln³⁺** doped phosphate glasses with and without aluminium and the results are presented in the next chapter. Thus the studies on these glass systems and those of earlier workers on silicate glasses should together provide useful information on the influence of **Al³⁺** ions on the optical properties of the lanthanide ions doped in different glass matrices in general.¹¹

3.2.1 Preparation of Calcium Alumino Borate Glasses

The glass samples with compositions in mol % **32.8CaO-16.4Al₂O₃-49.2B₂O₃-1 6Ln₂O₃** (Ln = Pr, Nd, **Sm**, **Eu**, Tb, Dy, Ho, Er or **Tm**) (CAB) were prepared by the following procedure. Calculated amounts of calcium carbonate (BDH), aluminum oxide (SD), boric acid (Analar) and respective rare earth oxides (Aldrich Chem. Co.) for 10 g of glass in single batch were ground to give a homogeneous mixture. The finely ground mixture was then placed in a silica crucible and heated in an electric furnace. A slow heating rate was initially maintained until the temperature reached 300 °C and the dehydration of **H₃BO₃** was complete. The temperature was subsequently raised to 830 °C

Chapter 3

and kept at this temperature until the decomposition of calcium carbonate was complete. This step was followed by rapidly raising the temperature to 950 °C. The crucible containing the melt was constantly agitated to ensure homogeneous mixing. Sufficient time was allowed for the melt to become visibly homogeneous and bubble free. Then the melt was poured into a slot in a stainless steel plate and quenched rapidly by pressing with another stainless steel plate. Typical weight loss on melting under experimental conditions indicated that the actual compositions should be within 0.5 % of the values quoted for the components. The samples were annealed at a temperature 20 °C below T_g and subsequently polished with commercial media and water free lubricant. The samples could be obtained with good transparency and uniform thickness of 0.2 cm and 2.0 cm diameter. The amorphous nature of the glass samples were confirmed by recording the powder x-ray **diffraction** spectra.

3.2.2 Results and Discussion

The absorption spectra of Pr^{3+} , Nd^{3+} , Sm^{3+} , Dy^{3+} , Ho^{3+} , Er^{3+} and Tm^{3+} ions in cabal glass of composition $32.8\text{CaO}-16.4\text{Al}_2\text{O}_3-49.2\text{B}_2\text{O}_3-1.6\text{Ln}_2\text{O}_3$ are reproduced in figures 3.4-3.10 respectively. The observed and calculated transition energies for Pr^{3+} , Nd^{3+} , Er^{3+} and Tm^{3+} ions doped **glasses** for which calculations are done as discussed in chapter 2 using the matrices with terms corresponding to all the J values show good agreement as shown by the small **rms** deviations (tables 3.9 and 3.10). The corresponding spectroscopic parameters are reproduced in table 3.11. In the case of Tm^{3+} the transition energies are found to be not sensitive to y and can be analyzed with six parameters only as observed by earlier **workers**.^{35,36} The eigenvector components of the energy matrices are reproduced in tables 3.12-3.15. The **Judd-Ofelt** parameters obtained from a least squares analysis of experimental oscillator strengths of Pr^{3+} , Nd^{3+} , Sm^{3+} , Dy^{3+} , Ho^{3+} , Er^{3+} and Tm^{3+} are given in tables 3.16. The experimental oscillator strengths are compared with those calculated using the resultant Judd-Ofelt parameters in tables 3.17-3.21. For Pr^{3+} , excluding the hypersensitive $^3\text{P}_2 \leftarrow ^3\text{H}_4$ transition improves the match between experimental and calculated oscillator strengths significantly. As the

number of transitions observed for the absorption spectra of Eu^{3+} and Tb^{3+} and limited due to strong self absorption below 400 nm by the parent glass matrix and as a result the **Judd-Ofelt** parameters could not be obtained reliably, no attempts were made to extend these calculations for these ions.

The energies and spectral profiles of certain transitions in the absorption spectra of Pr^{3+} and Nd^{34} ions throw light on their **coordination**.^{25,37,38} The $^3\text{P}_0 \leftarrow ^3\text{H}_4$ transition for Pr^{34} and $^2\text{P}_{1/2} \leftarrow ^4\text{I}_{9/2}$ transition for Nd^{34} give rise to values in the range 20,450 to 20,850 cm^{-1} and 23,100 to 23,400 cm^{-1} respectively indicating 8 or 9 coordination with oxide ligand **atoms**. The energies of 20,790 cm^{-1} for the $^3\text{P}_0 \leftarrow ^3\text{H}_4$ transition for Pr^{3+} and 23,337 cm^{-1} for the $^2\text{P}_{1/2} \leftarrow ^4\text{I}_{9/2}$ transition for Nd^{34} and observed profiles in the present system suggest predominantly 8-9 coordination. For Ln^{3+} ions doped in glasses eight coordination with C_2 symmetry may be visualized by four pairs of oxide ions coming from four tetrahedra constituted by AlO_4 or BO_4 units.³⁹ In the present system the Pr^{34} and Nd^{3+} may achieve eight coordination by occupying substitutional sites in the place of Ca^{2+} ions as well. This is especially so as Ca^{2+} shows 8-coordination in oxide matrices and its ionic radius (0.99 Å) is close to that of the Ln^{3+} ions under study (1.04-1.16 Å).⁴⁰

The Ω_2 values for Ln^{3+} ions in the present system and glasses in general are intermediate between much smaller values observed for crystalline oxides and fluorides and larger values reported for chelating ligands.^{33,34,41,42} The dopants in glassy systems are randomly distributed over non-equivalent sites with a distribution in the crystal-fields as evidenced by structure simulation studies⁴⁵ and large line widths observed in their optical⁴⁶ and esr **spectra**.⁴⁷ A large number of dopant ions will thus occupy sites with noncentro symmetric potential which is known to contribute significantly to Ω_2 .⁴⁸ Thus the Ω_2 values for Ln^{34} ions in glassy hosts are higher than in crystalline systems with similar ligand atoms. On the other hand covalency contributes significantly to Ω_2 for rare earth complexes with chelating ligands.^{43,44} Ω_2 in the present system shows an increasing

trend as we go higher up in the rare earth series showing a maximum in the middle of the series and decreases after Dy^{3+} ($4f^9$) (figure 3.11). This trend is different from the trends observed by earlier workers in **fluoride** and fluorozirconate glasses and in oxyfluoride glass matrices discussed later where Ω_2 shows an increasing trend along the **series**.^{34,49} Theoretical values for Ω_2 for free ions predict a decreasing trend with increasing atomic number.³³ However Ω_2 values for crystalline systems show much higher values than those of the free ions with significantly less **slope**. Such discrepancies in crystalline systems arise due to the influences of the dielectric of the **medium**, covalency and the nephelauxetic **effect**.^{6,33,48,50} The trends observed for glass matrices are quite different from those reported for crystalline **systems**.^{33,34} The much higher f_2 values with qualitatively different trends observed in glassy matrices may be understood in terms of the following factors unique for the glass systems. The dopant ions may occupy sites with different **coordination**. Even with sites with one type of coordination, differences in the distortions at the Ln^{3+} sites will lead to a distribution in the crystal fields. The sites with noncentro symmetric potential will lead to an enhancement of f_2 .^{5,48} Structural studies of Ln^{3+} ions in crystalline systems show a range of coordination number from 4 to 12 with strong preference for lower coordination number with increasing atomic number.^{24,51} Isomorphous series with single type of coordination are also **known**.^{13,26} Thus in glass matrices the Ln^{3+} ions can exhibit varied preferences such as occupying sites with single type of coordination over the entire series or with preference for lower coordination number as suggested above as we go along the series. Such variations in principle can account for the different trends observed for Ω_2 in different glass matrices. Crystalline borates show that end members such as Er^{3+} can have 6 or 10 coordination as suggested in the last section. The observed trend in Ω_2 presumably arises due to occupation of sites with 8-10 coordination over the entire series. Thus assuming that contribution to Ω_2 due to covalency is not much different, large distortion from cubic symmetry for the rare earth ions in the middle of the series such as Sm^{3+} , Eu^{3+} and Dy^{3+} may account for the observed trend. Ω_4 and Ω_6 show a rapid decrease followed by a

slow increase at the end as we go higher up in the series (figure 3.11). This is a common feature for Ln^{3+} ions in other glass hosts and crystalline systems such as Y_2O_3 as well.^{33,34} The values of Ω_4 and Ω_6 are strongly influenced by the vibrational levels associated with the central rare earth ion bound to the ligand atoms.^{33,48} Spectral studies of vibronic transitions for rare earth systems show that they are most intense for ions at the beginning and end of the series with Eu^{3+} exhibiting a minimum vibrational structure^{33,48}. Contribution due to vibrational interactions by terms common to f_4 and Ω_6 but not Ω_2 can qualitatively account for the observed trends in these cases.³³

The $^3\text{P}_2 \leftarrow ^3\text{H}_4$ transition for Pr^{3+} is known to be hypersensitive.⁴⁸ Its intensity is known to vary significantly with environment due to strong 4f-5d mixing and/or due to significant contribution by the terms corresponding to odd values of A, in eqn. (2.14) of chapter 2.^{42,53} The exceptional behavior of this transition is brought out by the significant changes in the fix ($\lambda=2,4,6$) values when it is excluded from the calculation (table 3.16).

The radiative lifetimes (τ_R) of fluorescent levels and branching ratios (PR) have been obtained for all transitions. These values are reproduced in tables 3.22-3.25. These parameters are of value particularly for the lasing transitions. The τ_R and β_R values for the lasing transitions are also reproduced separately in tables 3.26 and 3.27 respectively. The radiative properties of Ln^{3+} ions in glasses depend on a number of factors such as the network former and modifier in the glass and its refractive index.¹ For a number of rare earth ions doped in glasses both calculated and observed τ_R and β_R values are available.⁵⁴⁻⁵⁸ In such cases there is close agreement between measured and calculated branching ratios.^{42,53,59} Experimental lifetimes are generally lower than calculated values but show the same trend, viz., $^1\text{D}_2 \gg ^3\text{P}_0$ for Pr^{3+} , $^1\text{I}_{13/2} \gg ^1\text{I}_{11/2} \gg ^3\text{S}_{3/2} = ^3\text{F}_4$ for Er^{3+} , $^1\text{G}_4 \gg ^1\text{D}_2$ for Tm^{3+} . Our own calculated TR values follow the above trend. The experimental values for radiative lifetimes wherever available are found to lie between 60 and 80 % of calculated values depending on the quantum efficiency for the transition.

The differences between the measured and calculated lifetimes arise due to multiphonon relaxation on account of the intermediate energy levels and cross relaxation between pairs of ions.^{42,49,57-61} For transitions known to be potential lasers, the β_R values characterize the lasing power of the transition. The laser transition $^3P_0 \rightarrow ^3H_6$ of Pr^{3+} has a relatively lower β_R value in the tellurite glasses in the range 0.012 to 0.084 compared to much higher values for the phosphate glasses lying between 0.124 and 0.218.^{54-56,62} The β_R value obtained for the present ternary **alumino** borate glass is found to be comparable to that of phosphate glasses with a value of 0.201 lying on the higher side of the above range. The important lasing transition $^4F_{3/2} \rightarrow ^4I_{11/2}$ for Nd^{3+} has a β_R value ranging between 0.430 and 0.650 showing a strong influence of the glass former in the host matrix, viz., borate < fluoride < **phosphate**.^{1,54-56,63} The value for the present case, viz., 0.450 lies on the lower side within the same **range** β_R value for the lasing transition $^4S_{3/2} \rightarrow ^4I_{13/2}$ of Er^{3+} lies within the narrow limit of 0.24 to 0.28 reported for a number of glass systems.⁵⁴⁻⁵⁶

The emission spectra of 32 **8CaO-16 4Al₂O₃-49 2B₂O₃-1 6Ln₂O₃** (Ln= **Sm**, **Eu**, **Tb** and **Dy**) are reproduced in figures 3.12-3.15 **respectively**. The emission spectra of **Sm³⁺** and **Dy³⁺** consist of transitions from $^4G_{5/2}$ and $^4F_{9/2}$ respectively. The radiative properties, viz., the observed and calculated branching ratios (PR) and stimulated emission cross sections for the transitions of **Sm³⁺** and **Dy³⁺** ions doped in **CaO-Al₂O₃-B₂O₃** glass are given in table 3.28. The branching ratios derived from emission spectral intensities show good agreement with values calculated from Judd-Ofelt parameters in both the cases. The stimulated emission cross sections for the transitions of these ions are less in magnitude than for the transitions of other rare earth ions.^{42,60} The emission spectra of **Eu³⁺** and **Tb³⁺** consist of transitions only from the 5D_0 and 5D_4 levels respectively. The absence of emission transitions from higher excited states viz., 5D_1 (J= 1,2,3) of **Eu³⁺** and 5D_3 of **Tb³⁺** are due to the high phonon energy maximum of 1340-1480 cm⁻¹ of the host facilitating nonradiative **decay**.⁶

For **Eu** ions two intense emission transitions appear corresponding to ${}^5D_0 \rightarrow {}^7F_2$ at 615.5 nm in the red region and ${}^5D_0 \rightarrow {}^7F_1$ at 592.5 nm in the orange one. Their relative intensities denoted by R/O is a sensitive function of covalency and site asymmetry.^{17,18} In the case of **Dy**³⁺ two dominant emissions occur due to ${}^4F_{9/2} \rightarrow {}^6H_{13/2}$ at 574.8 nm in the yellow region and ${}^4F_{9/2} \rightarrow {}^6H_{15/2}$ at 483.0 nm in the blue one. The Y/B ratio in crystalline systems is shown to follow a trend parallel to the R/O ratio of **Eu**³⁺.¹⁸ The R/O ratio of **Eu**³⁺ and the Y/B ratio of **Dy**³⁺ doped in **CaO-Al₂O₃-B₂O₃** glass are compared with values obtained for these ions in **CaO-B₂O₃** glass system in table 3.29. The influence of **Al**³⁺ ions in borate glasses on the intensities of the hypersensitive transitions for **Eu**³⁺ and **Dy**³⁺ ions is not significant as evidenced by the small differences in the values of R/O and Y/B ratios between these two glass matrices.⁴⁸

The phonon side band spectrum of **Eu**³⁺ ion doped in this glass is also measured by monitoring the emission at 615.5 nm corresponding to the transition ${}^5D_0 \rightarrow {}^7F_2$.^{19,20} The phonon energies ($\hbar\omega$) and the electron phonon coupling strengths (g) for **CaO-Al₂O₃-B₂O₃** and **CaO-B₂O₃** glasses are also included in table 3.29. The phonon side band in this case is found to be a single unresolved band unlike in **CaO-B₂O₃** glass where two components were observed. The phonon energy maximum is found to be 1317 cm⁻¹. This may be identified with the B-O stretching frequencies in **BO₃** groups indicating that the **Eu**³⁺ ions are closely with these groups. The electron phonon coupling strength is found to be higher for **CaO-B₂O₃** than the **CaO-Al₂O₃-B₂O₃** glass system.

3.2.3 Conclusions

The absorption spectra of **Ln**³⁺ (**Pr**³⁺, **Nd**³⁺, **Sm**³⁺, **Dy**³⁺, **Ho**³⁺, **Er**³⁺, **Tm**³⁺) have been analyzed for spectral and Judd-Ofelt parameters. Analysis of absorption spectra using a full matrix diagonalisation procedure is found to lead to good match between experimental and calculated transition energies. The Judd-Ofelt phenomenological model provides a very useful framework to analyze the observed relative intensities and correlate results of different rare earth ions doped in a parent matrix of interest. The **Ln**³⁺ ion doped in glasses exhibit higher Ω_2 values compared to the same ions in crystalline

lattices with similar ligand atoms. This is attributed to enhanced contributions by large number of Ln^{3+} ions occupying sites with noncentro symmetric potential. Ω_2 in the present system shows an increasing trend as we go higher up in the rare earth series showing a maximum in the middle of the series and decreases after $\text{Dy}^{3+}(4f^9)$. The observed trend in Ω_2 presumably arises due to the dopant ions having 8-10 coordination over the entire series. with the rare earth ions in the middle of the series occupying sites with larger distortion from cubic symmetry. This will lead to larger contribution to Ω_2 due to noncentro symmetric potential for the rare earth ions in the middle of the series. The values for Ω_4 and Ω_6 show a rapid fall followed by a slowly increasing trend at the end with increasing atomic number suggesting a significant role in the contribution to intensity by vibrational interactions. A comparison of radiative lifetimes of different fluorescent levels in the Ln^{3+} ions under study shows that their relative values in different glassy hosts including the present system follow similar trends with regard to lifetimes of the excited states. The branching ratio for the laser transition ${}^3\text{P}_0 \rightarrow {}^3\text{H}_6$ for Pr^{3+} in the present system is found to be on the higher side of the range of values reported for this ion in different glass hosts. On the other hand for Nd^{3+} for the lasing transition ${}^4\text{F}_{3/2} \rightarrow {}^4\text{I}_{13/2}$ the value lies on the lower side of the range of values reported. For Er^{3+} for the transition of interest ${}^4\text{S}_{3/2} \rightarrow {}^4\text{I}_{13/2}$ the β_R lies within the narrow range observed for different types of glasses as host materials. The stimulated emission cross sections (σ_p) for the transitions of Sm^{3+} , Dy^{3+} ions are less by an order of magnitude than values reported for other rare earth ions. The branching ratios obtained from Judd-Ofelt parameters for these ions show good agreement with values derived from emission spectra. A comparison of the R/O and Y/B ratios for Sm^{3+} and Dy^{3+} ions in the $\text{CaO-Al}_2\text{O}_3\text{-B}_2\text{O}_3$ and $\text{CaO-B}_2\text{O}_3$ glasses shows that the presence of Al^{3+} ions do not influence the hypersensitive transitions in the emission spectra significantly. The phonon side band spectrum of Eu^{3+} ions in $\text{CaO-Al}_2\text{O}_3\text{-B}_2\text{O}_3$ glass matrix unlike in $\text{CaO-B}_2\text{O}_3$ shows a single component occurring at 1317 cm^{-1} due to association with BO_3 groups and its electron phonon coupling strength is found to be lower than that of $\text{CaO-B}_2\text{O}_3$ glass.

Table 3.9 Observed and calculated energy levels in cm^{-1} of Pr^{3+} and Tm^{3+} ions in 32 CaO -16 $4\text{Al}_2\text{O}_3$ -49 $2\text{B}_2\text{O}_3$ -1.6 Ln_2O_3 glass system

Pr^{3+}			Tm^{3+}		
Terms	E_{obs}	E_{cal}	Terms	E_{obs}	E_{cal}
from ^1H , (cm^{-1})		(cm^{-1})	from $^3\text{H}_6$	(cm^{-1})	(cm^{-1})
$^3\text{F}_2$	5320	5379	$^3\text{F}_4$	5890	5790
$^3\text{F}_3$	6639	6638	$^3\text{H}_5$	8297	8297
$^3\text{F}_4$	7063	7016	$^3\text{H}_4$	12675	12732
$^1\text{D}_2$	16983	16982	$^3\text{F}_3$	14660	14660
$^3\text{P}_0$	20790	20789	$^3\text{F}_2$	15232	15237
$^3\text{P}_1$	21321	21320	$^1\text{G}_4$	21504	21483
$^1\text{I}_6$	21689	21680	$^1\text{D}_2$	28248	28260
$^3\text{P}_2$	22421	22410			
rms		± 26			± 36

Table 3.10 Observed and calculated energy levels in cm^{-1} of Nd^{3+} and Er^{3+} ions in 32 CaO -16.4 Al_2O_3 -49.2 B_2O_3 -1.6 Ln_2O_3 glass system.

Nd^{3+}			Er^{3+}		
Terms	E_{obs}	E_{cal}	Terms	E_{obs}	E_{cal}
from*19a (cm^{-1})	(cm^{-1})	(cm^{-1})	from $^4\text{I}_{15/2}$	(cm^{-1})	(cm^{-1})
$^4\text{F}_{3/2}$	11402	11425	$^4\text{I}_{13/2}$	6538	6485
$^4\text{F}_{5/2}$	12422	12482	$^4\text{I}_{11/2}$	10198	10104
$^2\text{H}_{9/2}$	12562	12509	$^4\text{I}_{9/2}$	12441	12365
$^4\text{S}_{3/2}$	13360	13334	$^4\text{F}_{9/2}$	15384	15353
$^4\text{F}_{7/2}$	13487	13470	$^4\text{S}_{3/2}$	18497	18678
$^4\text{F}_{9/2}$	14658	14700	$^2\text{H}_{11/2}$	19275	19273
$^2\text{H}_{11/2}$	15713	15746	$^4\text{F}_{7/2}$	20546	20611
$^4\text{G}_{5/2}$	17123	17166	$^4\text{F}_{5/2}$	22261	22214
$^2\text{G}_{7/2}$	17467	17255	$^4\text{F}_{3/2}$	22696	22620
$^4\text{G}_{7/2}$	19043	19029	$^2\text{H}_{9/2}$	24660	24638
$^4\text{G}_{9/2}$	19535	19481	$^4\text{G}_{11/2}$	26609	26682
$^2\text{G}_{9/2}$	21190	21012	$^4\text{G}_{9/2}$	27525	27666
$^2\text{P}_{1/2}$	23337	23300	$^2\text{G}_{7/2}$	28192	28172
rms	± 36			± 43	

Table 3.11 Spectroscopic parameters for (in cm^{-1}) the Pr^{3+} , Nd^{3+} , Er^{3+} and Tm^{3+} ions in 32 8CaO -16 $\text{4Al}_2\text{O}_3$ -49 $\text{2B}_2\text{O}_3$ -1 $\text{6Ln}_2\text{O}_3$ glass system.

Parameter (cm^{-1})	Pr^{3+}	Nd^{3+}	Er^{3+}	Tm^{3+}
F^2	71302	73629	98605	105477
F^4	54280	53782	72666	78555
F^6	36664	34093	49864	58375
E^1	4851.98	4843.00	6628.00	7261.51
E^2	2247	23.50	31.72	34.21
E^3	476.78	503.70	658.40	685.05
a	21.10	21.10	18.20	14.67
β	-1681.70	-575.00	-615.00	-923.49
y	1340.00	1180.00	1395.00	0.00
γ	68033	877.00	2377.00	2663.90
E^1/E^3	10.18	9.61	10.06	10.59
E^2/E^3	0.047	0.046	0.048	0.049
rms	± 26	± 36	± 43	± 44

Table 3.12 Computed eigenvalues and eigenvector components for Pr^{3+} ion in 32 8CaO -16 $\text{4Al}_2\text{O}_3$ -49 $\text{2B}_2\text{O}_3$ -1.6 Pr_2O_3 glass system.

SL	J	E (cm^{-1})	Eigenvector components		
^3H	4	0	+0.9880 ^3H	+0.1478 ^1G	-0.0240 ^3F
^3H	5	1886	1.0000 ^3H		
^3H	6	3888	-0.0468 ^1I	+0.9989 ^3H	
^3F	2	5379	+0.9898 ^3F	+0.1416 ^1D	-0.0122 ^3P
^3F	3	6638	1.0000 ^3F		
^3F	4	7016	-0.1088 ^3H	+0.5987 ^1G	-0.7935 ^3F
^1G	4	9685	-0.1029 ^3H	+0.7872 ^1G	+0.6080 ^3F
^1D	2	16982	-0.1395 ^3F	+0.9516 ^1D	-0.2736 ^3P
^3P	0	20790	+0.9967 ^3P	+0.0807 ^1S	
^3P	1	21320	1.0000 ^3P		
^1I	6	21680	+0.9989 ^1I	+0.0468 ^3H	
^3P	2	22421	-0.0270 ^3F	+0.2726 ^1D	+0.9617 ^3P
^1S	0	50085	-0.0807 ^3P	+0.9967 ^1S	

Table 3.13 Computed eigenvalues and eigenvector components for Nd^{3+} ion in 32 8CaO-16 4Al₂O₃-49.2B₂O₃-1 6Nd₂O₃ glass system

SL	J	E(cm ⁻¹)	Eigenvector components							
T	9/2	0	+0.0030 ⁴ F	+0.0076 ⁴ G	-0.0166 ² G	+ 0.0147 ³ G'	+0.0549 ² H	-0.1648 ² H'	+0.9844 ⁴ I	
⁴ I	11/2	1861	+0.0071 ⁴ G	+0.0349 ² H	-0.0951 ² H'	+0.9947 ⁴ I	-0.0145 ² I			
	13/2	3846	+0.9978 ⁴ I	+0.0223 ² I	+0.0617 ² K					
⁴ I	15/2	5909	-0.9936 ⁴ I	-0.1125 ² K	+0.0083 ² L					
⁴ F	3/2	11425	-0.0555 ⁴ S	-0.0624 ² P	-0.0126 ⁴ D	+0.2279 ² D	-0.0646 ² D'	+0.9678 ⁴ F		
⁴ F	5/2	12482	+0.0030 ⁴ D	-0.1489 ² D	+0.0198 ² D'	-0.9874 ⁴ F	+0.0289 ² F	+0.0319 ² F'	+0.0202 ⁴ G	
² H	9/2	12509	-0.3354 ⁴ F	-0.1415 ⁴ G	+0.3255 ² G	-0.2709 ² G'	-0.2787 ² H	+0.7656 ² H'	+0.1554 ⁴ I	
⁴ S	3/2	13334	+0.9693 ⁴ S	+0.2279 ² P	+0.0150 ⁴ D	-0.0413 ² D	+0.0034 ² D'	+0.0805 ⁴ F		
⁴ F	7/2	13470	+0.0032 ⁴ D	+0.9652 ² F	-0.0309 ² F	-0.0393 ² F'	+0.0320 ⁴ G	-0.1994 ² G	+0.1577 ² G'	
⁴ F	9/2	14700	-0.8798 ⁴ F	+0.0293 ⁴ G	+0.1452 ² G	-0.0988 ² G'	+0.1349 ² H	-0.4133 ² H'	-0.0703 ⁴ I	
² H	11/2	15746	-0.2343 ⁴ G	-0.3430 ² H	+0.9024 ² H'	+0.0993 ⁴ I	-0.0532 ² I			
⁴ G	5/2	17166	-0.0087 ⁴ D	-0.0013 ² D	+0.0165 ² D'	+0.0252 ⁴ F	+0.0828 ² F	+0.0822 ² F'	+0.9926 ⁴ G	
² G	7/2	17255	-0.0021 ⁴ D	-0.2182 ⁴ F	-0.0160 ² F	-0.0157 ² F'	+0.6170 ⁴ G	-0.5747 ² G	+0.4906 ² G'	
⁴ G	7/2	19029	-0.0077 ⁴ D	+0.1366 ⁴ F	+0.0504 ² F	+0.0548 ² F'	+0.7827 ⁴ G	+0.4732 ² G	-0.3728 ² G'	
² K	13/2	19360	-0.0636 ⁴ I	-0.0982 ² I	+0.9931 ² K					
⁴ G	9/2	19481	+0.1875 ⁴ F	-0.8531 ⁴ G	+0.2940 ² G	-0.2728 ² G'	+0.1150 ² H	-0.2485 ² H'	-0.0328 ⁴ I	
² D	3/2	20802	-0.2015 ⁴ S	+0.6531 ² P	+0.1265 ⁴ D	-0.6731 ² D	+0.1524 ² D'	+0.2009 ⁴ F		
² G	9/2	21012	+0.2790 ⁴ F	+0.4966 ⁴ G	+0.6186 ² G	-0.4930 ² G'	-0.0073 ² H	-0.2213 ² H'	-0.0235 ⁴ I	
² K	15/2	21353	+0.1118 ⁴ I	-0.9718 ² K	+0.2073 ² L					
⁴ G	11/2	21532	+0.9639 ⁴ G	-0.2020 ² H	+0.1719 ² H'	+0.0166 ⁴ I	+0.0059 ² I			
² P	1/2	23300	+0.9736 ² P	+0.2279 ⁴ D						
² D	5/2	23589	+0.0262 ⁴ D	+0.9881 ² D	+0.0110 ² D'	-0.1495 ⁴ F	-0.0181 ² F	-0.0066 ² F'	+0.0071 ⁴ G	
² P	3/2	25692	-0.1281 ⁴ S	+0.7068 ² P	+0.0500 ⁴ D	+0.6456 ² D	-0.2197 ² D'	-0.1278 ⁴ F		
⁴ D	3/2	28326	+0.0133 ⁴ S	-0.0900 ² P	+0.8979 ⁴ D	+0.1656 ² D	+0.3974 ² D'	+0.0058 ⁴ F		
⁴ D	5/2	28420	+0.8736 ⁴ D	-0.0155 ² D	+0.4585 ² D'	+0.0033 ⁴ F	-0.1104 ² F	-0.1136 ² F'	+0.0338 ⁴ G	
² I	11/2	29096	-0.0651 ⁴ G	-0.3734 ² H	-0.1066 ² H'	+0.0168 ⁴ I	+0.9190 ² I			

Chapter 3

Table 3.14 Computed eigenvalues and eigenvector components for Er^{3+} ion in $32.8\text{CaO}-16.4\text{Al}_2\text{O}_3-49.2\text{B}_2\text{O}_3-1.6\text{Er}_2\text{O}_3$ glass system.

SL	J	E(cm^{-1})	Eigenvector components							
^4I	15/2	0	-0.9854 ^4I	+0.1690 ^4K	+0.0171 ^4L					
^4I	13/2	6486	-0.9955 ^4I	-0.0314 ^4I	+0.0887 ^4K					
^4I	11/2	10105	+0.1118 ^4G	-0.1067 ^2H	+0.3834 ^2H	+0.9083 ^4I	+0.0628 ^2I			
^4I	9/2	12366	-0.3465 ^4F	-0.0098 ^4G	-0.2743 ^2G	+0.2191 ^2G	-0.1931 ^2H	+0.4202 ^2H	+0.7366 ^4I	
^4F	9/2	15353	-0.7739 ^4F	-0.0898 ^4G	-0.2969 ^2G	+0.2227 ^2G	+0.0032 ^2H	-0.0769 ^2H	-0.4991 ^4I	
^4S	3/2	18679	+0.8238 ^4S	-0.4311 ^2P	+0.0420 ^2D	-0.2797 ^2D	-0.0184 ^2D	+0.2344 ^4F		
^2H	11/2	19274	-0.5801 ^4G	+0.1476 ^2H	-0.6987 ^2H	+0.3875 ^4I	-0.0562 ^2I			
^2F	7/2	20612	-0.0118 ^4D	-0.9609 ^4F	-0.0478 ^2F	-0.0557 ^2F	-0.0293 ^4G	-0.2133 ^2G	+0.1570 ^2G	
^4F	5/2	22214	+0.0479 ^2D	+0.3599 ^2D	-0.1409 ^2D	-0.9162 ^4F	-0.0431 ^2F	-0.0733 ^2F	+0.0388 ^4G	
^4F	3/2	22620	-0.4101 ^4S	-0.0630 ^2P	+0.0038 ^4D	-0.4486 ^2D	-0.0102 ^2D	+0.7914 ^4F		
^2H	9/2	24639	-0.4930 ^4F	+0.2293 ^4G	+0.4350 ^2G	-0.3876 ^2G	+0.2641 ^2H	-0.4126 ^2H	+0.3531 ^4I	
^4G	11/2	26680	-0.7896 ^4G	-0.3173 ^2H	+0.5017 ^2H	-0.1533 ^4I	+0.0213 ^2I			
^2G	9/2	27666	+0.0313 ^4F	-0.8918 ^4G	-0.0260 ^2G	+0.0649 ^2G	+0.0908 ^2H	-0.3800 ^2H	+0.2144 ^4I	
^2K	15/2	27835	-0.1682 ^4I	-0.9560 ^2K	-0.2403 ^2L					
^2G	7/2	28173	+0.0595 ^2D	+0.1966 ^4F	+0.1486 ^2F	+0.1501 ^2F	-0.6407 ^4G	-0.5161 ^2G	+0.4858 ^2G	
^2P	3/2	31874	-0.3483 ^4S	-0.6071 ^2P	+0.1733 ^2D	-0.4604 ^2D	-0.1758 ^2D	-0.4868 ^4F		
^2K	13/2	33136	+0.0747 ^4I	+0.3078 ^2I	+0.9484 ^2K					
^2P	1/2	33529	-0.9599 ^2P	+0.2800 ^4D						
^4G	5/2	33594	+0.0133 ^4D	-0.1093 ^2D	-0.0876 ^2D	+0.0344 ^4F	-0.1614 ^2F	-0.1870 ^2F	+0.9580 ^4G	
^4G	7/2	34229	+0.0393 ^4D	-0.1616 ^4F	+0.0498 ^2F	+0.0368 ^2F	-0.7391 ^4G	+0.5239 ^2G	-0.3841 ^2G	
^2D	5/2	34707	+0.3591 ^4D	+0.7501 ^2D	-0.4041 ^2D	+0.3783 ^4F	+0.0184 ^2F	-0.0283 ^2F	+0.0275 ^4G	
^4G	9/2	36665	-0.1902 ^4F	-0.3654 ^4G	+0.4914 ^2G	-0.3910 ^2G	-0.2800 ^2H	+0.5663 ^2H	-0.1915 ^4I	
^4D	5/2	39112	+0.6669 ^4D	-0.5309 ^2D	-0.4870 ^2D	-0.0957 ^4F	-0.0363 ^2F	-0.0869 ^2F	-0.1341 ^4G	
^4D	7/2	39606	+0.9727 ^4D	-0.0389 ^4F	+0.1702 ^2F	+0.1027 ^2F	+0.1065 ^4G	+0.0347 ^2G	-0.0097 ^2G	
^2I	11/2	41147	+0.1140 ^4G	-0.5597 ^2H	-0.1304 ^2H	+0.0312 ^4I	-0.8097 ^2I			
^2D	3/2	42505	-0.0813 ^4S	-0.2902 ^2P	+0.7284 ^4D	+0.5332 ^2D	+0.1875 ^2D	+0.2429 ^4F		
^4D	3/2	43310	+0.1561 ^4S	+0.5789 ^2P	+0.4546 ^4D	-0.4138 ^2D	-0.5025 ^2D	+0.0989 ^4F		
^2I	13/2	43895	+0.0571 ^4I	-0.9509 ^2I	+0.3041 ^2K					

Table **3.15** Computed eigenvalues and eigenvector components for Tm^{3+} ion in $32\text{CaO}-16\text{Al}_2\text{O}_3-49\text{B}_2\text{O}_3-1\text{6Tm}_2\text{O}_3$ glass system

SL	J	E (cm^{-1})	Eigenvector components		
^3H	6	0	+0.0931 ^1I	+0.9956 ^3H	
^3F	4	5790	-0.2896 ^3H	+0.5458 ^1G	+0.7862 ^3F
^3H	5	8297	1.0000 ^3H		
^3H	4	12732	+0.7716 ^3H	-0.3528 ^1G	+0.5292 ^3F
^3F	3	14660	1.0000 ^3F		
^3F	2	15237	+0.8772 ^3F	-0.4595 ^1D	-0.1384 ^3P
^1G	4	21483	+0.5662 ^3H	+0.7599 ^1G	-0.3190 ^3F
^1D	2	28260	+0.4355 ^3F	+0.6411 ^1D	+0.6318 ^3P
^1I	6	35171	+0.9956 ^1I	-0.0931 ^3H	
^3P	0	36007	+0.9776 ^3P	-0.2100 ^1S	
^3P	1	36658	1.0000 ^3P		
^3P	2	38548	-0.2016 ^3F	-0.6146 ^1D	+0.7626 ^3P
^1S	0	80949	+0.2100 ^3P	+0.9776 ^1S	

Table 3.16 The **Judd-Ofelt** parameters for lanthanide ions in **32.8CaO-16.4Al₂O₃-49.2B₂O₃-1.6Ln₂O₃** glass system.

Lanthanide ion	$\Omega_2 (10^{-20} \text{ cm}^2)$	$\Omega_4 (10^{-20} \text{ cm}^2)$	$\Omega_6 (10^{-20} \text{ cm}^2)$
Pr³⁺	3.330(4.84)	8.280(8.42)	14.040 (11.080)
Nd³⁺	3.660	5.340	4.460
Sm³⁺	3.814	4.448	2.362
Dy³⁺	6.132	1.818	1.559
Ho³⁺	4.244	2.301	1.396
Er³⁺	3.700	1.360	0.840
Tm³⁺	4.010	2.750	1.260

The values in parenthesis are obtained excluding $^3\text{P}_2 \leftarrow ^3\text{H}_4$ transition.

Table 3.17 Observed and calculated Oscillator strengths of **Pr³⁺** and **Tm³⁺** ions in **32.8CaO-16.4Al₂O₃-49.2B₂O₃-1.6Ln₂O₃** glass system

Pr³⁺			Tm³⁺		
Transition	P (10⁻⁶)		Transition	P (10⁻⁶)	
from ³H₄	obs	cal	from ³H₆	obs	cal
³F₂	5.77	5.52	³F₄	2.12	2.82
³F₃	12.57	13.28	³H₅	1.42	1.67
³F₄	4.65	7.98	³H₄	2.91	2.73
¹D₂	2.27	2.32	³F₃	2.97	3.04
³P₀	3.11	4.62	³F₂	0.49	0.53
³P₁	5.74	4.68	¹G₄	1.01	0.96
³P₂	12.47	7.68	¹D₂	3.38	2.99
rms	± 2.3			± 0.32	

Table 3.18 Observed and calculated Oscillator strengths of Nd^{3+} and Er^{3+} ions in 32 CaO -16 $4\text{Al}_2\text{O}_3$ -49 $2\text{B}_2\text{O}_3$ -1.6 Ln_2O_3 glass system

Nd^{3+}			Er^{3+}		
Transition	$P (10^{-6})$		Transition	$P (10^{-6})$	
from $^4\text{I}_{9/2}$	obs	cal	from $^4\text{I}_{13/2}$	obs	cal
$^4\text{F}_{3/2}$	1.74	2.34	$^4\text{I}_{13/2}$	0.84	0.85
$^4\text{F}_{5/2}$	5.85	6.29	$^4\text{I}_{11/2}$	0.61	0.39
$^4\text{F}_{7/2}$	6.11	6.00	$^4\text{I}_{9/2}$	0.13	0.22
$^4\text{F}_{9/2}$	0.69	0.49	$^4\text{F}_{9/2}$	1.47	1.56
$^2\text{H}_{11/2}$	0.21	0.13	$^4\text{S}_{3/2}$	0.43	0.31
$^4\text{G}_{5/2}$	16.78	16.84	$^2\text{H}_{11/2}$	4.72	5.46
$^4\text{G}_{7/2}$	6.18	5.39	$^4\text{F}_{7/2}$	1.27	1.31
$^4\text{G}_{9/2}$	1.47	0.99	$^4\text{F}_{5/2}$	0.31	0.36
$^2\text{P}_{1/2}$	0.51	0.64	$^4\text{G}_{11/2}$	10.19	9.79
$^4\text{D}_{3/2}$	12.06	12.08	$^2\text{G}_{7/2}$	0.99	1.17
rms	± 0.38			± 0.38	

Table 3.19 Observed and calculated oscillator strengths of Sm^{3+} in 32.8CaO-16.4Al₂O₃-49.2B₂O₃-1.6Sm₂O₃ glass system

Transition from $^6\text{H}_{5/2}$	Spectral region (nm)	f (10)	
		obs	cal
$^6\text{H}_{15/2} \rightarrow ^6\text{F}_{1/2} \rightarrow ^6\text{F}_{3/2}$	1505.1	331.2	329.8
$^6\text{F}_{5/2}$	1390.0	237.5	262.5
$^6\text{F}_{7/2}$	1225.0	297.5	356.1
$^6\text{F}_{9/2}$	1082.0	215.5	220.4
$^6\text{F}_{11/2}$	945.9	32.5	34.5
$^4\text{G}_{5/2}$	560.0	3.4	1.8
$^4\text{F}_{3/2}$	526.5	2.1	0.6
$^4\text{G}_{7/2} \rightarrow ^4\text{I}_{9/2} \rightarrow ^4\text{M}_{15/2} \rightarrow ^4\text{I}_{11/2} \rightarrow ^4\text{I}_{13/2}$	469.4	170.6	108.5
$^4\text{F}_{5/2} \rightarrow ^4\text{M}_{17/2} \rightarrow ^4\text{G}_{9/2} \rightarrow ^4\text{I}_{15/2}$	439.0	15.6	16.1
$(^6\text{P} \rightarrow ^6\text{P})_{5/2} \rightarrow ^4\text{L}_{13/2} \rightarrow ^4\text{F}_{7/2}$	406.7	635.2	614.2
$\text{P}_{3/2} \rightarrow \text{K}_{11/2} \rightarrow \text{L}_{15/2} \rightarrow \text{G}_{11/2}$			
$(^4\text{D}_{1/2} \rightarrow ^6\text{P}_{7/2} \rightarrow ^4\text{F}_{9/2}) \rightarrow ^4\text{L}_{17/2} \rightarrow ^4\text{K}_{13/2}$	374.0	176.2	134.2
$^4\text{D}_{3/2} \rightarrow (^4\text{D} \rightarrow ^6\text{P})_{5/2} \rightarrow ^4\text{H}_{7/2}$	361.5	144.6	141.4
rms		± 2.9	

Hypersensitive transitions

Table 3.20 Observed and calculated oscillator strengths of Dy^{3+} in 32 $\text{8CaO-16 4Al}_2\text{O}_3\text{-49 2B}_2\text{O}_3\text{-1 6Dy}_2\text{O}_3$ glass system

Transition	Spectral	P(10 ^{−8})	
from ⁶ H _{15/2}	region (nm)	obs	cal
⁶ H _{11/2}	1665.0	102.4	96.0
⁶ F _{11/2} • ⁶ H _{9/2}	1285.0	615.8	619.2
⁶ F _{9/2} ⁶ H _{7/2}	1090.0	212.9	203.5
⁶ F _{7/2} ⁶ H _{5/2}	902.0	164.5	150.3
⁶ F _{5/2}	803.0	90.7	65.9
⁶ F _{3/2}	753.0	18.9	12.5
⁴ I _{15/2} •	451.9	28.7	31.9
⁴ G _{11/2} •	425.0	10.5	6.7
⁴ F _{7/2} ⁴ K _{17/2} ⁴ I _{13/2}	380.9	178.0	118.4
⁴ M _{19/2} ⁶ P _{5/2} (⁴ P ⁴ D) _{3/2}	364.0	86.8	145.1
rms		±27	
Hypersensitive transitions			

Table 3.21 Observed and calculated oscillator strengths of Ho^{3+} in 32 8CaO -16 $4\text{Al}_2\text{O}_3$ -49 $2\text{B}_2\text{O}_3$ -1 $6\text{H}_2\text{O}$ glass system.

Transition from $^5\text{I}_8$	Spectral region (nm)	P (10^{-8})	
		obs	cal
$^5\text{I}_7$	1980.2	100.6	121.1
$^5\text{I}_6$	1190.0	76.3	88.4
$^5\text{I}_5$	898.7	16.0	15.8
$^5\text{F}_5$	6420	285.7	254.9
$^5\text{S}_2 \ ^5\text{F}_4$	537.0	309.3	318.1
$^5\text{F}_3$	486.0	118.8	91.9
$^5\text{F}_2 \ ^3\text{K}_8 \ ^5\text{G}_6$	452.0	1843.5	1845.3
$^5\text{G}_5$	417.0	254.4	271.5
$^5\text{G}_4 \ ^3\text{K}_7$	386.0	60.1	49.2
$^5\text{G}_2 \ ^3\text{H}_5 \ ^3\text{H}_6$	361.5	420.9	407.9
rms		± 18	

Hypersensitive transitions

Table 3.22 Electric dipole strengths (S_{ed}), magnetic dipole strengths (S_{md}), transition probabilities (A), total transition probabilities (A_T), radiative life times (τ_R) and branching ratios (β_R) for excited states of Pr^{3+} ion in 32 8CaO-16 4Al₂O₃-49 2B₂O₃-1 6Pr₂O₃ glass system

SLJ	S' L' J'	$S_{ed}/e^2 (10^{-27})$	$S_{md}/e^2 (10^{-27})$	$A (\text{sec}^{-1})$	$A_T (\text{sec}^{-1})$	$\tau_R (\mu\text{sec})$	$p\%$ (cal)
$^3\text{F}_3$	$^3\text{F}_2$	49.2	24.3	1			0.000
	$^3\text{H}_6$	14500	0.0	108			0.065
	$^3\text{H}_5$	497.0	0 0	192			0.115
	$^3\text{H}_4$	1290.0	0.0	1364	1666	600	0.818
$^1\text{D}_2$	$^1\text{G}_4$	288.0	0.0	565			0.112
	$^3\text{F}_4$	1930	0.0	961			0.191
	$^3\text{F}_3$	23.9	00	133			0.026
	$^3\text{F}_2$	71.8	0.254	573.503			0 113
	$^3\text{H}_6$	61.9	0.0	701			0.139
	$^1\text{H}_8$	2.0	00	36			0.007
	$^3\text{H}_4$	836	0.0	2063	5035	198	0.409
	$^1\text{D}_2$	4.4	0	0	6	0	0.00
$^3\text{P}_0$	$^1\text{G}_4$	35.2	0.0	1215			0.019
	$^3\text{F}_4$	100.0	0.0	6621			0.107
	$^3\text{F}_3$	0.0	0.0	0			0.000
	$^3\text{F}_2$	98.3	0.0	9066			0.147
	$^3\text{H}_6$	102.0	0.0	12411			0.201
	$^3\text{H}_5$	0.0	0.0	0			0.000
	$^3\text{H}_4$	142.0	0.0	32154	61475	16	0.523
	$^3\text{P}_0$	0.0	7.4	0			0.000
	$^1\text{D}_2$	250	0.697	19			0.000
	$^1\text{G}_4$	50.1	00	663			0.010
$^3\text{P}_1$	$^3\text{F}_4$	236.0	0.0	5811			0.092
	$^3\text{F}_3$	353.0	0 0	9402			0.150
	$^3\text{F}_2$	90.1	14 1	4950			0.079
	$^3\text{H}_6$	175.0	00	7794			0 124
	$^3\text{H}_5$	362.0	00	22338			0.356
	$^3\text{H}_4$	143.0	00	11616	62595	15	0 185

Chapter 3

Table 3.23 Electric dipole strengths (S_{ed}), magnetic dipole strengths (S_{md}), transition probabilities (A), total transition probabilities (A_T), radiative life times (TR) and branching ratios (PR) for excited states of Nd^{3+} ion in 32.8CaO-16.4Al₂O₃-49.2B₂O₃-1.6Nd₂O₃ glass system.

SLJ	S' L' J'	$S_{ed}/e^2 (10^{-21})$	$S_{md}/e^2 (10^{-22})$	A (sec ⁻¹)	A_T (sec ⁻¹)	τ_R (μ sec)	β_R (cal)
⁴ F _{3/2}	⁴ I _{13/2}	12.6	0.0	12			0.004
	⁴ I _{11/2}	93.5	0.0	240			0.079
	⁴ I _{11/2}	259.0	0.0	1364			0.451
	⁴ I _{9/2}	148.0	0.0	1402	3018	331	0.464
⁴ F _{5/2}	² H _{9/2}	14.8	0.0	0			0.000
	⁴ F _{3/2}	46.2	33.8	0			0.000
	⁴ I _{13/2}	102.0	0.0	112			0.029
	⁴ I _{11/2}	274	0		0.0	705	0.184
⁴ F _{7/2}	⁴ I _{11/2}	108.0	0.0	524			0.137
	⁴ I _{9/2}	301.0	0.0	2484	3828	261	0.648
	⁴ F _{7/2}	96.1	28.7	1			0.000
	⁴ S _{3/2}	1.56	0.0	0			0.000
⁴ F _{5/2}	⁴ F _{3/2}	64.5	0.0	2			0.000
	² H _{9/2}	15.4	16.0	2			0.000
	⁴ F _{3/2}	49.5	0.0	4			0.001
	⁴ I _{13/2}	478.0	0.0	775			0.244
⁴ I _{13/2}	⁴ I _{13/2}	348.0	0.0	1079			0.340
	⁴ I _{11/2}	204.0	0.153	1059			0.334
	⁴ I _{9/2}	26.5	0.919	243	3166	315	0.076
	⁴ F _{9/2}	59.8	39.1	0			0.000
² H _{11/2}	⁴ F _{7/2}	63.1	0.0	1			0.004
	⁴ S _{3/2}	23.9	0.0	0			0.002
	⁴ F _{5/2}	37.3	0.0	2			0.007
	² H _{9/2}	60.8	15.3	8			0.027
⁴ F _{3/2}	⁴ F _{3/2}	6.31	0.0	1			0.003
	⁴ I _{13/2}	80.7	0.0	150			0.461
	⁴ I _{13/2}	117	0.984	52			0.160
	⁴ I _{11/2}	446	0.309	30			0.093
⁴ I _{9/2}	⁴ I _{9/2}	9.55	0.0	77	325	3068	0.239
	² H _{11/2}	7.5	0.0	0			0.000
	⁴ F _{9/2}	396	0.0	2			0.000
	⁴ F _{7/2}	123.0	0.154	24			0.001
⁴ S _{3/2}	⁴ S _{3/2}	108.0	0.0	24			0.001
	⁴ F _{3/2}	170.0	0.022	70			0.004
	² H _{9/2}	13.8	0.0	5			0.000
	⁴ F _{3/2}	181.0	0.0246	140			0.009
⁴ I _{13/2}	⁴ I _{13/2}	2.1	0.0	11			0.000

Optical Properties of Lanthanide Ions in Borate Glasses

⁴ G _{7/2}	⁴ I _{13/2}	39.9	0.0	377			0.024
	⁴ I _{11/2}	199.0	0.0	2890			0.187
	⁴ I _{9/2}	560.0	0.0	11848	15396	64	0.769
	² G _{7/2}	204.0	30.5	6			0.000
	⁴ G _{5/2}	21.6	0.567	0			0.000
	² H _{11/2}	43.0	0.0	5			0.000
	⁴ F _{9/2}	185.0	0.0149	44			0.003
	⁴ F _{7/2}	124.0	1.07	74			0.006
	⁴ S _{3/2}	81.1	0.0	45			0.003
	⁴ F _{5/2}	221.0	0.653	191			0.016
	² H _{9/2}	70.9	0.0255	62			0.005
	⁴ F _{3/2}	89.6	0.0	121			0.010
	⁴ I _{15/2}	17.0	0.0	114			0.009
	⁴ I _{13/2}	136.0	0.0	1438			0.124
	⁴ I _{11/2}	407.0	0.0	6262			0.542
⁴ G _{9/2}	⁴ I _{9/2}	148.0	0.0	3188	11553	86	0.276
	⁴ G _{7/2}	105.0	17.9	5			0.000
	² G _{7/2}	168.0	0.0	5			0.000
	⁴ G _{5/2}	97.5	31.4	6			0.000
	² H _{11/2}	108.0	0.0211	14			0.001
	⁴ F _{9/2}	226.0	3.71	64			0.005
	⁴ F _{7/2}	248.0	0.233	132			0.011
	⁴ S _{3/2}	130.0	0.0	74			0.006
	⁴ F _{5/2}	119.0	0.0	100			0.008
	² H _{9/2}	95.3	1.29	87			0.007
	⁴ F _{3/2}	65.4	0.0	85			0.007
	⁴ I _{15/2}	185.0	0.0	1110			0.098
	⁴ I _{13/2}	557.0	0.0	5168			0.456
	⁴ I _{11/2}	261.0	0.0398	3493			0.308
	⁴ I _{9/2}	51.1	0.286	972	11321	88	0.085

Table 3.24 Electric dipole strengths (S_{ed}), magnetic dipole strengths (S_{md}), transition probabilities (A), total transition probabilities (AT), radiative life times (TR) and branching ratios (β_R) for excited states of Er^{3+} ion in $32.8\text{CaO}-16.4\text{Al}_2\text{O}_3-49.2\text{B}_2\text{O}_3-1.6\text{Er}_2\text{O}_3$ glass system.

S L J	S' L' J'	$S_{ed}/e^2 (10^{-22})$	$S_{md}/e^2 (10^{-23})$	A (sec^{-1})	A, (sec^{-1})	$\tau_R (\mu\text{sec})$	$\beta_R (\text{cal})$
$^4\text{I}_{13/2}$	$^4\text{I}_{13/2}$	1460	70.2	181	181	5512	1.000
$^4\text{I}_{11/2}$	$^4\text{I}_{13/2}$	1110	77.5	41			0.305
	$^4\text{I}_1$	32	43.3	0.0	93	135	0.694
$^4\text{I}_{9/2}$	$^4\text{I}_{11/2}$	25.0	41.7	5			0.035
	$^4\text{I}_{13/2}$	55.3	0.0	28			0.184
	$^4\text{I}_{15/2}$	25.2	0.0	119	153	6504	0.780
$^4\text{F}_{9/2}$	$^4\text{I}_{9/2}$	37.4	39.6	12			0.010
	$^4\text{I}_{11/2}$	133.0	16.2	71			0.059
	$^4\text{I}_{13/2}$	32.3	0.0	56			0.047
	$^4\text{I}_{15/2}$	116.0	0.0	1060	1201	832	0.882
$^4\text{S}_{3/2}$	$^4\text{F}_{9/2}$	3.14	0.0	1			0.000
	$^4\text{I}_{9/2}$	31.5	0.0	50			0.041
	$^4\text{I}_{11/2}$	7.17	0.0	28			0.023
	$^4\text{I}_{13/2}$	29.4	0.0	335			0.278
	$^4\text{I}_{15/2}$	19.3	0.0	792	1207	828	0.656
$^4\text{F}_{7/2}$	$^2\text{H}_{11/2}$	82.2	0.0	1			0.000
	$^4\text{S}_{3/2}$	2.1	0.0	0			0.000
	$^4\text{F}_{9/2}$	10.7	24.6	48			0.017
	$^4\text{I}_{9/2}$	54.8	5.82	137			0.050
	$^4\text{I}_{11/2}$	45.8	0.0	167			0.061
	$^4\text{I}_{13/2}$	40.5	0.0	359			0.131
	$^4\text{I}_{15/2}$	72.9	0.0	2012	2725	366	0.738
$^4\text{F}_{5/2}$	$^4\text{F}_{7/2}$	43.8	37.3	3			0.001
	$^2\text{H}_{11/2}$	24.2	0.0	2			0.001
	$^4\text{S}_{3/2}$	503	2.45	2			0.001
	$^4\text{F}_{9/2}$	67.2	0.0	91			0.044
	$^4\text{I}_{9/2}$	17.8	0.0	71			0.034
	$^4\text{I}_{11/2}$	195	0.0	145			0.070
	$^4\text{I}_{13/2}$	53.0	0.0	867			0.422
	$^4\text{I}_{15/2}$	18.9	0.0	870	2053	486	0.423
$^2\text{G}_{9/2}$	$^4\text{F}_{5/2}$	4.6	0.0	0			0.000
	$^4\text{F}_{7/2}$	27.8	0.0	1			0.000
	$^4\text{F}_{7/2}$	5.26	4.89	4			0.001
	$^2\text{H}_{11/2}$	41.4	2.89	20			0.007
	$^4\text{S}_{3/2}$	308	0.0	1			0.000
	$^4\text{F}_{9/2}$	12.8	0.0	25			0.009
	$^4\text{I}_{9/2}$	3.73	0.102	19			0.007

Optical Properties of Lanthanide Ions in Borate Glasses

${}^4G_{11/2}$	${}^4I_{11/2}$	516	4.18	526			0.194
	${}^4I_{13/2}$	78.0	0.0	1165			0.430
	${}^4I_{15/2}$	250	0.0	941	2706	369	0.347
	${}^2G_{7/2}$	163.0	9.2	3			0.000
	${}^4F_{3/2}$	13.2	0.0	2			0.000
	${}^4F_{5/2}$	12.7	0.0	2			0.000
	${}^4F_{7/2}$	828	0.0	38			0.001
	${}^2H_{11/2}$	31.3	132	71			0.003
	${}^4S_{3/2}$	10.9	0.0	11			0.000
	${}^4F_{9/2}$	170.0	0.944	532			0.026
	${}^4I_{6/2}$	294	0.0	181			0.009
	${}^4I_{8/2}$	684	0.002	654			0.032
	${}^4I_{13/2}$	94.9	2.2	1792			0.089
	${}^4I_{15/2}$	422.0	0.0	16833	20124	49	0.836

Table 3.25 Electric dipole strengths (S_{ed}), magnetic dipole strengths (S_{md}), transition probabilities (A), total transition probabilities (A_T), radiative life times (τ_R) and branching ratios (β_R) for excited states of Tm^{3+} ion in 32.8CaO-16.4Al₂O₃-49.2B₂O₃-1.6Tm₂O₃ glass system

S L J	S' L' J'	$S_{ed}/e^2 (10^{-27})$	$S_{md}/e^2 (10^{-27})$	$A (sec^{-1})$	$A_T (sec^{-1})$	$\tau_R (\mu sec)$	$\beta_R (cal)$
1D_2	3H_6	98.0	0.0	11150			0.370
	3F_4	256.0	0.0	14670			0.487
	3H_5	2.74	0.0	110			0.003
	3H_4	81.5	0.0	1539			0.051
	3F_3	844	0.0	1071			0.035
	3F_2	110.0	3.27	1369			0.045
1G_4	3G_5	125.0	0.0	196	30107	33	0.006
	3H_6	40.4	0.0	1123			0.474
	3F_4	146	0.599	183			0.077
	3H_5	104.0	0.0	670			0.283
	3H_4	119.0	11.3	307			0.129
	3F_3	68.0	0.0	60			0.025
	3F_2	30.8	0.0	21	2365	422	0.008

Table 3.26 Radiative lifetimes of fluorescent levels

Lanthanide ion	Level	τ_R (μsec)	Lanthanide ion	Level	τ_R (μsec)
Pr³⁺	³F₃	600	Er³⁺	⁴I_{13/2}	5512
	¹D₂	198		⁴I_{11/2}	7393
	³P₀	16		⁴I_{9/2}	6504
	³P₁	15		⁴F_{9/2}	832
Nd³⁺	⁴F_{3/2}	331	Tm³⁺	⁴S_{3/2}	828
	⁴F_{5/2}	261		⁴F_{7/2}	366
	⁴F_{9/2}	315		⁴F_{5/2}	486
	²H_{11/2}	3068		²G_{9/2}	369
	⁴G_{5/2}	64		⁴G_{11/2}	49
	⁴G_{7/2}	86		¹D₂	33
	⁴G_{9/2}	88		¹G₄	422

Table 3.27 Branching ratios of laser transitions for Pr^{3+} , Nd^{3+} , Er^{3+} and Tm^{3+} ions in 32 CaO -16 $4\text{Al}_2\text{O}_3$ -49 $2\text{B}_2\text{O}_3$ -1 $6\text{Ln}_2\text{O}_3$ glass system

Lanthanide ion	Transition	β_R (cal)
Pr^{3+}	$^3\text{P}_0 \rightarrow ^3\text{H}_6$	0.201
	$^3\text{P}_0 \rightarrow ^3\text{F}_2$	0.147
Nd^{3+}	$^4\text{F}_{3/2} \rightarrow ^4\text{I}_{9/2}$	0.464
	$^4\text{F}_{3/2} \rightarrow ^4\text{I}_{11/2}$	0.451
	$^4\text{F}_{3/2} \rightarrow ^4\text{I}_{13/2}$	0.079
Er^{3+}	$^4\text{S}_{3/2} \rightarrow ^4\text{I}_{13/2}$	0.278
	$^4\text{S}_{3/2} \rightarrow ^4\text{I}_{11/2}$	0.023
	$^4\text{S}_{3/2} \rightarrow ^4\text{I}_{9/2}$	0.041
	$^4\text{I}_{11/2} \rightarrow ^4\text{I}_{13/2}$	0.305
	$^4\text{I}_{13/2} \rightarrow ^4\text{I}_{15/2}$	1.000
Tm^{3+}	$^3\text{F}_4 \rightarrow ^3\text{H}_6$	1.000

Table 3.28 The radiative properties of Sm^{3+} and Dy^{3+} ions in $32.8\text{CaO}-16.4\text{Al}_2\text{O}_3-49\text{2B}_2\text{O}_3-1\text{6Ln}_2\text{O}_3$ glass system.

Transition	λ_p (nm)	A (sec^{-1})	β_R (cal)	β_R (obs)	σ_p (10^{-24} cm^2)
Samarium(III)					
$^4\text{G}_{5/2} \rightarrow ^6\text{H}_{5/2}$	563.4	11	0.038	0.269	30.2
$^4\text{G}_{5/2} \rightarrow ^6\text{H}_{7/2}$	599.2	107	0.375	0.601	304.2
$^4\text{G}_{5/2} \rightarrow ^6\text{H}_{9/2}$	644.8	112	0.392	0.127	294.9
$^4\text{G}_{5/2} \rightarrow ^6\text{H}_{11/2}$	704.2	31	0.107	0.002	139.2
$^4\text{G}_{5/2} \rightarrow ^6\text{H}_{13/2}$	788.8	3	0.012	-	41.4
$^4\text{G}_{5/2} \rightarrow ^6\text{F}_{3/2}$	919.0	2	0.004		
$^4\text{G}_{5/2} \rightarrow ^6\text{F}_{5/2}$	942.7	16	0.038		
$^4\text{G}_{5/2} \rightarrow ^6\text{F}_{7/2}$	1048.3	3	0.010		
$^4\text{G}_{5/2} \rightarrow ^6\text{F}_{9/2}$	1196.1	2	0.005		
Dysprosium(III)					
$^4\text{F}_{9/2} \rightarrow ^6\text{H}_{15/2}$	482.7	125	0.154	0.537	162.6
$^4\text{F}_{9/2} \rightarrow ^6\text{H}_{13/2}$	574.8	572	0.702	0.457	1191.1
$^4\text{F}_{9/2} \rightarrow ^6\text{H}_{11/2}$	660.9	59	0.073	0.003	
$^4\text{F}_{9/2} \rightarrow ^6\text{H}_{9/2} \quad ^6\text{F}_{11/2}$	758.3	31	0.038	0.003	
$^4\text{F}_{9/2} \rightarrow ^6\text{H}_{7/2} \quad ^6\text{F}_{9/2}$	879.7	17	0.021		
$^4\text{F}_{9/2} \rightarrow ^6\text{H}_{5/2} \quad ^6\text{F}_{7/2}$	1049.5	5	0.006		
$^4\text{F}_{9/2} \rightarrow ^6\text{F}_{5/2}$	1224.5	6	0.007		

Table 3.29 The emission intensity ratio (**R/O**) of Eu^{3+} , the emission intensity ratio (**Y/B**) of Dy^{3+} , phonon energy ($\hbar\omega$) and the electron phonon coupling strengths (g) for (a) $30\text{CaO}-69\text{B}_2\text{O}_3-1\text{Ln}_2\text{O}_3$ and (b) $32\text{CaO}-16\text{Al}_2\text{O}_3-49\text{B}_2\text{O}_3-1\text{Ln}_2\text{O}_3$ glass systems

Glass matrix	R/O [†]	Y/B [†]	$\hbar\omega$ (cm^{-1}) ± 10	g (10^{-3}) ± 1
CaO-B₂O₃	3.6	0.83	1083,1375	11.8
CaO-Al₂O₃-B₂O₃	3.50	0.88	1317	4.6

[†] see text

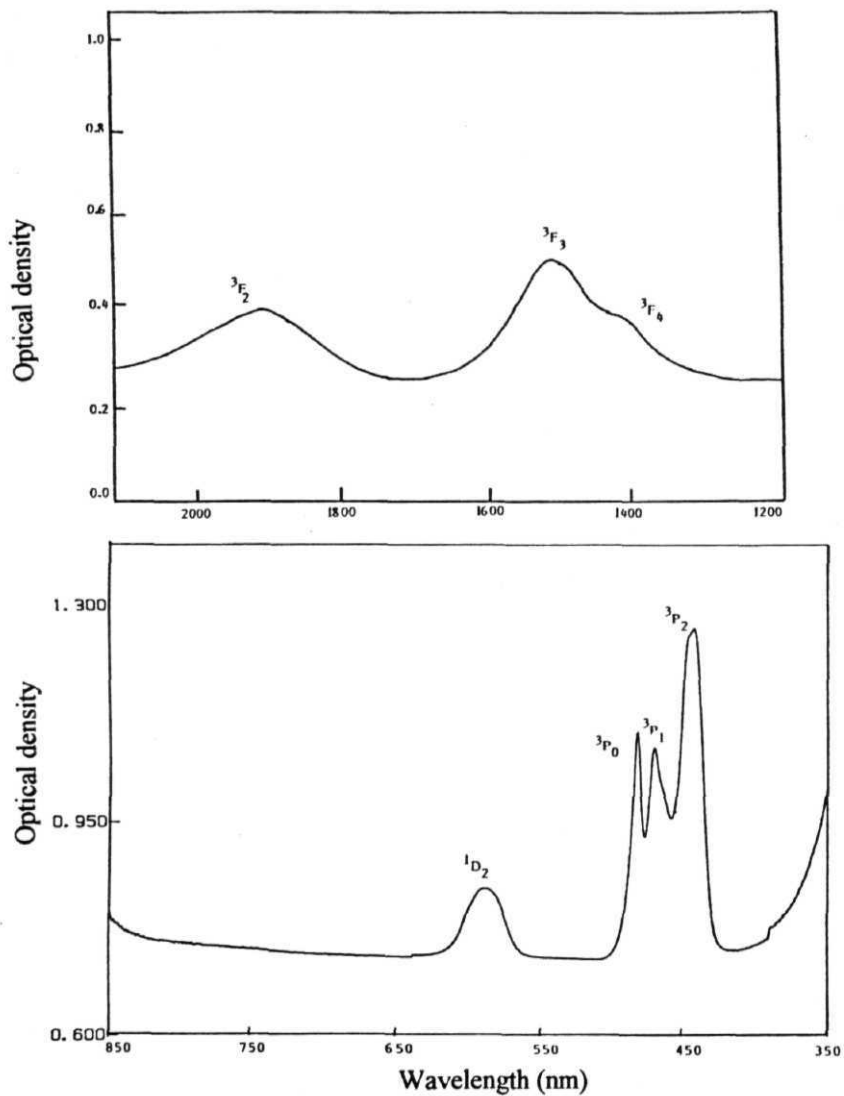


Figure 3.4 Absorption spectrum of Pr^{3+} ion doped in $\text{CaO-Al}_2\text{O}_3\text{-B}_2\text{O}_3$ glass system

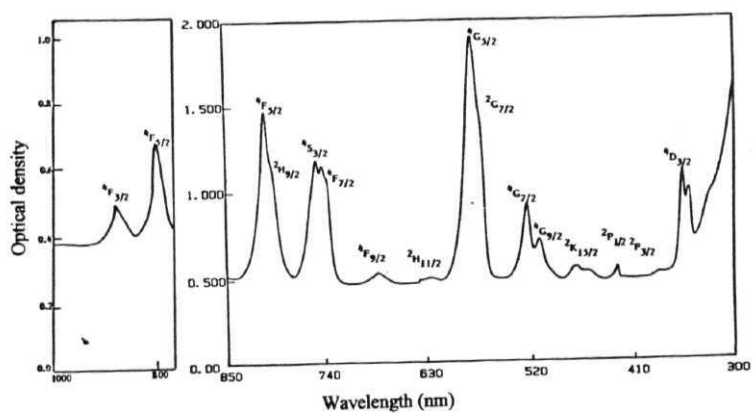


Figure 3.5 Absorption spectrum of Nd^{3+} ion doped in $\text{CaO-Al}_2\text{O}_3\text{-B}_2\text{O}_3$ glass system

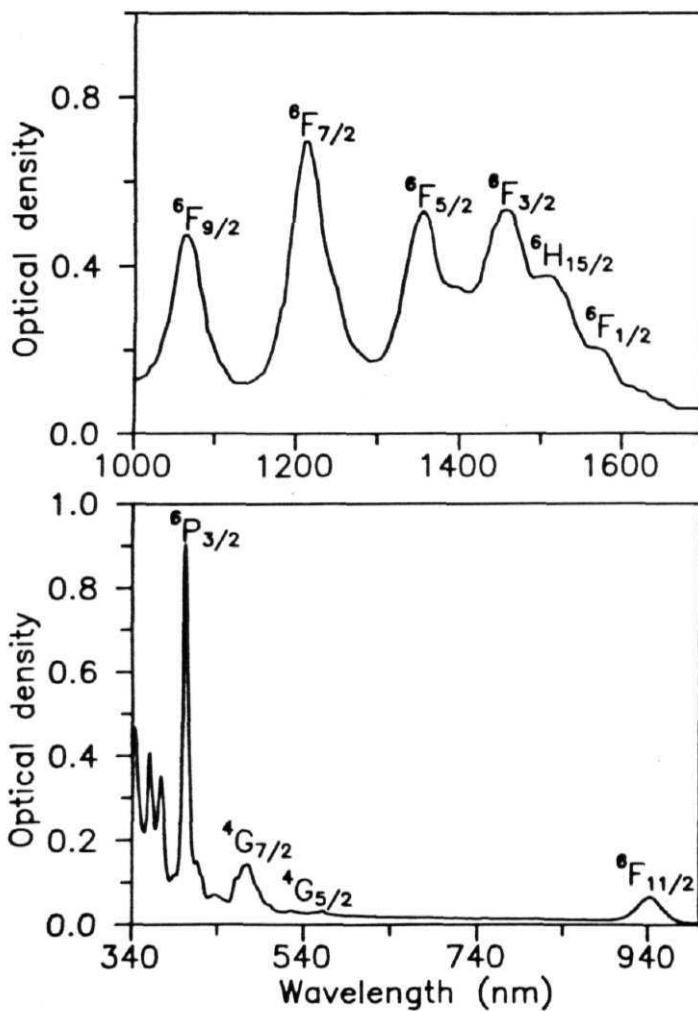


Figure 3.6 Absorption spectrum of Sm³⁺ ion doped in CaO-Al₂O₃-B₂O₃ glass system

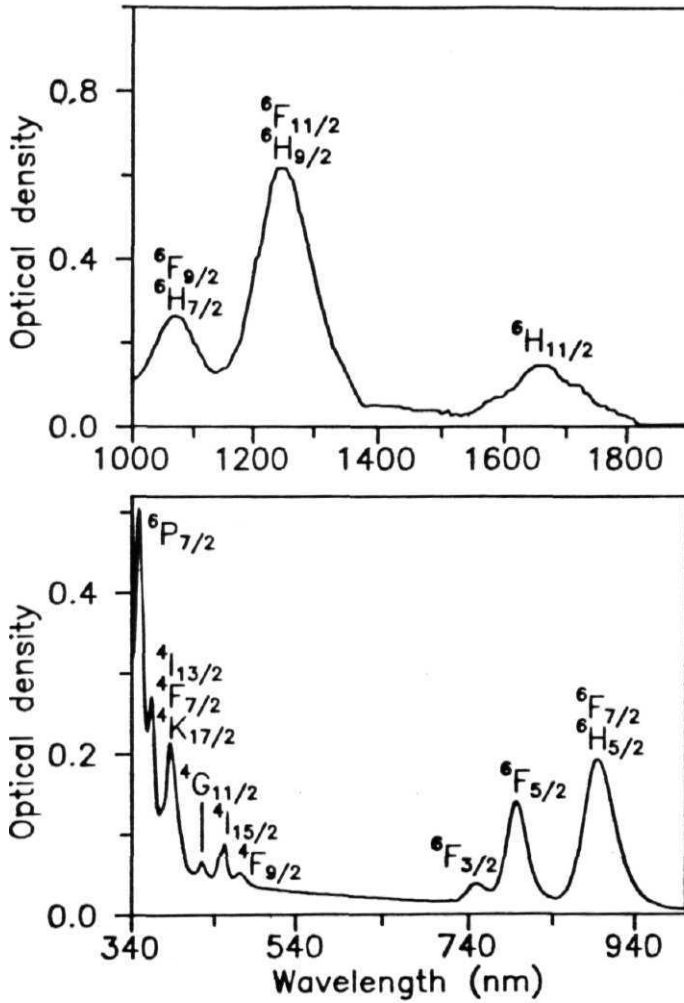


Figure 3.7 Absorption spectrum of Dy^{3+} ion doped in $\text{CaO-Al}_2\text{O}_3\text{-B}_2\text{O}_3$ glass system

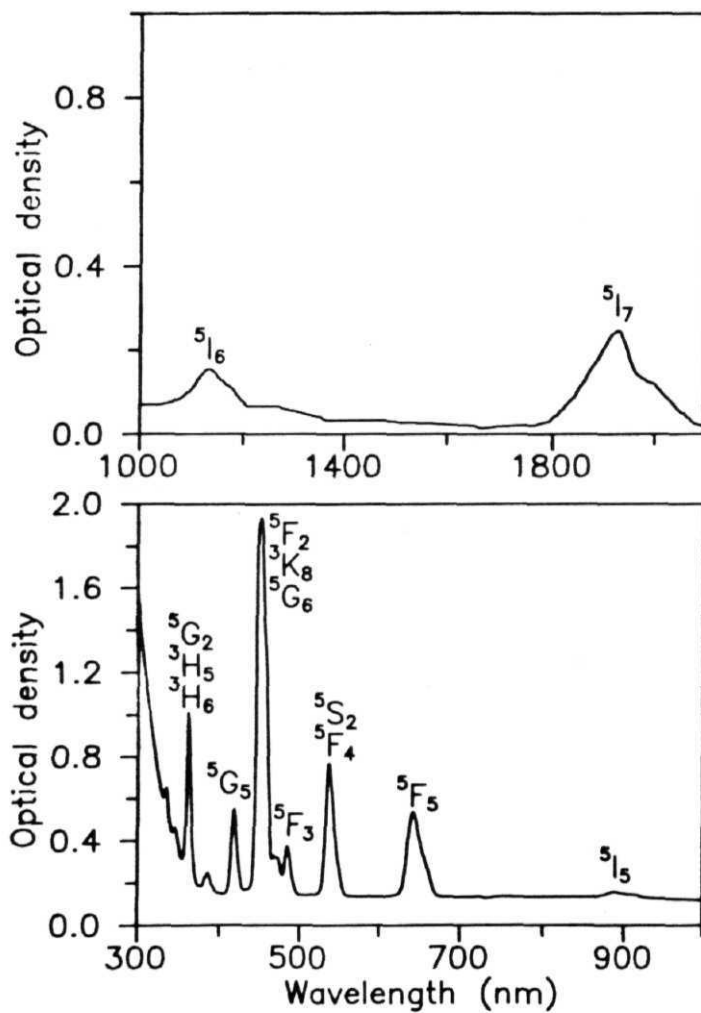


Figure 3.8 Absorption spectrum of Ho^{3+} ion doped in $\text{CaO-Al}_2\text{O}_3\text{-B}_2\text{O}_3$ glass system

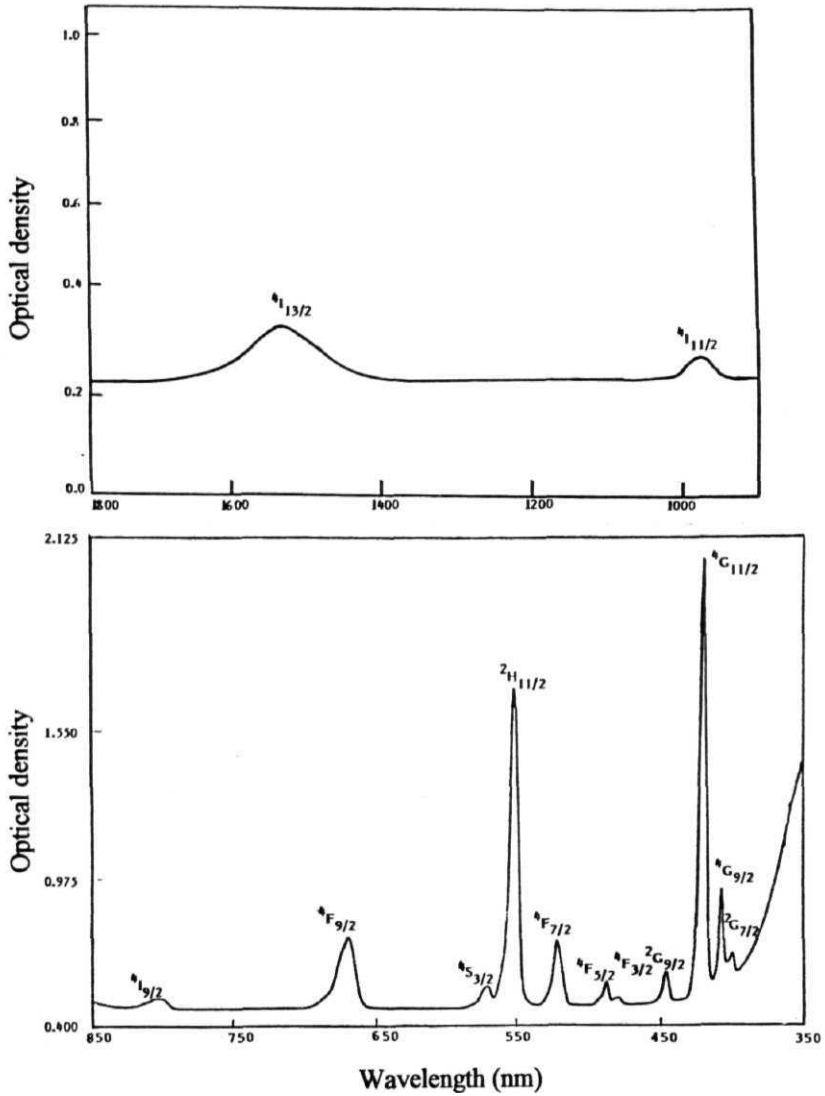


Figure 3.9 Absorption spectrum of Er^{3+} ion doped in $\text{CaO-Al}_2\text{O}_3\text{-B}_2\text{O}_3$ glass system

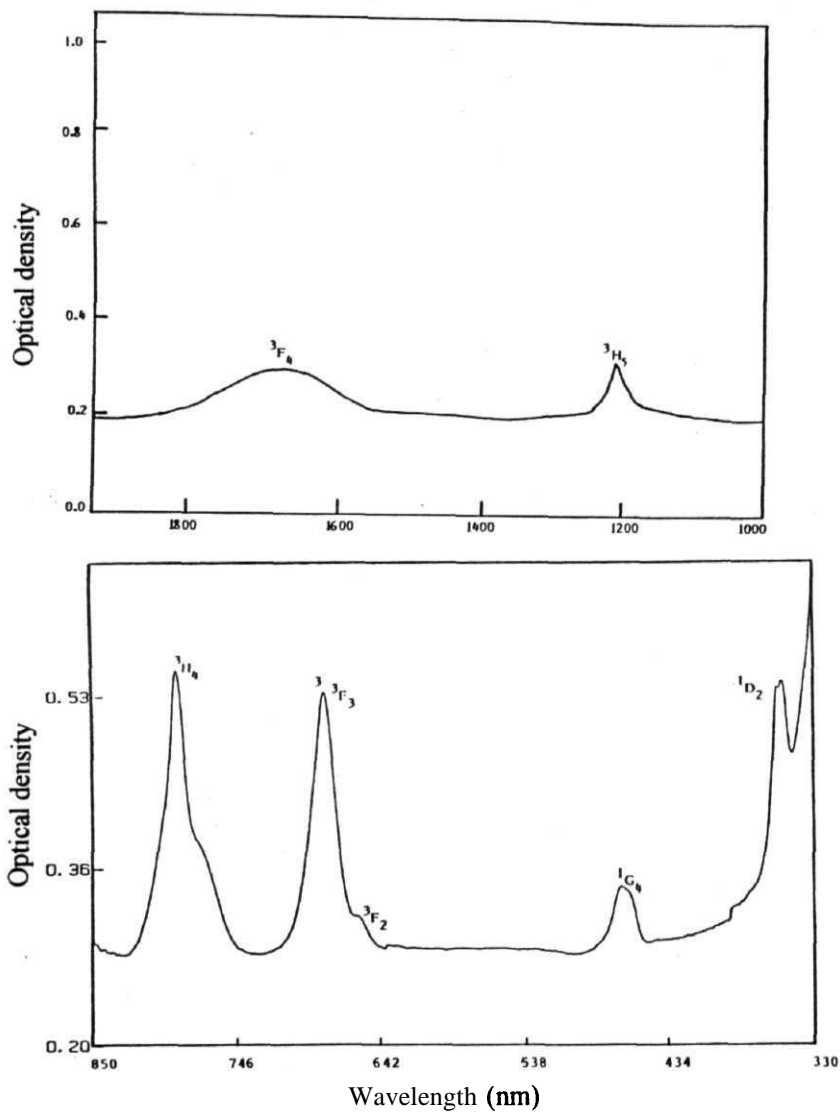


Figure 3.10 Absorption spectrum of Tm^{3+} ion doped in $CaO-Al_2O_3-B_2O_3$ glass system

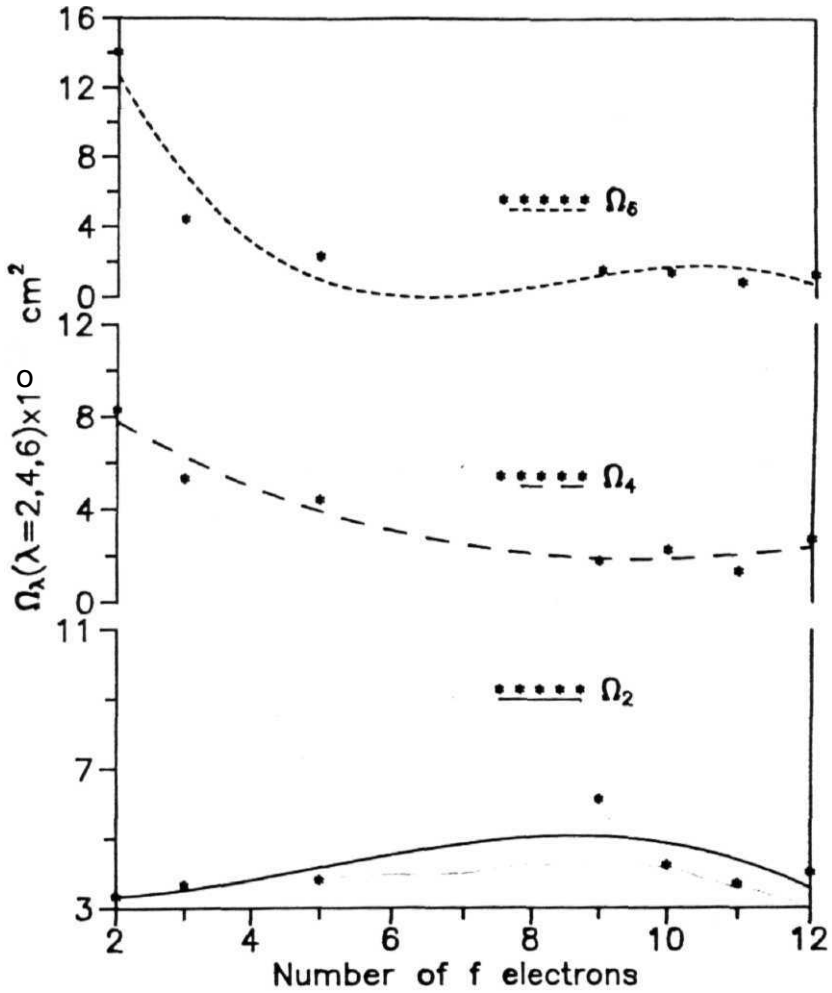


Figure 3.11 Dependence of intensity parameters (Ω_λ , $\lambda=2,4,6$) on atomic number of lanthanide ions doped in $\text{CaO-Al}_2\text{O}_3\text{-B}_2\text{O}_3$ glass system

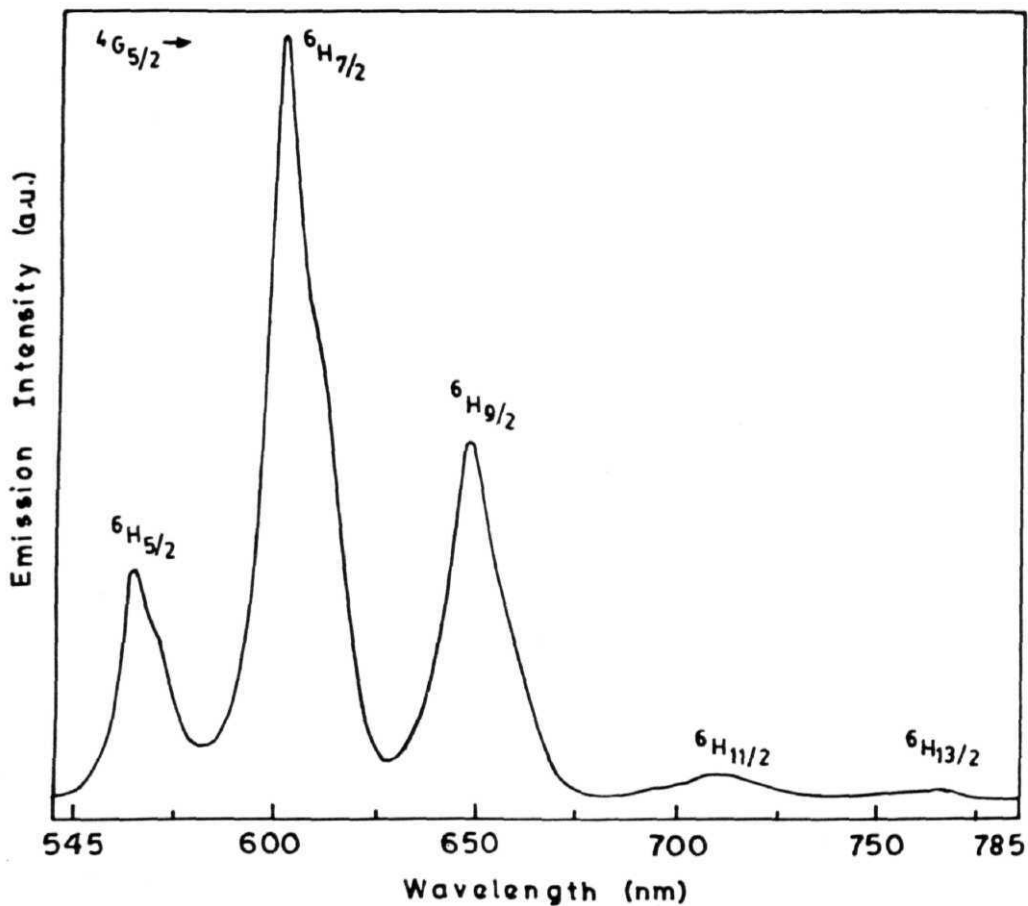


Figure 3.12 Emission spectrum of Sm^{3+} ion doped in $\text{CaO-Al}_2\text{O}_3\text{-B}_2\text{O}_3$ glass system
 $\lambda_{\text{ex}}=402$ nm.

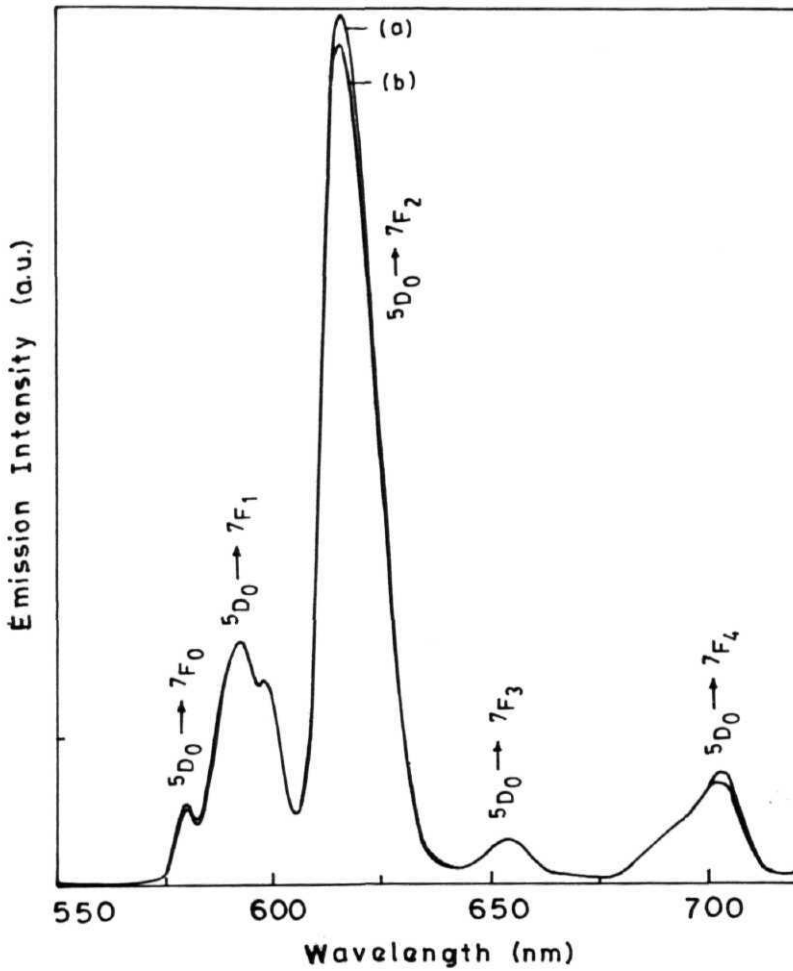


Figure 3.13 Emission spectrum of Eu^{3+} ion doped in $\text{CaO-Al}_2\text{O}_3\text{-B}_2\text{O}_3$ glass system
 $\lambda_{\text{ex}}=395 \text{ nm}$

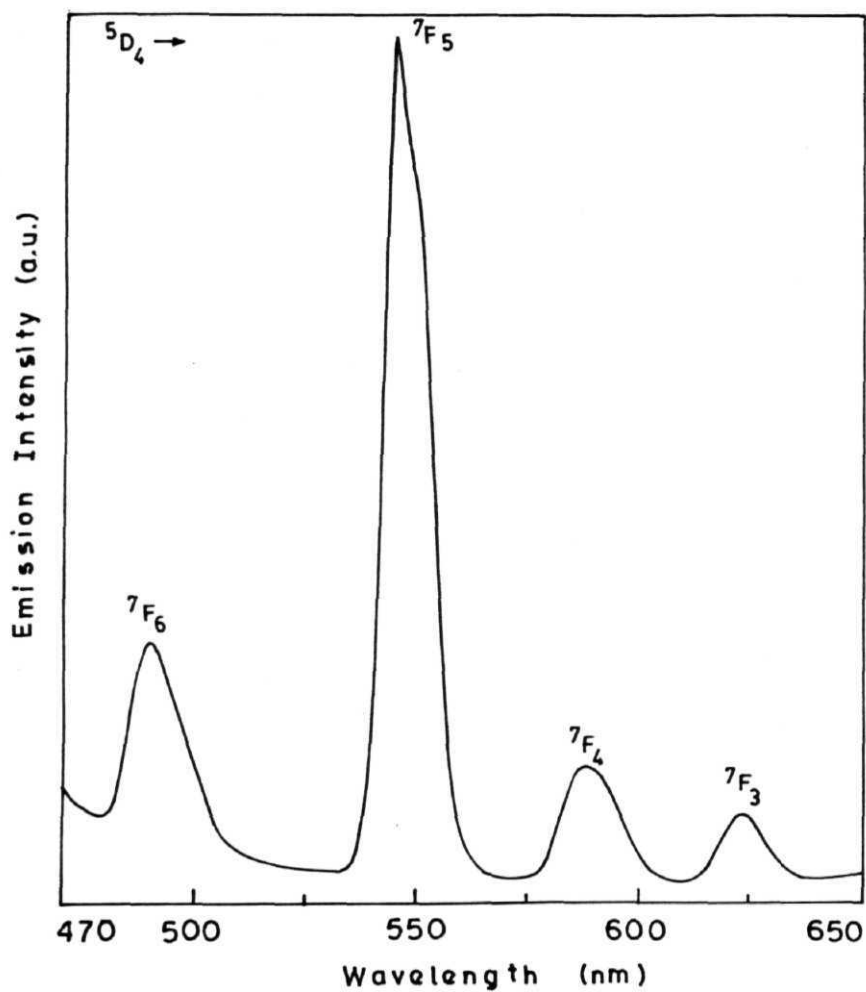


Figure 3.14 Emission spectrum of Tb^{3+} ion doped in $CaO-Al_2O_3-B_2O_3$ glass system $\lambda_{ex}=378$ nm.

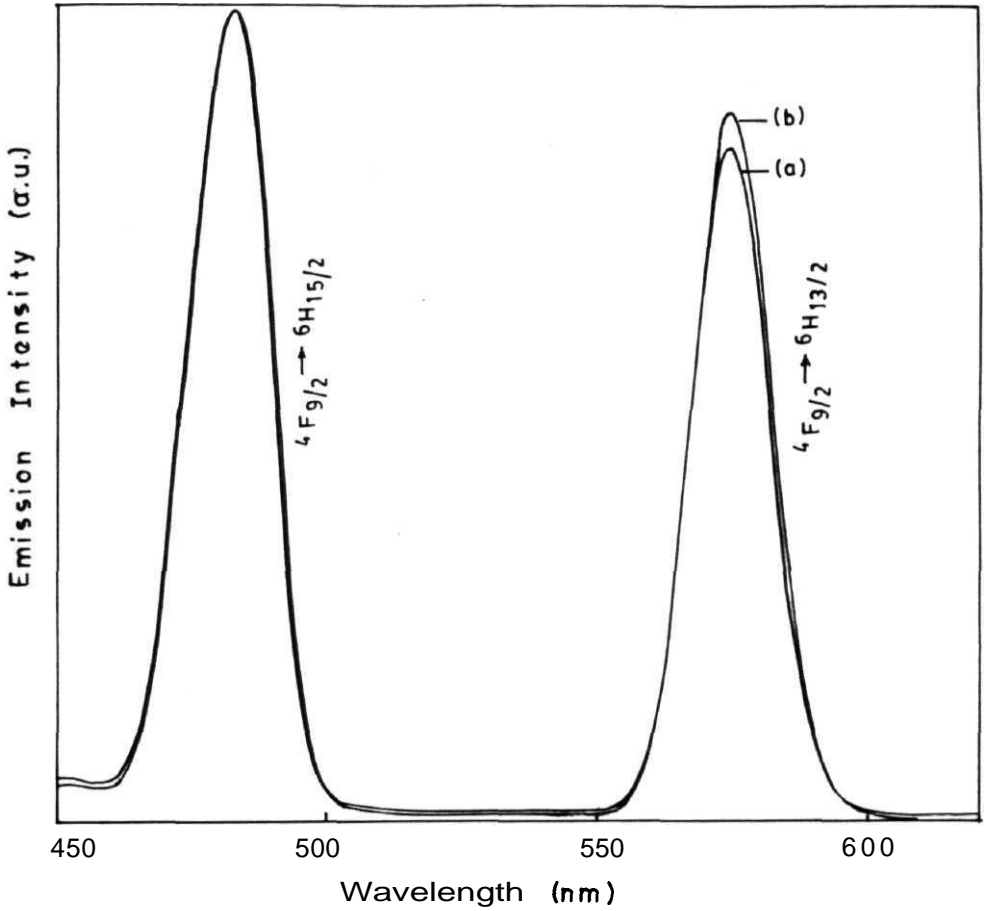


Figure 3.15 Emission spectrum of Dy^{3+} ion doped in $\text{CaO-Al}_2\text{O}_3\text{-B}_2\text{O}_3$ glass system $\lambda_{\text{ex}}=350$ nm.

Chapter 3

3.3 References

1. R. Reisfeld and C.K. Jorgensen, *Lasers and Excited States of Rare Earths* (Springer-Verlag, New York, 1977).
2. G. Fuxi, *Optical and Spectroscopic Properties of Glass* (Springer-Verlag, New York, 1992).
3. J.A. Caird, A.J. Ramponi and P.R. Staver, *J. Opt. Soc. Am. B.* **8** (1991) 1391.
4. J. Wang, L. Reekie, W.S. Brocklesby, Y.T. Chow and D.N. Payne, *J. Non-Cryst. Solids* **180** (1995) 207.
5. J. Wang, W.S. Brocklesby, J.R. Lincoln, J.E. Townsend and D.N. Payne, *J. Non-Cryst. Solids* **163** (1993) 261.
6. R. Reisfeld, *Structure and Bonding* **22** (Springer-Verlag, New York, 1975) 123.
7. K. Tanaka, T. Ohyagi, K. Hirao and N. Soga, *Bull. Chem. Soc. Jpn.* **66** (1993) 1121.
8. H. Imagawa, *Phys. Stat. Sol.* **30** (1968) 469.
9. C. Hirayama, *Phys. Chem. Glasses* **7** (1966) 52.
10. Y. Yan, A.J. Faber and H. Waal de, *J. Non-Cryst. Solids* **181** (1995) 283.
11. I.M. Thomas, S.A. Payne and G.D. Wilke, *J. Non-Cryst. Solids* **151** (1992) 183.
12. C.E. Weir and R.A. Schroeder, *J. Research NBS* **68A** (1964) 465, and refs. therein.
13. W.F. Bradley, D.L. Graf and R.S. Roth, *Acta Cryst.* **20** (1966) 283.
14. R. Bohlhoff, H.U. Bambauer and W. Hoffmann, *Naturwissenschaften* **10** (1970) 129.
15. J. Ysker St. and W. Hoffmann, *Naturwissenschaften* **10** (1970) 129.
16. B. Saubat, M. Vlasse and C. Fouassier, *J. Solid State Chem.* **34** (1980) 271.
17. E.W.J.L. Oomen and A.M.A. van Dongen, *J. Non-Cryst. Solids* **111** (1989) 205.
18. Q. Su, Z. Pai, L. Chi, H. Zhang, Z. Zhang and F. Zou, *J. Alloys Compds.* **192** (1993) 25.
19. S. Tanabe, S. Todoroki, K. Hirao and N. Soga, *J. Non-Cryst. Solids* **122** (1990) 59.

- 20 S. Tanabe, K. Hirao and N. Soga, *J. Non-Cryst. Solids* **142** (1992) 148.
- 21 Y.K Sharma, S.C Mathur, DC. Dube and S P. Tandon, *J. Mater. Sci.* **14** (1995) 71
- 22 E. Davis and N. Mott, *Philos. Mag.* **11** (1970) 903.
- 23 B G Wybourne, *Spectroscopic Properties of Rare Earths* (Interscience Publishers, New York, 1965).
24. KB. Yatsimirskii and N.K. Davidenko, *Coord. Chem. Rev.* **11** (1979) 223.
25. J. Lucas, *J. Less-Common Mets.* **112** (1985) 27.
- 26 M.A Marcus and A. Polman, *J. Non-Cryst. Solids* **136** (1991) 260.
- 27 C Dayanand, R.V.G.K. Sarma, G. Bhikshamaiah and M. Salagram, *J. Non-Cryst. Solids* **167** (1994) 122.
- 28 A Abdel-Kader, R. El-Mallawany and M.M. Elkholy, *J. Appl. Phys.* **73** (1993) 71.
- 29 W.C Gagel and J.D Mackenzie, *Phys. Chem. Glasses* **5** (1964) 113.
- 30 A.E Owen, *Phys. Chem. Glasses* **2** (1961) 87.
- 31 A.E Owen, *Phys. Chem. Glasses* **6** (1965) 253.
- 32 S.G. Bishop and P.J. Bray, *Phys. Chem. Glasses* **7** (1966) 73.
33. W.F. Krupke, *Phys. Rev.* **145** (1966) 325 and refs therein
- 34 R Reisfeld, *J. Less-Common Mets.* **112** (1985)9.
35. S.V.J. Lakshman and C.K. Jayasankar, *J. Phys.C: Solid State Phys.* **17** (1984) 2967.
- 36 W.T. Carnall, G.L Goodman, K Rajnak, and R.S Rana, *J. Chem. Phys.* **90** (1989)3443.
- 37 P. Caro and J. Derouet, *Bull. Soc. Chim. France* **1** (1972) 46
- 38 Q Su and Y. Lu, *Rare Earth Spectroscopy* (Eds) B. Jezowska-Trzebiatowska, J Legendziewicz and W. Strek, (World Scientific Publishing Co. Pte. Ltd., 1985) 379.
- 39 R Reisfeld and Y Eckstein, *J. Solid State Chem.* **5** (1972) 174.

40. A.F. Wells, *Structural Inorganic Chemistry* (The English Language Book Society, Oxford Univ. Press, Oxford, 1975).
41. R. Reisfeld and C.K. Jorgensen, *Hand Book on the Physics and Chemistry of Rare Earths*, (Eds.) K.A. Gschneidner and L. Eyring, 9 (North-Holland, New York, 1987) chap. 58.
42. M. Eyal, E. Greenberg, R. Reisfeld and N. Spector, *Chem. Phys. Letts.* **117** (1985) 108.
43. A.F. Kirby and R.A. Palmer, *Inorg. Chem.* 20 (1981) 4219
44. A.F. Kirby and R.A. Palmer, *Inorg. Chem.* 20 (1981) 1030.
45. G. Cormier and J.A. Capobianco, *J. Non-Cryst. Solids* **152** (1993) 225.
46. M.D. Shinn, W.A. Sibley, M.G. Drexhage and R.N. Brown, *Phys. Rev.* B27 (1983) 6635.
47. C.M. Broadbeck and L.E. Iton, *J. Chem. Phys.* 83 (1985) 4285
48. R.D. Peacock, *Structure and Bonding II* (Springer-Verlag, New York, 1975) 83 and refs. therein.
49. L. Wetenkamp, G.F. West and H. Tobben, *J. Non-Cryst. Solids* **140** (1992) 35
50. C.K. Jorgensen and R. Reisfeld, *J. Less-Common Mets.* 93 (1983) 107 and refs. therein.
51. F.A. Cotton and G. Wilkinson, *Advanced Inorganic Chemistry* (A Wiley-Interscience Publication, New York, 1988) 960.
52. E. Antic-Fidancev, M. Lemaitre-Blaise, P. Caro, B. Piriou and W. Strek, *Rare Earth Spectroscopy* (Eds.) B. Jezowska-Trzebiatowska, J. Legendziewicz and W. Strek, (World Scientific Publishing Co. Pte. Ltd., 1985) 354.
53. M. Malinowski, R. Wolski and W. Wolinski, *Solid State Commun.* 74 (1990) 17
54. S.V.J. Lakshman and A. Suresh Kumar, *J. Less-Common Mets.* **126** (1986) 257.
55. S.V.J. Lakshman and A. Suresh Kumar, *J. Phys. Chem. Solids* 49 (1988) 133
56. S.V.J. Lakshman and A. Suresh Kumar, *Phys. Chem. Glasses* 30 (1989) 35
57. G. Amaranath, S. Buddhudu, F.J. Baryant, L. Xi, B. Yu and S. Huang, *Mat. Res. Bull.* 25(1990) 1317.

- 58. G. Amaranath and S. Buddhudu, *J. Non-Cryst. Solids* **142** (1992) 252
- 59. J.L. Adam and W. A. Sibley, *J. Non-Cryst. Solids* 76 (1985) 267
- 60. G. Blasse, *Advances in Inorganic Chemistry* 35 (Academic Press, California, 1990) 319.
- 61. J. Sanz, R. Cases and R. Alcala, *J. Non-Cryst. Solids* 93 (1987) 377.
- 62. J. Hormadaly and R. Reisfeld, *J. Non-Cryst. Solids* 30 (1979) 337.
- 63. M.J. Weber, D.C. Ziegler and C.A. Angell, *J. Appl. Phys* 53 (1982) 4344.

Absorption and Emission Spectral Studies of Lanthanide Ions in Phosphate Glasses

Jorgenson and Reisfeld were the first to study in detail the optical properties of rare earth ions in glass systems.¹⁻³ Their works showed that borate, phosphate, germanate and tellurite glasses show distinct features with fluorescence emission being increasingly favored as we go along the above order. Their investigations gave an impetus to extend such studies to other glass matrices such as the fluoride glasses and the influence of glass modifiers such as Al^{3+} present in the glass matrix on the radiative properties of the Ln^{3+} ions. The radiative properties are strongly influenced by the glass formers and glass modifiers, as they in turn, strongly influence the characteristic properties of the glass such as the maximum phonon energy, dielectric constant or refractive index and the transparency or self absorption in the spectral region of interest.^{1,4-10} It is these properties which together play an important role with regard to radiative emission of the dopant ions. Systematic studies on the influence of glass modifier ions on the radiative properties are quite meager. The importance of such studies is shown for instance in the lasing system consisting of Nd^{3+} doped in silicate glass, where the presence of Al^{3+} leads to pronounced changes in the absorption spectra and in the life time of the $^4\text{F}_{3/2} \rightarrow ^4\text{I}_{11/2}$ laser transition.¹¹ Phosphate glasses are currently used as suitable matrix for commercial lasers.^{2,3} It is therefore considered appropriate to study on certain aspects of rare earth fluorescence in phosphate glass matrices. The present study deals with absorption and emission spectra of Ln^{3+} ions (Pr^{3+} , Nd^{3+} , Eu^{3+} , Dy^{3+} , Er^{3+} and Tm^{3+}) doped in the phosphate glasses $\text{CaO-Al}_2\text{O}_3\text{-P}_2\text{O}_5$ (CAP) and $\text{CaO-P}_2\text{O}_5$ (CP) by way of ascertaining the influence of the presence of Al^{3+} on the optical properties. Such a study will also fall in line with a similar study on the influence of Al^{3+} ions in borate glasses presented in the earlier chapter. The Judd-Ofelt theory has been

Chapter 4

quite successful in that three parameters enable characterization of absorption and emission spectra of a number of Ln^{3+} ions doped in crystalline and glass matrices of very different nature in a comprehensive manner.^{1,10-17} In this chapter the Judd-Ofelt parameters have been obtained from the absorption spectra of the rare earth ions mentioned above in the phosphate glass with and without Al^{3+} . Using the Judd-Ofelt parameters the radiative parameters have been obtained. The emission spectra have been measured for the Pr^{3+} , Eu^{3+} , Dy^{3+} , and Tm^{3+} ions. The influences of Al^{3+} ions on the absorption and emission spectral characteristics for the rare earth ions are presented.

4.1 Preparation of Phosphate Glasses

The glass samples with the compositions $20\text{CaO}-10\text{Al}_2\text{O}_3-69\text{P}_2\text{O}_5-1\text{Ln}_2\text{O}_3$ (CAP) and $30\text{CaO}-69\text{P}_2\text{O}_5-1\text{Ln}_2\text{O}_3$ (CP) ($\text{Ln} = \text{Pr}, \text{Nd}, \text{Eu}, \text{Dy}, \text{Er}, \text{Tm}$) were prepared in batches of 10 g as follows. Calculated amounts of respective rare earth oxide (Aldrich Chem. Co.), aluminium metal powder (SD) and calcium carbonate (BDH) were dissolved in the above sequence in required amount of phosphoric acid (SD). On making the volume of the solution to about 350 cm^3 a clear solution was obtained. The mixture was concentrated and quantitatively transferred into a platinum crucible. The solution was evaporated to dryness by slowly raising the temperature to 400°C . The temperature was subsequently increased to 1200°C for CAP glass and 1020°C for CP glass. The melt was kept at this temperature for nearly 20 min. The crucible containing the melt was constantly agitated to keep the melt bubble free and ensure homogeneous mixing. Then the melt was quenched to room temperature by quickly pouring it on a stainless steel plate having $2 \times 1 \times 0.3 \text{ cm}$ slot and pressing with another plate. Typical weight loss on melting under experimental conditions indicated that the actual compositions should be within 0.5 % of the values quoted for the components. Unlike the earlier described procedures,⁹ the above described method of mixing the components in the solution ensures thorough mixing of the starting materials as phosphates and also considerably brings down the temperature required to obtain the homogeneous melt. The samples were annealed at 160°C and polished with commercial media using a water free

lubricant The glass samples were obtained with good transparency and uniform thickness of 0.2 cm and 2.0 cm diameter.

4.2 Results and Discussion

The absorption spectra were recorded for the $20\text{CaO}-10\text{Al}_2\text{O}_3-69\text{P}_2\text{O}_5-1\text{Ln}_2\text{O}_3$ (CAP) and $30\text{CaO}-69\text{P}_2\text{O}_5-1\text{Ln}_2\text{O}_3$ (CP) the glass samples doped with Pr^{3+} , Nd^{3+} , Eu^{3+} , Dy^{3+} , Er^{3+} or Tm^{3+} ions. As the general features of the spectra are similar to those for the respective ions doped in $\text{CaO}-\text{Al}_2\text{O}_3-\text{B}_2\text{O}_3$ glass presented in the earlier chapter and differences occur only in shifts in the transition energies and their intensities these spectra are not reproduced. The spectroscopic parameters calculated using the appropriate **Hamiltonian** as discussed in chapter 2 for different Ln^{3+} ($\text{Ln}=\text{Pr}, \text{Nd}, \text{Er}, \text{Tm}$) ions are given in table 4.1. The corresponding observed and calculated transition energies for these ions are reproduced in tables 4.2 and 4.3 with their respective **rms** deviations. The small rms deviations show that the analysis of the spectra using a full matrix diagonalisation procedure leads to more reliable spectral parameters. The **Judd-Ofelt** parameters calculated from oscillator strengths of observed transitions are given in table 4.4. The observed oscillator strengths and the values obtained from Judd-Ofelt parameters are given in tables 4.5-4.9 along with their rms deviations. The small rms values indicate good agreement between observed and calculated values. The relatively larger deviations observed for Pr^{3+} arise due to the influence of hypersensitive transitions.¹⁷ The Ω_2 values for Ln^{3+} ions in these glasses are intermediate between much smaller values observed in crystalline oxides and larger values reported for chelating ligands.^{3,10,13,18-20} The Ω_2 values in both CAP and CP glasses show an increasing trend from A_f to $4f^0$ configuration and a decreasing trend there onwards (figure 4.1 and 4.2). These features are exactly the same as those observed for silicate glasses. The reasons for these observations have been presented in detail earlier. Thus our results show that they are applicable equally well for the Ln^{3+} doped CAP and CP glasses as well. On the other hand, in fluoride and fluorozirconate glasses an increasing trend has been reported for f_2 .^{10,15} The possible explanation for this is given in the next chapter by way of

explaining similar trend obtained for the **oxyfluoride** glass hosts. Reisfeld and Eckstein have suggested 8-coordination for the end members in the phosphate glasses which is the coordination suggested for the early member, Nd^{3+} as well for the present **systems**.⁹ Thus assuming that contribution to f_2 due to covalency is not much different, large distortion from cubic symmetry for the rare earth ions in the middle of the series such as Sm^{3+} , Eu^{3+} and Dy^{3+} may account for the observed trend. Ω_4 and Ω_6 show a rapid decrease followed by a slow increase, a feature common for all the glasses studied so far.^{10,15} The reasons for the observed trends in these cases have been presented in detail in the earlier chapter.

Unlike in borate glasses discussed in the chapter 3, presence of Al^{3+} ions results in higher Ω_2 values for CAP glass than for CP glass for all the rare earth ions under study. The higher Ω_2 values observed give evidence of a stronger dipolar field due to the presence of Al^{3+} ions in the proximity and noncentro symmetric placement of the nearest oxygen **neighbors** NMR studies in related systems also provide evidence for the proximity of AlO_4 tetrahedra to the Ln^{3+} ion.²¹ Studies on optical spectra of Nd^{3+} doped silicate glasses with and without Al^{3+} ions also show a similar result ¹¹

The radiative transition probabilities (A) and branching ratios (β_R) calculated from Judd-Ofelt parameters are given in tables 4.10-4.12 for selective transitions. These values are comparable with those reported for the corresponding ions doped in fluoride **glasses**.¹⁵ The CAP glass containing Al^{3+} ions show the following differences in the A values compared to CP glass. All the transitions for Pr^{3+} and Dy^{3+} except for the transition ${}^4\text{F}_{9/2} \rightarrow {}^6\text{H}_{13/2}$ in the latter show lower A values for CAP glass. All the three transitions originating from ${}^4\text{F}_{3/2}$ of Nd^{3+} , and the hypersensitive transitions ${}^5\text{D}_0 \rightarrow {}^7\text{F}_2$ of Eu^{3+} , ${}^4\text{F}_{9/2} \rightarrow {}^6\text{H}_{13/2}$ of Dy^{3+} and ${}^3\text{F}_4 \rightarrow {}^3\text{H}_6$ of Tm^{3+} show higher A values. For the laser transition ${}^4\text{F}_{3/2} \rightarrow {}^4\text{I}_{11/2}$ of Nd^{3+} in particular the A value for CAP glass is much higher than CP glass. In all other cases for the above ions and for all transitions in Er^{3+} the A values remain unaffected. An increase in A value signifies a decrease in the radiative life time.

Previous studies show that the life times derived from the Judd-Ofelt theory are in close agreement with experimental values.¹⁵ It will be therefore of interest to measure the life times for the present systems for confirmation

For Pr^{3+} , Eu^{3+} and Dy^{3+} the emission spectral data are adequate for calculating the β_R (exptl). For these cases the β_R (exptl), the average emission wavelength (λ_p), the emission line width ($\Delta\lambda_p$) and the stimulated emission cross sections (σ_p) calculated as discussed in chapter 2 are also included in table 4.9 and 4.10 for CAP and CP glasses. The calculated and experimental β_R values show good agreement for Pr^{3+} and Eu^{3+} for both the glasses. For Dy^{3+} the agreement is less satisfactory for both CAP and CP glasses. In Dy^{3+} doped fluoride glasses also this is found to be the case.¹⁶

The room temperature emission spectra of Pr^{3+} doped CAP and CP glasses are reproduced in figure 4.3. The most striking difference is in the relative intensities of the $^1\text{D}_2 \rightarrow ^3\text{H}_4$ transition compared to $^3\text{P}_0 \rightarrow ^3\text{H}_6$ transition which is significantly higher for the CP glass. The higher relative intensity for the former transition may arise due to preferential population of the $^1\text{D}_2$ level from $^3\text{P}_{0,1}$ levels by nonradiative decay in the CP glass matrix. The higher β_R obtained from Judd-Ofelt parameters for this transition in the CP glass compared to CAP glass also supports this observation. Similar observations have been reported by Blasse and coworkers for many crystalline systems.²²

The emission spectra of Eu^{3+} doped CAP and CP glasses showed better resolution at 77 K and are reproduced in figure 4.4. The $^5\text{D}_0 \rightarrow ^7\text{F}_0$ transition occurring at $17,271 \text{ cm}^{-1}$ and $17,259 \text{ cm}^{-1}$ for CAP and CP glasses respectively suggest 8-9 coordination for Eu^{3+} ions.²³ The relative intensity ratio of $(^5\text{D}_0 \rightarrow ^7\text{F}_2)/(^5\text{D}_0 \rightarrow ^7\text{F}_1)$ is a measure of ligand field asymmetry.^{24,25} The higher value observed for this ratio for the CAP glass indicates that Eu^{3+} ions occupy sites of higher asymmetry in this glass. Higher

Chapter 4

asymmetry for Eu^{3+} sites in CAP glass is also suggested by higher Ω_2 value for this glass as discussed earlier.

The phonon side bands for Eu^{3+} in the CAP and CP glasses appear at 440.0 and 440.2 nm respectively (figure 4.5). This band is due to the P-O^- stretching mode of the phosphate anion as shown by Tanabe *et al* for the phonon side band around 442 nm in the excitation spectra of Eu^{3+} doped fluoride glasses containing aluminium phosphate.⁷ The respective electron phonon coupling strengths^{7,26} for the stretching mode of P-O with Eu^{3+} ions are 10.3×10^{-3} and 14.3×10^{-3} . A higher electron phonon coupling strength for CP glass will imply more non-radiative decay.^{7,26,27} One would therefore expect less fluorescent emission in general in CP glass. This is indeed found to be the case for Eu^{3+} emission in CP glass compared to CAP glass as seen by comparison of normalized emission spectra for the two glasses. Evidence for higher nonradiative decay in the CP glass matrix is also provided by the higher relative intensity observed for the $^1\text{D}_2 \rightarrow ^3\text{H}_4$ transition compared to $^3\text{P}_0 \rightarrow ^3\text{H}_6$ transition for Pr^{3+} in this glass as discussed above. Further evidence for more favored nonradiative decay in CP glass is also provided by the $^1\text{G}_4 \rightarrow ^3\text{H}_6$ transition for Tm^{3+} ion as discussed below. These results are in accordance with higher non-radiative decay suggested by the higher electron phonon coupling strength for this glass.^{7,26,27}

The room temperature emission spectra of Dy^{3+} in CAP and CP glasses are reproduced in figure 4 6. Recently Qiang Su *et al* have shown in well characterized crystalline systems that the intensity ratio $(^4\text{F}_{9/2} \rightarrow ^6\text{H}_{13/2}) / (^4\text{F}_{9/2} \rightarrow ^6\text{H}_{15/2})$ for Dy^{3+} shows a behavior parallel to the $(^5\text{D}_0 \rightarrow ^7\text{F}_2) / (^5\text{D}_0 \rightarrow ^7\text{F}_1)$ ratio for Eu^{3+} .^{24,25} It is shown that the R/O and Y/B ratios increase with increase in covalency and site asymmetry. Previous works and our present studies also show that covalency and site asymmetry result in a significant enhancement of the Judd-Ofelt parameter Ω_2 .^{11,12,18} Thus one would expect

that Ln^{3+} (Eu, Dy) doped CAP glasses with significantly higher Ω_2 values would exhibit higher values for these ratios. This is indeed found to be the case.

The emission spectra of Tm^{3+} doped CAP and CP glasses at 77 K and 300 K are shown in figure 4.7. The spectra at 77 K show better resolution and a slight reduction in the emission intensity. Depending upon the nature of the absorption and emission spectra of the host matrix and their temperature dependence, a reduction in the emission intensities can result with increasing of temperature.^{1,8} However for a definite conclusion in the present systems a more detailed work is required. The relative intensity of $^1\text{G}_4 \rightarrow ^3\text{H}_6$ transition compared to $^3\text{P}_0 \rightarrow ^3\text{H}_6$ transition is noticeably larger for Tm^{3+} doped CP glass. This effect is similar to the observation of higher relative intensity observed for $^1\text{D}_2 \rightarrow ^3\text{H}_4$ transition compared to $^3\text{P}_0 \rightarrow ^3\text{H}_6$ transition for Pr^{3+} ions in this glass. Non-radiative decay as mentioned earlier is more favored in CP glass. This will lead to population of $^1\text{G}_4$ level being more favored on excitation to next higher energy $^1\text{D}_2$ level in Tm^{3+} ions. This in turn would result in the enhancement in the relative intensity of $^1\text{G}_4 \rightarrow ^3\text{H}_6$ emission in the CP glass compared to CAP glass.²⁸

4.3 Conclusions

All the rare earth ions studied give rise to higher Ω_2 values in the CAP glass matrix than for the same ions in the CP glass matrix. The transition probabilities (A) have been calculated for the important transitions for Pr^{3+} , Nd^{3+} , Er^{3+} and Pr^{3+} . For the same transitions the A values are higher for Nd^{3+} and lower for Pr^{3+} in CAP glass compared to CP glass. For Eu^{3+} , Dy^{3+} and Tm^{3+} the hypersensitive transitions show higher A values for the CAP glass. The A values are nearly the same for Er^{3+} in the two matrices. β_R (cal) and β_R (exptl) show good agreement for Pr^{3+} and Eu^{3+} . For Dy^{3+} the agreement is less satisfactory. The larger f_2 values and the higher intensity ratios, $(^3\text{D}_0 \rightarrow ^7\text{F}_2)/(^3\text{D}_0 \rightarrow ^7\text{F}_1)$ in Eu^{3+} and $(^4\text{F}_{9/2} \rightarrow ^6\text{H}_{13/2})/(^4\text{F}_{9/2} \rightarrow ^6\text{H}_{15/2})$ in Dy^{3+} in the CAP glass indicate that the presence of Al^{3+} leads to sites with higher asymmetry. The higher relative emission intensities for

the $^1D_2 \rightarrow ^3H_4$ compared to $^3P_0 \rightarrow ^3H_6$ in Pr^{3+} and for the $^1G_4 \rightarrow ^3H_4$ compared to $^1D_2 \rightarrow ^3F_4$ in Tm^{3+} doped CP glasses arise due to higher non-radiative decay in this glass. Phonon side band studies in the excitation spectra of Eu^{3+} also leads to higher electron phonon coupling strength for Eu^{3+}/CP glass indicating higher non-radiative decay rate for this system.

Table 4.1 The spectroscopic parameters of Pr^{3+} , Nd^{3+} , Er^{3+} and Tm^{3+} ions doped in $20\text{CaO}-10\text{Al}_2\text{O}_3-69\text{P}_2\text{O}_5-1\text{Ln}_2\text{O}_3$ (CAP) and $30\text{CaO}-69\text{P}_2\text{O}_5-1\text{Ln}_2\text{O}_3$ (CP) glass systems

Parameters	Pr^{3+}		Nd^{3+}		Er^{3+}		Tm^{3+}	
cm^{-1}	CAP	CP	CAP	CP	CAP	CP	CAP	CP
F^2	72528	72525	78416	78655	100466	100634	105382	104936
F^4	56538	56876	56113	55615	76289	76179	81228	79617
F^6	39652	39700	43081	43361	57154	57941	61737	60097
E^1	5037.9	5047.2	5335.0	5340.0	6998.0	7025.0	7422.8	7319.9
E^2	22.7	22.6	26.1	26.4	32.3	32.5	33.7	33.8
E^3	477.7	478.1	506.4	506.1	648.8	646.6	675.4	675.9
a	224	23.7	24.3	25.2	25.7	25.3	20.7	20.6
β	-15335	-1449.7	-670.0	-675.0	-860.0	-885.0	-1226.9	-1066.2
ξ	699.9	699.8	875.0	879.0	2427.0	2433.0	2658.4	2662.0
EVE^3	10.55	10.56	10.54	10.55	10.79	10.86	10.99	10.83
E^2/E^3	0.0475	0.0473	0.0515	0.0522	0.0498	0.0503	0.0499	0.0500
rms	± 37	$+20$	± 59	± 64	± 50	$+58$	± 43	± 50

Table 4.2 Observed and calculated energy levels in cm^{-1} of Pr^{3+} and Tm^{3+} ions in **20CaO-10Al₂O₃-69P₂O₅-1Ln₂O₃ (CAP)** and **30CaO-69P₂O₅-1Ln₂O₃ (CP)** glass systems.

Pr^{3+}					Tm^{3+}				
Terms	CAP		CP		Terms	CAP		CP	
from E_{obs}	E_{cal}	E_{obs}	E_{cal}		from	E_{obs}	E_{cal}	E_{obs}	E_{cal}
$^3\text{H}_4$	cm^{-1}	cm^{-1}	cm^{-1}	cm^{-1}	$^3\text{H}_6$	cm^{-1}	cm^{-1}	cm^{-1}	cm^{-1}
$^3\text{F}_2$	5256	5311	5220	5246	$^3\text{F}_4$	5886	5850	5836	5744
$^3\text{F}_3$	6605	6613	6553	6547	$^3\text{H}_5$	8278	8278	8291	8290
$^3\text{F}_4$	6695	6942	6920	6920	$^3\text{H}_4$	12626	12735	12620	12704
$^1\text{D}_2$	16920	16939	16920	16915	$^3\text{F}_3$	14598	14598	14535	14535
$^3\text{P}_0$	20833	20841	20833	20827	$^3\text{F}_2$	15197	15181	15151	15100
$^3\text{P}_1$	21367	21375	21367	21361	$^1\text{G}_4$	21598	21619	21505	21515
$^3\text{P}_2$	22522	22498	22512	22482	$^1\text{D}_2$	28011	28004	27933	27949
rms	± 24		± 20			± 44		± 51	

Table 4.3 Observed and calculated energy levels in cm^{-1} of Nd^{3+} and Er^{3+} ions in $20\text{CaO}-10\text{Al}_2\text{O}_3-69\text{P}_2\text{O}_5-1\text{Ln}_2\text{O}_3$ (CAP) and $30\text{CaO}-69\text{P}_2\text{O}_5-1\text{Ln}_2\text{O}_3$ (CP) glass systems

Nd^{3+}					Er^{3+}				
Terms	CAP		CP		Terms	CAP		CP	
from E_{obs}	E_{cal}	E_{obs}	E_{cal}		from	E_{obs}	E_{cal}	E_{obs}	E_{cal}
$^4\text{I}_{9/2}$	cm^{-1}	cm^{-1}	cm^{-1}	cm^{-1}	$^4\text{I}_{15/2}$	cm^{-1}	cm^{-1}	cm^{-1}	cm^{-1}
$^4\text{F}_{3/2}$	11441	11485	11467	11462	$^4\text{I}_{13/2}$	6631	6631	6623	6648
$^4\text{F}_{5/2}$	12468	12509	12484	12491	$^4\text{I}_{11/2}$	10225	10259	10235	10286
$^4\text{S}_{3/2}$	13405	13384	13405	13360	$^4\text{I}_{9/2}$	12469	12394	12531	12411
$^4\text{F}_{7/2}$	13487	13487	13487	13469	$^4\text{F}_{9/2}$	15384	15279	15384	15285
$^4\text{F}_{9/2}$	14662	14768	14641	14757	$^4\text{S}_{3/2}$	18467	18510	18467	18529
$^2\text{H}_{11/2}$	15974	15988	15974	15964	$^2\text{H}_{11/2}$	19230	19201	19230	19216
$^4\text{G}_{5/2}$	17153	17209	17153	17187	$^4\text{F}_{7/2}$	20534	20507	20492	20510
$^2\text{G}_{7/2}$	17421	17265	17452	17213	$^4\text{F}_{5/2}$	22173	22144	22173	22164
$^4\text{G}_{7/2}$	19047	19064	19047	19032	$^4\text{F}_{3/2}$	22472	22516	22573	22530
$^4\text{G}_{9/2}$	19569	19490	19569	19470	$^2\text{G}_{9/2}$	24630	24648	24630	24666
$^2\text{G}_{9/2}$	21052	21068	21008	21036	$^4\text{G}_{11/2}$	26525	26534	26455	26528
$^2\text{K}_{13/2}$	21756	21790	21739	21796	$^4\text{G}_{9/2}$	27472	27470	27472	27452
$^2\text{P}_{1/2}$	23310	23307	23310	23297					
$^4\text{D}_{3/2}$	28653	28571	28571	28673					
rms	± 50		± 52			± 44		± 58	

Table 4.4 The Judd-Ofelt parameters for lanthanide ions doped in **20CaO-10Al₂O₃-69P₂O₅-1Ln₂O₃** (CAP) and **30CaO-69P₂O₅-1Ln₂O₃** (CP) glass systems.

Lanthanide ion	Glass matrix	Ω_2 (10^{-20} cm ²)	ft_4 (10^{-20} cm ²)	Ω_6 (10^{-20} cm ²)
Pr³⁺	CP	-2.264	7.900	7.188
	CP*	-0.392	8.001	4.847
	CAP	0.860	6679	5.892
	CAP*	2.341	6.759	4.056
Nd³⁺	CP	3.179	2.564	4.067
	CAP	5.656	3.335	4.367
Eu³⁺	CP	5.530	2.147	2.502
	CAP	7.474	1.759	1.630
Dy³⁺	CP	6.513	1.843	1.824
	CAP	9 899	0.876	1.681
Er³⁺	CP	5 009	3.026	1.088
	CAP	6.192	3699	0914
Tm³⁺	CP	3 485	1.402	0.872
	CAP	3.386	1.841	0.753

Values are calculated excluding the hypersensitive transition $^3P_2 \leftarrow ^3H_4$

Table 4.5 Observed and calculated oscillator strengths of Pr^{3+} and Tm^{3+} ions in $20\text{CaO}-10\text{Al}_2\text{O}_3-69\text{P}_2\text{O}_5-1\text{Ln}_2\text{O}_3$ (CAP) and $30\text{CaO}-69\text{P}_2\text{O}_5-1\text{Ln}_2\text{O}_3$ (CP) glass systems

Pr^{3+}					Tm^{3+}				
Transition	CAP (10^{-6})		CP (10^{-6})		Transition	CAP (10^{-6})		CP (10^{-6})	
from $^3\text{H}_4$	obs	cal	obs	cal	from $^3\text{H}_6$	obs	cal	obs	cal
$^3\text{F}_2$	3.77	3.28	3.07	2.44	$^3\text{F}_4^*$	1.22	2.23	-	
$^3\text{F}_3$ $^3\text{F}_4$	8.44	10.82	9.64	12.62	$^3\text{H}_5$	1.67	1.19	1.39	1.17
$^1\text{D}_2$	2.06	1.17	2.36	1.39	$^3\text{H}_4$	2.91	2.09	2.01	2.13
$^3\text{P}_0$	2.51	3.91	2.55	4.65	$^3\text{F}_3$ $^3\text{F}_2$	1.85	2.38	2.33	2.34
$^3\text{P}_1$	5.54	3.98	6.92	4.74	$^1\text{G}_4$	1.02	0.75	0.83	0.68
$^3\text{P}_2^*$	9.72	3.86	11.99	4.67	$^1\text{D}_2$	2.56	2.09	1.60	1.65
rms	± 2.70		± 3.40			± 0.41		± 0.01	

Hypersensitive transition

Table 4.6 Observed and calculated oscillator strengths of Nd^{3+} ions in $20\text{CaO}-10\text{Al}_2\text{O}_3-69\text{P}_2\text{O}_5-1\text{Nd}_2\text{O}_3$ (CAP) and $30\text{CaO}-69\text{P}_2\text{O}_5-1\text{Nd}_2\text{O}_3$ (CP) glass systems

Transition	C	AP	(10^{-6})	CP	(10^{-6})
from $^4\text{I}_{9/2}$		obs	cal	obs	cal
$^4\text{F}_{3/2}$		1.68	1.70	1.12	1.36
$^4\text{F}_{5/2}$		5.75	5.75	5.08	5.03
$^4\text{S}_{3/2} \rightarrow ^4\text{F}_{7/2}$		5.81	6.08	5.26	5.56
$^4\text{F}_{9/2}$		0.55	0.48	0.34	0.42
$^2\text{H}_{11/2}$		0.11	0.13	0.12	0.11
$^4\text{G}_{5/2} \rightarrow ^2\text{G}_{7/2}$		19.71	19.78	12.26	12.35
$^4\text{G}_{7/2} \rightarrow ^4\text{G}_{9/2}$		5.68	4.75	4.76	3.66
$^2\text{K}_{15/2} \rightarrow ^2\text{G}_{9/2} \rightarrow ^4\text{G}_{11/2}$		1.55	0.98	1.22	0.82
$^2\text{P}_{1/2}$		0.42	0.43	0.33	0.33
$^4\text{D}_{3/2} \rightarrow ^4\text{D}_{1/2}$		8.14	8.38	6.27	6.50
rms		± 0.36		± 0.32	

Hypersensitive transition

Table 4.7 Observed and calculated oscillator strengths of Eu^{3+} ions in $20\text{CaO}-10\text{Al}_2\text{O}_3-69\text{P}_2\text{O}_5-1\text{Eu}_2\text{O}_3$ (CAP) and $30\text{CaO}-69\text{P}_2\text{O}_5-1\text{Eu}_2\text{O}_3$ (CP) glass systems

Transition from $^7\text{F}_0$	CAP			CP		
	Spectral region (nm)	10^{-6}		Spectral region (nm)	10^{-6}	
		obs	cal		obs	cal
$^5\text{D}_2$	462.1	0.19	0.19	462.5	0.14	0.14
$^5\text{L}_6$	390.1	0.98	0.95	390.8	1.46	1.44
$^5\text{G}_4$ $^5\text{G}_6$	373.2	0.16	0.29	373.2	0.26	0.49
$^5\text{D}_4$	359.6	0.16	0.78	359.2	0.20	0.09
$^5\text{H}_6$				315.5	0.71	0.65
rms		± 0.01			± 0.01	

Hypersensitive transition

Table 4.8 Observed and calculated oscillator strengths of Dy^{3+} ions in $20\text{CaO}-10\text{Al}_2\text{O}_3-69\text{P}_2\text{O}_5-1\text{Dy}_2\text{O}_3$ (CAP) and $30\text{CaO}-69\text{P}_2\text{O}_5-1\text{Dy}_2\text{O}_3$ (CP) glass systems.

CAP				CP		
Transition	Spectral	10 [*]		Spectral	10 ⁻⁶	
from ⁶ H _{15/2}	region (nm)	obs	cal	region (nm)	obs	cal
⁶ H _{11/2}	1658.1	0.88	1.15	1682.0	1.10	1.03
⁶ F _{11/2} ⁶ H _{9/2}	1253.9	7.88	7.90	1277.9	5.99	6.05
⁶ F _{9/2} ⁶ H _{7/2}	1095.0	1.22	1.43	1091.9	1.66	1.99
⁶ H _{5/2}	965.9	0.04	0.04	977.9	0.12	0.05
⁶ F _{7/2}	891.9	1.21	1.37	895.9	1.56	1.61
⁶ F _{5/2}	799.3	0.59	0.69	801.7	0.80	0.75
⁶ F _{3/2}	750.0	0.12	0.13	752.6	0.18	0.14
⁴ I _{13/2}	459.7	0.77	0.48	460.2	0.74	0.47
⁴ G _{11/2}	421.9	0.11	0.03	422.8	0.18	0.06
⁴ F _{7/1} ⁴ K _{17/2} ⁴ I _{13/2}	378.5	1.76	1.11	379.7	2.25	1.22
⁴ M _{19/2} ⁶ P _{3/2}	360.6	1.61	1.48	361.4	1.41	1.65
(⁴ P ⁴ D) _{3/2}						
rms		±0.25			±0.35	

Table 4.9 Observed and calculated oscillator strengths of Er^{3+} ions in $20\text{CaO}-10\text{Al}_2\text{O}_3-69\text{P}_2\text{O}_5-1\text{Er}_2\text{O}_3$ (CAP) and $30\text{CaO}-69\text{P}_2\text{O}_5-1\text{Er}_2\text{O}_3$ (CP) glass systems

Transition from $^4\text{I}_{15/2}$	CAP (10^{-6})		CP (10^{-6})	
	obs	cal	obs	cal
$^4\text{I}_{13/2}$	1.52	1.48	1.66	1.45
$^4\text{I}_{11/2}$	0.74	0.67	0.64	0.66
$^4\text{I}_{9/2}$	0.27	0.47	0.37	0.38
$^4\text{F}_{9/2}$	1.79	3.08	1.85	2.66
$^4\text{S}_{3/2}$	0.77	0.52	0.64	0.54
$^2\text{H}_{11/2}^*$	10.28	10.60	8.50	8.57
$^4\text{F}_{7/2}$	1.83	2.37	1.92	2.25
$^4\text{F}_{5/2} \ ^4\text{F}_{3/2}$	0.82	0.96	0.81	0.99
$^2\text{G}_{9/2}$	0.66	1.01	0.63	0.92
$^4\text{G}_{11/2}^*$	19.21	19.04	15.42	15.39
$^4\text{G}_{9/2}$	4.83	2.89	3.73	2.55
rms	± 0.59		± 0.30	

* Hypersensitive transition

Table 4.10 The calculated radiative properties(A, PR) for selected transitions of Nd^{3+} , Er^{3+} and Tm^{3+} ions doped in $20\text{CaO}-10\text{Al}_2\text{O}_3-69\text{P}_2\text{O}_5-1\text{Ln}_2\text{O}_3$ (CAP) and $30\text{CaO}-69\text{P}_2\text{O}_5-1\text{Ln}_2\text{O}_3$ (CP) glass systems.

Transition	CAP		CP	
	A sec^{-1}	β_R	A sec^{-1}	β_R
Neodymium(III)				
$^4\text{F}_{3/2} \rightarrow ^4\text{I}_{13/2}$	230	0.10	209	0.11
$^4\text{F}_{3/2} \rightarrow ^4\text{I}_{11/2}$	1140	0.51	999	0.53
$^4\text{F}_{3/2} \rightarrow ^4\text{I}_{9/2}$	867	0.39	685	0.36
Erbium(III)				
$^4\text{I}_{13/2} \rightarrow ^4\text{I}_{15/2}$	180	1.00	180	1.00
$^4\text{I}_{11/2} \rightarrow ^4\text{I}_{13/2}$	38	0.26	37	0.25
$^4\text{I}_{11/2} \rightarrow ^4\text{I}_{15/2}$	107	0.74	112	0.75
$^4\text{S}_{3/2} \rightarrow ^4\text{I}_{9/2}$	65	0.06	63	0.05
$^4\text{S}_{3/2} \rightarrow ^4\text{I}_{11/2}$	27	0.02	30	0.02
$^4\text{S}_{3/2} \rightarrow ^4\text{I}_{13/2}$	303	0.26	352	0.27
$^4\text{S}_{3/2} \rightarrow ^4\text{I}_{15/2}$	752	0.66	874	0.66
Thulium(III)				
$^3\text{F}_4 \rightarrow ^3\text{H}_6$	166	1.00	144	1.00
$^3\text{H}_4 \rightarrow ^3\text{H}_5$	20	0.03	15	0.02
$^3\text{H}_4 \rightarrow ^3\text{F}_4$	68	0.08	67	0.08
$^3\text{H}_4 \rightarrow ^3\text{H}_6$	740	0.89	745	0.90

Table 4.11 The radiative properties for the emission levels of Pr^{3+} , Eu^{3+} and Dy^{3+} ions doped in $20\text{CaO}-10\text{Al}_2\text{O}_3-69\text{P}_2\text{O}_5-1\text{Ln}_2\text{O}_3$ (CAP) glass system

Transition	λ_p nm	$\Delta\lambda_p$ nm	A sec ⁻¹	β_R cal exptl		σ_p cm ² 10 ⁻²⁰
Praseodymium(III)						
³ P ₀ → ³ H ₄	482.4	18.9	23590	0.66	0.66	385.7
³ P ₀ → ³ H ₅	523.6	10.9	0	0	0.19	0
³ P ₀ → ³ H ₆	609.8	19.4	4729	0.13	0.12	192.0
³ P ₀ → ³ F ₂	638.0	8.4	2137	0.06	0.03	239.5
¹ D ₂ → ³ H ₄	596.1	19.6	912	0.38	-	33.3
Europium(III)						
⁵ D ₀ → ⁷ F ₀	579.0	3.9	0	0	0.02	0
⁵ D ₀ → ⁷ F ₁	591.2	11.9	60	0.15	0.28	3.5
⁵ D ₀ → ⁷ F ₂	612.0	9.9	284	0.70	0.66	19.1
⁵ D ₀ → ⁷ F ₃	651.4	7.8	0	0	0.02	0
⁵ D ₀ → ⁷ F ₄	699.0	8.2	35	0.09	0.01	5.9
Dysprosium(III)						
⁴ F _{9/2} → ⁶ H _{15/2}	483.8	15.5	106	0.11	0.44	2.2
⁴ F _{9/2} → ⁶ H _{13/2}	572.8	12.5	708	0.75	0.55	34.9
⁴ F _{9/2} → ⁶ H _{11/2}	661.0	13.2	78	0.08	0.01	6.4
⁴ F _{9/2} → ⁶ H _{9/2}	758.6	9.1	35	0.04	0.01	7.2
$\Gamma_{11/2}$						

Table 4.12 The **radiative** properties for the emission levels of Pr^{3+} , Eu^{3+} and Dy^{3+} ions doped in $30\text{CaO}-69\text{P}_2\text{O}_5-1\text{Ln}_2\text{O}_3$ (CP) glass system.

Transition	λ_p nm	$\Delta\lambda_p$ nm	A sec ⁻¹	β_R cal exptl		σ_p cm ² 10 ⁻²⁰
Praseodymium(III)						
³ P ₀ → ³ H ₄	482.2	15.4	27473	0.70	0.65	554.4
³ P ₀ → ³ H ₅	523.0	10.1	0	0	0.19	0
³ P ₀ → ³ H ₆	610.0	15.8	5681	0.14	0.12	286.5
³ P ₀ → ³ F ₂	637.0	7.6	0	0	0.03	0
¹ D ₂ → ³ H ₄	596.0	17.1	1078	0.50	-	45.7
Europium(III)						
⁵ D ₀ → ⁷ F ₀	579.4	3.9	0	0	0.02	0
⁵ D ₀ → ⁷ F ₁	591.8	9.9	60	0.17	0.35	4.7
⁵ D ₀ → ⁷ F ₂	612.6	11.4	211	0.60	0.60	13.2
⁵ D ₀ → ⁷ F ₃	651.2	7.7	0	0	0.01	0
⁵ D ₀ → ⁷ F ₄	698.4	8.1	41	0.12	0.02	8.1
Dysprosium(III)						
⁴ F _{9/2} → ⁶ H _{15/2}	483.8	143	121	0.16	0.51	2.7
⁴ F _{9/2} → ⁶ H _{13/2}	572.8	11.8	528	0.70	0.48	27.9
⁴ F _{9/2} → ⁶ H _{11/2}	662.4	13.5	53	0.07	0.01	4.4
⁴ F _{9/2} → ⁶ H _{9/2}	758.2	9.9	28	0.04	0.01	5.4
F _{11/2}						

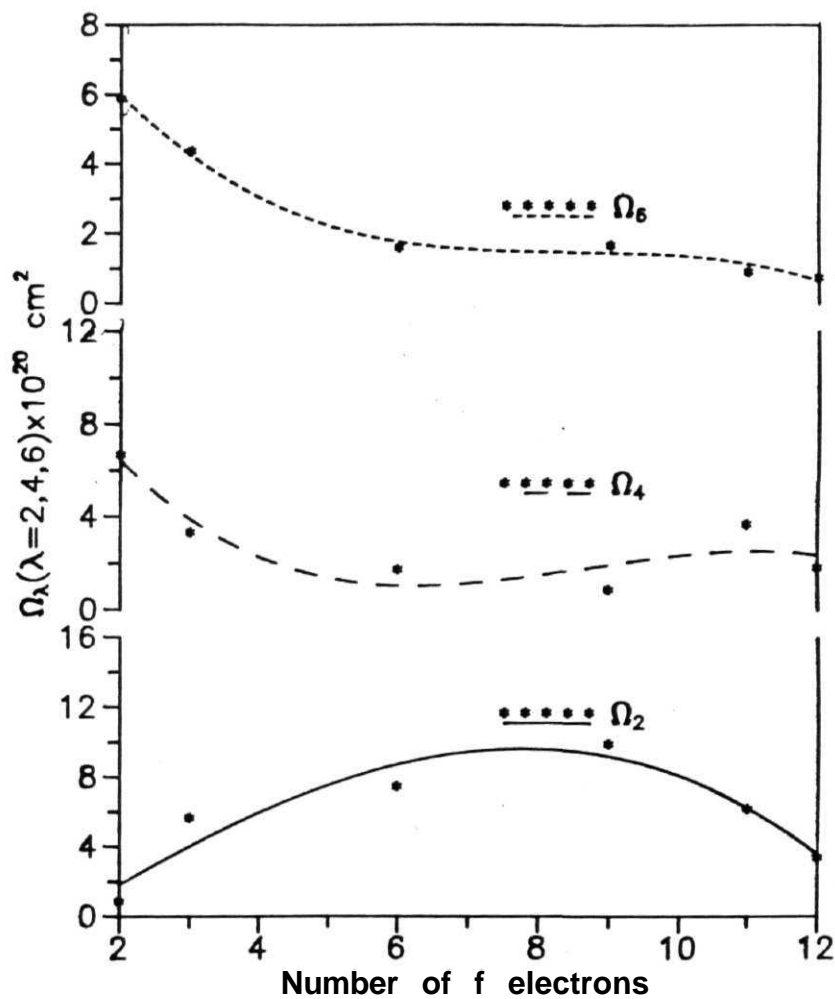


Figure 4.1 Dependence of intensity parameters Ω_λ ($\lambda=2,4,6$) on atomic number of rare earth ions in $\text{CaO-Al}_2\text{O}_3\text{-P}_2\text{O}_5$ (CAP) glass system.

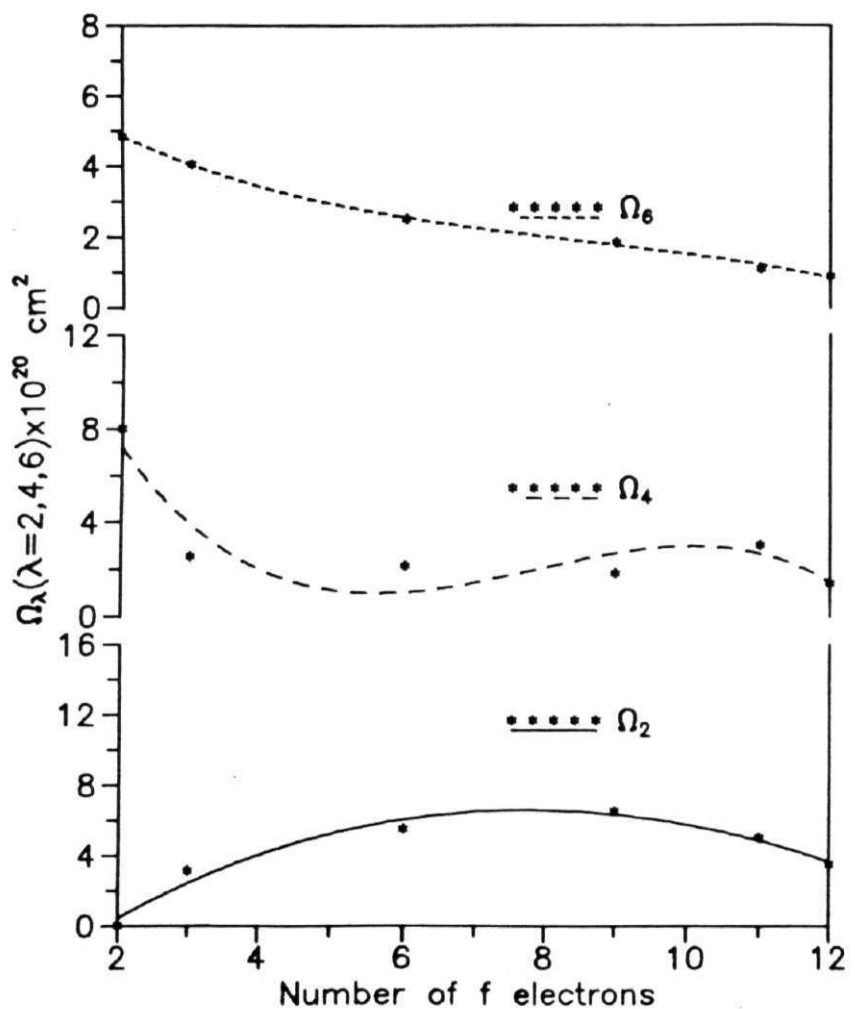


Figure 4.2 Dependence of intensity parameters Ω_λ ($\lambda=2, 4, 6$) on atomic number of rare earth ions in $\text{CaO-P}_2\text{O}_5$ (CP) glass system.

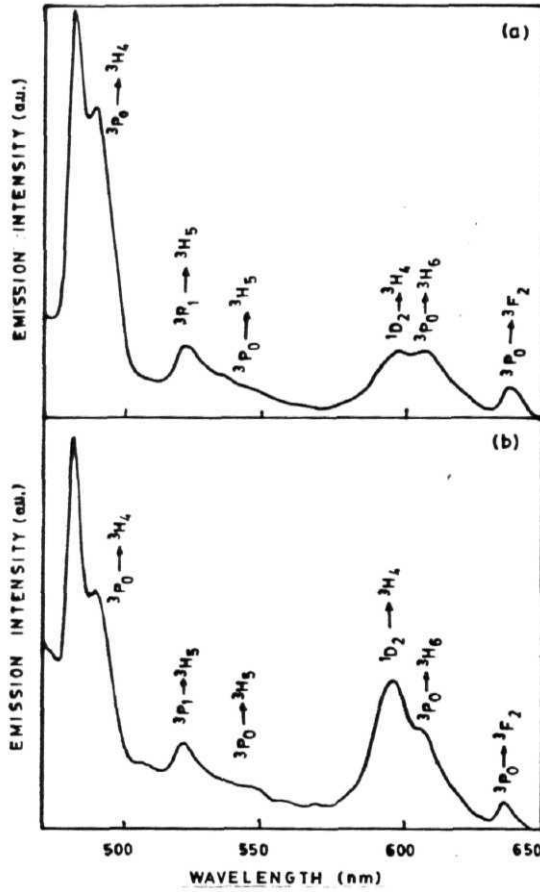


Figure 4.3 The emission spectra of Pr^{3+} ions in (a) $\text{CaO-Al}_2\text{O}_3\text{-P}_2\text{O}_5$ (CAP) and (b) $\text{CaO-P}_2\text{O}_5$ (CP) glasses at 300 K. $\lambda_{\text{ex}} = 445$ nm.

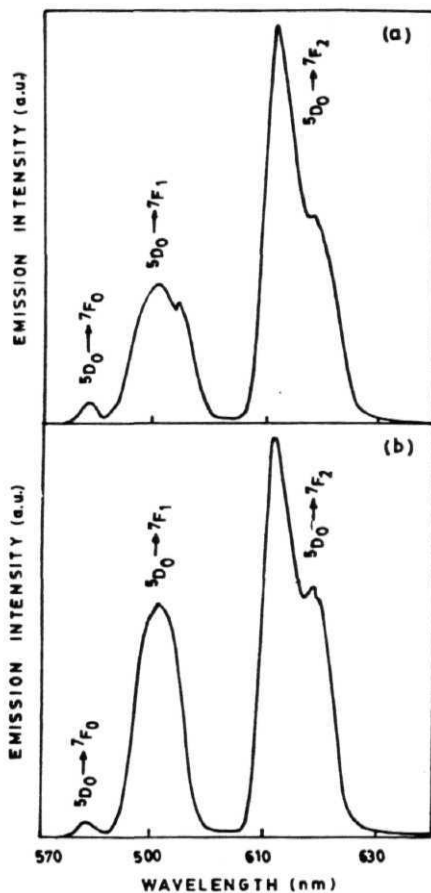


Figure 4.4 The emission spectra of Eu^{3+} ions in (a) $\text{CaO-Al}_2\text{O}_3\text{-P}_2\text{O}_5$ (CAP) and (b) $\text{CaO-P}_2\text{O}_5$ (CP) glasses at 77 K. $\lambda_{\text{ex}} = 395$ nm.

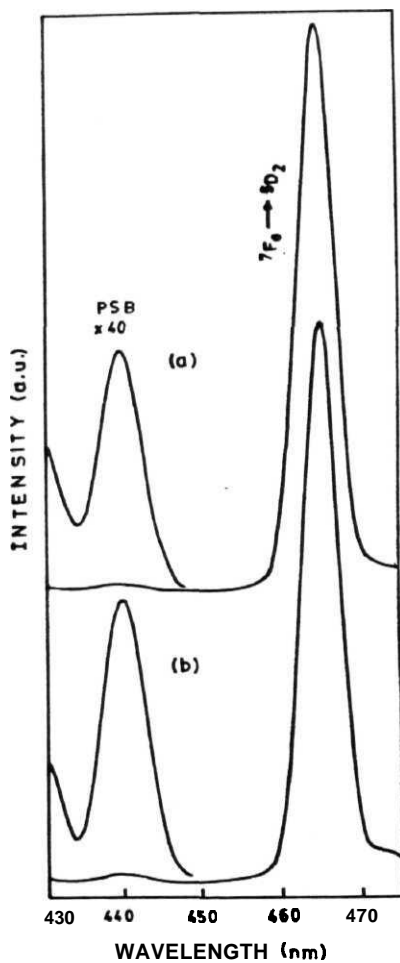


Figure 4.5 The excitation spectra of Eu^{3+} ions in (a) $\text{CaO-Al}_2\text{O}_3\text{-P}_2\text{O}_5$ (CAP) and (b) $\text{CaO-P}_2\text{O}_5$ (CP) glasses at 300 K with phonon side band (PSB) $\lambda_{\text{em}} = 613 \text{ nm}$. Base lines are shifted for clarity

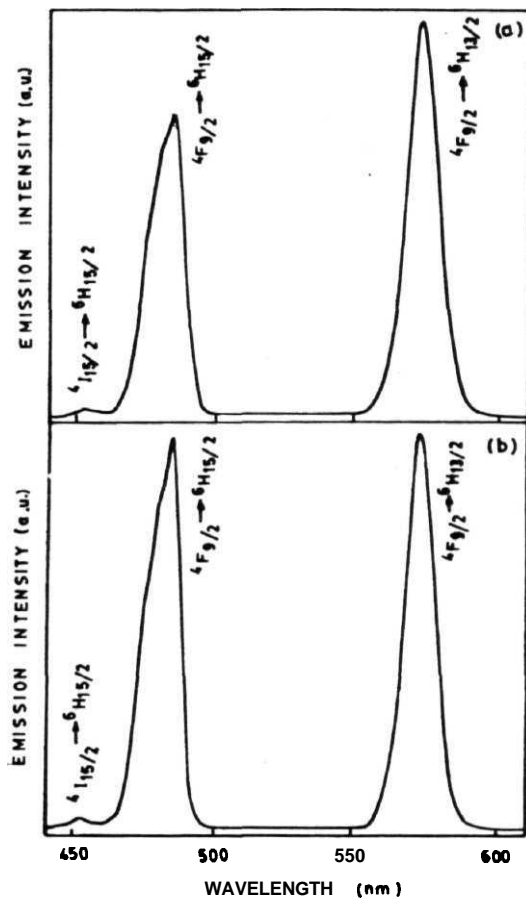


Figure 4.6 The emission spectra of Dy^{3+} ions in (a) $\text{CaO-Al}_2\text{O}_3\text{-P}_2\text{O}_5$ (CAP) and (b) $\text{CaO-P}_2\text{O}_5$ (CP) glasses at 300 K $\lambda_{\text{ex}} = 350$ nm.

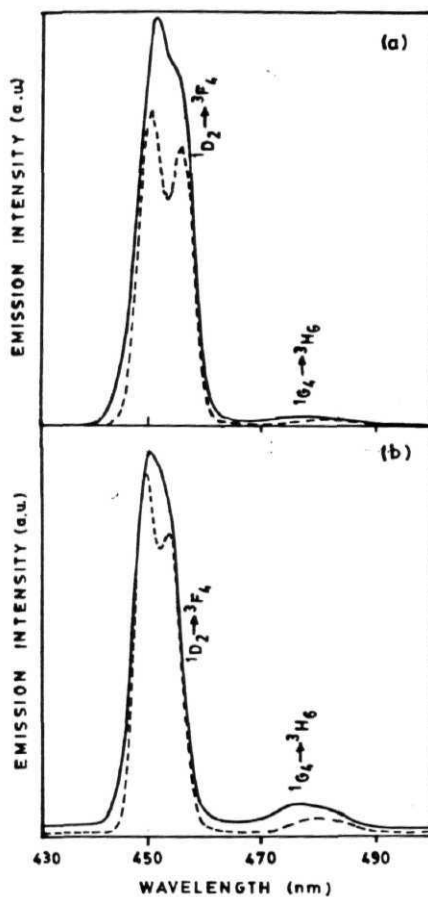


Figure 4.7 The emission spectra of Tm^{3+} ions in (a) $\text{CaO-Al}_2\text{O}_3\text{-P}_2\text{O}_5$ (CAP) and (b) $\text{CaO-P}_2\text{O}_5$ (CP) glasses at 300 K (solid line) and 77 K (dotted line) $\lambda_{\text{ex}} = 357 \text{ nm}$

References

- 1 **R** Reisfeld, *Structure and Bonding* **22** (Springer-Verlag, New York, 1975) 123.
2. R. Reisfeld and C.K. **Jorgensen**, *Lasers and Excited States of Rare Earths* (Springer-Verlag, New York, 1977).
3. **R** Reisfeld and C **K** Jorgensen, *Hand Book on the Physics and Chemistry of Rare Earths*, (Eds.) K.A. Gschneidner and L. Eyring, 9 (North-Holland, New York, 1987) chap. 58.
4. J.W.M. Verwey and G. Blasse, *Chem. Mater.* 2 (1990) 458.
- 5 E.W.J.L. **Oomen**, *J. Lumin.* SO (1992) 317
6. M.D. Shinn, W.A. Sibley, M.G. Drexhage and R.N. Brown, *Phys. Rev.* 27 (1983) 6635.
7. **S** Tanabe, **K** Hairo and N. **Soga**, *J. Non-Cryst. Solids* **142** (1992) 148.
8. R. Reisfeld and Y. Eckstein, *J. Chem. Phys.* 63 (1975) 4001
9. **R** Reisfeld and Y. Eckstein, *J. Solid State Chem.* 5 (1972) 174
- 10 R. Reisfeld, *J. Less-Common Mets.* **112** (1985) 9
11. **I.M.** Thomas, S.A. Payne and G D. Wilke, *J. Non-Cryst. Solids* **151** (1992) **183**
12. C K. Jorgensen and R. Reisfeld, *J. Less-Common Mets.* 93 (1983) 107
- 13 M. **Eyal**, E. Greenberg, R. Reisfeld and N. Spector, *Chem. Phys. Lett.* **117** (1985) 108.
- 14 W.T. **Carnall**, **J.P** Hessler and F. Wagner, Jr., *J. Phys. Chem.* 82 (1978) 2152.
- 15 L. **Wetenkemp**, G.F. West and H. Tobben, *J. Non-Cryst. Solids* **140** (1992) 35.
16. V.M. Orera, P.J. Alonso, R. Cases and R. Alcala, *Phys. Chem. Glasses* 29 (1988) 59.
17. R.D. Peacock, *Structure and Bonding* **22** (Springer-Verlag, New York 1975) 83
- 18 W.F. Krupke, *Phys. Rev.* **145** (1966) 325.
19. A.F. **Kirby** and R.A. Palmer, *Inorg. Chem.* **20** (1981) 4219.
- 20 A.F. Kirby and R.A. Palmer, *Inorg. Chem.* 20 (1981) 1030.

- 21 T. Fujiyama, T. **Yokoyama**, M. Hori and M Sasaki, *J. Non-Cryst. Solids* **135** (1991)198.
- 22 C de **Mello** Donega, A Meijerink and G. Blasse, *J. Phys. **Chem.** Solids* 56 (1995) 673.
- 23 G Boulon, M. **Bouderbala**, and J. Seriot, *J. Less-Common **Mets.*** **112** (1985) 41
- 24 P.K Gallagher, C.R Kurkjian, P.M Bridenbaugh, *Phys. Chem. Glasses* 6 (1965) **95**.
- 25 Q Su, Z **Pai**, L. Chi, H Zhang, Z Zhang and F. Zou, *J. Alloys **Compds.*** **192** (1993)25.
- 26 S Tanabe, S. Todoroki, K Hairo and N. Soga, *J. Non-Cryst. Solids* **122** (1990) **59**
27. T. Miyakawa and D.L. Dexter, *Phys. Rev.* **B1** (1970) **2961**.
- 28 B C Joshi and M C **Joshi**, *J. Non-Cryst. Solids* **142** (1992) 171.

Absorption and Emission Spectral Studies of Lanthanide Ions in Lead Oxyfluoride Glasses

Lead bearing oxyhalide glasses were first identified and characterized by Rao *et al.*^{1,4} Their characterization studies include **thermodynamic** and electrical properties of these **glasses**. They have also put forward a structural model for these glasses based on x-ray absorption fine structure. The oxyhalide glasses have distinctly different structural features compared to borate, phosphate and silicate **glasses**.¹⁻⁴ In this chapter we present the results of the optical properties of rare earth ions doped in the lead based oxyfluoride glass as host **matrix**. The glasses are characterized by a structure consisting of octahedrally situated Pb^{2+} ions and the network is made of covalent Pb-O and ionic Pb-F bonds.¹ These glasses further show good conductivity¹ and hence Ln^{3+} ions doped PbO-PbF_2 glass system can provide an impetus for further studies for device **applications**. These oxyfluoride glasses can be prepared with relative ease and show good thermal stability and insensitivity to **moisture**.¹ The rare earth ions may occupy sites with large interionic distances thereby precluding concentration quenching. They have phonon energy characteristics permitting observation of fluorescence for a number of rare earth ions over a wide spectral region.⁵ Glass matrices as hosts are attractive as they can be prepared with relative ease and enable systematic variation in the composition of the glass matrices and associated properties such as thermal stability and refractive **index**.¹ The latter in particular is known to bring about changes in the emission properties of the dopant ions as **well**. While the optical properties of rare earth ions in borate, phosphate and tellurite glasses have been reported earlier by Reisfeld and Jorgenson and others,^{6,8} their optical properties in fluoride glass matrices have been reported in some detail in recent literature.⁹⁻¹⁴ Thus the present studies in oxyfluoride glasses can fill the gap and provide an overall understanding of the subject.

Chapter 5

For convenience of presentation, the results of our absorption and emission spectral studies of lanthanide ions in the **PbO-PbF₂ oxyfluoride** glass system, are covered as follows.

- i. *Absorption and emission spectral studies of Pr^{3+} and Tm^{3+} ions in $30\text{PbO}-70\text{PbF}_2$ glass:* In this part we present both the absorption and emission spectral studies of these two ions with the related electronic configurations $4f^2$ ($^3\text{H}_4$) and $4f^{12}$ ($^3\text{H}_6$) respectively.
- ii. *Optical properties of Nd^{3+} , Ho^{3+} and Er^{3+} ions doped in $30\text{PbO}-70\text{PbF}_2$ glasses:* These ions give rise to a large number of narrow absorption transitions in the ultraviolet, visible and near infrared region many of which are hypersensitive and can therefore be profitably compared. Further Nd^{3+} $4f^3$ ($^4\text{I}_{9/2}$) and Er^{3+} $4f^{11}$ ($^4\text{I}_{15/2}$) have related electronic configurations. Thus the absorption spectral studies of the above ions doped in $30\text{PbO}-70\text{PbF}_2$ glass are presented together in this section. Due to the limitations of the experimental facility the emission spectra of Nd^{3+} could not be recorded. The emission spectra of Ho^{3+} and Er^{3+} could however be measured and thus the results of the emission spectral studies of these ions doped in $30\text{PbO}-70\text{PbF}_2$ glass are also presented in this part.
- iii. *Absorption and emission spectral studies of Sm^{3+} and Dy^{3+} ions in oxyfluoride glasses:* Sm^{3+} and Dy^{3+} have the related electronic configurations of $4f^6$ ($^6\text{H}_{5/2}$) and $4f^9$ ($^6\text{H}_{5/2}$) respectively. These two ions give rise to a large number of absorption and emission transitions over a wide spectral region. Thus the absorption and emission spectral studies of Sm^{3+} and Dy^{3+} ions in $30\text{PbO}-70\text{PbF}_2$ glass are presented separately in this part.
- iv. *Absorption and emission spectral studies of Eu^{3+} doped in $\text{PbO}-\text{PbF}_2$ glass system:* Compared to the rare earth ions mentioned above Eu^{3+} $4f^6$ ($^7\text{F}_0$) gives rise to only a limited number of absorption transitions over a wide region. The emission and excitation spectra of Eu^{3+} are more informative. Thus, the composition

dependent absorption and emission spectral studies of Eu³⁺ are presented separately in this part.

- v. *Tb fluorescence as a probe for cluster formation in lead oxyfluoride glasses:*
The absorption spectral study of Tb³⁺ 4f⁸ (⁷F₆) is not much informative. The emission studies on the other hand are of considerable value. Tb³⁺ gives rise to pronounced emission transitions from ⁵D₃ and ⁵D₄ levels which appear in the blue and the green regions respectively. The integrated intensity ratio of the transitions falling into these two regions is a sensitive function of cluster formation of the dopant ions. As it is considered more interesting to investigate the use of this ion as a probe for cluster formation, studies in this direction are carried out and the results are presented separately in this part.

Preparation of PbO-PbF₂ Oxyfluoride Glasses:

The glass samples with compositions in mol % 30PbO-70PbF₂-xLn³⁺ (where x=0.2 and 1.35 in wt. % Ln=Pr, Nd, Sm, Dy, Ho, Er or Tm) were prepared by a procedure very similar to that described by Rao *et al* except for the modifications required for introduction of the rare earth ion of interest.¹ Reagent grade Pb₃O₄, PbF₂ and respective rare earth oxides (Aldrich Chem. Co.) have been used as starting materials. The following details regarding the starting materials relevant to glass preparation are noted from the literature.¹⁵ Pb₃O₄ decomposes to PbO at 500 °C with evolution of oxygen and finally melts at 890 °C. The melting temperature of PbF₂ is 855 °C. The weighed quantities of the starting materials for 10 g of glass in single batch were ground to give a homogeneous mixture. The finely ground mixture was then placed in a silica crucible and heated in an electric furnace. A slow heating rate was initially maintained until the temperature reached 600 °C and the decomposition of Pb₃O₄ was complete. The temperature was then rapidly increased to 850 to 900 °C when a brown melt was obtained. The crucible containing the melt was constantly agitated to keep the melt bubble free and ensure homogeneous mixing. The molten state was retained for about 10 min, and the melt was poured into a slot in a stainless steel plate and quenched

rapidly by pressing with another stainless steel **plate**. The inner surface of the silica crucible in contact with the melt is found to be slightly affected. But the composition of the glass is not substantially influenced on this account or on account of possible loss of starting materials. For the preparation of each sample a new crucible was used each time. Typical weight loss on melting under experimental conditions indicated that the actual compositions lie within 1 % of the values quoted for the components. The samples were annealed at a temperature 20 °C below T_g and subsequently polished with commercial media and water free lubricant. The samples could be obtained with good transparency and uniform thickness of 0.2 cm and 2.0 cm diameter. For some of the studies it was required to prepare **PbO-PbF₂** glass of different compositions with varying concentrations of Eu^{3+} . Thus samples with the compositions **30PbO-70PbF₂-xEu³⁺** and **70PbO-30PbF₂-xEu³⁺** (where $x=0.2$ and 2.0 in wt. %) were prepared by an analogous procedure taking the starting materials corresponding to the desired **stoichiometry**. Similarly for Tb^{3+} emission and energy transfer studies samples with varying concentrations of the required dopant ions, the exact compositions of which are given below were prepared by altering the amounts of the rare earth oxide taken at the beginning of the preparations suitably.

- (i) **30PbO-70PbF₂-xTb³⁺** (where $x=0.1, 0.2, 0.5, 1.0$ and 2.0 in wt. %)
- (ii) **30PbO-70PbF₂-xPr³⁺-yTb³⁺** (where $x=0.5$ and $y=0.0, 0.12, 0.25, 0.5, 0.75, 1.0, 1.25$ in wt. %).
- (iii) **30PbO-70PbF₂-xPr³⁺-yTb³⁺** (where $x=0.0, 0.2, 0.5, 0.7$ and $y=0.5$ in wt. %).

5.1 Absorption and Emission Spectral Studies of **Pr³⁺** and **Tm³⁺** Ions in **PbO-PbF₂** Glass

The optical spectral studies of **Pr³⁺** (**4f²**) and **Tm³⁺** (**4f³**) have several features of interest. Laser action has been observed in **Pr³⁺** and **Tm³⁺** incorporated crystalline and glassy systems.¹⁶⁻¹⁸ Application of Judd-Ofelt theory in the case of **Pr³⁺** is less successful unlike in the case of other **Ln³⁺** ions.¹⁹ Both these ions exhibit hypersensitive transitions in their absorption spectra.^{19,20} Absorption and emission spectral studies of these rare earth ions provide scope for extending the work to cross relaxation studies in **Pr³⁺** and upconversion studies in **Tm³⁺** ion.²¹⁻²⁴ In continuance of our works in individual **Ln³⁺** ions doped in these glasses, preliminary investigations on the energy transfer when **Pr³⁺** and **Tb³⁺** were codoped in the **PbO-PbF₂** glass were also carried out. Interestingly these investigations revealed an hitherto unreported energy transfer from **Pr³⁺** to **Tb³⁺** with the former as donor. Hitherto reported works show that **Pr³⁺** acts only acceptor.²⁵⁻²⁸ The results of these studies are also submitted here.

5.1.1 Results and Discussion

The absorption spectra of the oxyfluoride glasses, 30**PbO**-70**PbF₂**-1.35 wt. % **Pr³⁺** and 30**PbO**-70**PbF₂**-1.35 wt. % **Tm³⁺** are reproduced in figures 5.1 and 5.2 respectively. The spectroscopic parameters derived from the transition energies in the absorption spectra of **Pr³⁺** and **Tm³⁺** are given in table 5.1. The observed and calculated transition energies are reproduced in table 5.2 along with rms deviations. The small rms values show that the agreement between the observed and calculated transition energies is quite good. In the case of **Tm³⁺** six parameters viz., **E¹**, **E²**, **E³**, **a**, **β** and **ξ** were found to be adequate for getting a good fit as reported by earlier workers.^{29,30} Self absorption by the sample in the ultraviolet region precluded the observation of **³P₂ ← ³H₆** and **¹D₂ ← ³H₆** transitions for **Tm³⁺**. The Judd-Ofelt parameters obtained from a least square fit of observed oscillator strengths of **Pr³⁺**, and **Tm³⁺** are given in tables 5.3. The observed oscillator strengths are compared with those calculated using the resultant Judd-Ofelt

parameters in table 5.4 along with their respective deviations. The small **rms** values show that observed and calculated oscillator strengths are in good agreement. In the analysis of **Pr³⁺** spectrum exclusion of the hypersensitive transition $^3P_2 \leftarrow ^3H_4$ leads to non-negative values of Ω_2 with improved match between observed and calculated oscillator strengths (table 5.4).¹⁹ The larger rms values observed between observed and calculated oscillator strengths in the case of **Pr³⁺** arises due to 4f-5d mixing^{9,31} which is known to bring about contributions to intensities through U^λ matrix elements with odd values of λ which are usually taken to be negligible for the calculation of the **Judd-Ofelt parameters**.⁶⁻⁸ The transition $^3P_0 \leftarrow ^3H_4$ occurs at 20,704 cm⁻¹ indicating 8-9 coordination around the **Ln³⁺** ion.³² The glass matrix **PbO-PbF₂** is known to be made of **OPb₄** tetrahedra and **PbO₂F₄** octahedra with **O-Pb-O** linkages.¹ In such a solid the eight coordination for the dopant **Ln³⁺** ions can be visualized with the **Ln³⁺** ion being surrounded predominantly by eight F⁻ ions from six **PbO₂F₄** octahedra as shown in figure 5.3. It is seen in this instance that **Ln³⁺** ions occupy sites with **D_{2h}** or lower micro **symmetry**. However in a glass matrix other types of sites with **Ln³⁺** ions surrounded by more or less than eight ligand atoms of different types cannot be ruled out although the number of such sites may be significantly **less**. Ω_2 is known to be sensitive to bonding of the **Ln³⁺** ions and in the present case they are found to be significantly low both for **Pr³⁺** and **Tm³⁺** ions. The f_i^* ($\lambda=2,4,6$) values for the present system are much smaller than those reported for glass matrices with oxide ligands and comparable to **Ln³⁺** (**Pr, Tm**) ions in fluoride **glasses**.^{7,8,10,11,33} Thus the values of Judd-Ofelt parameters support the above suggested coordination with **Ln³⁺** predominantly surrounded by fluoride ligands.

The emission spectra of oxyfluoride glasses, **30PbO-70PbF₂-0.2 wt. % Pr³⁺** and **30PbO-70PbF₂-0.2 wt. % Tm³⁺** are given in figures 5.4 and 5.5 respectively and their radiative properties are given in table 5.5. The radiative lifetimes of important emission levels calculated from Judd-Ofelt parameters are given in table 5.6. The emission spectrum of **Pr³⁺** consists of the bands originating from 3P_1 , 3P_0 and 1D_2 levels. The

relative intensities of emission bands originating from 3P_1 level decreased at 77 K (figure 5.4). Thus at higher temperature the enhanced Boltzmann population of higher Stark components of the ground state 3H_4 facilitating direct excitation to 3P_1 and/or the thermal excitation from 3P_0 to 3P_1 result in enhanced fluorescence from this level. According to Judd-Ofelt theory only four bands are allowed from 3P_0 level by the dipole mechanism: $^3P_0 \rightarrow ^3H_{4,6}$ and $^3P_0 \rightarrow ^3F_{2,4}$. The presence of the $^3P_0 \rightarrow ^3H_5$ band arises due to strong J-J mixing.³⁴ The emission spectrum of Tm^{3+} consists of bands originating from 1D_2 and 1G_4 levels. The transitions $^1D_2 \rightarrow ^3H_5$, $^3F_{4,3}$ and $^1G_4 \rightarrow ^3H_4$ are not observed with significant intensities. The line widths ($\Delta\lambda_p$) of the emission bands of Pr^{3+} and Tm^{3+} in the present case are comparable with values reported for phosphate and fluoride glasses.^{26,35} Branching ratios calculated from Judd-Ofelt parameters show fairly good agreement with experimental values obtained from emission spectra (table 5.5). The values of stimulated emission cross section (σ_p) obtained in the present system are comparable with the values reported by Reisfeld *et al* for fluoride glass matrices.⁹

Glass matrices are known to bring about marked differences in the relative fluorescence of the dopant ions due to the multiphonon nonradiative decay characteristic of the host matrix. Figure 5.6 compares the normalized emission spectra of Pr^{3+} in PbO-PbF₂ and a representative phosphate glass CaO-P₂O₅. The PbO-PbF₂ glass doped with Pr^{3+} shows significantly higher fluorescence (figure 5.6). Similar observations on the influence of glass matrices on Eu^{3+} fluorescence have been reported earlier for germanate and tellurite glasses.⁷ The higher fluorescence emission in these glasses is known to arise due to a much lower phonon energy maximum characteristic of the glass matrix. It may therefore be concluded that the characteristic phonon energy for the PbO-PbF₂ glass is comparable to other glass matrices such as the fluoride glasses which also show good Pr^{3+} fluorescence.^{9,14} This conclusion is also substantiated by infrared spectral data for this matrix presented in section 5.4 and our experimental observations on the fluorescence studies of Eu^{3+} and Tb^{3+} doped in PbO-PbF₂ glass as discussed in sections 5.4 and 5.5 respectively.

Energy transfer between rare earth ions codoped in glass matrices have been investigated in a number of systems.²⁵⁻²⁸ As the present oxyfluoride glass matrix is investigated for the first time, preliminary works on energy transfer were carried out for this glass matrix. For this purpose the rare earth ions Pr^{3+} and Tb^{3+} are chosen. Emission spectra of $30\text{PbO}-70\text{PbF}_2-x\text{Pr}^{3+}-y\text{Tb}^{3+}$ (where $x=0.5$ wt. % and $y=(a) 0.0$, (b) 0.12, (c) 0.25, (d) 0.5, (e) 0.75, (f) 1.0, (g) 1.25 wt. %) are reproduced in figure 5.7. With increasing Tb^{3+} concentration the emission spectral intensities of Pr^{3+} show a systematic decrease. These observations show that energy transfer takes place from Pr^{3+} to Tb^{3+} . The energy transfer efficiency (η_T), probability (P_{da}) and donor-acceptor distance (R) for Pr^{3+} to Tb^{3+} as a function of c^2 where c is the sum of the concentrations of donor and acceptor in wt. % were calculated from integrated emission spectral intensities of Pr^{3+} and are given in table 5.7. A plot of c^2 vs. P_{da} is linear for $c^2=1.0$ to 3.06 as shown in figure 5.8 supporting dipole-dipole mechanism. Deviations from linearity observed at low concentrations ($c^2<1.0$) presumably arise due to diffusion, transfer involving higher moments and/or back transfer.^{18,19,33} Energy transfer from Tb^{3+} to Pr^{3+} is known.²⁵⁻²⁸ Energy transfer in the reverse path viz., Pr^{3+} to Tb^{3+} is observed for the first time. The maximum phonon energy for PbO-PbF_2 glass is markedly low (930 cm^{-1}) compared to borate and phosphate glasses discussed in the earlier chapters. Thus the unusual observation of Pr^{3+} to Tb^{3+} energy transfer may arise due to the nature of the host. Energy transfer from Tb^{3+} to Pr^{3+} is also examined by keeping Tb^{3+} concentration constant and varying the concentrations of Pr^{3+} . Emission spectra of $30\text{PbO}-70\text{PbF}_2-x\text{Pr}^{3+}-y\text{Tb}^{3+}$ (where $x=(a) 0.0$, (b) 0.2, (c) 0.5 (d) 0.7 and $y=0.5$ wt. %) are reproduced in figure 5.9. The emission intensities of Tb^{3+} decreased drastically even with small addition of Pr^{3+} (0.2 wt. %) and further additions do not affect the emission intensities significantly.

5.1.2 Conclusions

Analysis of absorption spectra of 30PbO-70PbF₂-1.35 wt. % Ln³⁺ (Ln=Pr, Tm) using full matrix diagonalisation procedure leads to good match between experimental and calculated transition energies. The $^3P_0 \leftarrow ^3H_4$ transition of Pr³⁺ occurring at 20,704 cm⁻¹ suggests 8-9 coordination. Eight coordinated Ln³⁺ ions with D_{2h} or lower symmetry, predominantly surrounded by the fluoride ligands from the PbO₂F₄ units of the PbO-PbF₂ glass has been proposed. This suggestion derives support also from the Judd-Ofelt parameters which are significantly small and close to values reported for Ln³⁺ ions in fluoride glasses. The β_R values calculated from Judd-Ofelt parameters are in close agreement with values obtained from the emission spectra. The stimulated emission cross section (σ_p) values are found to be close to those reported for these ions in fluoride glasses. Thus oxyfluoride glass can be considered for many applications suggested for the fluoride glasses. The relative intensities of emission bands originating from 3P_1 level of Pr³⁺ are temperature dependent. This is attributed to enhanced contributions due to Boltzmann population of higher Stark components of the ground state, 3H_4 and thermal excitation from 3P_0 to 3P_1 state. The presence of $^3P_0 \rightarrow ^3H_5$ band indicates strong J-J mixing.³⁴ Fluorescence emission in Pr³⁺ doped in the present glass is found to be significantly higher than in a representative phosphate glass of composition CaO-P₂O₅. It is concluded that the dominant phonon energy responsible for nonradiative emission in the oxyfluoride glass should be of similar magnitude as in tellurite and germanate glasses. Results of preliminary investigations of energy transfer studies in the oxyfluoride glass codoped with Pr³⁺ and Tb³⁺ show that Pr³⁺ can act both as donor as well as acceptor. Thus energy transfer of Pr³⁺ → Tb³⁺ is reported for the first time.

Chapter 5

5.2 Optical Properties of Nd^{3+} , Ho^{3+} and Er^{3+} Ions Doped in PbO-PbF_2 Glasses

In this section we present the results of detailed investigations of the absorption spectra of Nd^{3+} ($4f^3$), Ho^{3+} ($4f^{10}$) and Er^{3+} ($4f^{11}$). It may be noted that the electronic configurations of Nd^{3+} and Er^{3+} are related. Their absorption spectra are analyzed using the same matrix elements taking into account that only the sign of ξ , the spin-orbit coupling changes as described in chapter 2. All the three ions give rise to large number of transitions in the visible and near infrared regions and hence the Judd-Ofelt parameters can be reliably **evaluated**.³² As all the three ions give rise to emission spectral transitions of interest the radiative parameters including the branching ratios and transition probabilities are derived from the Judd-Ofelt parameters. While considerable attention has been bestowed on the behavior of hypersensitive transitions of Ln^{3+} ions in solutions, relatively little attention is given on the behavior of these transitions for Ln^{3+} doped in glasses.^{19,20,36} The variations in the structure sensitive Judd-Ofelt parameters and the hypersensitive transitions in the absorption spectra are compared with observations in **borate**, phosphate and fluoride glasses as host materials. The study of variations in the **Judd-Ofelt** parameters as we go along the rare earth series is of particular interest as shown by **Krupke**.³⁷ A comparison of these parameters for crystalline systems with the trends predicted on the basis of crystal field theory and vibronic contributions show qualitative agreement.³⁷ Results of a similar study in glasses in comparison with crystalline hosts should therefore be of interest. To our knowledge such a study in glasses is **limited**.^{37,38} We present here the variations in the Ω_2 , Ω_4 and Ω_6 parameters for Ln^{3+} ions in PbO-PbF_2 glass host. Stimulated emission cross sections have also been obtained for Ho^{3+} and Er^{3+} ions as their emission spectra could be **recorded**.

5.2.1 Results and Discussion

The absorption spectra of the oxyfluoride glasses, 30PbO-70PbF_2 -1.35 wt. % Ln^{3+} ($\text{Ln}=\text{Nd}$, Ho and Er) are reproduced in figures 5.10-5.12 **respectively**. The spectroscopic parameters derived from the transition energies in the absorption spectra

of Nd³⁺ and Er³⁺ are given in table 5.1. The observed and calculated transition energies are reproduced in table 5.8 along with the **rms deviations**. The small **rms** values **signify** a good match between the observed and calculated **values**. The ⁴I_{9/2}→²P_{1/2} transition is characteristic of Nd³⁺ **coordination**.³² This transition occurring at 23,397 **cm⁻¹** for the present glasses suggests 8-9 **coordination**.³² 8-9 coordination is also supported by our absorption spectral studies of Pr³⁺ and emission spectral studies of Eu³⁺ doped PbO-PbF₂ glasses. The Judd-Ofelt parameters obtained from a least squares analysis of observed oscillator strengths for Nd³⁺, Er³⁺ and Tm³⁺ ions in 30PbO-70PbF₂ glass are compared with values obtained for the same ions in fluoride, borate and phosphate glasses in table 5.9. The observed oscillator strengths and those calculated using the resultant Judd-Ofelt parameters for Nd³⁺, Er³⁺ and Tm³⁺ ions in PbO-PbF₂ glass are given in tables 5.10-5.12 along with their respective rms deviations. The small rms values show good agreement between observed and calculated oscillator strengths. The values of Ω_λ ($\lambda=2,4,6$) for the oxyfluoride glass are intermediate between those reported for oxide glasses of the type borate, phosphate **etc.**, and the fluoride glasses (table 5.9).^{6-9,39-43} It is known that the Judd-Ofelt parameters, Ω_2 in particular, increase with increasing covalency of the chemical bond between the rare earth ion and the ligand **anions**.^{7,19,44,45} Oomen and van Dongen have suggested that instead of looking at the variation of any single Judd-Ofelt parameter it is convenient to look at the variation of the sum of the Judd-Ofelt parameters ($\Sigma\Omega_\lambda$, $\lambda=2,4,6$) which increases with increasing **covalency**.⁴⁶ The sum of the Judd-Ofelt parameters increases in the order, fluoride < oxyfluoride < borate < phosphate glasses (table 5.9). It is of interest to study the variation in the Judd-Ofelt parameters across the lanthanide series with the Ln³⁺ ions doped in the same host **material**. For this purpose, the Judd-Ofelt parameters for the different rare earth ions in the present host material are plotted against the number of 4f electrons as shown in figure 5.13. Krupke evaluated the variations of Ω_λ as a function of electronic configuration as we go along the series on a crystal field model.³⁷ The theoretical trends show decreasing Ω_λ ($\lambda=2,4,6$) along the rare earth **series**. In real systems with hosts such

as Y_2O_3 the Ω_2 values show a decreasing trend and Ω_4 and Ω_6 show shallow minima.³⁷ Our results show a decreasing trend for Ω_4 and Ω_6 in agreement with the predicted trends. On the other hand Ω_2 shows an increasing trend. Ω_4 and Ω_6 are mainly influenced by the dielectric of the media.^{7,19,44} On the other hand Ω_2 is sensitive to covalency and/or asymmetry around the lanthanide site.^{7,19,44,45} The Ω_2 values in glass systems in general shows a different trend across the lanthanide series unlike Ln^{3+} doped in crystalline Y_2O_3 .³⁷ The reasons for the discrepancy between glass and crystalline systems have been stated earlier in chapter 3. The observed trend for the oxyfluoride glass also qualitatively differs from the trends observed for borate and phosphate glasses as well. The discrepancy may be explained as follows. Ln^{3+} ions doped in glass matrices may occupy sites with same coordination over the entire series as suggested for the borate and phosphate glasses. On the other hand, the early members of the series with large ionic size may favor higher coordination number of 8 to 12 and the end members with relatively smaller ionic size tend to occupy sites with 6 to 8 coordination.⁵ The lowering of coordination number with reduction in the ionic size of the rare earth ion towards the end of the series should in principle lead to shortening of the metal ligand bonds and in turn enhancement of covalency.⁴⁷ This should result in the enhancement of Ω_2 as we go along the series as observed.

The positions, intensities and/or profiles of the hypersensitive transitions of Ln^{3+} ions are markedly influenced by their ligand environment.^{6-8,19,20} The $^4\text{G}_{5/2} \rightarrow ^4\text{I}_{9/2}$ of Nd^{3+} , $^5\text{G}_2 \rightarrow ^5\text{H}_5$, $^3\text{H}_6 \rightarrow ^5\text{I}_8$ and $^5\text{F}_2 \rightarrow ^3\text{K}_8$, $^5\text{G}_6 \rightarrow ^5\text{I}_6$ of Ho^{3+} and $^2\text{H}_{11/2} \rightarrow ^4\text{I}_{15}$ and $^4\text{G}_{11/2} \rightarrow ^4\text{I}_{15}$ of Er^{3+} are hypersensitive and follow the quadrupole selection rules ($\Delta S=0$, ΔL , $\Delta J \leq 2$). The line positions and shape of these hypersensitive transitions are compared for the present oxyfluoride glasses with those of borate and phosphate glasses investigated in our laboratory in figures 5.14 and 5.15 for Nd^{3+} and Er^{3+} respectively. The transitions exhibit significant variations in the energies and profiles. The position of $^4\text{G}_{5/2} \rightarrow ^4\text{I}_{9/2}$ transition of Nd^{3+} shifts towards longer wavelength with the hosts in the order, oxyfluoride < borate < phosphate which shows the enhancement of covalency of the

chemical bond between the Nd^{3+} and the ligand atoms. This is also in accordance with the trend in Ω_2 . The effective band width of this transition is smaller for oxyfluoride glasses compared to phosphate and borate glasses. This indicates that the distribution in the crystal fields due to differences in the site symmetries of Nd^{3+} is narrower for the present oxyfluoride glass compared to borate and phosphate glasses. In the case of Ho^{3+} the line positions and profiles of hypersensitive transitions are not showing noticeable difference between oxyfluoride and borate glasses. For Er^{3+} the effective band width of the hypersensitive transition ${}^2\text{H}_{11/2} \leftarrow {}^4\text{I}_{15/2}$ is higher in oxyfluoride glass compared to phosphate and borate glasses in contrast to the observation for the hypersensitive transition for Nd^{3+} discussed earlier. This is because of smaller ionic size of the Er^{3+} with preference for lower coordination of 6 to 8 compared to Nd^{3+} which prefers 8-9 coordination.⁴⁸ 8-9 coordination is also evidenced by the ${}^2\text{P}_{1/2} \leftarrow {}^4\text{I}_{9/2}$ transition of Nd^{3+} which is known to be characteristic of coordination of the ion as discussed earlier.³²

To highlight further the influence of host matrices on the hypersensitive transitions, the sum of the Judd-Ofelt parameters are plotted against the oscillator strengths for the hypersensitive and intense nonhypersensitive transitions for Nd^{3+} , Ho^{3+} and Er^{3+} doped in fluoride, oxyfluoride, phosphate and borate glasses (figures 5.16-5.18). These plots show that the oscillator strengths for nonhypersensitive transitions remain constant for Ho^{3+} and Er^{3+} . For Nd^{3+} however the plot shows a small slope. On the other hand the oscillator strengths for the hypersensitive transitions increase linearly with increase in the sum of Judd-Ofelt parameters for all the three cases of Nd^{3+} , Ho^{3+} and Er^{3+} . The oscillator strengths for the hypersensitive transition ${}^4\text{G}_{5/2} \leftarrow {}^2\text{G}_{7/2} \leftarrow {}^4\text{I}_{9/2}$ of Nd^{3+} increases by a factor of 1.35, ${}^5\text{G}_2 \leftarrow {}^3\text{H}_5$, ${}^3\text{H}_6 \leftarrow {}^5\text{I}_8$ and ${}^5\text{F}_2 \leftarrow {}^3\text{K}_8$, ${}^5\text{G}_6 \leftarrow {}^5\text{I}_8$ of Ho^{3+} increase by a factor of 0.36 and 2.43 respectively and ${}^2\text{H}_{11/2} \leftarrow {}^4\text{I}_{15/2}$ and ${}^4\text{G}_{11/2} \leftarrow {}^4\text{I}_{15/2}$ of Er^{3+} increase by a factor of 1.49 and 0.84 respectively. Thus it may be concluded that only those hypersensitive transitions where the factor is significantly higher than unity are quite sensitive to structural changes. For Nd^{3+} the nonhypersensitive transitions are also showing small slope due to less shielding effect and/or vibrational contribution to the

Chapter 5

intensity of Nd^{3+} ion which is known to be significant for the early members of the lanthanide series compared to the end members such as Ho^{3+} and Er^{3+} ions.^{47,49}

The emission spectra of oxyfluoride glasses, $30\text{PbO}-70\text{PbF}_2-0.2$ wt. % Ln^{3+} ($\text{Ln}=\text{Er}, \text{Ho}$) are given in figures 5.19 and 5.20 respectively with assignments of the transitions. The fluorescence of these rare earth ions in oxide glasses are seldom observed. This is because the higher phonon energies characteristic of the oxide glass matrices facilitate the nonradiative decay from the excited energy levels to closely situated levels lying just below which enhances the fluorescence quenching. In other words the number of phonons P given by, $P = \Delta E / \hbar\omega$ where ΔE is the energy difference between the two levels and $\hbar\omega$ is the phonon energy of host matrices, is less for Ho^{3+} and Er^{3+} compared to other rare earth ions such as Eu^{3+} and Tb^{3+} which give rise to significant emission in the same host. The maximum phonon energy for the present oxyfluoride glass host is 930 cm^{-1} being much smaller than the values reported for silicate, phosphate and borate glasses facilitates the radiative emission in the rare earth ions under study.⁷

The radiative properties of these ions viz., the radiative transition probability, calculated branching ratios and stimulated emission cross sections are given in table 5.13. These values are compared with values reported for fluoride and oxide glasses.^{6,8,39,43} It may be noted that the stimulated emission cross sections for various transitions are lower than the corresponding values for fluoride glasses. The radiative transition probabilities for these ions in the present system are comparable with those reported for fluoride glasses and lower than the values reported for oxide glasses.^{6-8,39-43} The branching ratio for the important laser transition viz., ${}^4\text{F}_{3/2} \rightarrow {}^4\text{I}_{11/2}$ of Nd^{3+} is higher for the present case compared to fluoride glasses.^{39,42} It will therefore be of interest to investigate this system in further detail.

5.2.2 Conclusions

The Ω_2 values and the sum of the Judd-Ofelt parameters $\Sigma\Omega_\lambda$, ($\lambda=2,4,6$) for the Nd^{3+} , Ho^{3+} and Er^{3+} rare earth ions doped in $30\text{PbO}-70\text{PbF}_2$ glass are intermediate

between their values in fluoride glasses and oxide glasses such as borates as host matrices indicating that the rare earth ions occupy sites in the oxyfluoride glass with intermediate ionic character in accordance with the systematic change in the ligand atoms for the three glass matrices. This observation also lends support to the sensitivity of the **Judd-Ofelt** parameter to small but significant variations in the ionic character of the rare earth ions depending on the ligand atoms. Unlike in borate and phosphate glasses Ω_2 in oxyfluoride glasses shows an increasing trend along the lanthanide series as in the case of **fluoride** glasses. This trend suggests increasing covalent character for the rare earth ions with decreasing ionic size. The lanthanides with decreasing ionic size are known to show preference for lower coordination which in turn would result in increasing covalency due to shorter **ligand-metal** bonds. In other words, the different trends in Ω_2 observed indicates that while Ln^{3+} ions exist with same coordination over the entire series for the borate and phosphate glasses, they show a preference for lower coordination at the end of the series in oxyfluoride and fluoride glasses Ω_4 and Ω_6 which are influenced only by the dielectric of the medium and vibrational levels follow the same trends as in crystalline systems. The profiles of the hypersensitive transitions suggest that the crystal fields due to the differences in the site symmetries of Nd^{3+} with 8-9 coordination is much narrower than that of Er^{3+} ions with 6-8 coordination. The hypersensitive transitions of rare earth ions in glass hosts have not been investigated in detail earlier. A plot of $\Sigma\Omega_\lambda$, ($\lambda=2,4,6$) against oscillator strengths of hypersensitive and nonhypersensitive transitions for different glass host matrices show that the oscillator strengths of the hypersensitive transitions are markedly affected by the nature of the ligand atoms while those of nonhypersensitive transitions remain almost unaffected. The hypersensitive transitions which are most sensitive to ligand environment have been **identified** The observation of emission spectra at room temperature for Ho^{3+} and Er^{3+} is attributed to favorable phonon energy maximum characteristic of the matrix. The stimulated emission cross sections for Er^{3+} and Ho^{3+} are lower than the values for fluoride glasses. The radiative transition probabilities for all the three ions are comparable to those reported for fluoride **glass**

5.3 Absorption and Emission Spectral Studies of Sm^{3+} and Dy^{3+} Ions in Oxyfluoride Glasses

Optical properties of trivalent samarium and dysprosium ions doped in glass matrices have received much less attention than other lanthanide ions despite many features of interest. Samarium has promising characteristics for spectral hole burning studies.^{50,51} Codoping of Sm^{3+} as sensitizer with Eu^{3+} can strongly influence the emission of the lasing transition ${}^5\text{D}_0 \rightarrow {}^7\text{F}_2$ in the latter.⁵² The decay of excited states in Sm^{3+} involves different mechanisms depending on the nature of the parent matrix." The $3.02 \mu\text{m}$ ${}^6\text{H}_{13/2} \rightarrow {}^6\text{H}_{15/2}$ transition in Dy^{3+} has been identified as a laser transition.⁵³ The hypersensitive transition ${}^6\text{F}_{11/2} \rightarrow {}^6\text{H}_{15/2}$ of Dy^{3+} at $1.34 \mu\text{m}$ has potential for fiber amplifiers.⁵⁴ The yellow to blue intensity ratio of the emission lines in Dy^{3+} exhibits features similar to the red to orange intensity ratio of Eu^{3+} and throws light on the nature of metal-ligand bonding.⁵⁵ Sm^{3+} and Dy^{3+} in general have low emission efficiencies compared to other rare earth ions.⁵⁶ It is therefore of interest to understand the influence of parent matrices, the mechanism of fluorescence quenching and the influence of other Ln^{3+} ions present as donors or acceptors on their optical properties. In this work the Judd-Ofelt parameters for Sm^{3+} and Dy^{3+} ions doped in PbO-PbF_2 glass have been evaluated from their absorption spectra and the radiative properties derived. The variations in the relative intensities of the emission lines in Dy^{3+} is compared with Eu^{3+} in different glass matrices. The stimulated emission cross sections for a number of transitions for trivalent samarium and dysprosium are being reported to the best of our knowledge for the first time. The calculated radiative properties are compared with the results of emission spectra and experimentally measured lifetimes. The influence of dopant concentration on the lifetimes are presented as well.

5.3.1 Results and Discussion

The room temperature absorption spectra of oxyfluoride glasses, 30PbO-70PbF_2 -1.35 wt. % Ln^{3+} ($\text{Ln}=\text{Sm}, \text{Dy}$), showed features identical to those reported for fluoride

glass matrices and are reproduced in figures 5.21 and 5.22 respectively. The spectral energies with assignments and the observed and calculated oscillator strengths are given in table 5.14 and 5.15 respectively along with the respective **rms** deviations. The small **rms** values show good agreement between observed and calculated oscillator strengths. The overlapping transitions marked b in table 5.14 principally contribute to the rms deviation. This is found to be the case in the earlier works as well.^{11,57} The Judd-Ofelt parameters obtained are given in table 5.3. These values are of the same order as those reported for **Sm³⁺** and **Dy³⁺** in fluoride glasses and significantly lower than the values reported for oxide glasses.^{8,11,57,58} These results show that the lanthanide ions under study are situated in sites with crystal field and metal ligand bonding which are closely similar in the fluoride rich 30PbO-70PbF₂ glass and fluoride glasses.¹⁹

The emission spectra of oxyfluoride glasses, 30PbO-79PbF₂-0.2 wt. % **Ln³⁺** (Ln=Sm, Dy) are reproduced in figures 5.23 and 5.24 respectively. The assignments made are based on previous works^{11,57,58} The emission spectra show the following features of interest. Unlike in the case of phosphate and borate glasses the emission lines corresponding to ⁴G_{5/2}→⁶H_{11/2}, ⁶H_{13/2} for **Sm³⁺** and ⁴F_{9/2}→⁶H_{11/2}, ⁶H_{9/2}, ⁶F_{11/2} for **Dy³⁺** could be observed even at room temperature. In this respect these systems behave more like the fluoride glasses. Similar results are obtained in the case of the present glass doped with **Eu³⁺** and **Tb³⁺** where the observation of a large number of emission transitions particularly in the high energy region could be observed as in the fluoride glasses unlike in borate and phosphate glasses in which they are found to be very weak or not observed.^{7,13} The close similarity between **Ln³⁺** doped oxyfluoride and fluoride glasses arises for the following reasons. At low dopant concentrations, even when the **Ln³⁺** ions occur as near neighbors, they are far apart and preclude energy transfer. This observation is also in accordance with the structure proposed earlier for **Ln³⁺** ions in the oxyfluoride glass in section 5.1 and in fluoride glass matrices.⁵⁹ Secondly the ionic environment and the consequent low phonon energy maxima of ~ 650 cm⁻¹ and ~ 930

Chapter 5

cm^{-1} characterizing fluoride and oxyfluoride glasses respectively prevent multiphonon nonradiative decay.

The two dominant emissions for Dy^{3+} occur due to ${}^4\text{F}_{9/2} \rightarrow {}^6\text{H}_{13/2}$ at 575.1 nm in the yellow region and ${}^4\text{F}_{9/2} \rightarrow {}^6\text{H}_{15/2}$ at 481.0 nm due to blue emission. Qiang Su *et al* have shown in crystalline systems that the Y/B ratio of Dy^{3+} emissions follows a trend parallel to the red to orange intensity ratio (${}^3\text{D}_0 \rightarrow {}^7\text{F}_2 / {}^3\text{D}_0 \rightarrow {}^7\text{F}_1$) of Eu^{3+} as these ratios are influenced by site asymmetries and electronegativities of the ligand atoms in a similar manner.⁵⁵ It would be of interest to compare the trends in the above ratios in glass systems.. The Y/B ratio of Dy^{3+} emissions for the present system is found to be 1.58 compared to 1.23 for fluoride glasses.⁵⁸ Comparison of R/O of Eu^{3+} and Y/B in Dy^{3+} in glasses show different trends, viz., silicate > fluoride > phosphate > borate > oxyfluoride for Eu^{3+} and oxyfluoride > silicate \sim fluoride > phosphate > borate for Dy^{3+} .^{58,60-62} The low values of Ω_2 for the two ions indicate that they occupy highly ionic sites with small distortions from cubic symmetry. It is therefore unlikely that these two ions occupy very different sites in the oxyfluoride glass leading to the above discrepancy with respect to different glass matrices. The differences in the relative trends of the R/O ratio of Eu^{3+} and Y/B ratio of Dy^{3+} may be accounted for as follows. The ratio for Eu^{3+} is likely to follow a more systematic trend with changes in coordination and electronegativity of the ligand atoms than the ratio for Dy^{3+} for the following reason. In the case of Eu^{3+} the ${}^7\text{F}_{0(1)} \leftrightarrow {}^5\text{D}_{1(0)}$ transition is purely magnetic dipole and its intensity exhibits little sensitivity to the metal ligand interactions. Only the ${}^7\text{F}_{0(2)} \leftrightarrow {}^5\text{D}_{1(2)}$ transition being electric dipole in nature and hypersensitive is affected. As a result Eu^{3+} shows systematics with covalency and symmetry of the central ion. In Dy^{3+} , on the other hand both the transitions are electric dipole one of which is hypersensitive. Richardson has shown that intensity calculations of f-f transitions in such cases is very sensitive to the differences in charges and polarizabilities of the ligand atoms in the axial and equatorial positions even when the coordination geometries are similar.⁶³ In the present glass the Ln^{3+} ion is bound to

two different types of ions, *viz.*, monovalent F and divalent O²⁻ ions. In such cases it is unlikely that the R/O ratio of Eu³⁺ and Y/B ratio of Dy³⁺ in different glass matrices will follow a parallel trend.

The radiative properties of Ln³⁺ (Sm³⁺ and Dy³⁺) ions *viz.*, the radiative transition probability (A), observed and calculated branching ratios (PR) and stimulated emission cross sections (σ_p) are given in table 5.16. The radiative transition probabilities for these ions in the present system are comparable with those reported for fluoride glasses and lower than the values reported for borate and phosphate glasses.^{7,8,11,57,58} The observed branching ratios were measured by area method excluding the transitions which occur in near infrared region. This may result in a systematic error in the observed branching ratios. The errors should however be negligible as the emission lines in the near infrared region are relatively very weak.^{57,58} The branching ratios calculated from absorption spectral data show good agreement with values obtained from emission spectral data. To our knowledge the σ_p values for different transitions for Sm³⁺ and Dy³⁺ ions have not been reported so far. The σ_p values suggest that they are an order of magnitude less than the values reported for various transitions in this region of wavelengths for other rare earth ions. The low emitting efficiencies reported for Sm³⁺ and Dy³⁺ (1 %) compared to other rare earth ions such as Eu³⁺ (10 %) and Tb³⁺ (70 %) can account for the low σ_p values obtained.⁵⁶

The lifetimes (τ_M) of the ⁴G_{5/2} fluorescent level of Sm³⁺ and ⁴F_{9/2} of Dy³⁺ are measured at 0.2 and 1.35 wt. % dopant concentrations. The fluorescent decay curves are reproduced in figures 5.25 and 5.26 for Sm³⁺ and Dy³⁺ respectively. The decay curves were analyzed taking into account various possibilities on the basis of analyses reported in literature for these ions.¹¹ These include fitting the data to single exponential, double exponential and expressions that include cross relaxation in the case of Sm³⁺. The best fits were judged by means of error analyses. For samples with 0.2 wt. % of Ln³⁺ (Sm³⁺,

Dy^{3+}), good fits of the decay curves to single exponential are obtained as shown in figures 5.25 and 5.26 for Sm^{3+} and Dy^{3+} respectively. The calculated radiative lifetimes (τ_R) and measured lifetimes (τ_M) for $^4\text{G}_{5/2}$ level of Sm^{3+} and $^4\text{F}_{9/2}$ level of Dy^{3+} are given in table 5.16. The lifetimes calculated from Judd-Ofelt parameters are significantly higher than the measured values. The corresponding values for quantum efficiencies are 52 % and 49 % for Sm^{3+} and Dy^{3+} ions respectively. The corresponding values for these ions in fluoride glasses are 92 % and 64 % respectively.^{11,57,58} Thus the agreement between measured and calculated lifetimes in the case of fluoride glasses is better.^{11,57,58} The reason for the same is not far to seek. The PbO-PbF_2 glasses have a phonon energy maximum of 930 cm^{-1} compared to the low phonon energy maximum of 650 cm^{-1} for fluoride glasses.¹² In such a case the multiphonon nonradiative decay will be far more facilitated in the present glass system leading to lesser agreement between calculated and measured lifetimes.

The decay curve for the emission level $^4\text{F}_{9/2}$ of Dy^{3+} follows single exponential for both the concentrations studied although the higher concentration of the dopant ion resulted in the reduction of the lifetime to 0.740 msec (figure 5.26). The shortening of the lifetime of the emission level for this ion may be attributed to concentration quenching. In the case of Sm^{3+} ions with increasing concentration, the decay curve became non exponential and fitting with single exponential led to large errors. Unlike in the case of Dy^{3+} , energy transfer by cross relaxation is important for Sm^{3+} . If cross relaxation is responsible for non exponential decay, the expression derived by Inokuti and Hirayama⁶⁴ and Eisenthal and Siegel⁶⁵ for donor-acceptor transfer can be used. In the present case the non excited Sm^{3+} ions act as acceptor and the expression is valid if the number of excited ions are small compared to the total number of active ions. The emission intensity versus time in this case is given by¹¹

$$\phi(t) = \frac{\int_0^{\infty} \exp\left(-\frac{t'}{\tau} - \frac{4\pi}{3} N_A (t' C_{DA}^{(s)})^{3/s} \Gamma\left(1 - \frac{3}{s}\right)\right) dt'}{\int_0^{\infty} \exp\left(-\frac{t'}{\tau} - \frac{4\pi}{3} N_A (t' C_{DA}^{(s)})^{3/s} \Gamma\left(1 - \frac{3}{s}\right)\right) dt'} \quad (1)$$

where $s = 6, 8$ or 10 depending on whether the dominant mechanism of the interaction is dipole-dipole, dipole-quadrupole or quadrupole-quadrupole, respectively, N_A is the concentration of acceptor ions, $\Gamma(x)$ is the gamma function and $C_{DA}^{(s)}$ is the parameter of the dominant contribution to the donor acceptor transfer related to the transition probability by

$$W_{DA} = \frac{C_{DA}^{(s)}}{R^s} \quad (2)$$

where R is the distance between ions involved in the transfer.

The best fit for the decay curve for the emission level ${}^4G_{5/2}$ of Sm^{3+} with higher concentration of 1.35 wt % is obtained using eqn. (1) with $s = 6$, $C_{DA} = 5.63 \times 10^{-41} \text{ cm}^6 \text{ sec}^{-1}$ and the energy transfer probability $W_{DA} = 5.9 \text{ sec}^{-1}$ (figure 5.25). The fact that eqn. (1) well accounts for the radiative decay from the excited state ${}^4G_{5/2}$ of Sm^{3+} shows that there is strong cross relaxation. Cross relaxations in Sm^{3+} occur involving the levels ${}^4G_{5/2}$, ${}^6H_{9/2} \rightarrow {}^6F_{9/2}$, ${}^6F_{7/2}$, ${}^6F_{9/2}$, ${}^6F_{7/2}$, ${}^6F_{9/2}$ and ${}^6F_{5/2}$, ${}^6F_{11/2}$. The results also show that the dominant interaction in the relaxation mechanism is dipole-dipole in the present case as in the fluoride and borate glass matrices.^{11,66} However in some cases dipole-quadrupole and even quadrupole-quadrupole interactions have been proposed.^{11,57}

5.3.2 Conclusions

The Judd-Ofelt parameters for Sm^{3+} and Dy^{3+} in the oxyfluoride glass, $30\text{PbO}-70\text{PbF}_2$, are significantly less than those reported for these ions doped in borate and phosphate glasses and comparable to the fluoride glasses. For Dy^{3+} the ratio of the emission spectral intensities of transitions in the yellow to blue regions is 1.58 compared to 1.23 reported for fluoride glasses. The radiative transition probabilities (A) are comparable to those reported for fluoride glasses and lower than the values reported for oxide glasses. The strong similarities in the spectral characteristics of these ions doped in oxyfluoride and fluoride glasses suggest that Ln^{3+} ions occupy sites with similar ionic character and symmetry. This is also in accordance with the sites proposed in the earlier section for Ln^{3+} ions in these glasses. The branching ratios calculated from absorption spectral data show good agreement with those obtained from emission spectral data. The stimulated emission cross sections for Sm^{3+} and Dy^{3+} ions are an order of magnitude less than the values for other rare earth ions. This accounts for the low emission efficiencies observed in general for these ions compared to other rare earth ions such as Eu^{3+} and Tb^{3+} . The quantum efficiencies for $^4\text{G}_{5/2}$ of Sm^{3+} and for $^4\text{F}_{9/2}$ of Dy^{3+} are 52 % and 49 % respectively. These values are less than those observed for fluoride glasses. The higher phonon energy maximum for the oxyfluoride glasses accounts for the lower quantum efficiencies. The fluorescent decay processes follow single exponential at low concentrations. At higher dopant concentrations Dy^{3+} decay exhibits only a single exponential with reduction in the lifetime due to concentration quenching. The fluorescent decay of Sm^{3+} at higher dopant concentrations shows that energy transfer involving cross relaxation plays a significant role in the radiative decay process.

5.4 Absorption and Emission Spectral Studies of Eu³⁺ Doped in Pb-PbF₂ Glass System

The absorption and emission spectra of Ln³⁺ (Eu, Tb, Dy) show characteristic features not exhibited by other rare earth ions. They give rise to hypersensitive transitions both in their absorption and emission spectra. The relative emission intensities of transitions occurring in the low energy region (570-710 nm) to those in the high energy region (440-570 nm) are quite sensitive to the host matrix.⁷ Hypersensitive transitions invariably appear as intense emission bands in the low energy region and are influenced by the micro symmetry and covalency of the rare earth ions.⁵⁵ Eu³⁺ ion has the additional feature of interest in that phonon side band studies can give information about the electron-phonon coupling strength with the host lattice and also throw light on whether the nonradiative or radiative decay is favored.⁶⁷ In favorable cases information on the nature of the matrix and the binding of the rare earth ion to the matrix can be obtained as discussed earlier in the alkali and alkaline earth borate glasses. The present study reports the absorption and emission spectral studies of Eu³⁺ doped PbO-PbF₂ glass system. The absorption spectra were analyzed using the Judd-Ofelt model and radiative parameters calculated for the laser transition ⁵D₀→⁷F₂. The features exhibited by Judd-Ofelt and radiative parameters, phonon side bands and the hypersensitive transitions due to change in the composition of the host matrix and concentration of Eu³⁺ ions are presented.

5.4.1 Results and Discussion

The oscillator strengths of oxyfluoride glasses, 30PbO-70PbF₂-2.0 wt. % Eu³⁺ and 70PbO-30PbF₂-2.0 wt. % Eu³⁺ are given in table 5.17 along with their Judd-Ofelt parameters. The applicability of Judd-Ofelt parametric fit for Eu³⁺ has been successful in crystalline systems such as Y₂O₃, YAlO₃, molten salts and glasses *e.g.*, phosphates and fluorides.⁸⁶⁸ In most of the glass matrices only three transitions are observed in the absorption spectra of Eu³⁺ in the 300 to 1200 nm region unlike in the cases of rare earth

ions such as Nd^{3+} , Ho^{3+} etc., where a large number of transitions are observed. In the present system four transitions are observed (table 5.17). This renders the fitting of their intensities according to the **Judd-Ofelt** model meaningful although the errors in such cases can be higher than those reported for the earlier mentioned rare earth ions. The good match obtained between observed and calculated oscillator strengths (table 5.17) also shows the applicability of the model for the present systems. The Judd-Ofelt parameter Ω_2 is sensitive to ligand atoms to which Ln^{3+} ion is bound. The f_l values for Eu^{3+} for the two glasses are intermediate between the larger values reported for oxide ligands such as the phosphate and the smaller values reported for fluoride glasses (table 5.17).⁸ This suggests that Eu^{3+} is bound to both the oxide and fluoride ions as the ligands. An enhanced Ω_2 value for the PbO rich glass suggests the presence of more oxide ions in the coordination sphere leading to a more covalent environment due to replacement of fluoride ions by oxide ions. The ${}^5\text{D}_0 \rightarrow {}^7\text{F}_0$ transition is characteristic of Eu^{3+} coordination.⁶⁹ This transition occurring at $17,277 \text{ cm}^{-1}$ for the present glasses suggests 8-9 coordination. 8-9 coordination is also supported by our absorption spectral studies of Pr^{3+} and Nd^{3+} doped PbO-PbF_2 glasses as discussed earlier

The excitation spectra of Eu^{3+} doped glasses monitored by the emission at 612 nm corresponding to the ${}^5\text{D}_0 \rightarrow {}^7\text{F}_2$ transition are reproduced in figure 5.27. The low intensity peak present in the higher energy side of ${}^7\text{F}_0 \rightarrow {}^5\text{D}_2$ transition is the phonon side band associated with this transition.⁶⁷ The energy gap between the phonon side band and ${}^7\text{F}_0 \rightarrow {}^5\text{D}_2$ transition peak corresponds to the phonon energy, $\hbar\omega$.⁶⁷ The intensity ratio of phonon side band to the pure electronic transition ${}^7\text{F}_0 \rightarrow {}^5\text{D}_2$ gives the electron phonon coupling strength, g . The values estimated for f_{ICO} , the electron phonon coupling strength, g and IR active maximum phonon energy, $\hbar\nu_{\text{max}}$ are listed in table 5.18. The IR spectrum of PbO-PbF_2 glass shows a broad absorption peak at around 900 cm^{-1} supporting the assignment of the peak at 445 nm in the excitation spectra (figure 5.27) to phonon side band with a phonon energy of 930 cm^{-1} . These oxyfluoride glasses are thus

characterized by a markedly higher $\hbar\omega$ and $h\nu_{\max}$ than those reported for fluoride glasses viz., 260-600 cm⁻¹ and 470-650 cm⁻¹ respectively.¹² These values are however, lower than the value ($\hbar\omega=1060$ cm⁻¹) reported for the phosphate group in the fluorophosphate glasses.⁶⁷ Thus the non radiative decay for Eu³⁺ in these glasses will be more in the present system than in fluoride glasses but less than in phosphate glasses

The $^5D_0 \rightarrow ^7F_2$ laser transition of Eu³⁺ is purely electric dipole in nature and can therefore be expected to lead to reliable values for the radiative parameters unlike other transitions which arise due to J mixing ($^5D_0 \rightarrow ^7F_0$ and $^5D_0 \rightarrow ^7F_3$) or pure magnetic dipole transition ($^5D_0 \rightarrow ^7F_1$) or have contributions both from magnetic dipole and electric dipole mechanisms.⁷⁰ The transition probability $A(\psi J)$, the total transition probability $AT(V/J)$, and branching ratios, β_R , evaluated from the Judd-Ofelt parameters and the branching ratio and stimulated emission cross section σ_p derived from emission spectra for this transition are reproduced in table 5.19. The β_R value obtained from the Judd-Ofelt parameters and that derived from the emission spectra show good agreement. It will be informative to compare these values with systems with more commonly encountered glass forming anions. For this purpose we have also included the data of some of the phosphate glasses studied in our laboratory in table 5.19. The lower σ_p and $A(\psi J)$ values observed for the oxyfluoride glasses arise due to higher refractive indices (n) and lower Ω_2 values for these glasses compared to the phosphate glasses.

The emission spectra of Eu³⁺ in PbO-PbF₂ glasses are reproduced in figure 5.28. The most striking feature is the observance of the transitions in the high energy region which to our knowledge is restricted to the three glass systems viz., tellurites, germanates and fluorides.⁷ These glasses have characteristically low phonon energies. Our results suggest that in these oxyfluoride glasses also the phonon energies are low enough to lead to the observation of high energy lines in the region 440-570 nm. The emission spectra further show that the relative integrated intensities of low energy lines

$^5D_0 \rightarrow ^7F_J$ to high energy lines $^5D_{1,2} \rightarrow ^7F_J$ denoted by **RI** are sensitive both to the composition of the glasses as well as concentration of Eu^{3+} ions in the glass of same composition. An increase in the PbO content in the glass matrix is found to lead to an increase in the RI value (table 5.18). An increase in the Eu^{3+} concentration for the same glass leads to a decrease in the relative intensities of the transitions $^5D_{1,2} \rightarrow ^7F_J$ in the high energy region. The RI for 30PbO-70PbF₂ glass increases from 7.3 to 30.0 on increasing the Eu^{3+} concentration from 0.2 to 2 wt. % whereas for the 70PbO-30PbF₂ glass it does not significantly vary. The decrease in the relative emission intensities of the transitions in the high energy region can occur due to glass matrices characterized by high phonon energies or due to clustering of the Ln^{3+} ions. For the two glasses under investigation the phonon energies which are mainly characterized by the presence of the glass former PbO will be nearly the same. The reduction in the value of RI should therefore arise due to a higher tendency to form clusters in the PbO rich glass. Increasing **clustering** can also be brought about by increase in the Eu^{3+} concentration. Evidence for the same is also seen in the marked enhancement in the RI values with increasing Eu^{3+} concentration in the same glass. The influence of clustering due to the nature of the host matrix and concentration of rare earth ions leading to a marked increase in the RI value is well demonstrated for the rare earth ion, Tb^{3+} doped in crystalline and glass systems.¹³

The two dominant emissions for Eu^{3+} occur due to $^5D_0 \rightarrow ^7F_2$ at 612 nm in the red region and $^5D_0 \rightarrow ^7F_1$ at 592 nm due to orange emission. Their relative intensities denoted by **R/O** is a sensitive function of covalency and site **asymmetry**.^{45,46,55} The **R/O** value is found to be higher when the Eu^{3+} ion is bound to more covalent atoms or present in higher **asymmetry**.^{45,46,55} In such a case in the PbF₂ rich glass the higher ionic environment due to presence of larger number of fluoride ions around the Eu^{3+} ion as suggested by the lower f_2 values should lead to smaller R/O values for this glass. This is indeed found to be the case (table 5.18).

5.4.2 Conclusions

Absorption and emission spectra of **Eu³⁺** doped in **PbO-PbF₂** glasses suggest that **Ln³⁺** ion is 8-9 coordinated, the ion being bound to both oxide and fluoride ions. For the laser transition the calculated and experimental branching ratios agree well. The transition probabilities for this transition are higher for the oxyfluoride glasses than for phosphate glasses signifying higher lifetimes for **⁵D₀** level in these glasses. Our results show that in these glasses the phonon energies are low enough to lead to the observation of high energy lines in the region 440-580 nm. The phonon energy maximum is found to be 930 cm⁻¹. The electron-phonon coupling strengths evaluated from the phonon side band are nearly the same and are 10.2x10⁻³ and 9.5x10⁻³ for 30PbO-70PbF₂-2.0 wt. % **Eu³⁺** and 70PbO-30PbF₂-2.0 wt. % **Eu³⁺** respectively. The relative emission intensities are sensitive functions of glass composition and concentration of **Eu³⁺** ions. These oxyfluoride glasses are characterized by low energy phonons as in tellurite, germanate and fluoride glasses and are quite different from borate and phosphate glasses in this respect. The variations in the relative integrated intensities of the low energy lines to high energy lines within these glass systems provide evidence for increasing tendency to form clusters of the rare earth ions with increasing PbO content and increase in the concentration of the **Eu³⁺** ions.

5.5 Tb³⁺ Fluorescence as a Probe for Ouster Formation in Lead Oxyfluoride Glasses

A knowledge of pairing and **clustering of** lanthanide ions even when doped in low concentrations in different matrices is invaluable as it has bearing on their fluorescence properties and related phenomena such as energy transfer and upconversion. The emission spectral studies of Tb³⁺ incorporated single crystals and glasses show that Tb³⁺ fluorescence can be used as an incisive probe to determine pair or cluster formation of the dopant ions in these **matrices**.¹³ Based on such studies the parent matrices can be broadly classified into two groups, one showing extensive clustering and the other showing the so called standard behavior where pairing and clustering occur to a significantly lesser extent especially at low concentrations of the dopant ions. The present work deals with the concentration dependence of fluorescence in Tb³⁺ doped 30PbO-70PbF₂ glass.

5.5.1 Results and Discussion

The emission spectra of the 0.5 and 2.0 wt. % of Tb³⁺ doped 30PbO-70PbF₂ glasses are reproduced in figure 5.29 as illustrative examples. The emission lines originating from ⁵D₄ and ⁵D₃ energy levels are indicated in the spectra. The emission transitions from these two levels occur in the green and blue regions respectively. The intensities of the blue and green emissions are obtained by integrating the area over the corresponding part of the spectrum. In the low wavelength region, slight systematic errors in intensity measurements can be present due to background emissions. The extent of such errors were evaluated while obtaining the relative intensities of the green to blue emissions. The ratios of integrated emission intensities of transitions from ⁵D₄ and ⁵D₃ energy levels ($\Sigma I(^5D_4)/\Sigma I(^5D_3)$) with estimated errors and the ratios of the number of Tb³⁺ ions to the total number of cations (x_{Tb}) in the 30PbO-70PbF₂ glass are given in table 5.20. A plot of x_{Tb} against ($\Sigma I(^5D_4)/\Sigma I(^5D_3)$) is shown in figure 5.30. This figure

also reproduces two plots due to van Dongen indicating the variations in this ratio for varying concentrations of Tb³⁺ ions doped in different crystalline materials and glasses.¹³

The energy levels of Tb³⁺ are shown in figure 5.31 The energy gap between ⁵D₃ and ⁵D₄ levels approximates the energy difference within the ⁷F₁ (J = 0, 6) multiplet. The emissions at wavelengths below 480 nm originate from the ⁵D₃ level situated around 26,300 cm⁻¹ above the ground state, ⁷F₆. At longer wavelengths the ⁵D₄→⁷F₁ transitions are observed Figure 5.30 shows that the ratio ($\Sigma I(^5D_4)/\Sigma I(^5D_3)$) is a very sensitive function of Tb³⁺ concentration. It exhibits two distinct trends depending on whether homogeneous distribution or clustering of Tb³⁺ takes place in the host material The full line gives the behavior of the above mentioned intensity ratio for materials with dominant blue emission at low Tb³⁺ concentrations which shifts to green emission at relatively higher Tb³⁺ concentrations This behavior has been referred to as standard behavior and is characteristic of materials in which the Tb³⁺ ions are homogeneously distributed. The dotted line is found for materials with markedly negligible blue emission and is indicative of clustering even at low Tb³⁺ concentrations Cross relaxation involving ⁵D₃→⁵D₄ and ⁷F₆→⁷F₁ energy levels is responsible for the enhancement of emission intensities from blue to green region above the critical concentration.¹³ The intensity ratio of emissions from the ⁵D₄ and ⁵D₃ levels for our sample are found to be close to the full line indicating homogeneous distribution for samples with Tb³⁺ concentration up to 2.0 wt. % and cluster formation at higher concentrations. However the values of this ratio for the concentrations of Tb³⁺ ions investigated are found to be systematically lower than the values reported for other materials displaying standard behavior This is also brought out by the significantly larger relative intensities for the high energy transitions for our sample in the low concentration region (figure 5.29) compared to the observations for these transitions for Tb³⁺ doped fluoride glasses in the same range of dopant concentrations¹³ This shows that pairing and clustering occur to a lesser extent in PbO-PbF₂ glass compared to other samples following standard behavior Our results further show that concentration dependence of Tb³⁺ fluorescence can enable differentiating the

Chapter 5

extent to which ion-ion interaction takes place even in **materials** following standard behavior.

The observed deviation from the standard behavior can be attributed to the nature of sites available for occupation by Ln^{3+} ions in general and Tb^{3+} ions in particular. In the present glass doped with Pr^{3+} , Nd^{3+} and Eu^{3+} , the transitions $^3\text{P}_0 \leftarrow ^3\text{H}_4$ of Pr^{3+} and $^2\text{P}_{1/2} \leftarrow ^4\text{I}_{9/2}$ of Nd^{3+} in the absorption spectra and $^5\text{D}_0 \rightarrow ^7\text{F}_0$ of Eu^{3+} in the emission spectrum, which characterize coordination of the Ln^{3+} ion are found to occur at 20,704 cm^{-1} , 23,397 cm^{-1} , 17,277 cm^{-1} respectively and support eight coordination.^{32,59,69} The structure of PbO-PbF_2 glass suggests that eight coordination of Tb^{3+} ions can be achieved by eight fluoride and oxide ligands from six PbO_2F_4 octahedra as shown in figure 5.3, the octahedra being linked by **Pb-O-Pb linkages**.¹ Two octahedra contribute a pair each and four octahedra one ligand atom each leading to eight coordination. The lanthanide ion will occupy sites with D_{2h} or lower micro symmetry with large separation between these ions even if they happen to be near **neighbors** The observed results indicating weak interaction between the Tb^{3+} ions is in conformity with the nature of the sites occupied by these ions as suggested earlier.

5.5.2 Conclusions

The Tb^{3+} concentration dependence of emission spectral intensities in the PbO-PbF_2 glass closely follows the standard behavior characteristic of homogeneous distribution of the probe ions The systematic deviation from the standard behavior shows that pairing and clustering occur to a lesser extent in this glass than in other systems exhibiting standard behavior. This result is also in conformity with the nature of the sites occupied by the rare earth ions. The results show that the concentration dependence of the emission spectra of Tb^{3+} throws light not only on whether pairing and clustering occur but also on the extent to which interactions between the probe ions differ in systems exhibiting standard behavior.

Table 5.1 The spectroscopic parameters of Pr^{3+} , Nd^{3+} , Er^{3+} and Tm^{3+} ions doped in **30PbO-70PbF₂** glass system.

Parameters (cm^{-1})	Pr^{3+}	Nd^{3+}	Er^{3+}	Tm^{3+}
F²	70530	77165	98510	104836
F⁴	51989	51840	72566	80456
F^6	34626	38346	54088	59669
E¹	4778.80	5048.00	6750.00	7323.28
E^2	22.53	26.29	32.15	33.45
E^3	476.16	508.80	640.11	678.46
a	22.98	24.34	12.46	14.67
β	-1341.78	-630.00	-545.00	-959.00
y	1215.00	1436.00	1608.00	0.00
ξ	720.10	868.80	2460.90	2664.10
EVE^3	9.91	9.92	10.55	10 79
E^2/E^3	0.047	0.052	0.050	0.049
rms	± 23	± 66	± 42	± 41

Table 5.2 Observed and calculated energy levels in cm^{-1} of Pr^{3+} and Tm^{3+} ions in $30\text{PbO}-70\text{PbF}_2$ glass system.

Pr^{3+}			Tm^{3+}		
Terms	E_{obs}	E_{cal}	Terms	E_{obs}	E_{cal}
from $^3\text{H}_{\infty}$ (cm^{-1})		(cm^{-1})	from $^3\text{H}_{\infty}$	(cm^{-1})	(cm^{-1})
$^3\text{F}_2$	5173	5208	$^3\text{F}_4$	5935	5908
$^3\text{F}_3$	6557	6552	$^3\text{H}_3$	8298	8298
$^3\text{F}_4$	6916	6937	$^3\text{H}_4$	12809	12784
$^1\text{D}_2$	16939	16947	$^3\text{F}_3$	14660	14660
$^3\text{P}_0$	20790	20785	$^3\text{F}_2$	15218	15217
$^3\text{P}_1$	21369	21365	$^1\text{G}_4$	21706	21725
$^3\text{P}_2$	22563	22532			
rms	± 20			± 16	

Table 5.3 The Judd-Ofelt parameters for lanthanide ions doped in 30PbO-70PbF₂ glass system.

Lanthanide ion	$\Omega_2 (10^{-20} \text{ cm}^2)$	$\Omega_4 (10^{-20} \text{ cm}^2)$	$\Omega_6 (10^{-20} \text{ cm}^2)$
Pr ³⁺	0.02	7.88	4.81
Nd ³⁺	1.53	3.62	3.82
Sm ³⁺	1.16	2.66	1.43
Eu ³⁺	2.64	2.29	1.41
Dy ³⁺	2.13	2.10	1.04
Ho ³⁺	1.49	1.69	1.27
Er ³⁺	3.21	1.34	0.61
Tm ³⁺	2.50	2.35	1.16

Table 5.4 Observed and calculated oscillator strengths of Pr³⁺ and Tm³⁺ ions in 30PbO-70PbF₂ glass system.

Pr ³⁺			Tm ³⁺		
Transition	P (10 ⁻⁶)		Transition	P (10 ⁻⁶)	
from ³ H ₄	obs	cal	from ³ H ₆	obs	cal
³ F ₂	3.89	3.91	³ F ₄	2.38	2.74
³ F ₃	7.92	8.03	³ H ₅	2.59	1.79
³ F ₄	3.27	3.79	³ H ₄	2.66	2.74
¹ D ₂	3.88	1.30	³ F ₃	3.29	3.50
³ P ₀	4.04	5.68	³ F ₂	0.51	0.63
³ P ₁	7.31	5.77	¹ G ₄	1.65	0.92
³ P ₂	1687	425			
rms	+3.93			±0.19	

Table 5.5 The radiative properties for the emission levels of **Pr³⁺** and **Tm³⁺** doped in **30PbO-70PbF₂** glass system.

Transition	λ_p (nm)	$\Delta\lambda_p$ (nm)	A (sec ⁻¹)	β_R cal	β_R exptl	σ_p (10 ⁻²⁰ cm ²)
Praseodymium(III)						
³ P ₀ → ³ H ₄	4876	18.0	50647	0.74	0.73	6.66
³ P ₀ → ³ H ₅	540.0	17.0	-	-	0.10	
³ P ₀ → ³ H ₆	6110	15.0	6718	0.10	0.13	261
³ P ₀ → ³ F ₂	642.0	10.0	81	0	0.04	0.05
³ P ₁ → ³ H ₅	526.6	134	26950	0.41	-	6 48
¹ D ₂ → ³ H ₄	595.0	22.0	1519	0.39	-	0 36
Thulium(III)						
¹ D ₂ → ³ H ₄	452.8	10.0	15345	42.2		2.70
¹ G ₄ → ³ H ₆	482.0	11.0	1441	43.5		0 29
¹ D ₂ → ³ H ₅	5250	14.0	162	05		0.03
¹ G ₄ → ³ H ₄	6520	14.0	295	8.9		0.05
¹ D ₂ → ³ F ₄	662.0	16.0	1817	50		091
¹ D ₂ → ³ F ₃	767.0	10.4	1172	3.2		1.63

Table 5.6 Calculated radiative lifetimes of fluorescent levels for **Pr³⁺** and **Tm³⁺** ions in **30PbO-70PbF₂** glass system

Lanthanide ion	Level	τ_R ((isec)
Pr³⁺	³F₃	813
	¹D₂	257
	³P₀	14
	³P₁	15
Tm³⁺	¹D₂	27
	¹G₄	301

Table 5.7 Calculated values of energy transfer efficiencies (η_T), transfer probabilities (**P_{da}**) and donor-acceptor distances (R) for **Pr³⁺→Tb³⁺** ions doped in **30PbO-70PbF₂** glass system.

S. No	Donor Conc wt. %	Acceptor Conc. wt. %	c ² or (D+A) ²	D-A distance R(A)	E.T efficiency (η_T) ± 0.05	E.T probability (P_{da}) sec ⁻¹ ± 0.05
1.	0.5	0.12	0.39	18.20	0.11	130.81
2.	0.5	0.25	0.56	17.21	0.33	493.47
3.	0.5	0.50	1.00	15.74	0.49	992.03
4.	0.5	0.75	1.56	14.67	0.52	1085.16
5.	0.5	1.00	2.25	13.85	0.60	1533.33
6.	0.5	1.25	3.06	13.18	0.63	1753.62

E.T. = Energy transfer

Table 5.8 Observed and calculated energy levels in cm^{-1} of Nd^{3+} and Er^{3+} ions in $30\text{PbO}-70\text{PbF}_2$ glass system.

Nd^{3+}			Er^{3+}		
Terms from $^4\text{I}_{9/2}$	E_{obs} (cm^{-1})	E_{cal} (cm^{-1})	Terms from $^4\text{I}_{15/2}$	E_{obs} (cm^{-1})	E_{cal} (cm^{-1})
$^4\text{F}_{3/2}$	11520	11502	$^4\text{I}_{13/2}$	6717	6738
$^4\text{F}_{5/2}$	12475	12514	$^4\text{I}_{11/2}$	10362	10383
$^4\text{S}_{3/2}$	13408	13367	$^4\text{I}_{9/2}$	12532	12462
$^4\text{F}_{7/2}$	13610	13483	$^4\text{F}_{9/2}$	15405	15374
$^4\text{F}_{9/2}$	14643	14753	$^4\text{S}_{3/2}$	18501	18569
$^4\text{G}_{5/2}$	17199	17261	$^2\text{H}_{11/2}$	19297	19295
$^2\text{G}_{7/2}$	17559	17273	$^4\text{F}_{7/2}$	20601	20611
$^4\text{G}_{7/2}$	19135	19077	$^4\text{F}_{5/2}$	22311	22266
$^4\text{G}_{9/2}$	19580	19515	$^4\text{F}_{3/2}$	22686	22638
$^2\text{G}_{9/2}$	21021	21039	$^2\text{G}_{9/2}$	24734	24779
$^2\text{K}_{15/2}$	21767	21783	$^4\text{G}_{11/2}$	26695	26651
$^2\text{P}_{1/2}$	23397	23309	$^2\text{G}_{9/2}$	27578	27620
rms		± 66			± 42

Table 5.9 Comparison of Judd-Ofelt parameters for lanthanide ions doped in fluoride, oxyfluoride, borate and phosphate glass **systems**

Lanthanide ion	Glass matrix	f_i^2 (10^{-20} cm^2)	f_i^U (10^{-20} cm^2)	Ω_6 (10^{-20} cm^2)	$\Sigma\Omega_\lambda$ 10^{-20} cm^2
Nd³⁺	Fluoride	1.950	3.650	4.170	9.770
	Oxyfluoride	1.528	3.620	3.821	8.969
	Borate	3.660	5.340	4.460	13.460
	Phosphate	5.656	3.335	4.367	13.358
Ho³⁺	Fluoride	2.430	1.670	1.840	5.940
	Oxyfluoride	1.485	1.696	1.265	4.446
	Borate	4.244	2.301	1.396	7.941
	Phosphate	5.600	2.720	1.870	10.190
Er³⁺	Fluoride	2.540	1.390	0.960	4.890
	Oxyfluoride	3.216	1.338	0.609	5.163
	Borate	3.700	1.360	0.840	5.900
	Phosphate	6.192	3.699	0.914	10.805

Table 5.10 Observed and calculated oscillator strengths of Nd^{3+} in 30PbO-70PbF₂ glass system.

Transition from ⁴ I(w region (nm)	Spectral	P(10 ⁿ⁸)	
		obs	cal
³ F _{3/2}	868.1	162.0	216.6
⁴ F _{3/2}	801.6	667.3	645.4
⁴ S _{3/2} ⁴ F _{7/2}	740.2	632.1	652.1
⁴ F _{9/2}	682.9	38.5	51.6
⁴ G _{5/2} ² G _{7/2}	581.4	1210.7	1213.2
⁴ G _{7/2}	522.6	513.4	482.4
⁴ G _{9/2}	510.7	124.3	115.5
² P _{1/2}	427.4	28.5	55.2
rms		±26	

Hypersensitive transitions

Table 5.11 Observed and calculated oscillator strengths of Ho^{3+} in 30PbO-70PbF₂ glass system.

Transition from $^5\text{I}_8$	Spectral region (nm)	P(10^{-8})	
		obs	cal
%	1980.2	114.8	121.8
$^5\text{I}_6$	1190.0	65.7	90.4
$^5\text{I}_5$	898.7	10.2	16.1
$^5\text{F}_5$	642.0	234.8	238.9
$^5\text{S}_2$ $^5\text{F}_4$	537.0	325.0	314.6
$^5\text{F}_3$	486.0	70.9	95.9
$^5\text{F}_2$ $^3\text{K}_8$ $^5\text{G}_6^*$	452.0	1001.5	1009.8
$^5\text{G}_5$	417.0	218.7	231.3
$^5\text{G}_4$ $^3\text{K}_7$	386.0	117.1	43.7
$^5\text{G}_2$ $^3\text{H}_5$ $^3\text{H}_6^*$	361.5	298.3	253.5
rms		± 30	
Hypersensitive transitions			

Table 5.12 Observed and calculated oscillator strengths of Er^{3+} in $30\text{PbO}-70\text{PbF}_2$ glass system.

Transition from $^4\text{I}_{13/2}$	Spectral region (nm)	P (10^{-6})	
		obs	cal
$^4\text{I}_{13/2}$	1488.7	92.3	82.6
$^4\text{I}_{11/2}$	965.1	34.0	38.7
$^4\text{I}_{9/2}$	797.9	18.0	33.7
$^4\text{F}_{9/2}$	649.1	185.7	173.7
$^4\text{S}_{3/2}$	540.5	53.1	28.1
$^2\text{H}_{11/2}$	518.2	633.8	633.8
$^4\text{F}_{7/2}$	485.4	110.8	134.9
$^4\text{F}_{5/2}$	448.2	59.8	54.3
$^4\text{F}_{3/2}$	440.8	47.5	45.6
$^2\text{G}_{9/2}$	404.3	147.1	109.4
$^4\text{G}_{11/2}^{\circ}$	374.6	1243.4	1245.3
$^4\text{G}_{9/2}$	362.6	145.3	150.1
rms		± 13	

Hypersensitive transitions

Table 5.13 The radiative properties of Nd³⁺, Ho³⁺ and Er³⁺ ions in 30PbO-70PbF₂ glass system

Transition	λ_p nm	A sec ⁻¹	β_R cal	σ_p 10 ⁻²² cm ²
Neodymium(III)				
⁴ F _{3/2} → ⁴ I _{9/2}	869.0	1923	0.350	
⁴ F _{3/2} → ⁴ I _{11/2}	1034.0	2853	0.520	
⁴ F _{3/2} → ⁴ I _{13/2}	1298.0	607	0.110	
Holmium(III)				
³ S ₂ → ³ I ₈	542.5	1319	0.509	29.4
³ F ₄ → ³ I ₈	542.5	3515	0.804	78.4
³ F ₅ → ³ I ₈	651.0	1927	0.772	64.4
³ S ₂ → ³ I ₇	758.4	998	0.386	55.3
³ F ₄ → ³ I ₇	758.4	390	0.089	21.6
Erbium(III)				
² H _{11/2} → ⁴ I _{15/2}	532.0	6564	0.957	135.5
⁴ S _{3/2} → ⁴ I _{15/2}	549.9	816	0.669	19.2
⁴ F _{9/2} → ⁴ I _{15/2}	677.0	1394	0.873	51.6
⁴ S _{3/2} → ⁴ I _{13/2}	845.0	976	0.260	
⁴ S _{3/2} → ⁴ I _{11/2}	1221.0	75	0.020	
⁴ S _{3/2} → ⁴ I _{9/2}	1637.0	119	0.030	
⁴ I _{13/2} → ⁴ I _{15/2}	1484.0	560	1.000	
⁴ I _{11/2} → ⁴ I _{13/2}	2744.0	97	0.250	

Table 5.14 Observed and calculated oscillator strengths of Sm^{3+} in $30\text{PbO}-70\text{PbF}_2$ glass system.

Transition from ${}^6\text{H}_{5/2}$	Spectral region (nm)	$\text{Px}10^8$	
		obs	cal
${}^6\text{H}_{15/2} \rightarrow {}^6\text{F}_{1/2} \rightarrow {}^6\text{F}_{3/2}$	1505.1	147.8	151.5
${}^6\text{F}_{5/2}$	1390.0	182.6	173.2
${}^6\text{F}_{7/2}$	1225.0	247.1	249.9
${}^6\text{F}_{9/2}$	1082.0	123.1	156.0
${}^6\text{F}_{11/2}$	945.9	21.2	24.0
${}^4\text{G}_{5/2}$	560.0	3.1	1.1
${}^4\text{F}_{3/2}$	526.5	1.4	0.2
${}^4\text{G}_{7/2} \rightarrow {}^4\text{I}_{9/2} \rightarrow {}^4\text{M}_{15/2} \rightarrow {}^4\text{I}_{11/2} \rightarrow {}^4\text{I}_{13/2}^{\text{b}}$	469.4	147.2	73.8
${}^4\text{F}_{5/2} \rightarrow {}^4\text{M}_{17/2} \rightarrow {}^4\text{G}_{9/2} \rightarrow {}^4\text{I}_{15/2}$	439.0	11.1	10.8
$({}^6\text{P} \rightarrow {}^6\text{P})_{5/2} \rightarrow {}^4\text{L}_{13/2} \rightarrow {}^4\text{F}_{7/2} \rightarrow {}^6\text{P}_{3/2}$	406.7	410.0	425.1
$\text{K}_{11/2} \rightarrow \text{L}_{15/2} \rightarrow \text{G}_{11/2}$			
$({}^4\text{D}_{1/2} \rightarrow {}^6\text{P}_{7/2} \rightarrow {}^4\text{F}_{9/2}) \rightarrow {}^4\text{L}_{17/2} \rightarrow {}^4\text{K}_{13/2}$	374.0	103.2	93.8
${}^4\text{D}_{3/2} \rightarrow ({}^4\text{D} \rightarrow {}^6\text{P})_{5/2} \rightarrow {}^4\text{H}_{7/2}$	361.5	148.0	96.3
rms		± 28	

* Hypersensitive transition

^b See text

Table 5.15 Observed and calculated oscillator strengths of Dy³⁺ in 30PbO-70PbF₂ glass system.

Transition from ⁶ H _{15/2}	Spectral region (nm)	Px 10⁸	
		obs	cal
⁶ H _{11/2}	1665.0	39.2	64.4
⁶ F _{11/2} [▲] ⁶ H _{9/2}	1285.0	382.4	380.6
⁶ F _{9/2} ⁶ H _{7/2}	1090.0	207.2	213.0
⁶ F _{7/2} ⁶ H _{5/2}	902.0	153.5	130.1
⁶ F _{5/2}	803.0	90.7	50.9
⁶ F _{3/2}	753.0	10.6	9.6
⁴ I _{13/2} [▲]	451.9	31.2	21.2
⁴ G _{11/2}	425.0	12.2	84
⁴ F _{7/2} ⁴ K _{17/2} ⁴ I _{13/2}	380.9	104.8	106.3
⁴ M _{19/2} ⁶ P _{3/2} (⁴ P ⁴ D) _{3/2}	364.0	90.7	117.3
rms		± 19	

[▲] Hypersensitive transition

Table 5.16 The radiative properties of Sm^{3+} and Dy^{3+} in 30PbO-70PbF₂ glass system.

Transition	λ_p (nm)	A (sec ⁻¹)	β_R (cal)	β_R (obs)	σ_p (10 ⁻²⁴ cm ²)	τ_M (msec)	τ_R (msec)
Samarium(III)							
$^4G_{5/2} \rightarrow ^6H_{5/2}$	562.5	9	0.044	0.118	30.2	2.33	4.46
$^4G_{5/2} \rightarrow ^6H_{7/2}$	598.5	92	0.432	0.636	304.2		
$^4G_{5/2} \rightarrow ^6H_{9/2}$	645.5	71	0.332	0.188	294.9		
$^4G_{5/2} \rightarrow ^6H_{11/2}$	705.5	26	0.123	0.032	139.2		
$^4G_{5/2} \rightarrow ^6H_{13/2}$	780.5	2	0.012	0.025	41.4		
$^4G_{5/2} \rightarrow ^6F_{3/2}$	916.6	1	0.004				
$^4G_{5/2} \rightarrow ^6F_{5/2}$	946.8	8	0.038				
$^4G_{5/2} \rightarrow ^6F_{7/2}$	1053.8	2	0.010				
$^4G_{5/2} \rightarrow ^6F_{9/2}$	1208.3	1	0.005				
Dysprosium(III)							
$^4F_{9/2} \rightarrow ^6H_{13/2}$	481.0	136	0.220	0.384	162.6	0.79	1.60
$^4F_{9/2} \rightarrow ^6H_{13/2}$	575.1	390	0.630	0.608	1191.1		
$^4F_{9/2} \rightarrow ^6H_{11/2}$	661.9	35	0.057	0.004			
$^4F_{9/2} \rightarrow ^6H_{9/2} \quad ^6F_{11/2}$	758.3	25	0.040	0.004			
$^4F_{9/2} \rightarrow ^6H_{7/2} \quad ^6F_{9/2}$	877.1	22	0.035				
$^4F_{9/2} \rightarrow ^6H_{5/2} \quad ^6F_{7/2}$	1030.5	7	0.012				
$^4F_{9/2} \rightarrow ^6F_{5/2}$	1199.5	3	0.005				

Table 5.17 Observed and calculated oscillator strengths of Eu³⁺ transitions in PbO-PbF₂ glasses and their Judd-Ofelt parameters

Transition from Fo	30PbO-70PbF ₂		70PbO-30PbF ₂	
	P (10 ⁻⁸)		P (10 ⁻⁸)	
	obs	cal	obs	cal
³ D ₂ [*]	8.3	8.3	10.2	10.2
³ L ₆	99.4	100.9	73.3	74.1
³ G ₄ ³ G ₆	39.6	33.5	30.9	27.9
³ D ₄	9.0	12.7	13.0	14.8
rms	±3.5		±1.7	
Ω ₂ (10 ⁻²² cm ²)	264.1		376.5	
Ω ₄ (10 ⁻²² cm ²)	228.8		308.6	
Ω ₆ (10 ⁻²² cm ²)	140.5		119.0	

Hypersensitive transition

Table 5.18 The phonon energy ($\hbar\omega$), the maximum energy peak in IR spectra ($h\nu_{\max}$), the electron-phonon coupling strength (g), refractive index (η) and the relative emission intensities RI and R/O for Eu³⁺ doped PbO-PbF₂ glass systems.

Glass matrix	$\hbar\omega$ (cm ⁻¹)	$h\nu_{\max}$ (cm ⁻¹)	g(10 ⁻³)	η	RI ^a	R/O ^a
	±10	±5	±1	±0.004		
30PbO-70PbF ₂	926	940	10.2	1.779	7.3	0.9
70PbO-30PbF ₂	927	960	9.5	1.600	30.5	1.2

^a see text

Table 5.19 The radiative properties of the laser transition ${}^5D_0 \rightarrow {}^7F_2$ for Eu^{3+} in PbO-PbF_2 and phosphate glasses

Glass matrix	λ_p	$\Delta\lambda_p$	A	A_1	$\sigma_p \times 10^{22}$	β_R	
	(nm)	(nm)	(sec^{-1})	(sec^{-1})	(cm^2)	cal	exp
30PbO-70PbF₂	611.4	10.2	171	348	9.8	0.48	0.46
70PbO-30PbF₂	611.6	10.2	170	327	12.1	0.52	0.53
CaO-Al₂O₃-P₂O₅	612.0	9.9	284	407	19.1	0.70	0.66
CaO-P₂O₅	612.6	11.4	211	354	13.2	0.60	0.60

Table 5.20 Ratios of intensities of transitions from 5D_4 and 5D_3 levels and of Tb^{3+} ions to the total number of cations (x_{Tb}) in PbO-PbF_2 glass system.

Concentration of Tb^{3+} wt. % ± 0.004	$x_{\text{Tb}} (10^{-4})$	$\frac{\sum I({}^5D_4)}{\sum I({}^5D_3)}$
0.1	14.988 ± 0.637	0.335 ± 0.007
0.2	29.931 ± 0.636	0.485 ± 0.008
0.5	74.495 ± 0.633	1.038 ± 0.014
1.00	147.926 ± 0.629	2.896 ± 0.057
2.0	291.513 ± 0.620	7.897 ± 0.354

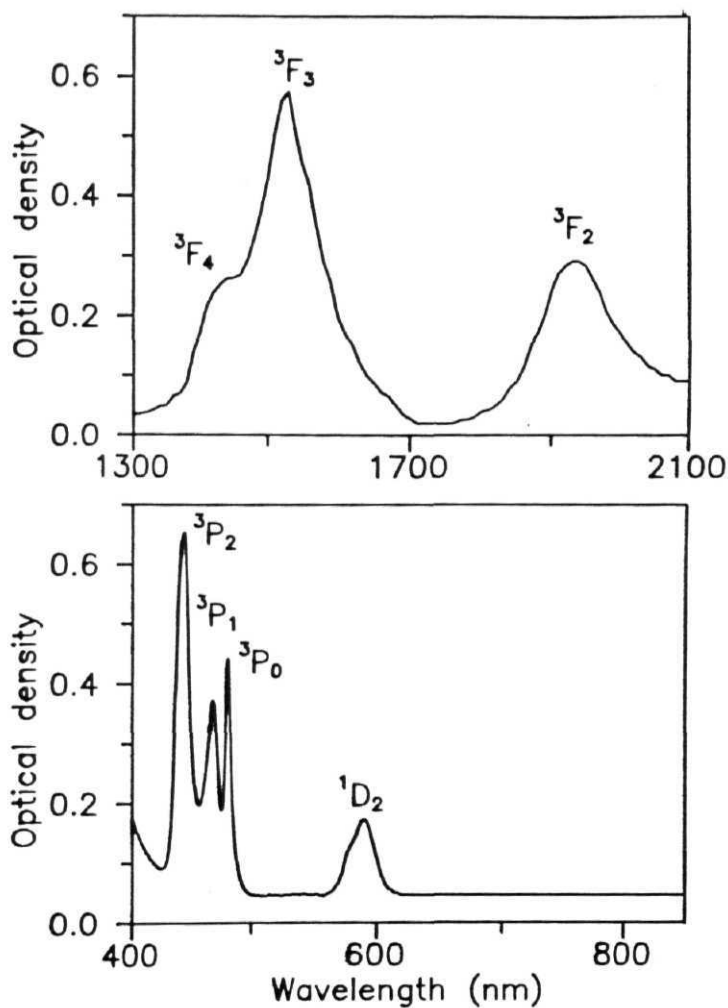


Figure 5.1 Absorption spectrum of Pr^{3+} in $30\text{PbO}-70\text{PbF}_2$ glass system.

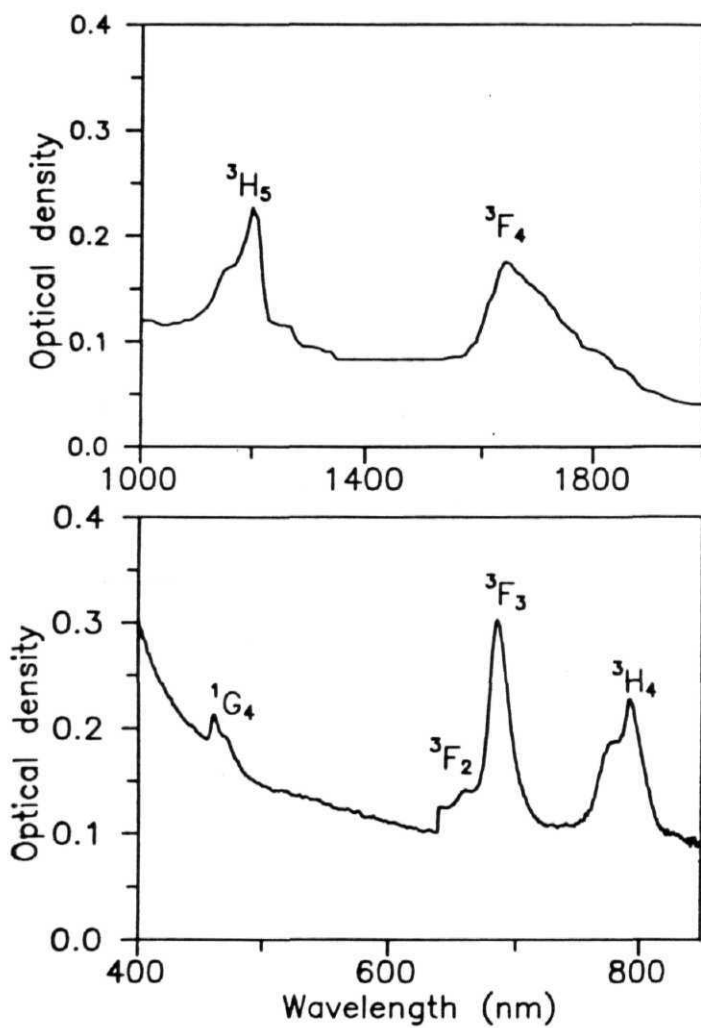


Figure 5.2 Absorption spectrum of Tm^{3+} in 30PbO-70PbF₂ glass system.

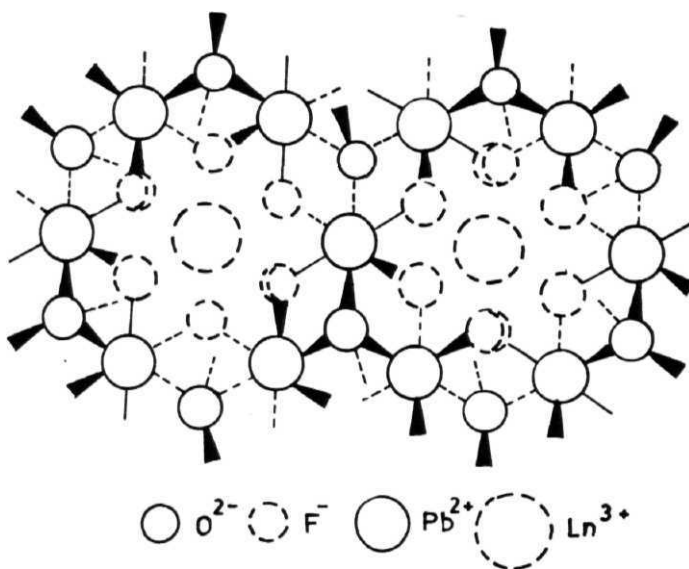


Figure 5.3 Illustration of the suggested Ln^{3+} site in 30PbO-70PbF₂ glass system made of [OPb₄] and [PbO₂F₄] units.

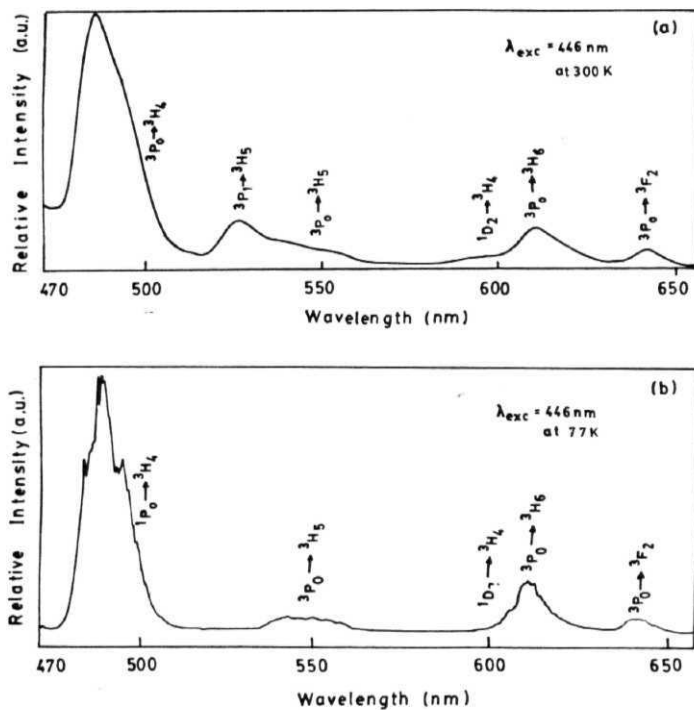


Figure 5.4 Emission spectra of Pr^{3+} in 30PbO-70PbF₂ glass system at (a) 300 K and (b) 77 K. $\lambda_{\text{ex}}=446 \text{ nm}$.

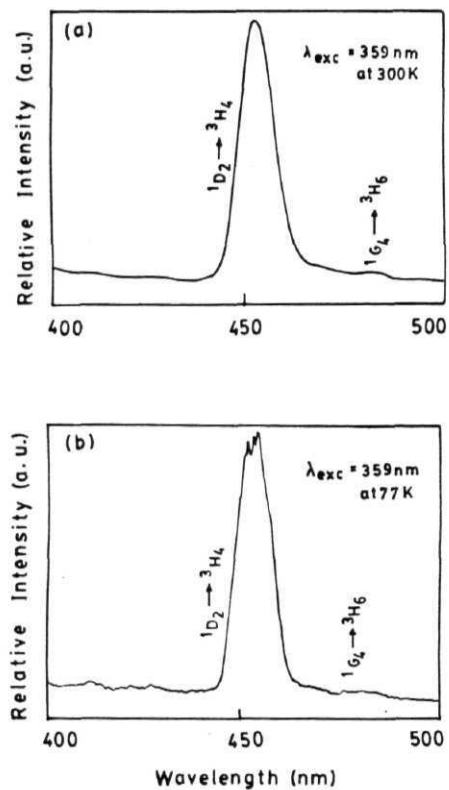


Figure 5.5 Emission spectra of Tm^{3+} in 30PbO-70PbF₂ glass system at (a) 300K and 77K. $\lambda_{\text{ex}}=359 \text{ nm}$.

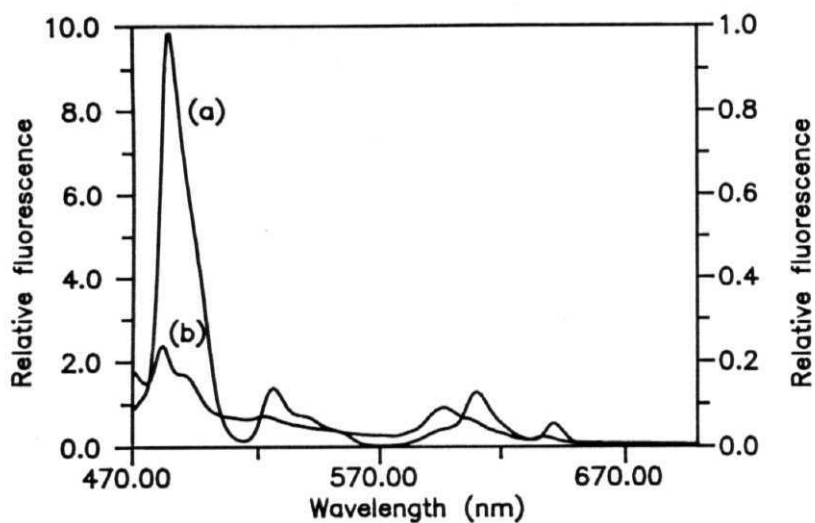


Figure 5.6 Emission spectra of Pr^{3+} in (a) $30\text{PbO}-70\text{PbF}_2$ (b) $30\text{CaO}-69\text{P}_2\text{O}_5$ glass systems normalized for the absorption. $\lambda_{\text{ex}}=446\text{ nm}$.

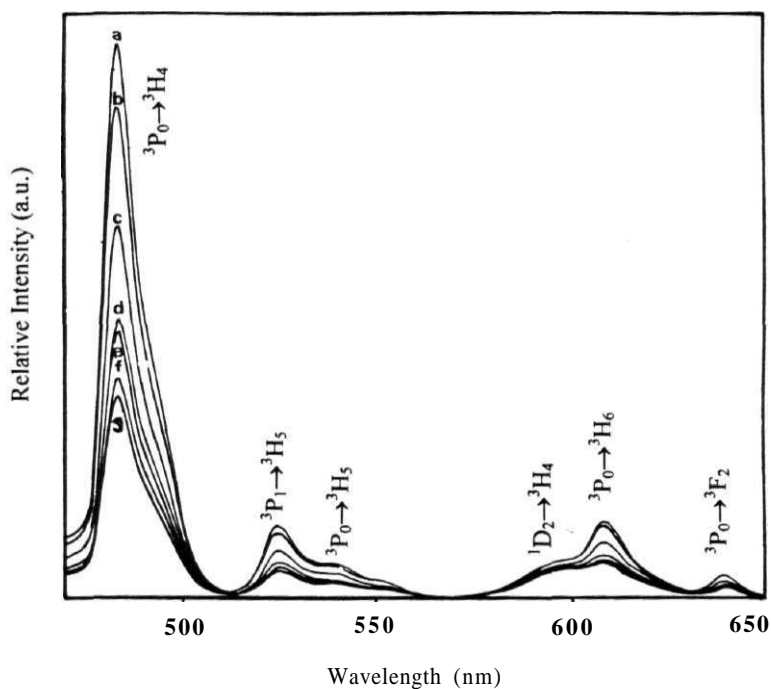


Figure 5.7 Room temperature emission spectra of Pr^{3+} in $30\text{PbO}-70\text{PbF}_2-x\text{Pr}^{3+}-y\text{Tb}^{3+}$ glass (a) 0.5Pr^{3+} (b) $0.5\text{Pr}^{3+}-0.125\text{Tb}^{3+}$ (c) $0.5\text{Pr}^{3+}-0.25\text{Tb}^{3+}$ (d) $0.5\text{Pr}^{3+}-0.5\text{Tb}^{3+}$ (e) $0.5\text{Pr}^{3+}-0.75\text{Tb}^{3+}$ (f) $0.5\text{Pr}^{3+}-1.00\text{Tb}^{3+}$ (g) $0.5\text{Pr}^{3+}-1.25\text{Tb}^{3+}$. $\lambda_{\text{ex}}=446\text{nm}$

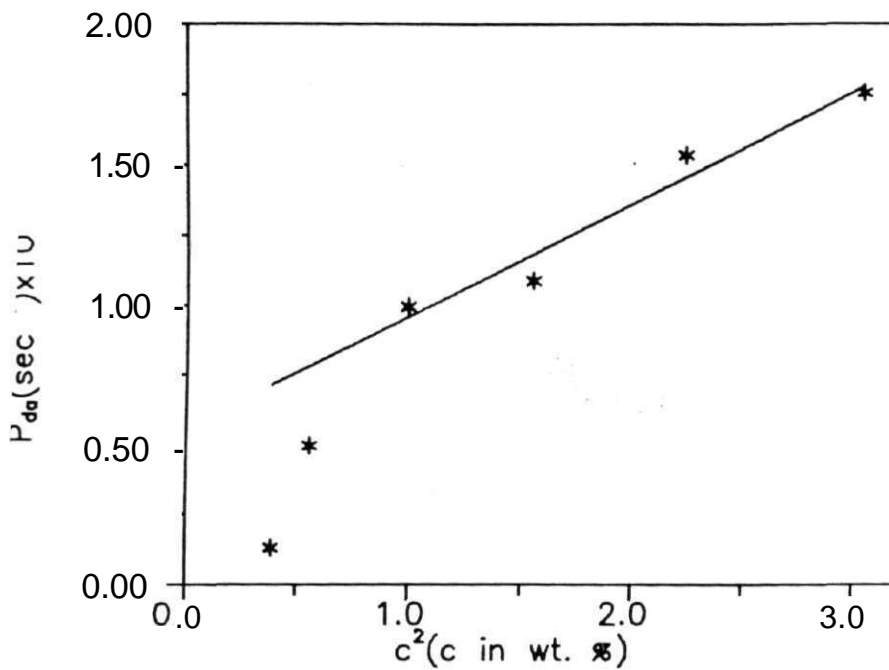


Figure 5.8 Variation of energy transfer probability (P_d) with c^2 where c is the sum of the donor (Pr^{3+}) and acceptor (Tb^{3+}) concentrations.

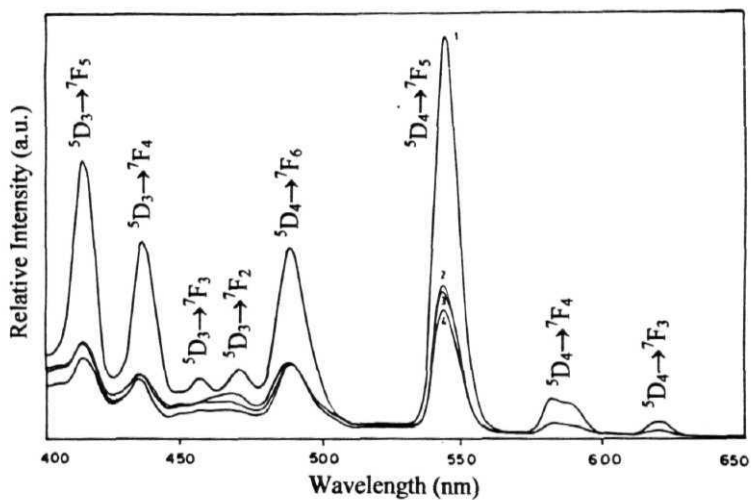


Figure 5.9 Room temperature emission spectra of Tb^{3+} in $30\text{PbO}-70\text{PbF}_2-x\text{Tb}^{3+}-y\text{Pr}^{3+}$ glass. (1) 0.5Tb^{3+} (2) $0.5\text{Tb}^{3+}-0.7\text{Pr}^{3+}$ (3) $0.5\text{Tb}^{3+}-0.5\text{Pr}^{3+}$ (4) $0.5\text{Tb}^{3+}-0.2\text{Pr}^{3+}$. $\lambda_{\text{ex}}=377$ nm

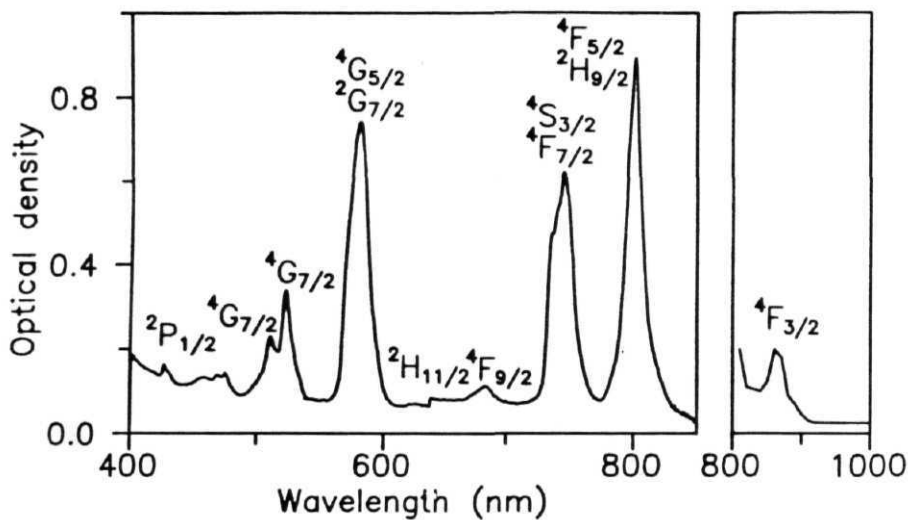


Figure 5.10 Absorption spectrum of Nd^{3+} in 30PbO-70PbF₂ glass system.

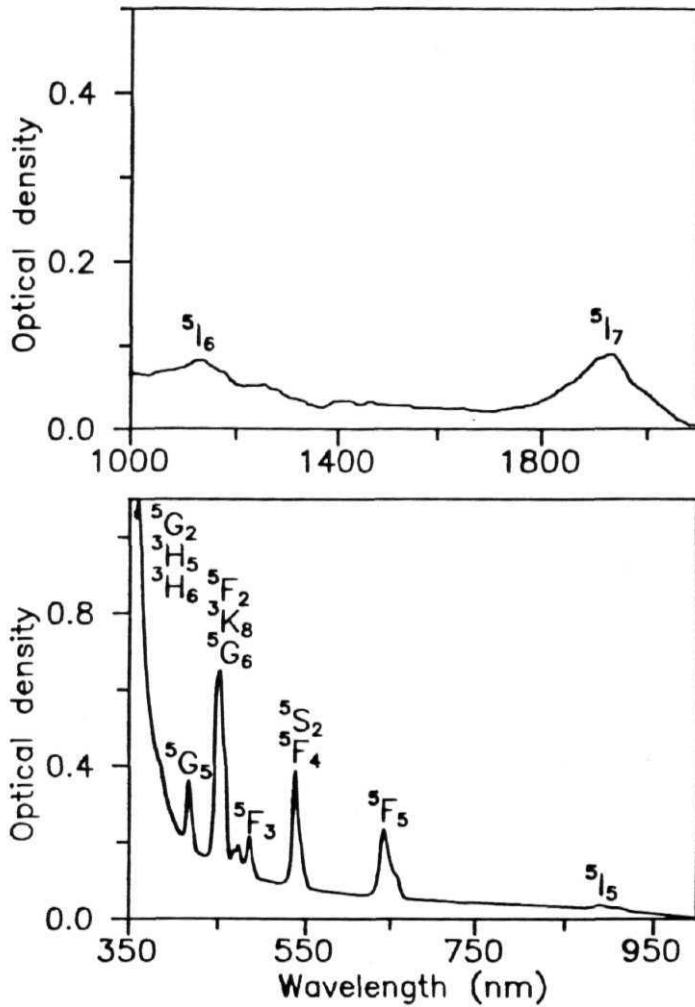


Figure 5.11 Absorption spectrum of Ho^{3+} in 30PbO-70PbF_2 glass system.

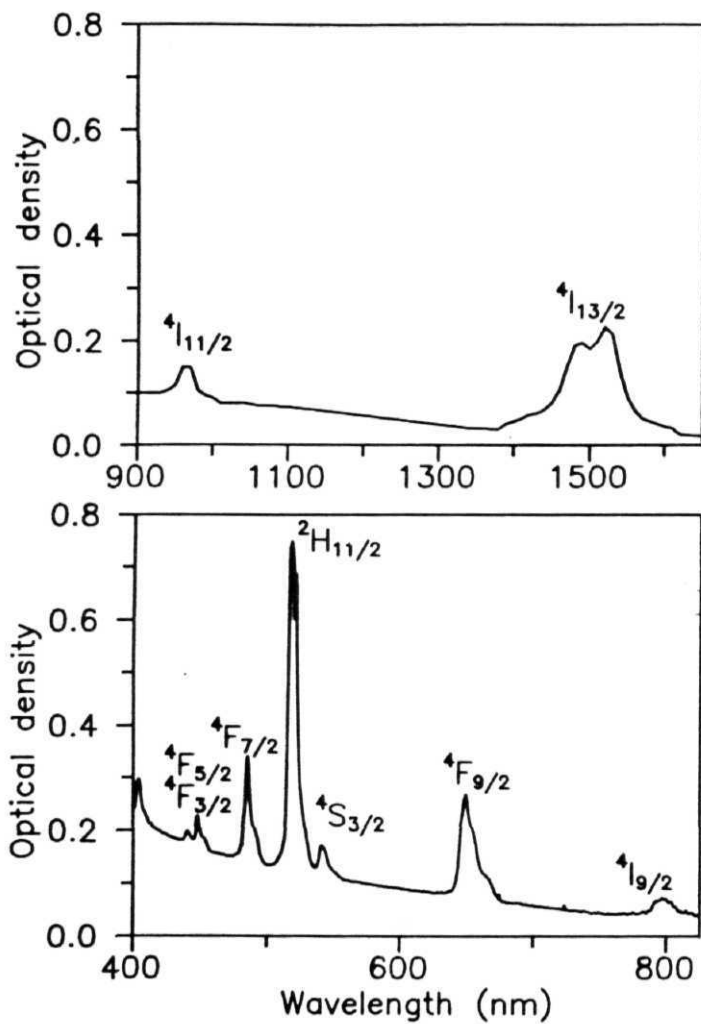


Figure 5.12 Absorption spectrum of Er^{3+} in 30PbO-70PbF₂ glass system

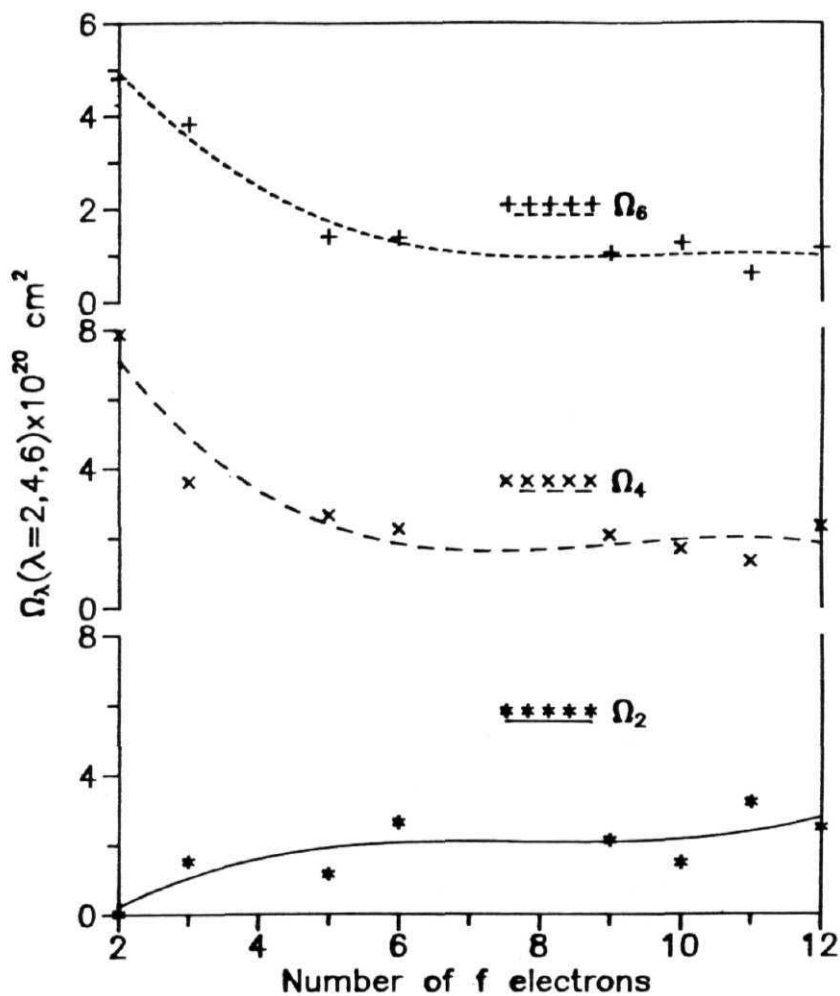


Figure 5.13 Dependence of intensity parameters (Ω_λ , $\lambda=2,4,6$) of atomic number of lanthanide ions in 30PbO-70PbF₂ glass system.

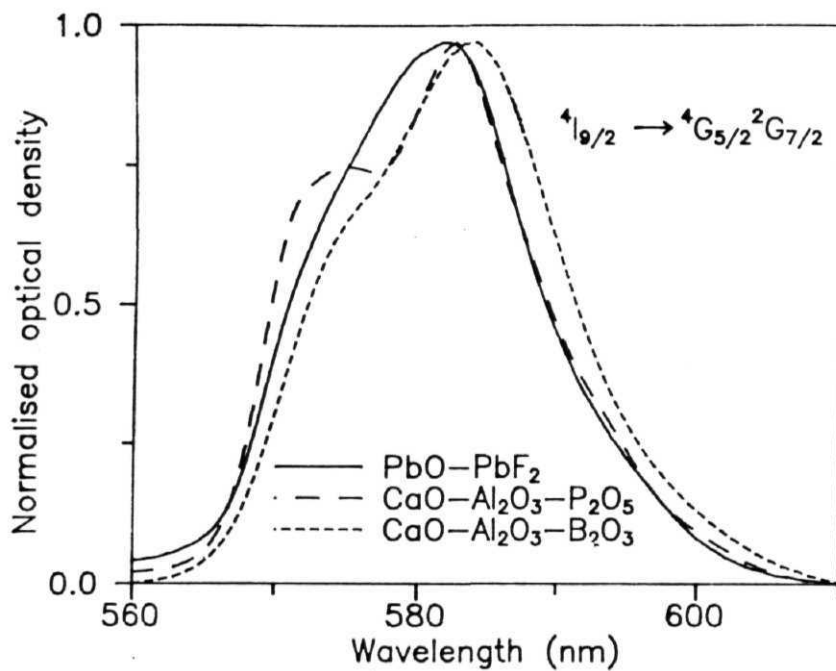


Figure 5.14 Comparison of line position and profile of hypersensitive transition $^4G_{5/2}$ $^2G_{7/2} \leftarrow ^4I_{9/2}$ of Nd^{3+} in oxyfluoride, borate and phosphate glass matrices

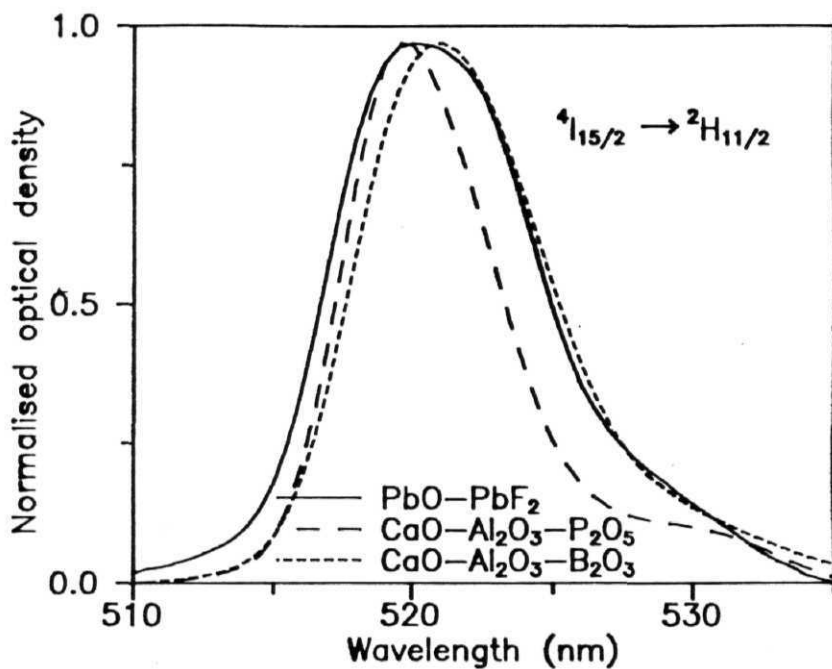


Figure 5.15 Comparison of line position and profile of hypersensitive transition $^4I_{15/2} \leftarrow ^2H_{11/2}$ of Er^{3+} in oxyfluoride, borate and phosphate glass matrices.

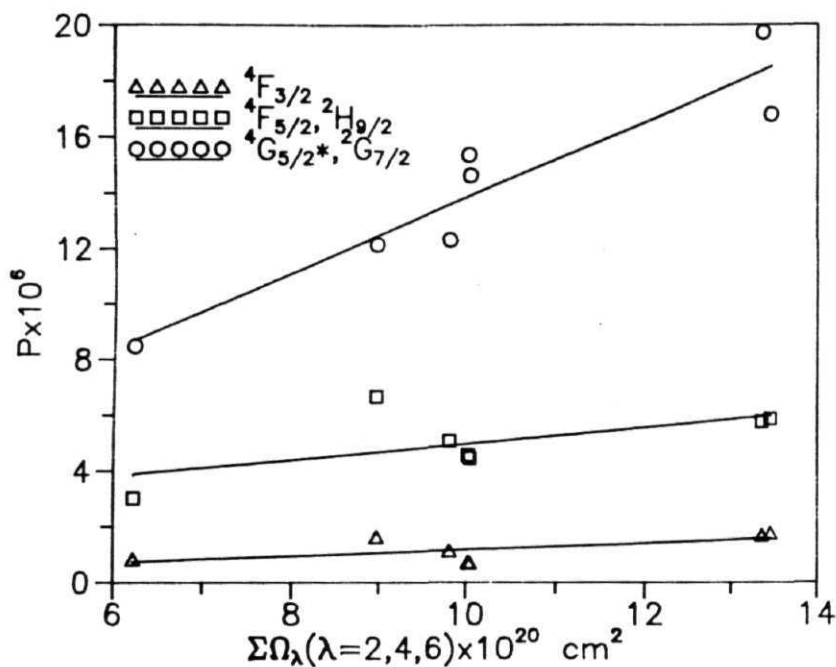


Figure 5.16 A plot of the sum of Judd-Ofelt parameters against the oscillator strengths of the hypersensitive and intense non hypersensitive transitions of Nd^{3+} in fluoride, oxyfluoride, borate and phosphate glass matrices.

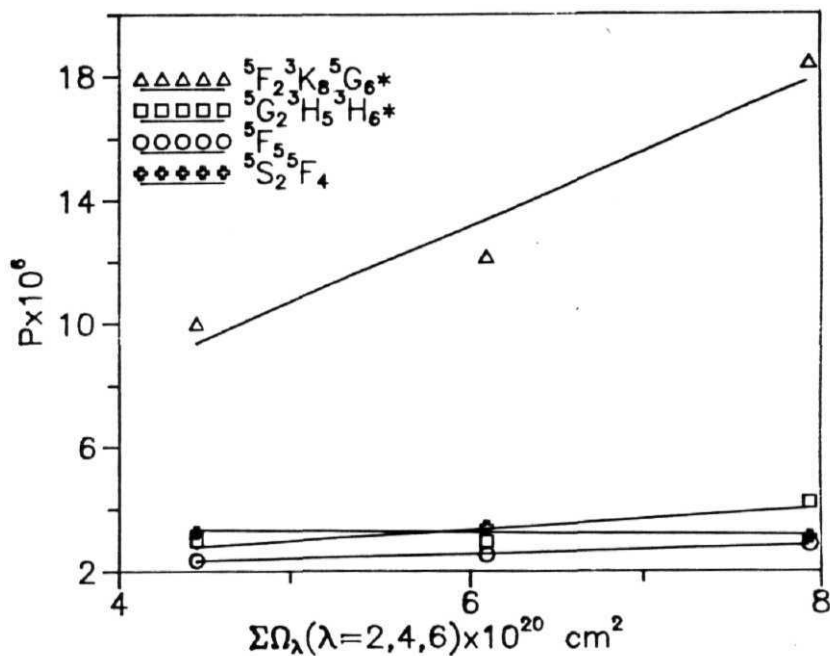


Figure 5.17 A plot of the sum of Judd-Ofelt parameters against the oscillator strengths of the hypersensitive and intense non hypersensitive transitions of Ho^{3+} in fluoride, oxyfluoride, borate and phosphate glass matrices

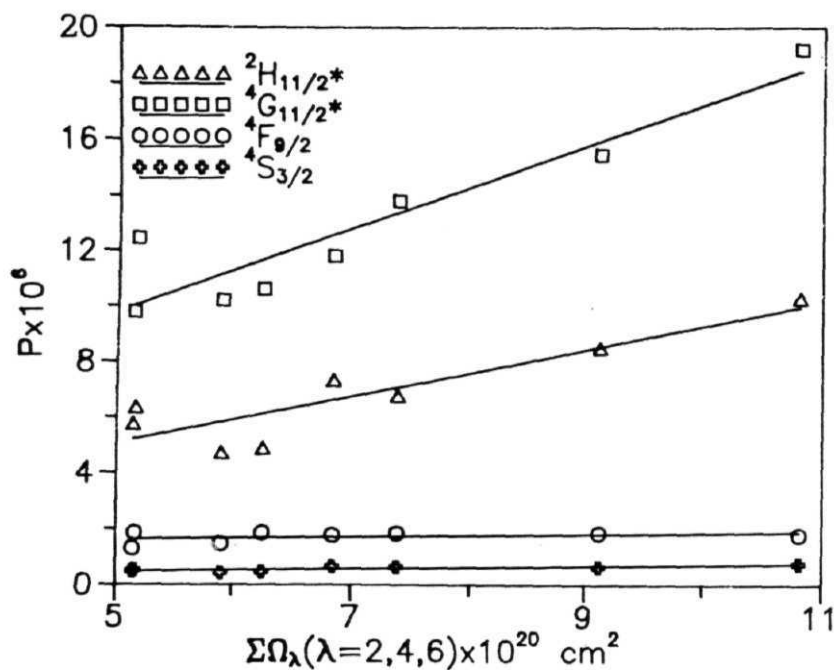


Figure 5.18 A plot of the sum of Judd-Ofelt parameters against the oscillator strengths of the **hypersensitive** and intense non hypersensitive transitions of Er^{3+} in fluoride, oxyfluoride, borate and phosphate glass matrices.

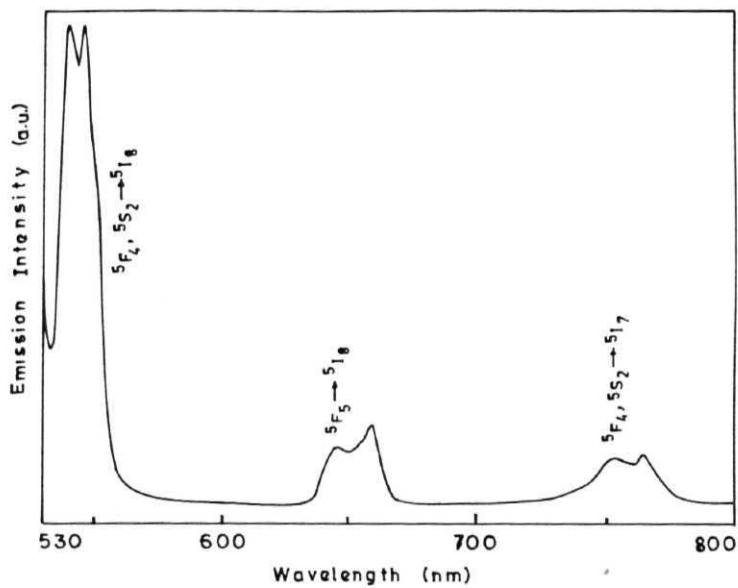


Figure 5.19 Emission spectrum of **Ho³⁺** in 30PbO-70PbF₂ glass system. λ_{ex} =452 nm.

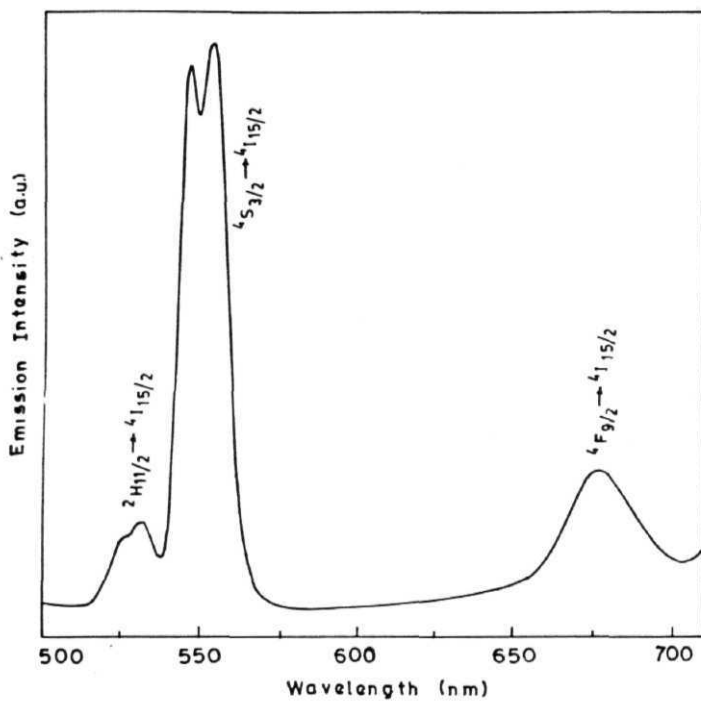


Figure 5.20 Emission spectrum of Er^{3+} in 30PbO-70PbF₂ glass system. λ_{ex} =379 nm.

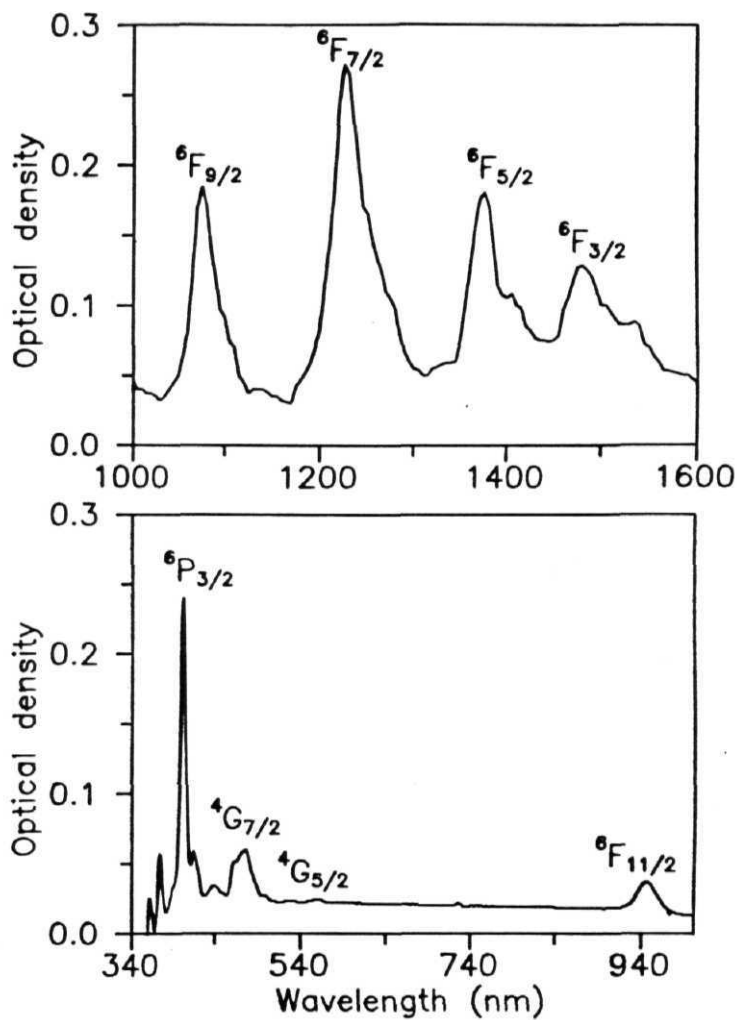


Figure 5.21 Absorption spectrum of Sm^{3+} in 30PbO-70PbF₂ glass system.

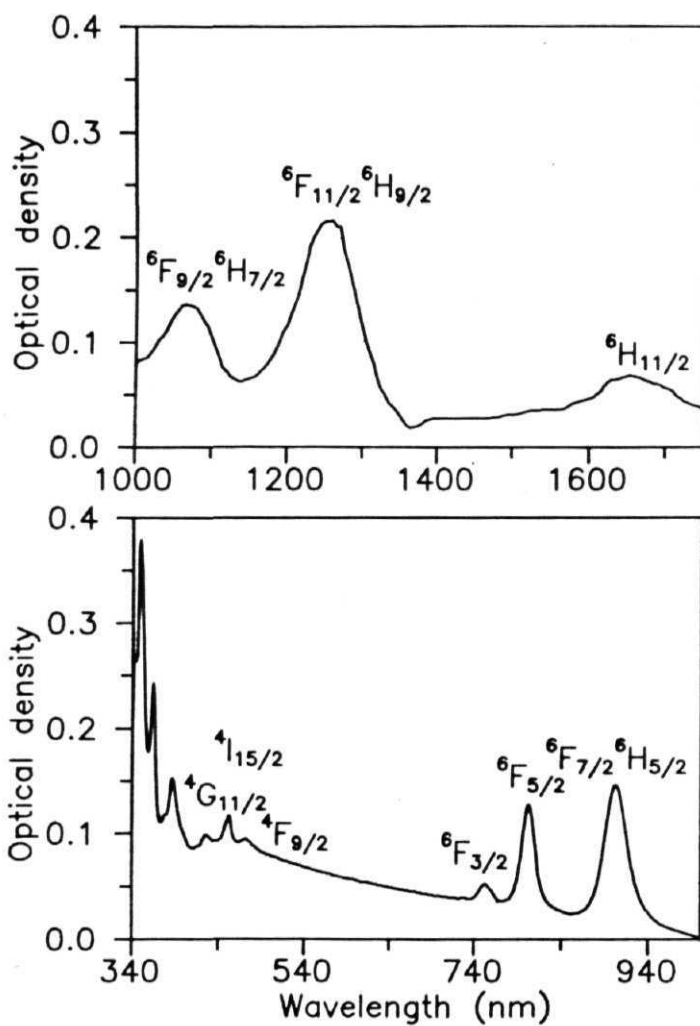


Figure 5.22 Absorption spectrum of Dy^{3+} in 30PbO-70PbF₂ glass system.

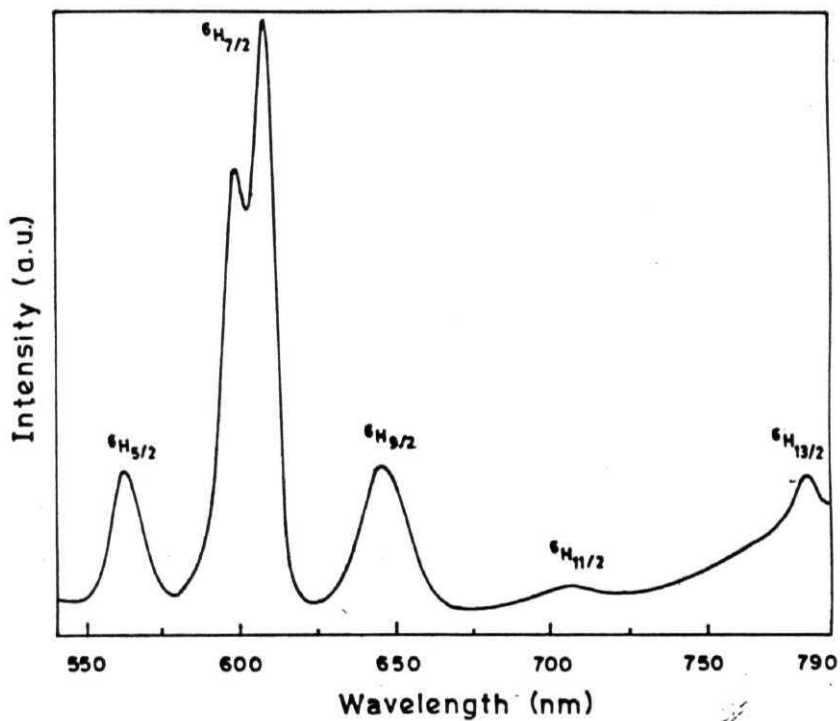


Figure 5.23 Emission Spectrum of 0.2 wt. % of Sm^{3+} at room temperature in 30PbO-70PbF₂ glass. The transitions are from the $^4\text{G}_{5/2}$ to the indicated levels. $\lambda_{\text{ex}}=402$ nm.

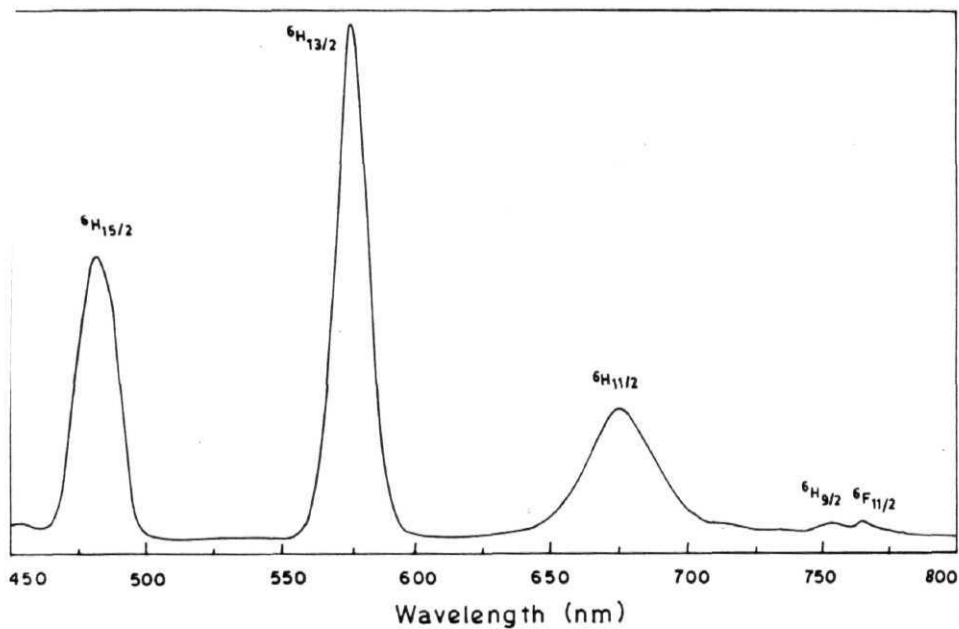


Figure 5.24 Emission Spectrum of 0.2 wt. % of Dy^{3+} at room temperature in $30\text{PbO}-70\text{PbF}_2$ glass. The transitions are from the ${}^4\text{F}_{9/2}$ to the indicated levels. $\lambda_{\text{ex}}=350$ nm.

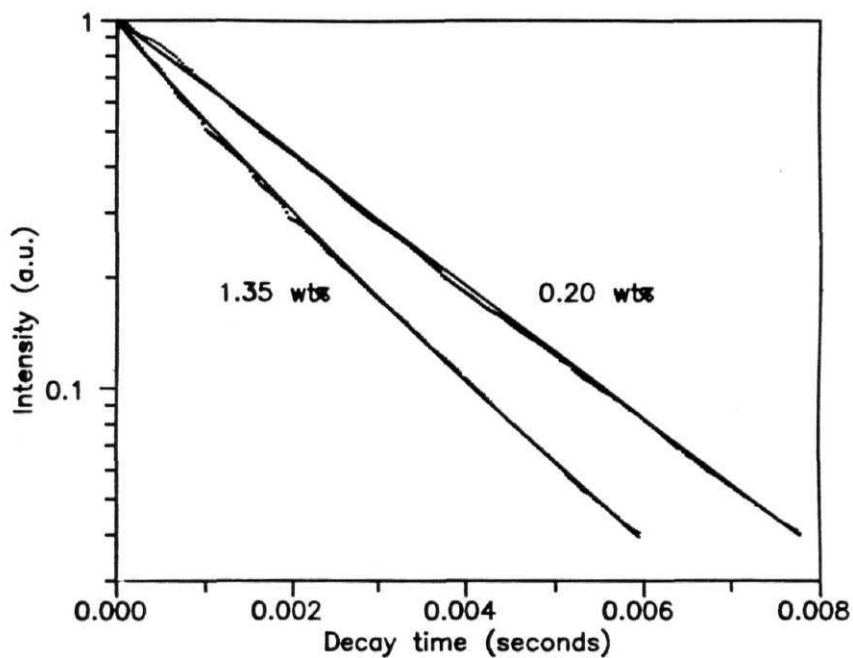


Figure 5.25 Luminescence decays at room temperature in $30\text{PbO-}70\text{PbF}_2$ glasses with 0.2 and 1.35 wt. % of Sm^{3+} . The lines represent the best fits of the experimental results to single exponential and eqn. (1) for 0.2 and 1.35 wt. % of Sm^{3+} respectively.

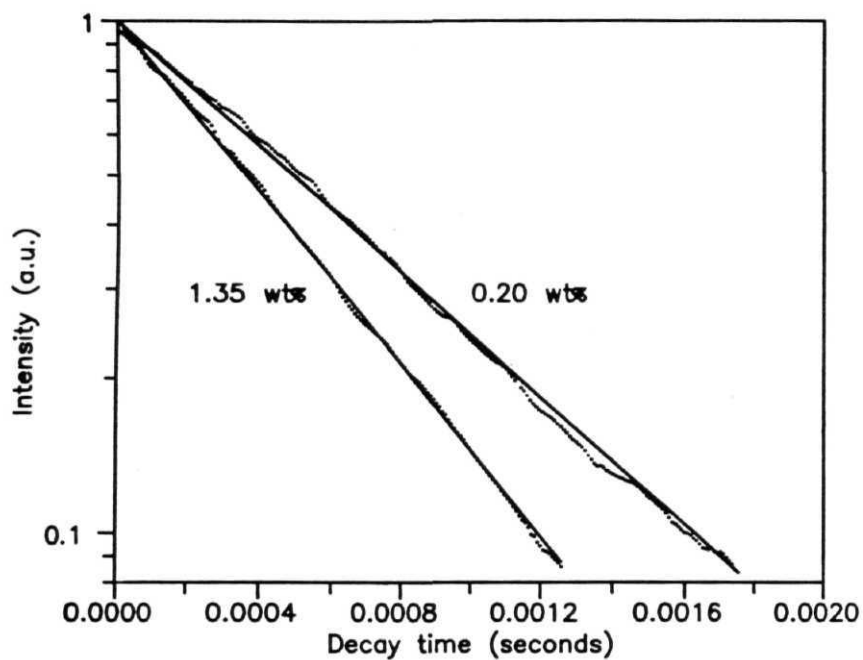


Figure 5.26 Luminescence decays at room temperature in 30PbO-70PbF₂ glasses with 0.2 and 1.35 wt. % of Dy^{3+} . The lines represent the best fits of the experimental results to single exponential for 0.2 and 1.35 wt % of Dy^{3+} ions.

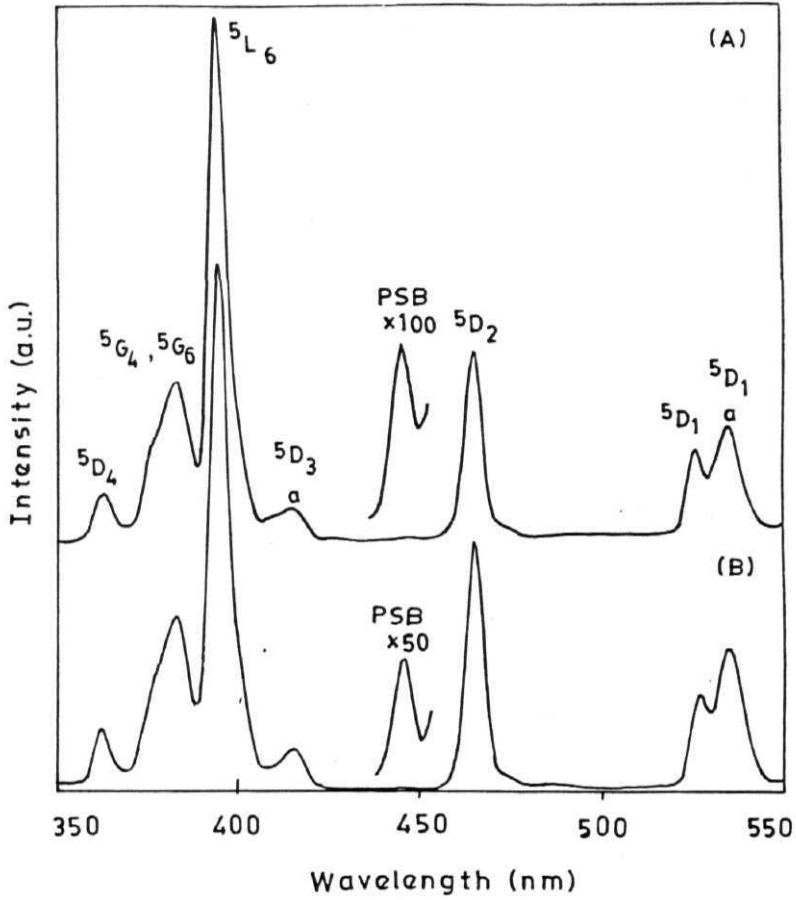


Figure 5.27 Room temperature excitation spectra of Eu³⁺ doped 30PbO-70PbF₂ (A) and 70PbO-30PbF₂ (B) glasses. PSB indicates phonon side band. $\lambda_{em}=612$ nm. The transitions marked (a) are from ⁷F₁ state and the rest are from ⁷F₀ state to higher energy states.

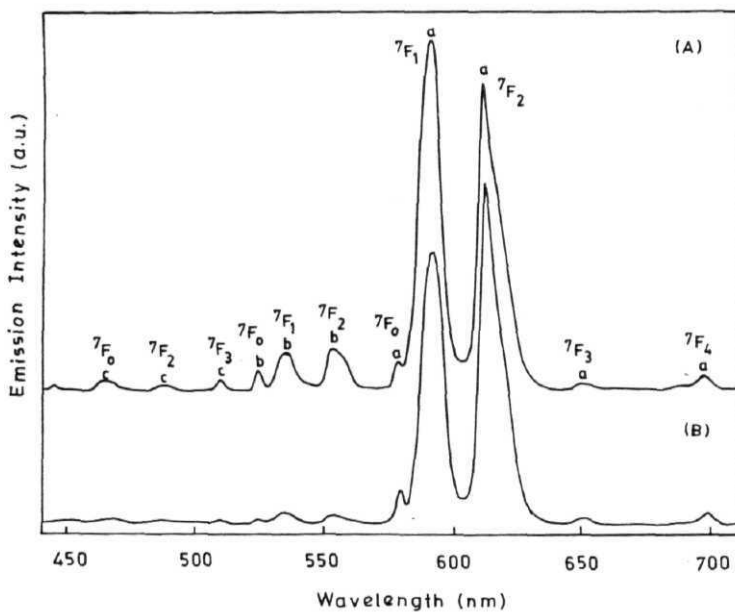


Figure 5.28 Room temperature emission spectra of Eu^{3+} doped $30\text{PbO}-70\text{PbF}_2$ (A) and $70\text{PbO}-30\text{PbF}_2$ (B) glasses. $\lambda_{\text{ex}}=395$ nm. The transitions marked (a), (b) and (c) are from D_0 , ${}^5\text{D}_1$ and ${}^5\text{D}_2$ states **respectively** Base lines are shifted efor clarity.

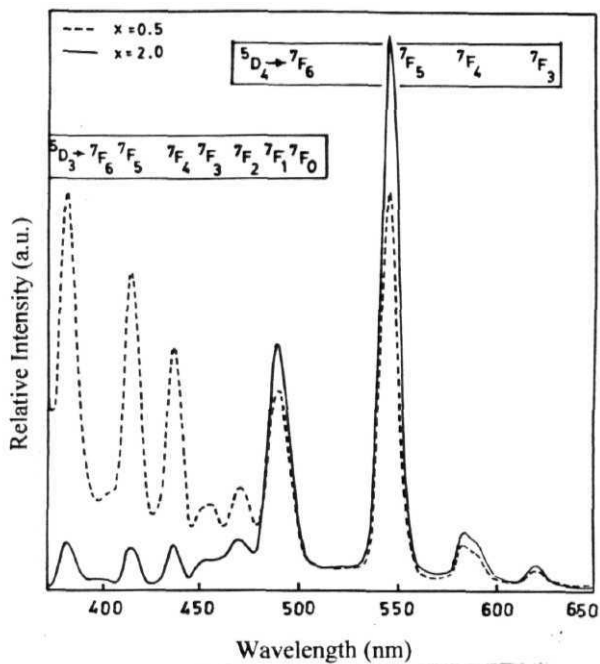


Figure 5.29 Emission spectra of PbO-PbF₂-xTb³⁺ glasses for x=0.5 and 2.0 wt %.

$\lambda_{ex}=352$ nm

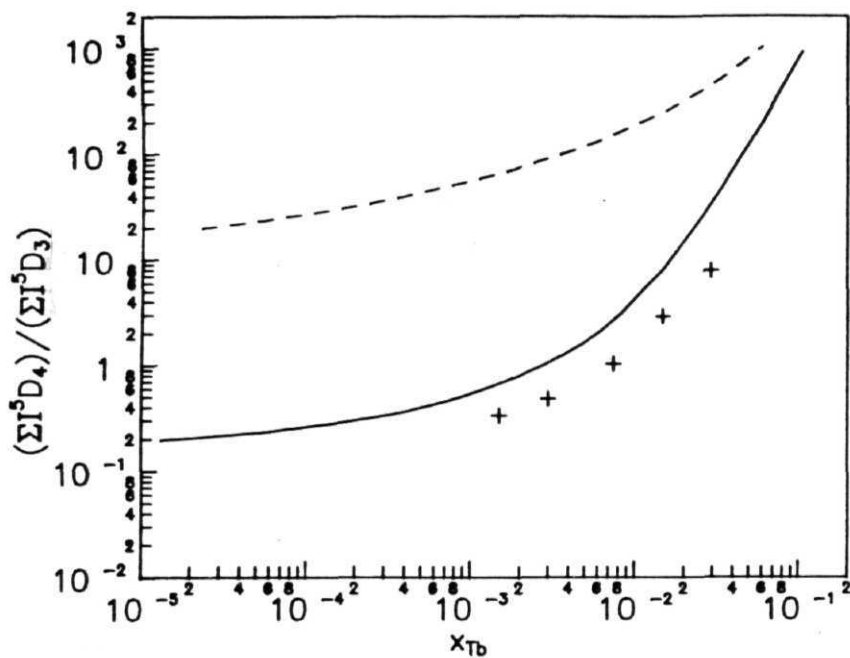


Figure 5.30 Ratio integrated 5D_4 to 5D_3 emission intensity for Tb^{3+} doped 30PbO-70PbF₂ glass. x_{Tb} is the amount of Tb^{3+} ions/total amount of cations. See text for explanation of the lines

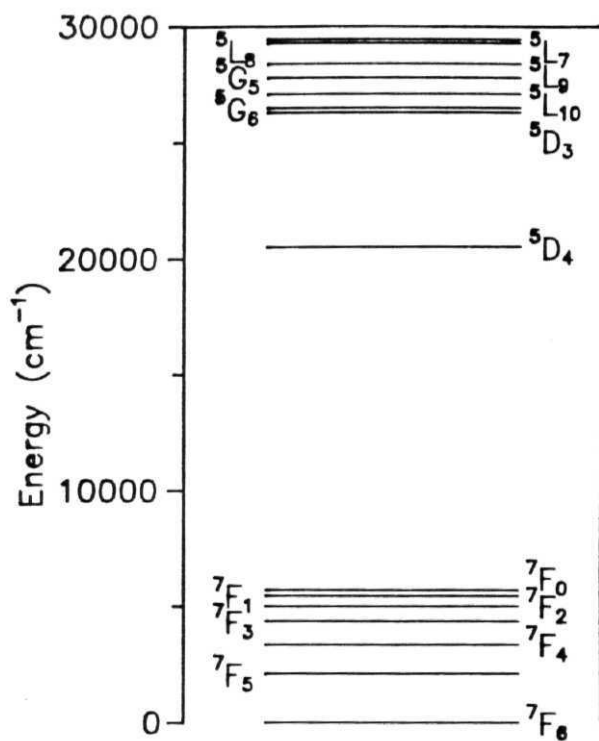


Figure 5.31 Energy level scheme of Tb^{3+} ion

References

1. B.G. Rao, H.G. Keshava Sunder, and K.J. Rao, *J. Chem. Soc. Faraday Trans. I* 80(1984)3491.
2. B.G. Rao and K.J. Rao, *Phys. Chem. Glasses* 25 (1984) 11.
3. K.J. Rao, J. Wong and B.G. Rao, *Phys. Chem. Glasses* 25 (1984) 57
4. K.J. Rao, B.G. Rao and S.R. Elliott, *J. Mater. Sci.* 20 (1985) 1678
5. J. Wang, W.S. Brocklesby, L.R. Lincoln, J.E. Townsend and D.N. Payne, *J. Non-Cryst. Solids* 163 (1993) 261.
6. R. Reisfeld and C.K. Jorgensen, *Lasers and Excited States of Rare Earths* (Springer-Verlag, New York, 1977).
7. R. Reisfeld, *Structure and Bonding* 22 (Springer-Verlag, New York, 1975) 123.
8. R. Reisfeld and C.K. Jorgensen, *Hand Book on the Physics and Chemistry of Rare Earths* (Eds.) K.A. Gschneidner and L. Eyring 9 (North Holland, Amsterdam, 1987) chap. 58.
9. M. Eyal, E. Greenberg, R. Reisfeld and N. Spector, *Chem. Phys. Lett.* 117 (1985) 108.
10. R. Cases, M.A. Chamarro, R. Alcala and V.D. Rodriguez, *J. Lumin.* 48 & 49 (1991) 509.
11. V.D. Rodriguez, I.R. Martin, R. Alcala and R. Cases, *J. Lumin.* 55 (1992) 23
12. S. Todoroki, K. Hirao and N. Soga, *J. Non-Cryst. Solids* 143 (1992) 46.
13. A.M.A. van Dongen, *J. Non-Cryst. Solids* 139 (1992) 271.
14. J. Sanz, R. Cases and R. Alcala, *J. Non-Cryst. Solids* 93 (1987) 377.
15. R. C. Weast, *Handbook of Chemistry and Physics* (The Chemical Rubber Co., Ohio, 1972)B-63.
16. Z. Mazurak, E. Lukowiak, B. Jezowska-Trzebiatowska, D. Schultze and Ch. Waligora, *J. Phys. Chem. Solids* 45 (1984) 487
17. M. Galczynski and W. Strek, *J. Phys. Chem. Solids* 52 (1991) 681.
18. J.N. Carter, R.G. Smart, A.C. Tropper and D.C. Hanna, *J. Non-Cryst. Solids* 140 (1990) 10.

- 19 R D Peacock, *Structure and Bonding* **22** (Springer-Verlag, New York, 1975) 83
- 20 D.E. Henrie, R L Fellows and G.R Choppin, *Coord. Chem. Rev.* **18** (1976) **199**
- 21 A.B Arauzo, R Cases and R Alcala, *Phys. Chem. Glasses* **35** (1994) **202**
- 22 R C Naik, N.P. Karanjikar and M.A.N Razvi, *J. Lumin.* **54** (1992) 139.
23. E.W.J.L. Oomen, *J. Non-Cryst. Solids* **140** (1990) 150
- 24 S. Tanabe, K Tamai, K Hirao and N. Soga, *Phys. Rev.* **41** (1993) 2507.
- 25 B.C Joshi, M C Joshi and B.D Joshi, *J. Phys. Chem. Solids* **52** (1991) **939**
- 26 B.C Joshi and M.C Joshi, *J. Non-Cryst. Solids* **142** (1992) 171.
- 27 S.C Goh, R Pattie, C. Byrne and D Coulson, *Appl. Phys. Lett.* **67** (1995) **768**
- 28 H C. Kandpal, A.K Agarwal and H.B Tripathi, *Ind. J. Pure & Appl. Phys.* **17** (1979)583.
- 29 S.V.J. Lakshman and C.K. Jayasankar, *J. Phys. C, Solid State Phys.* **17** (1984) 2967.
- 30 Y. Subramanyam, L R. Moorthy and S.V.J. Lakshman, *J. Non-Cryst. Solids* **139** (1992)67
- 31 M Malinowski, R Wolski and W. Wolinski, *Solid State Commun.* **74** (1990) **17**
- 32 K.B. Yatsimirskii and N.K. Davidenko, *Coord. Chem. Rev.* **11** (1979) 223 and refs. therein.
- 33 L. Wetenkamp, G.F. West and H. Tobben, *J. Non-Cryst. Solids* **140** (1992) 35.
34. W. Strek, C Szafranski, P. Deren, K. Jablonski and B. Jezowska-Trzebiaatowska, *Rare Earth Spectroscopy (Eds.) B Jezowska-Trzebiaatowska, J Legendziewicz and W Strek* (World Scientific, Philadelphia, 1985) 340.
- 35 G. Amaranath, S Buddhuu, F J. Bryant, X. Luo, B. Yu and S. Huang, *Mat. Res. Bull.* **25**(1990) 1317.
- 36 D.G. Karraker, *Inorg. Chem.* **6** (1967) **1863**
37. W.F. Krupke, *Phys. Rev.* **145** (1966) 325.
- 38 R. Reisfeld, *J. Less-Common Mets.* **112** (1985) 9.

Chapter S

39. B. Villacampa, V.M. Orera, R.I. Merino, R. Cases, P.J. Alonso and R. Alcala, *Mat. Res. Bull.* 26 (1991) 741.
40. K. Tanimura, M.D. Shinn, W.A. Sibley, M.G. Drexhage and R.N. Brown, *Phys. Rev.* 5 30(1984)2429.
41. M.D. Shinn, W.A. Sibley, M.G. Drexhage and R.N. Brown, *Phys. Rev. B* 11 (1983)6635.
42. S. Buddhudu and F.J. Bryant, *Spectrochimica Acta* 44A (1988) 1381
43. E.V. Uhlmann, M.C. Wienberg, N.J. Kreidl, L.L. Burgner, R. Zanoni and K.H. Church, *J. Non-Cryst. Solids* 178 (1994) 15.
44. C.K. Jorgensen and R. Reisfeld, *J. Less-Common Mets.* 93 (1983) 107
45. H.C. Kandpal and K.C. Joshi, *J. Non-Cryst. Solids* 101 (1988) 243
46. E.W.J.L. Oomen and A.M. A. va Dongen, *J. Non-Cryst. Solids* 111 (1989) 205.
47. F.A. Cotton and G. Wilkinson, *Advanced Inorganic Chemistry* (A Wiley-interscience Publication, New York, 1988) 960.
48. M.A. Marcus and A. Polman, *J. Non-Cryst. Solids* 136 (1991) 260.
49. B.G. Wybourne, *Spectroscopic Properties of Rare Earths* (Interscience Publishers, New York, 1965).
50. K. Hirao, S. Todoroki, D.H. Cho and N. Soga, *Opt. Lett.* 18 (1993) 1586.
51. A. Kurita, T. Kushida, T. Izumitani and M. Matsukawa, *Opt. Lett.* 19 (1994) 314
52. R. Reisfeld and L. Bohem, *J. Solid State Chem.* 4 (1972) 417.
53. G. Fuxi, *Optical and Spectroscopic Properties of Glass* (Springer-Verlag, New York, 1992).
54. K. Wei, D.P. Machewirth, J. Wenzel, E. Snitzer and G.H. Sigel, Jr., *Opt. Lett.* 19 (1994) 904.
55. Q. Su, Z. Pai, L. Chi, H. Zhang, Z. Zhang and F. Zou, *J. Alloys Compds.* 192 (1993)25.
56. G. Blasse, *Advances in Inorganic Chemistry* 35 (Academic Press, California, 1990)319.
57. M. Canaujo, R. Cases and R. Alcala, *Phys. Chem. Glasses* 29 (1988) 187.

- 58 V M Orera, P.J Alonso, R Cases and R Alcala, *Phys. Chem. Glasses* 29 (1988) **59**
- 59 J. Lucas, *J. Less-Common Metals* **112**(1985) 27
- 60 R. Reisfeld, A. Honigbaum, G. Michaeli, L. Harel and M Ish-shalom, *Isreal J. Chem.* 7(1969)613.
61. R Reisfeld, E Greenberg, R.N. Brown, M.G. Drexhage and C.K Jorgensen, *Chem. Phys. Lett.* 95 (1983) **91**
- 62 G.S. Raghuvanshi, H.D Bist and H.C Kandpal, *J. Phys. Chem. Solids* 43 (1982) 781.
63. F S Richardson, J.D. Saxe, S.A Davis and T.R Faulkner, *Molec. Phys.* 42 (1981) 1401.
- 64 M Inokuti and F. Hirayama, *J. Chem. Phys.* 43 (1965) 1978.
- 65 K.B Eisenthal and S. Siegel, *J. Chem. Phys.* 41 (1964) 652.
- 66 Z Zhang, X Jiang, Z. Li, P. Wu and S. Xu, *J. Lumin.* 40 (1988) 657.
67. S Tanabe, K. Hirao and N. Soga, *J. Non-Cryst. Solids* 111 (1992) 148.
- 68 W.T. Carnall, J.P. Hessler and F. Wagner Jr., *J. Phys. Chem.* 82 (1978) **2152**
69. G Boulon, M. Boudierbala and J. Seriot, *J. Less-Common Metals.* **112**(1985)**41**.
70. M.J Weber, *Optical Properties of Ions in Crystals* (Eds.) H.M. Crosswhite and H.W. Moos (Interscience, New York, 1967) 467.

Summary

The optical properties of Ln^{3+} ions in glass matrices provide scope for a wide range of studies both from fundamental as well as application point of view. The present work throws light on the nature of information one can obtain from two points of view, one pertaining to the spectral characteristics of the doping lanthanide ion and the other pertaining to the nature of the host matrix.

From the point of view of the spectral characteristics of the Ln^{3+} ions the following points emerge. It is important to study both the absorption as well as emission spectra as they are interrelated. The study of absorption spectra has two aspects, one dealing with the transition energies leading to the derivation of the spectral parameters such as the Racah parameters, spin-orbit coupling **etc.**, and the other dealing with the analyses of spectral intensities. The former study is of limited value. In the present work the analyses of transition energies are carried out for Pr^{3+} , Nd^{3+} , Er^{3+} and Tm^{3+} ions where they are fairly simple. For this purpose, a full matrix diagonalisation procedure is adopted instead of the Taylor series method commonly followed. For Pr^{3+} and Tm^{3+} in view of the observed transitions being limited, incorporating relationships between matrix elements and observed transition energies as conditions to be satisfied in the least square fit procedure leads to better fit and hence to more reliable spectral parameters. With regard to the analyses of intensities, **Judd-Ofelt** theory is of great value in spite of the simplifications made in this theory. The model is particularly valuable as it helps in the evaluation of the radiative parameters *viz.*, transition probabilities (A), branching ratios (β_R) and excited state lifetimes (τ_R) providing a link between absorption and emission spectral **studies**. The Judd-Ofelt parameters can be reliably evaluated for Pr^{3+} , Nd^{3+} , Sm^{3+} , Dy^{3+} , Ho^{3+} , Er^{3+} and Tm^{3+} . While for Eu^{3+} these parameters can be obtained reliably in favorable cases it is difficult to evaluate them for Gd^{3+} and Tb^{3+} . Hypersensitive transitions which occur both in absorption and emission spectra throw light on the local structure of the lanthanide ions. The emission spectral studies can be carried out with existing experimental facilities for Pr^{3+} , Sm^{3+} , Eu^{3+} , Tb^{3+} , Dy^{3+} , Er^{3+} , Ho^{3+} and Tm^{3+} . Emission spectra provide direct information on the influence of the host

matrix on nonradiative decay. Evaluation of radiative parameters from the Judd-Ofelt parameters can be profitably compared with emission spectral data particularly for the lanthanide ions where both absorption as well as emission data are available.

From host materials point of view the information can be obtained based on (i) absorption spectral features, (ii) emission spectral features and (iii) phonon side band studies. The glass matrices investigated include borate, phosphate and oxyfluoride glasses. The observations made in these glasses are given below.

Borate Glasses: The borate glasses where the cations are changed show the following characteristics. The transitions in the absorption spectra of Nd^{3+} ions show a red shift with increasing ionic radius of the cation present as major constituent. The energy parameters show a corresponding decrease. The ionic size of the constituent cations and coordination preferences intrinsic to the Nd^{3+} and Er^{3+} ions as evidenced by structural characteristics shown by related crystalline borates account for the variations in the Judd-Ofelt parameters. The Judd-Ofelt parameter f_2 for Nd^{3+} in different borate glasses and the red to orange emission intensities of the Eu^{3+} show increasing covalent character for the dopant with increasing ionic size of the cation. The phonon side bands of the ${}^7\text{F}_0 \rightarrow {}^5\text{D}_2$ transition of Eu^{3+} show components due to BO_3 and BO_4 groups. An increase in the BO_4 component accompanied by a corresponding increase in the electron phonon coupling strength in the order $\text{Li}^+ < \text{Ca}^{2+} < \text{Ba}^{2+}$ provide evidence for increasing dimensionality. The optical band gaps for the undoped glasses show decreasing trend with increasing cationic radius. The phonon side band spectrum of Eu^{3+} ions in $\text{CaO-Al}_2\text{O}_3\text{-B}_2\text{O}_3$ glass matrix unlike in $\text{CaO-B}_2\text{O}_3$ shows a single component due to association with BO_3 groups and its electron phonon coupling strength is lower than that of $\text{CaO-B}_2\text{O}_3$ glass

Phosphate Glasses: All the rare earth ions studied give rise to higher Ω_2 values in the $\text{CaO-Al}_2\text{O}_3\text{-P}_2\text{O}_5$ (CAP) glass matrix than for the same ions in the $\text{CaO-P}_2\text{O}_5$ (CP) glass matrix showing that presence of Al^{3+} leads to higher asymmetry at the lanthanide sites. For the same transitions the transition probabilities (A) are higher for Nd^{3+} and lower for Pr^{3+} in CAP glass compared to CP glass. For Eu^{3+} , Dy^{3+} and Tm^{3+} the

hypersensitive transitions show higher A values for the CAP glass. The A values are nearly the same for Er^{3+} in the two matrices. The β_R values calculated from Judd-Ofelt parameters are in close agreement with values obtained from the emission spectra. The relative intensity of $^1\text{D}_2 \rightarrow ^3\text{H}_4$ transition compared to $^3\text{P}_0 \rightarrow ^3\text{H}_6$ in Pr^{3+} , $^1\text{G}_4 \rightarrow ^3\text{H}_6$ compared to $^1\text{D}_2 \rightarrow ^3\text{F}_4$ transition in Tm^{3+} and the phonon side band spectra of Eu^{3+} indicate higher nonradiative decay in the CP glass.

Oxyfluoride Glasses: The f_2 values, the observation of high energy emission transitions for Eu^{3+} and Tb^{3+} , room temperature observation of emission for Ho^{3+} and Er^{3+} and the stimulated emission cross section (σ_p) values comparable to those reported for Ln^{3+} ions in fluoride glasses, all point out that oxyfluoride glasses in many respects closely resemble the fluoride glasses. Thus oxyfluoride glass can be considered for many applications suggested for the fluoride glasses.

Energy transfer studies in the oxyfluoride glass codoped with Pr^{3+} and Tb^{3+} show that Pr^{3+} can act both as donor as well as acceptor. Thus energy transfer of $\text{Pr}^{3+} \rightarrow \text{Tb}^{3+}$ is reported for the first time.

The stimulated emission cross sections for Sm^{3+} and Dy^{3+} ions are an order of magnitude less than the values for other rare earth ions. The fluorescent decay processes for these ions follow single exponential except for Sm^{3+} at higher concentrations. At higher dopant concentrations. The fluorescent decay of Sm^{3+} at higher dopant concentrations shows that energy transfer involving cross relaxation plays a significant role in the radiative decay process.

The Tb^{3+} concentration dependence of emission spectral intensities in the PbO-PbF_2 glass closely follows the standard behavior characteristic of homogeneous distribution of the rare earth ion. Based on the observed results it has been suggested that Tb^{3+} fluorescence can be used as a powerful probe to throw light not only on whether pairing and clustering occur but also on the extent to which interactions between the probe ions differ in systems exhibiting standard behavior.

Phonon side band studies show that in these glasses the phonon energies are low enough to lead to the observation of high energy emissions in the region 440-580 nm. The phonon energy maximum is found to be 930 cm^{-1} . The electron-phonon coupling strengths evaluated from the phonon side bands for oxyfluoride glasses of different compositions are nearly the same.

Ω_2 in the borate and phosphate glasses shows an increasing trend as we go higher up in the rare earth series showing a maximum in the middle of the series and decreases after $\text{Dy}^{3+}(4f^9)$. This trend is explained as due to the dopant ions having 8-10 coordination over the entire series, with the rare earth ions in the middle of the series occupying sites with larger distortions. Unlike in borate and phosphate glasses Ω_2 in oxyfluoride glasses shows an increasing trend along the lanthanide series as in the case of fluoride glasses. This trend suggests increasing covalent character for the rare earth ions with decreasing ionic size. The lanthanides with decreasing ionic size are known to show preference for lower coordination which in turn would result in increasing covalency due to shorter ligand-metal bonds. In other words, the different trends in Ω_2 observed indicates that while Ln^{3+} ions exist with same coordination over the entire series for the borate and phosphate glasses, they show a preference for lower coordination at the end of the series in oxyfluoride and fluoride glasses. Ω_4 and Ω_6 which are influenced only by the dielectric of the medium and vibrational levels follow the same trends as in crystalline systems.

The hypersensitive transitions of rare earth ions in glass hosts have not been investigated in detail earlier. A plot of $\Sigma\Omega_\lambda$, ($\lambda=2,4,6$) against oscillator strengths of hypersensitive and nonhypersensitive transitions for the rare earth ions Nd^{3+} , Ho^{3+} and Er^{3+} for different glass host matrices show that the oscillator strengths of the hypersensitive transitions are markedly affected by the nature of the ligand atoms while those of nonhypersensitive transitions remain almost unaffected. The hypersensitive transitions which are most sensitive to ligand environment have been identified.

Thermal and Optical Properties of **PbO-KF** Glasses

The studies on the lead bearing oxyfluoride glasses **PbO-PbF₂** showed several features of **interest**. This promoted looking into related systems. An attempt is made to extend the above studies to other oxyfluoride glass systems such as **PbO-KF**. Emission spectral studies of rare earth ions in this glass matrices could not be made due to interference by very significant lead fluorescence. As a result the investigations were **modified**. The influence of composition on lead fluorescence, optical absorption edge, refractive index and thermal stability are investigated instead for this glass system. These results are presented here.

The glass samples were prepared by a procedure similar to that described for **PbO-PbF₂** glass. Differential scanning calorimetric studies were carried out using a **Perkin-Elmer DSC-IV** unit. All other experimental measurements were made as described in chapter 2.

The range of glass composition in the **PbO-KF** systems extends from 70 to 30 mol % **PbO**. The densities, molar volumes and refractive indices obtained for different glass compositions are reproduced in table 1. The onset of crystallization for the **70PbO-30KF** glass was found to occur at 732 K. For the remaining compositions crystallization occurs beyond 500 °C, the maximum limit used for calorimetric studies.

The range of composition in which **PbO-KF** glass is formed is comparable to the ranges for the related glass systems such as **PbO-PbF₂** and **PbO-PbCl₂**^{1,2}. The variations of densities and molar volumes with composition show linear dependence (figure 1). The molar refractivity (**R_m**) is given by³

Appendix 1

$$R_m = \frac{\eta^2 - 1}{\eta^2 + 2} \left(\frac{M}{\rho} \right)$$

where η is the refractive index, M the molecular weight and ρ is the density. Accordingly R_m is found to increase with increasing refractive index and molar volume. Replacement of PbO by KF enhances the refractive index of the glass, a result similar to the PbO-PbF₂ system where replacement of PbO by PbF₂ is found to increase the refractive index. The glass transition temperatures (T_g) for the PbO-xKF glasses are higher than those reported for the corresponding PbO-xPbF₂ glasses.¹ Further, larger the concentration of PbO, greater is the glass transition temperature. The difference between crystallization temperature (T_c) and glass transition temperature (T_g) which gives a measure of stability and could be obtained for 70PbO-30KF is found to be 172 K.¹ This value is much greater than the value (37 K) for the corresponding PbO-PbF₂.¹ Thus KF contributes significantly more to thermal stability than PbF₂.

The infrared absorption spectra of PbO-KF glasses are reproduced in figure 2. A broad absorption band around 950 cm⁻¹ and another band at 460 cm⁻¹ are observed and these absorptions may be assigned to Pb-O and K-F bonds respectively.^{1,4} Figure 2 shows that the peak at 950 cm⁻¹ becomes broader and shifts to higher wavenumbers with increasing PbO content presumably due to the presence of PbO_nF_m polyhedra.¹ That the stretching frequency of the K-F bond in glass occurs at 460 cm⁻¹ compared to 405 cm⁻¹ for KF shows the influence of formation of the Pb-O-K-F network on the K-F bond.

The absorption spectra of the PbO-KF glasses are shown in figure 3. The absorption edges occur in the ultra violet region 300 to 420 nm. With increasing KF the absorption edge significantly shifts to shorter wavelengths. In samples for which the shifts to shorter wavelengths are significant, a weak absorption band overlapping with the absorption edge appears at 26,300 cm⁻¹. This band is relatively more pronounced for the composition 40PbO-60KF. This absorption band arises due to the ¹S₀→³P₁ transition,

the ground state 1S_0 and the excited state 3P_1 arising from $6s^2$ and $6s6p$ configurations respectively of Pb^{2+} .^{5,6}

The optical band gap for glasses can be derived from their absorption spectra. Satisfactory values for band gaps can be obtained by plotting the quantity $(\alpha h \omega)^{1/2}$ where $\alpha(\omega)$ is the absorption coefficient, as a function of $h \omega$ as suggested by Davis and Mott for amorphous materials in which the optical transitions are indirect.⁷ The values of $(\alpha h \omega)^{1/2}$ are obtained from the absorption spectra. The optical band gap (E_{opt}) can be obtained by extrapolation of the linear region of the plot to $(\alpha h \omega)^{1/2} = 0$ (figure 4). The values of E_{opt} thus obtained are given in table 1. A plot of E_{opt} against PbO concentration shows that E_{opt} decreases almost linearly with increasing PbO concentration in the range of compositions under study (figure 5). Such a trend may be explained as follows. The optical band gap is closely related to the energy gap between valence band and conduction band.¹⁴ In glasses the latter is strongly influenced by the anions.⁸ The s and p orbitals of Pb^{2+} and p orbitals of oxygen interact with each other to form bonding and anti bonding states which contribute to valence band and conduction band respectively. Replacement of typically ionic KF by highly covalent PbO results in the presence of strong -Pb-O-Pb- covalent linkages.¹ This in principle should result in a reduction of the band gap between the valence band and the conduction band and in turn the optical band gap, as we replace KF by PbO. Similar trend but to a lesser extent is observed for the PbO-PbF₂ glass as well (table 1).

The width (AE) of the tails of localized states within the optical band gap can be obtained using the Urbach's relationship.⁹ According to this relationship AE can be calculated from the slope of the linear part of the $\log \alpha(h \omega)$ plots. The AE values thus obtained are given in table 1. AE shows an increase with increasing PbO, reaches a maximum at 50 mol % of PbO, and then decreases with further increase in the PbO content. The range of AE values for many of the glasses reported lie in the range

Appendix 1

obtained by us.^{10,11} It has been suggested that the widths of the tails of the localized states for different materials have the same physical origin and is attributed to the phonon assisted indirect electronic transitions.¹²

The normalized emission spectra of **PbO-KF** glasses with varying composition are reproduced in figure 6. For mercury like ions the excited state energy levels occur in the order $^3P_0 < ^3P_1 < ^3P_2 < ^1P_1$.^{13,14} The excitation band occurring at $32,250\text{ cm}^{-1}$ for these glass samples can be assigned to $^1S_0 \rightarrow ^1P_1$. The emission spectra of PbO-KF glasses could be resolved into three gaussian components with peak maxima at $18,850$, $21,420$ and $22,650\text{ cm}^{-1}$ and assigned to $^3P_0 \rightarrow ^1S_0$, $^3P_1 \rightarrow ^1S_0$ and $^1P_1 \rightarrow ^1S_0$ respectively. The Stoke's shift for 3P_1 and 1P_1 levels show a wide range and as large as $20,000\text{ cm}^{-1}$ and $9,800\text{ cm}^{-1}$ respectively.^{6,13,15} Our assignments imply Stoke's shift of $9,600\text{ cm}^{-1}$ and $\sim 4,880\text{ cm}^{-1}$ respectively for these two transitions. Cooling the samples down to a temperature of 80 K did not show any significant changes in the emission spectra. The emission lines are found to be superimposed with sharp transitions separated by 400 cm^{-1} in the region $19,000$ to $23,000\text{ cm}^{-1}$. These transitions arise due to the vibrational levels of this magnitude as suggested by the infrared spectra discussed earlier. Increasing concentration of lead shows that the emission intensities of all the observed transitions decrease with increasing lead content as we go from **30PbO-70KF** to **70PbO-30KF**. Thus it is clear that these emissions are due to lead, the resulting decrease arising from concentration quenching. However the extent to which the relative intensities of these transitions vary on increasing lead content shows a marked behavior. The relative intensities of the three gaussians is found to be **19:11:70** for **30PbO-70KF**. As the concentration of lead increases, the relative intensities show a systematic change and for the lead rich sample **70PbO-30KF** attain the values **55:6:39**. In other words the component corresponding to $^1P_1 \rightarrow ^1S_0$ shows a marked decrease with increasing lead concentration. These results suggest significant non radiative decay from 1P_1 and 3P_1 to 3P_0 states. In principle the nonradiative decay from 1P_1 to the closely lying 3P_1 should be more effective than from 3P_1 to 3P_0 which are farther apart. However the large line

widths leading to strong overlaps between the three emission lines and the occurrence of vibrational levels superimposed on them and a glass lattice characterized by high energy phonons (950 cm^{-1}) suggest that multiphonon nonradiative decay will be facilitated in these systems and thus can account for the observed results.

On account of interference due to lead fluorescence, emission studies of a number of rare earth ions cannot be carried out in this glass matrix. It was however found that rare earth ions such as Pr^{3+} , Sm^{3+} and Ho^{3+} could be doped and their emission spectra studied.

Table 1 Density, molar volume, glass transition temperature (T_g), the optical band gap (E_{opt}), Urbach energy (AE) and the refractive index (η) for different glass compositions.

Composition PbO:KF mol%	Density (g/cm^3) ± 0.04	Molar volume (cm^3) ± 0.2	T_g (K) ± 1	E_{opt} (eV) ± 0.03	AE (eV) ± 0.001	Refractive index (η) ± 0.001
70:30	6.72	25.9	559	3.13(3-30)	0.123	1.410
60:40	5.72	27.5	550	3.34	0.126	
50:50	4.99	28.1	543	3.39	0.139	1.590
40:60	4.16	29.8	518	3.63	0.134	
30:70	3.53	30.5	-	3.74(3.39)	0.111	1.653

The values in parentheses are for PbO-PbF₂ glasses.

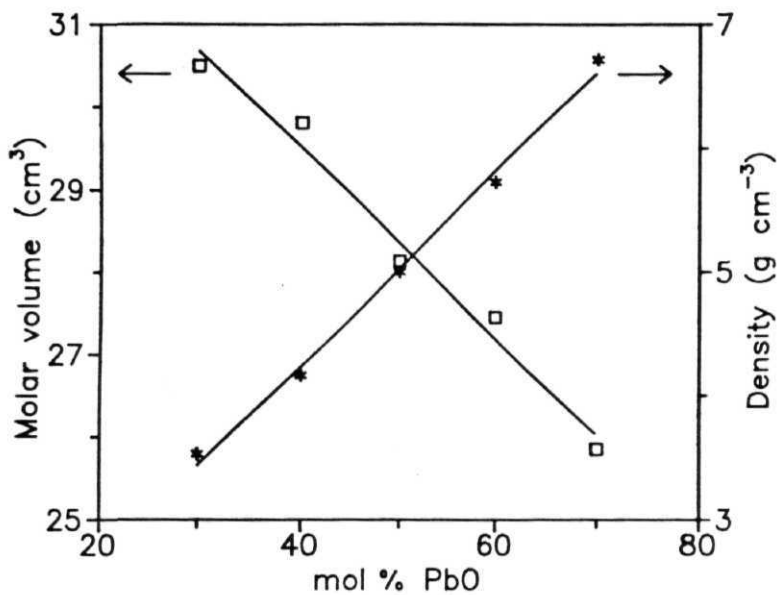


Figure 1 Variations of density (*) and molar volume (•) against mol % of PbO.

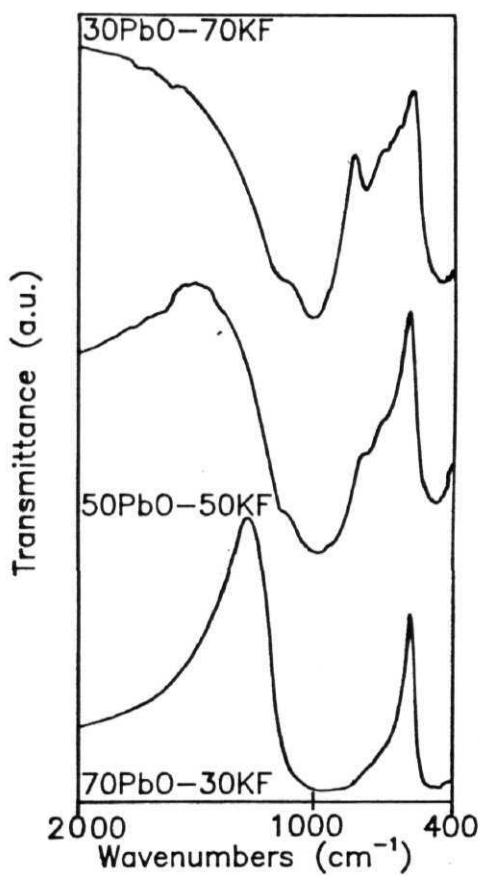


Figure 2 Infrared spectra of PbO-KF glasses for different compositions.

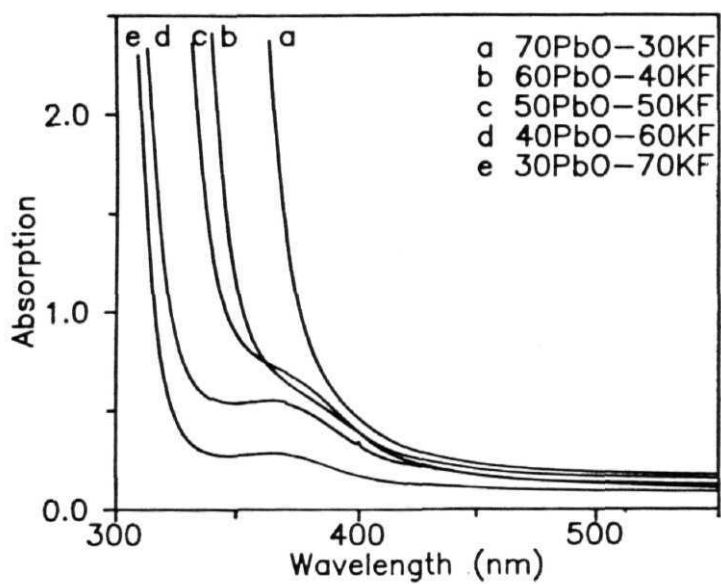


Figure 3 Absorption spectra of PbO-KF glasses for different compositions.

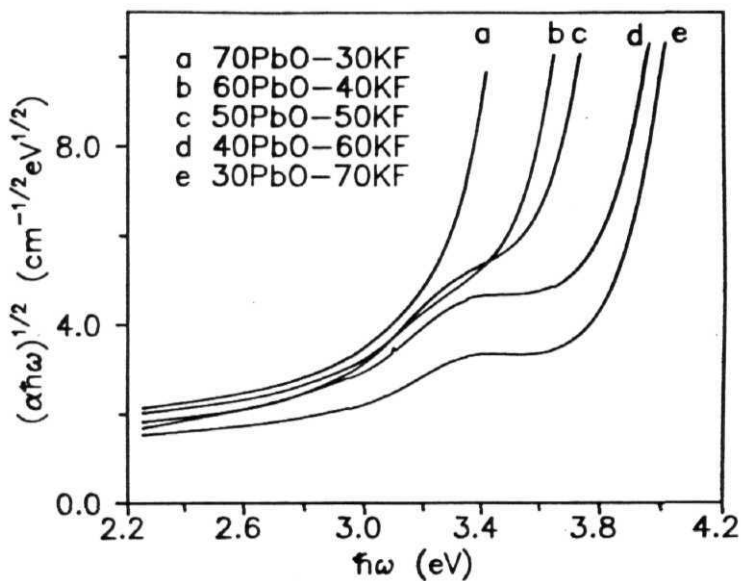


Figure 4 $(\alpha \hbar \omega)^{1/2}$ as a function of photon energy for PbO-KF glasses with varying composition.

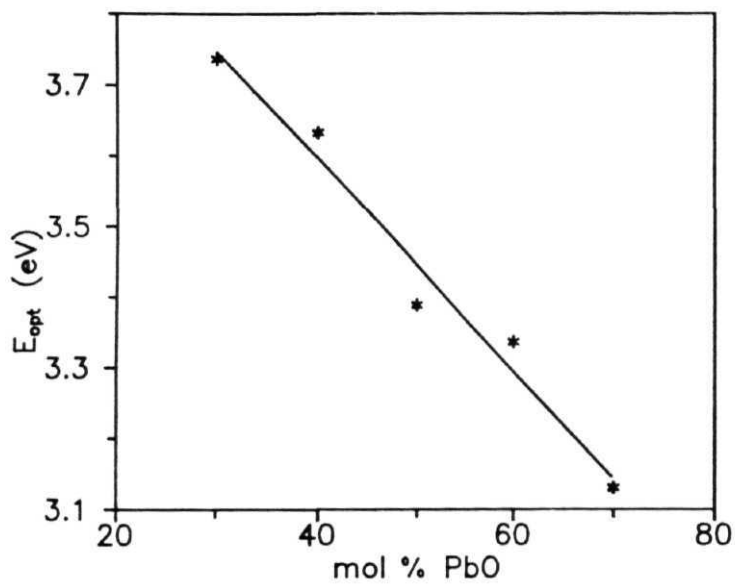


Figure 5 Optical band gap energy (E_{opt}) against mol % of PbO.

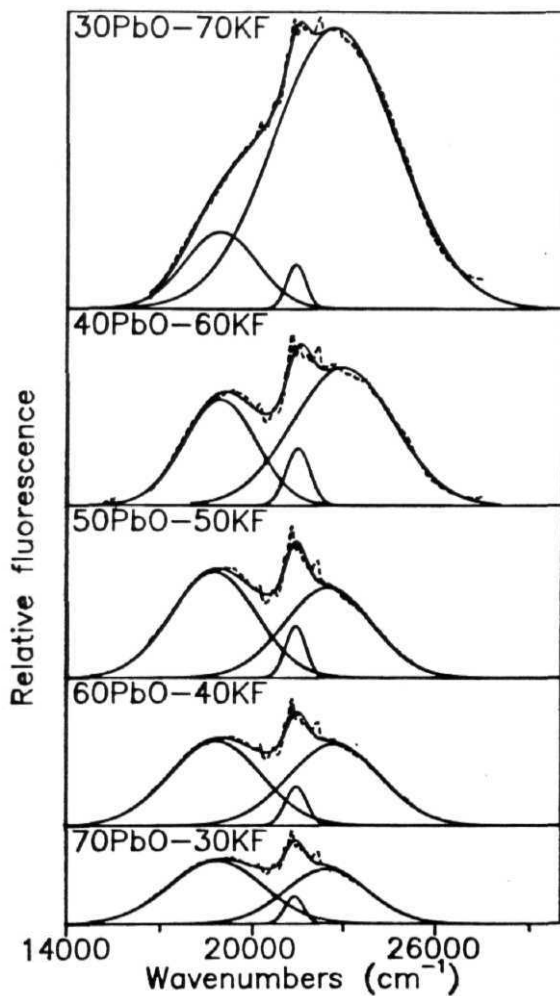


Figure 6 The normalized emission spectra of Pb^{2+} ion in PbO-KF glasses. The solid curves represent the resolved gaussians of the spectra. The dashed curves are the experimental spectra.

References

1. B.G. Rao, H.G. Keshava Sunder and **K.J** Rao, *J. Chem. Soc., Faraday Trans. 1* **80** (1984) 3491
2. **K.J** Rao, B.G. Rao and S.R. Elliott, *J. Mater. Sci.* 20 (1985) 1678
3. I. Fanderlik, *Optical Properties of Glass* (Glass Science and Technology, Elsevier, New York) 5 (1983) 92.
- 4 **C.N.R.** Rao, *Chemical Applications of Infrared Spectroscopy* (Academic press, New York) (1963) 346.
5. **H.F** Folkerts and **G** Blasse, *Chem. Mater.* 6 (1994) 969
- 6 R. Reisfeld and N. Lieblch, *J. Non-Cryst. Solids* 12 (1973) 207.
7. E. Davis and **N** Mott, *Philos. Mag.* 22 (1970) 903.
- 8 G. Fuxi, *Optical and Spectroscopic Properties of Glass* (Springer-Verlag, New York) (1992) 62
- 9 **F** Urbach, *Phys. Rev.* 92 (1953) 1324.
- 10 **C** Dayanand, R.V.G.K. **Sarma**, **G** Bhikshamaiah and **M** Salagram, *J. Non-Cryst. Solids* **167** (1994) 122.
11. A. **Abdel-Kader**, R. El-Mallawany and MM. Elkholy, *J. Appl. Phys.* 73 (1993) 71.
12. K.L. Chopra and **S.K** Bahl, *Thin Solid Films* **11** (1972) 377.
- 13 **C.** Bettinali and G. Ferraresso, *J. Non-Cryst. Solids* 1 (1968) 91
- 14 **A** Paul, *Phys. Chem. Glasses* **11** (1970) 46.
15. A. Meijerink, H. Jetten and **G** Blasse, *J. Solid State Chem.* 76 (1988) 115.